United Arab Emirates University

Scholarworks@UAEU

5-2017

Regioselective Synthesis of Biologically Active Pyrazolone Nucleosides and their Benzoyl Analogues

Heba Ahmed Ghanim Aboukhousa

Follow this and additional works at: https://scholarworks.uaeu.ac.ae/philosophy_dissertations

Part of the Biology Commons

Recommended Citation

United Arab Emirates University

College of Science

REGIOSELECTIVE SYNTHESIS OF BIOLOGICALLY ACTIVE PYRAZOLONE NUCLEOSIDES AND THEIR BENZOYL ANALOGUES

Heba Ahmed Ghanim Aboukhousa

This dissertation is submitted in partial fulfilment of the requirements for the degree of Doctor of Philosophy
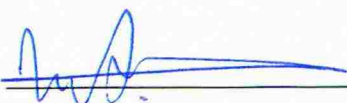
Under the Supervision of Dr. Ibrahim Mahmoud Abdou

May 2017

Declaration of Original Work

I, Heba Ahmed Ghanim Aboukhousa, the undersigned, a graduate student at the United Arab Emirates University (UAEU), and the author of this dissertation entitled *"Regioselective Synthesis of Biologically Active Pyrazolone Nucleosides and their Benzoyl Analogues"*, hereby, solemnly declare that this dissertation is my own original research work that has been done and prepared by me under the supervision of Dr. Ibrahim Abdou in the College of Science at UAEU. This work has not previously been presented or published, or formed the basis for the award of any academic degree, diploma or a similar title at this or any other university. Any materials borrowed from other sources (whether published or unpublished) and relied upon or included in my dissertation have been properly cited and acknowledged in accordance with appropriate academic conventions. I further declare that there is no potential conflict of interest with respect to the research, data collection, authorship, presentation and/or publication of this dissertation.

Student's Signature: _____   Date: 26/12/2017

Approval of the Doctorate Dissertation

This Doctorate Dissertation is approved by the following Examining Committee Members:

1) Advisor (Committee Chair): Dr. Ibrahim M. Abdou

   Title: Associate Professor

   Department of Chemistry

   College of Science

   Signature _____   Date __4 | 10 | 2017__

2) Member: Dr. Haythem A. Saadeh

   Title: Associate Professor

   Department of Chemistry

   College of Science

   Signature _____   Date __4/5/2017__

3) Member: Dr. Ahmed H. Al-Marzouqi

   Title: Associate Professor

   Department of Biochemistry

   College of Medicine & Health Sciences

   Signature _____   Date __4/5/2017__

4) Member (External Examiner): Prof. Gamal A.El-Hiti

   Title: Professor

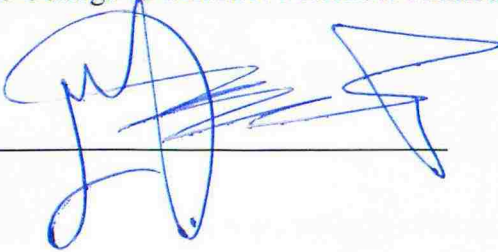   Applied of Medical Sciences

   Institution: University of King Saud University, KSA

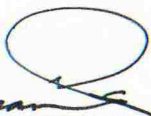   Signature _____   Date __04-05-2017__

This Doctorate Dissertation is accepted by:

Dean of the College of Science: Professor Ahmed A. Murad

Signature _____ Date 5/12/2017

for Dean of the College of Graduate Studies: Professor Nagi T. Wakim

Signature _____Ali Hassan_____ Date __20/12/2017__

Copy __1__ of __8__

Advisory Committee

1) Advisor: Dr. Ibrahim Abdou

   Title: Associate Professor

   Department of Chemistry

   College of Science

2) Co-advisor: Professor Alaa Salem

   Title: Professor

   Department of Chemistry

   College of Science

3) Member: Professor Abdu Adem

   Title: Professor

   Department of Pharmacology

   College of Medicine & Health Sciences

Abstract

Increasing incidence of anticancer and antimicrobial resistance are the most common concerns in the medical field. Cancer is a serious disease that can affect almost every tissue lineage in the human body and poses great challenges to medicinal science. In addition, many antibiotics have a tendency to becoming resistant and are prone to severe adverse effects after long term use. Hence, there is an urgent need to discover and develop novel antitumor drug molecules which could effectively inhibit proliferative pathways with fewer side effects. Also, increasing demand to synthesize novel antimicrobial agents that are active against resistant strains.

This research aimed to design, synthesis, physical studies and biochemical evaluated of some novel pyrazolones and their corresponding ribonucleoside, deoxyribonucleoside and benzoyl analogues for their *in vitro* antimicrobial and anticancer activities.

Antimicrobial properties of the title compounds were investigated against Gram positive and Gram negative bacterial as well as fungal strains. Anticancer activity was performed against HL60 cell lines. Antimicrobial activity results revealed that the synthesized azo conpound **113c**, and the synthesized nucleosides conpounds **116a** and **118c** were found to be the most effective agents with better MIC values, compared to some existing antimicrobial drugs, such as Ceftriaxone and Amphotericin B. On the other hand, the results of anticancer study indicated that the synthesized nucleosides **117a, 122a,b** and **123** were found to be most potent anticancer agent against the cancerous HL60 cell line while the synthesized nucleosides **117e,f**, **122a** and the bezoylated compounds **124c,d,f**, and **124g** showed

good affect against the A-549 cell line. Also, pyrazolones derivatives are more sensitive against the lung cancer.

Binding affinity and selectivity of the synthesized compounds towards *ct*-DNA were studied at different conditions of pH and solvents; The results showed that compound **118c** interact and stabilize the *ct*-DNA which can be anti-cancer agent.

Therefore, these compounds, open new avenues for the development of anti-bacterial and anti-cancer therapeutic agents for the treatment of infectious and cancer diseases. Also, these results give an insight into the structure-activity relationships, which are tremendously important for the design of further new antimicrobial and anticancer agents.

Keywords: Design, Synthesis, Pyrazolone , Nucleosides, Anti-microbial, Anti-cancer, *ct*-DNA.

Title and Abstract (in Arabic)

تصنيع نيكليوزيدات البيرازولين و مشتقاته البنزوايليه بتفاعلات انتقائية المكان ذات نشاط حيوي

الملخص

تهدف هذه الدراسة إلى تطوير وتخليق بعض نيوكليسيدات البيرازول الجديدة المحتويه على ذرات الفلور وهى تعتبرمن أكثر البروتوكولات الصناعية تحدياً، ويرجع ذلك إلى وجود مراكز متعددة النشاط على جزيئ السكر والتي تتحكم في التراكيب الفراغية للمنتجات النهائيه. من المتوقع أن يكون لهذه المركبات الجديده نشاط بيولوجى متميز نظراً الى أن إدخال عدة ذرات من الفلور في أماكن مختلفة من حلقة البيرازولون أدت الى تغيير سلوكها التفاعلى وزادت من تعزيز الأنشطة البيولوجية للمنتجات النهائية. تم خلال هذه الدراسة تصميم وتخليق عدد من المركبات الجديدة عن طريق تفاعلات انتقائية أدت الى الحصول على متشابهات الصيغ (O- و N-isomers) من كل من نيوكليسيدات البيرازولين ومشتقاته البنزويليه ثم التأكد من بنائها الجزيئي من خلال استخدام التقنيات الطيفية الحديثه. تمت دراسة تأثير المركبات الجديدة كمثبط لسرطان الدم و سرطان الرئة. و أوضحت نتائج الدراسات المعملية أن المركبات 117a،122b ، 122a و 123aهم الأكثر تأثيرا ونشاطا ضد خلايا الدم السرطانيه (اللوكيميا) بينما المركبات 124f, 117e ,117f, 122a, 124c, 124d و 124f لها تأثير كبيرعلى خلايا سرطان الرئة. كما تمت دراسة تأثير المركبات الجديدة على بعض انواع البكتيريا إيجابية الجرام والبكتيريا سالبية الجرام وقد أظهرت النتائج أن المركبات 113c، 116a و 118c لها فعالية أكبر مقارنة مع بعض مضادات البكتيريا الموجودة، مثل سيفترياكسون والأمفوتريسين B.

كما انه تمت دراسة التقارب الملزم والانتقائية للمركبات المصنعة مع الحمض النووي في ظروف مختلفة من الرقم الهيدروجيني والمذيبات. وأظهرت النتائج أن المركب 118c ارتبط بالحمض النووي و ساعد على استقرارة مما يمكنه أن يكون عامل مضاد للسرطان. نتائج هذه الدراسة قد تؤدي إلى تطوير معالجات الأورام السرطانية وكذلك استحداث مجموعه جديدة من المضادات البكتيريه في جامعة الإمارات العربية المتحدة والذي قد يساعد مستقبلا في مجال تصميم الأدوية.

مفاهيم البحث الرئيسية: بيرازولون، نيوكليسيدات، تفاعلات انتقائية، مضادات الخلايا السرطانية، مضادات الميكروبات.

Acknowledgments

My thanks first go to Allah for this opportunity and for helping me in sustaining through these, the best and toughest, years of my life.

Then I would like to express thanks to my advisor Dr. Ibrahim Abdou, Associate Professor, Chemistry Department, College of Science, UAE University, thank you for allowing me to grow as a research scientist.

I am grateful also to my advisory committee members, Professor Alaa Salm, and Professor Abdou Adm for their assistance during my Ph.D journey.

Besides my advisory committee, I would like to thank the member of my examination committy for their insightful comments and encouragement.

I gratefully acknowledge Professor Ahmed Murad, Dean, College of Science UAE University, for his tremendous support, enormous help and wise guidance.

I would like to express my special appreciation and thanks for Dr. Ruwaya Al-Kendi, Assistant Dean for Research and Graduate Studies, College of Science, UAE University. I would like to thank you for the continuous support of my Ph.D study, for your patience and motivation. Your guidance and advices help me in all the time. Thank you for believing in me.

I do greatly appreciate the massive support from Professor Sulaiman Alkaabi, Dr. Asma Asma Al Menhali, and Professor Sayed Marzouk

I am thankful to Professor Fatthi Allan, Math Department, UAEU, for his constant encouragement and support (May Allah have mercy on him).

My sincere thanks also goes to Mr. Ahmed Taha, Main Library, for providing me with the relevant reference materials.

Dedication

To My mom, Bent Abdullah,

A strong and gentle soul who taught me to trust in Allah,

believe in hard work and that so much could be done with little,

without your support, I would never have finished this endeavor

Table of Contents

List of Tables

List of Figures

List of Schemes

List of Abbreviations

A-549	Lung carcinoma from human cell line
Abs	Absorption
Ac	Acetyl
CD	Circular dichroism
CdA	2-Chloro-2´-deoxyadenosine
CDCl$_3$	Deuterated chloroform
CEF	Ceftriaxone
COSY	Two dimensional nuclear correlation spectroscopy
ct-DNA	Calf thymus DNA
DMF	Dimethyl formamide
DMSO	Dimethyl sulfoxide
DMSO-d_6	Deuterated dimethyl sulfoxide
DNA	Deoxyribonucleic acid
EDTA	Ethylenediaminetetraacetic acid
EGFR	Epidermal growth factor receptor
Et	Ethyl
EtOAc	Ethyl acetate
EtOH	Ethanol
FT-IR	Fourier transform infrared spectroscopy
G	Gram(s)
gCOSY	Gradient two dimensional nuclear correlation spectroscopy
gHMBC	Gradient two dimensional nuclear heteronuclear multiple-bond correlation spectroscopy

h or hr	Hour(s)
HBA	Hydrogen bond acceptor
HBD	Hydrogen bond donor
Hep G2	Human liver cancer cell line
HL$_{60}$	Human promyelocytic leukemia cells
HMBC	Two dimensional nuclear heteronuclear multiple-bond correlation spectroscopy
HPLC	High performance liquid chromatography
HSQC	Two dimensional nuclear heteronuclear single-quantum correlation spectroscopy
HT29	Caucasian colon adenocarcinoma grade II cell line
IC$_{50}$	The half maximal inhibitory concentration
K562	Chronic myelogenous leukemia
KB	Keratin-forming tumor cell line
KBr	Potassium bromide
LC/MS	High performance liquid chromatography/mass spectrometry
LSER	Linear solvation energy relationship
M$^+$H	Parent plus a proton
M$^+$Na$^+$	Parent plus sodium ion
MDA-MB-231	Human breast adenocarcinoma cell line
MDR	Breast adenocarcinoma cells
MeOH	Methanol
Mg	Milligram(s)
MIC	Minimum inhibitory concentration
Min	Minute

mL	Milliliter
Mol	Mole(s)
Mmol	Millimole(s)
MW	Microwave
Mtb H37Rv	Mycobacterium tuberculosis H37Rv
NBS	N-bromosuccinimide
NMR	Nuclear magnetic resonance
OVCAR3	Human ovary carcinoma cell
PDB	Protein data bank
RNA	Ribonucleic acid
SD	Standard deviation
THF	Tetrahydrofuran
T_m	Melting temperature
TMS	Tetramethylsilane
TLC	Thin layer chromatography
TMSO*f*	Trimethylsilyl triflate
TsNHNH$_2$	Tosylhydrazones
UV-Vis	Ultraviolet–visible spectroscopy

Chapter 1: Introduction

1.1 Overview

Pyrazolones, which are five-membered heterocyclic ring containing two nitrogen atoms, are important organic compounds in pharmaceutical and agrochemical industries (Figure 1). Pyrazolones are one of the oldest synthetic pharmaceutically active compounds. Compounds containing pyrazole moiety are known to exhibit non-steoriodal anti-inflammatory proprieties that show anti pyretic and analgesic activities [1]. Pyrazolones are also used as multi drug resistant (MDR) reversal agents such as: antimicrobial, antiviral, anti-fungal, anti-cancer, anti-allergic, antidepressant, antibacterial [2-5] antidiabetic, anti-malarial, anaxiolytic, antineoplastic activities, antipyretic, anticonvulsant, anticholinergic, tyrosinase inhibitor ability, anti-HIV, anti-viral, anti-tuberculosis, antiparasitic, anti-microbial, hypoglycaemic and anti-tumor [6-10].
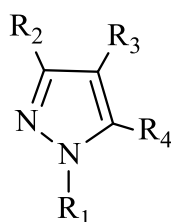
Figure 1: Structure of pyrazoles

1.2 Statement of the Problem

Since cancer is considered the third leading cause of death in the UAE, this study will focus on the synthesis of newly synthesized pyrazolone nucleosides to be used in the treatment of cancer. Drug discovery programs focus on the development

of novel chemotherapeutics to reduce cancer's risk [1], delay the spread of cancer, or in some cases destroy it completely [2]. The chemotherapeutic agents are either naturally occurring compounds that have been isolated from plants or synthetic compounds. Nucleosides containing fluorine atoms have several medical applications such as antiviral, antifungal and antiinflamatory agents [3, 4].

This research aimed to develop some novel pyrazoline nucleosides which may have potential activities against cancer cells. Pyrazoline derivatives are known to have antiproliferative effect against many types of cancer. For example, in the last decade, many Pyrazolone nucleosides were discovered and been used for treatment of cancer [11]. The new designed pyrazolone nucleosides as well as the benzoyl ester expected to have new anticancer prosperities. The results of this project may lead to development of anticancer agents in the UAEU.

Furthermore, new and reemerging infectious diseases will continue to pose serious global health threats into the 21st century and according to the World Health Organization report, these are still the leading cause of death among humans worldwide. Among infectious diseases, tuberculosis claims approximately two million deaths per year worldwide. In addition, agents that reduce the duration and complexity of the current therapy and solve the problem of resistance to conventional antibiotics would have a major impact on the overall cure rate to combat bacterial infection. Subsequently, there is an urgent need for the development of new drug candidates with newer targets and alternative mechanism of action. The research is focused as well in using some of the novel pyrazolones derivatives against common pathogenic bacteria.

1.3 The Chemistry of Pyrazoles

Pyrazole is a tautomeric compound. Unsubstituted pyrazole can be represented in three tautomeric forms (Scheme 1). While substited pyrazole exist in five possible tautomeric structures (Scheme 2) [12].
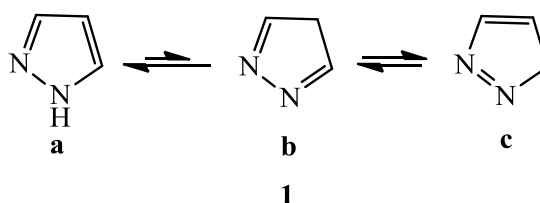
Scheme 1: Tautomeric forms of unsubstituted pyrazole
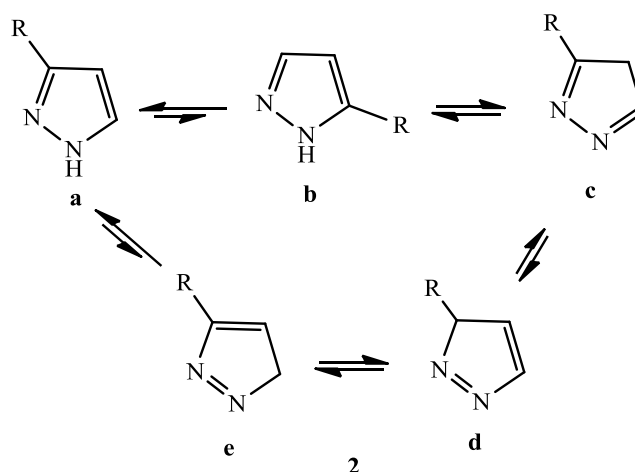
Scheme 2: Five tautomeric forms of 3-substituted pyrazole derivative

1.3.1 Naturally Occurring Pyrazoles

Naturally occurring pyrazoles were isolated after 1950s as pyrazole. 3-*N*-nonylpyrazole isolated from *Houttuynia Cordata*, a plant of the *piperaceae* family in tropical Asia (Figure 2). This naturally occuring pyrazole showed antimicrobial

activity [13]. The other natural pyrazole derivative, *levo-β*-(1-pyrazolyl)alanine, was isolated from watermelon seeds (*Citrullus Vulgaris*) by Japanies researchers [13].

3-n-nonylpyrazole
(an antimicrobial agent)
3

levo-B-(1-pyrazoyl)alanine
(an amino acid)
4
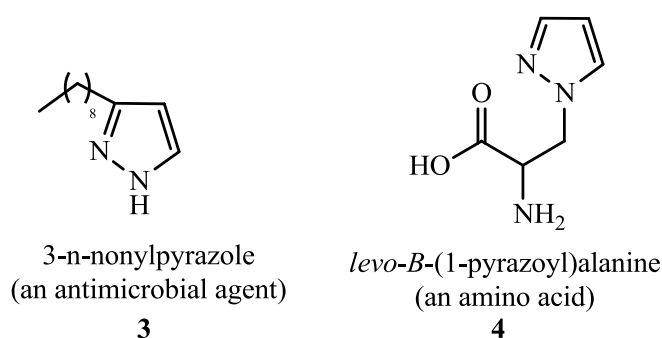
Figure 2: Two examples of naturally occurring pyrazoles

1.4 Synthesis of Pyrazoles

Because of the excellent bioactivity and wide range of application associated with pyrazoles have targeted pyrazolines to be synthesized. Many methods have been developed for preparation of substituted pyrazoles. In general, pyrazoles are synthesized by (i) the reaction of 1,3-diketones with hydrazines, (ii) 1,3-dipolar cycloaddition of diazo compounds with alkynes and (iii) the reaction of α,β-unsaturated aldehydes or ketones with hydrazines. [14].

1.4.1 Pyrazoles from 1,3-Diketones

The first method used to synthesize pyrazole was explored by Knorr in 1883 [15], which employed the reactions of 1,3-dicarbonyl compounds **5** with arylhydrazines to afford pyrazole derivatives **6** and **7** (Scheme 3). The condensation of 1,3-diketones with arylhydrazines in the presence of catalysts generally produced a mixture of two regioisomers. The yields of pyrazole isomers usually depend on the reaction conditions.

a: R = Me, R$_1$= phenyl, Ar = *p*-bromophenyl,(94:6);
b: R = CF$_3$, R$_1$= *p*-nitrophenyl, Ar = *p*-SO$_2$NH$_2$Ph,(99.5:0.5);
c: R = Me, R$_1$= phenyl, Ar = *p*-SO$_2$NH$_2$Ph,(96:4);
d: R = CF$_2$H, R$_1$= , *p*-methoxyphenyl, Ar = *p*-SO$_2$NH$_2$Ph,(99.8:0.2)
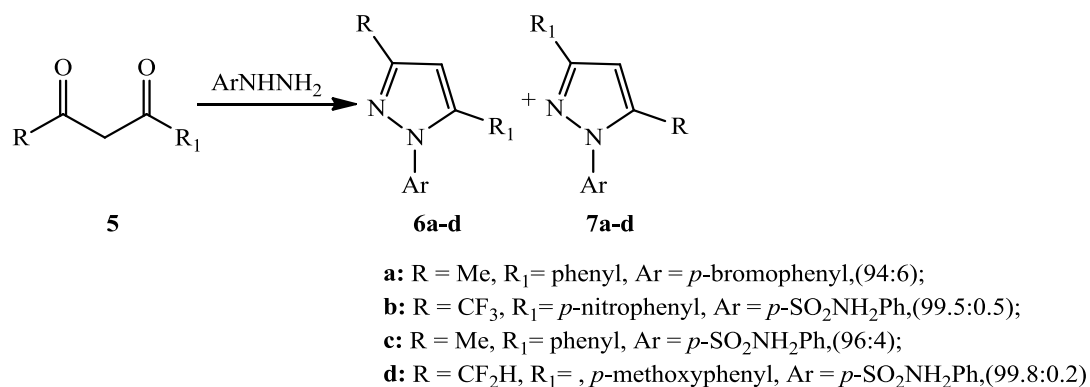
Scheme 3: Synthesis of pyrazoles from 1,3-diketones and arylhydrazines

Recently, an efficient one-pot synthesis of disubstituted pyrazoles was achieved by employing lithium enolates **8** and acid chlorides **9**. The reaction proceeded by generating 1,3-dicarbonyl compound **5** in situ**.** The intermediate then cyclized with hydrazine to afford disubstituted pyrazole **10** (Scheme 4) [16].

10a: R$_1$ = *p*-bromophenyl, R$_2$ = -*p*-methoxyphenyl ,(89%)
10b: R$_1$ = *p*-bromophenyl, R$_2$ = -CH$_2$CH$_2$CH$_2$CH$_2$Cl ,(49%)
10c: R$_1$ = *p*-nitrophenyl, R$_2$ = -*p*-methoxyphenyl ,(72%)
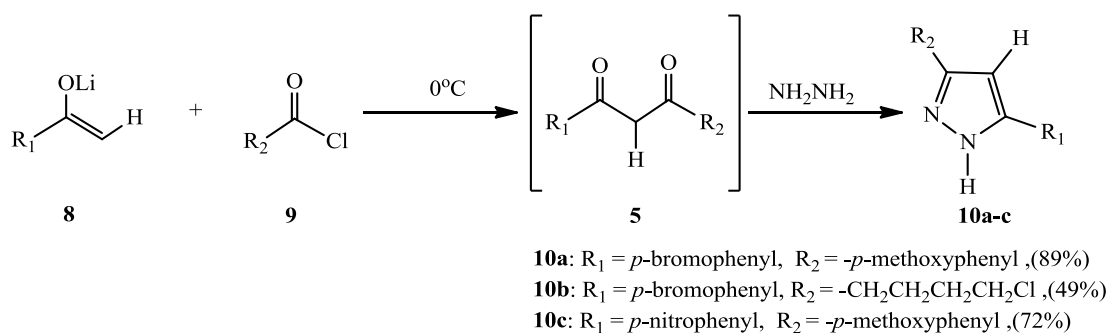
Scheme 4: Synthesis of disubstituted pyarzoles from lithium enolates and acid chlorides

1.4.2 Pyrazoles from 1,3-Dipolar Cycloaddition Reactions

Alkynes react with diazonium ion to afford pyrazoles via [3+2]-cycloaddition. Aggarwal [17] reported one-pot 1,3-dipolar cycloaddition of diazoles with alkynes for the preparation of 3,5-disubstituted pyrazoles (Scheme 5). First,

diazonium ions **12** were generated in-situ from the reaction tosylhydrazones (TsNHNH$_2$) and aldehydes **11** in basic condition, which then underwent cycloaddition with terminal alkynes to produce pyrazole derivatives **13**.

13a: Ar = *p*-chlorophenyl, (74%)
13b: Ar = *p*-bromophenyl, (82%)
13c: Ar = *o*-methoxyphenyl, (81%)
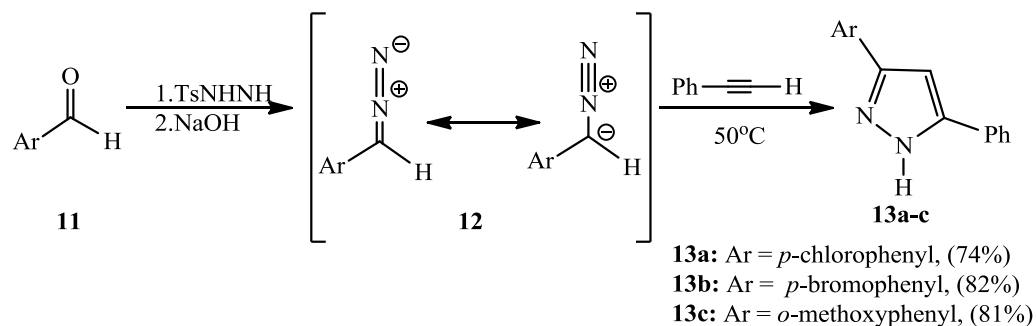
Scheme 5: Synthesis of pyrazoles via 1,3-dipolar cycloaddition

In the reaction between *N*-monosubstituted hydrazones **14** and nitroolefines **15**, 1,3,4,5-tetrasubstituted pyrazoles **16** were obtained in moderate to good yields (Scheme 6) [18].

16a: R$_1$ = Me, R$_2$ = *p*-chlorophenyl, R$_3$ = Ph, R$_4$ = Me, (92%)
16b: R$_1$ = -CH$_2$Ph, R$_2$ = *p*-chlorophenyl, R$_3$ = *p*-toly, R$_4$ = H, (96%)
16c: R$_1$ = Ph, R$_2$ = -CH$_2$CH$_3$, R$_3$ = Ph, R$_4$ = H, (76%)
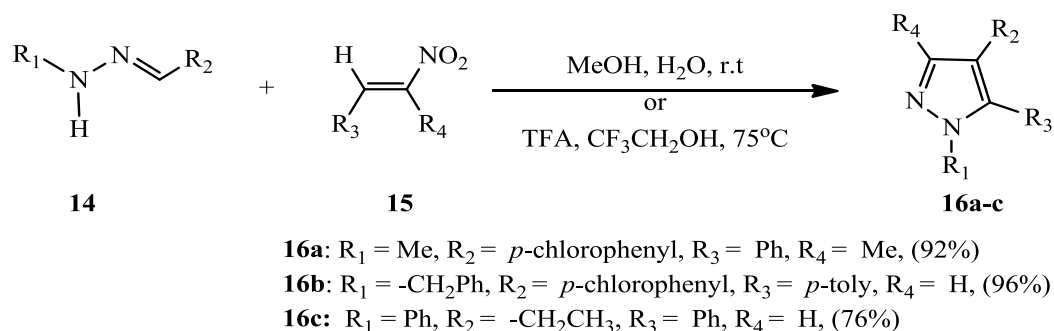
Scheme 6: Synthesis of pyrazoles from nitroolefines

1.4.3 Pyrazoles from *α,β*-Unsaturated Aldehydes

Another strategy for the synthesis of pyrazoles is the cyclocondensation of an appropriate hydrazine with *α,β*-unsaturated aldehydes or ketones [19]. Example, the

α,β-unsaturated ketone **17** reacted with hydrazine to give the desired product. Katritzky reported the synthesize of the 1,3,5-trisubstituted pyrazoles **19** by the reaction of α-benzotriazolyl-α,β-unsaturated ketones **17** with arylhydrazines (Scheme 7) [20]. Pyrazolines **18** were first produced and then oxidized to pyrazoles **19** in the presence of base.

19a: R = H, Ar = Ph, Ar' = *p*-chlorophenyl, (82%)
19b: R = H, Ar = Ph, Ar' = *p*-cynophenyl, (92%)
19c: R = Ph, Ar = *p*-methoxyphenyl, Ar' = *p*-toly, (90%)
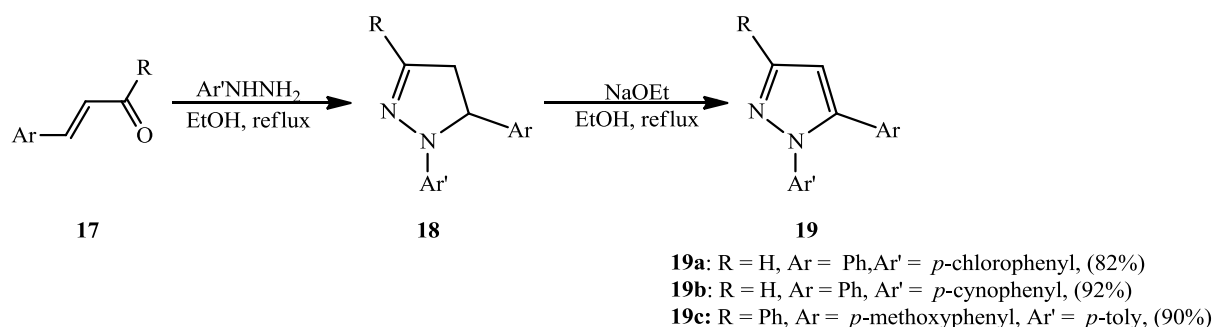
Scheme 7: Synthesis of pyrazoles from α,β-unsaturated ketones and arylhydrazines

The reaction of hydrazine with α,β-alkynic aldehydes or ketones produced two pyrazole products **21, 22**. For instance, the reactions between propargyl ketones **20** and hydrazine gave two pyrazole isomers **21** and **22** (Scheme 8) [21]. Notably, the regioselectivity of the reaction depend on the type of hydrazine substitutents. For example, methyl hydrazine afforded pyrazoles **21** as major product while aryl hydrazine yielded pyrazoles **22** as major product.

a: R = Me, **21** (78%), **22** (30%)
b: R= *p*-methoxyphenyl, **21** (14%), **22** (86%)
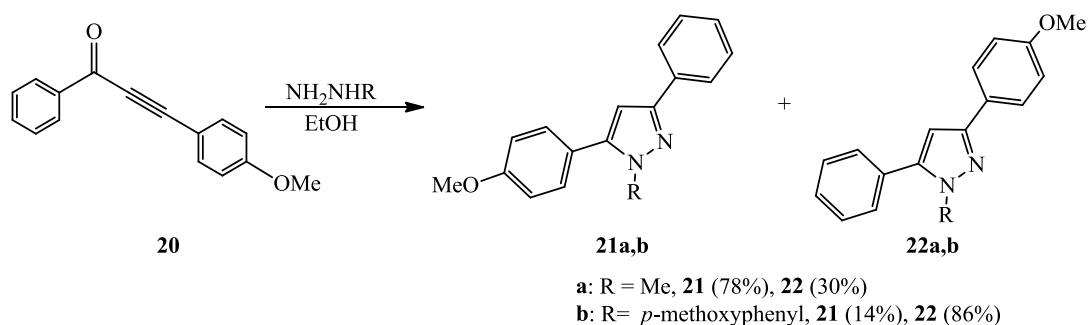
Scheme 8: Synthesis of pyrazoles from alkynones and hydrazines

1.4.4 Pyrazoles Catalyzed by Palladium

Pyrazoles were also synthesized by the reaction between *N*-tosyl-*N*-propargylhydrazine **23** and aryl iodides in the presence of palladium catalyst (Scheme 9) [22]. Initially, cyclocondensation led to the formation of *N*-tosyl-3-arylpyrazoles **24**, followed by detosylation yielded 3-aryl-1*H*-pyrazoles **25.**

25a: R = Thienyl, (85%)
25b: R = *o*-methoxyphenyl, (93%)
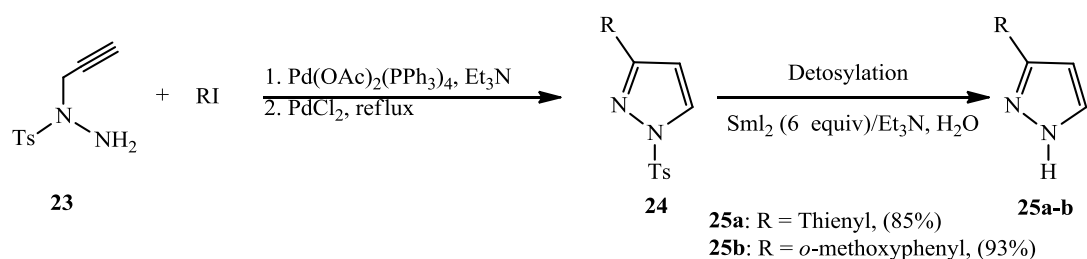
Scheme 9: Synthesis of 3-aryl(vinyl)pyrazoles from *N*-tosyl-*N*-propargylhydrazines

1.5 Pyrazolone Nucleosides

Nucleosides are the key to life as they building blocks of both DNA and RNA in Nature. In medicine, many drugs contain synthetic nucleosides or nucleoside analogues are used for the treatment of disease, especially cancer and viral infection [23]. As a result, designing expeditious routes are of paramount importance to organic and medicinal chemists, and the glycosylation step between nucleobase and carbohydrate is often the key step. To date, all reported nonenzymatic methods to synthesize nucleosides have required the use of protecting groups on the carbohydrate moiety to deactivate the inherently reactive hydroxyl groups on the sugar ring [24]. Three general glycosylation methods dominate in nucleoside synthesis. The Fischer method [25] employs nucleophilic displacement of an α-halogenose by the metal salt of a heterocycle to furnish the nucleoside in the manner

of nucleophilic substitution reaction with inversion in the configuration of the stereochemistry of anomeric carbon [26]. The fusion method consists of heating a per-acylated sugar with a nucleobase [27]. The most popular and mildest method is the Vorbrüggen variant [28] of the Hilbert−Johnson using a fully protected sugar in a coupling reaction with a silylated nucleobase in the presence of Lewis acids ($SnCl_4$ or TMSOTf), but other reactions exist [29] to provide the protected nucleoside. The greatest challenge is the achievement of a good stereoselectivity to avoid the formation of α/β diastereomeric mixtures, which are quite difficult to separate [30].

1.5.1 Stereoselectivity and Glycosylation Reaction

In most frequently nucleosides studied mechanisms, oxocarbenium ions have been proved to be the intermediates in glycosylation reactions, which mean those reactions underwent S_N1 mechanism. Woerpel and coworkers [31-34] were active in studying these intermediates and their conformations when attacked by nucleophiles. They have established a model to explain the highly stereoselective reaction between nucleophiles and five-membered-ring oxocarbenium ions [31]. They futured a model to explaine the selectivity through using *C*-glycosylation as a model by taking into account the favored conformations of both oxocarbenium ions and products (Scheme 10). The favored conformation of the oxocarbenium ion was an envelope **26.** This allowed the nucleophile to attack the ion from inside face leading to the staggered product **27**, which is lower in energy, due to a stereoelectronic effect. On the same area, Reissig provided an example of Woerpel's stereoselectivity in his study of lactols [35].
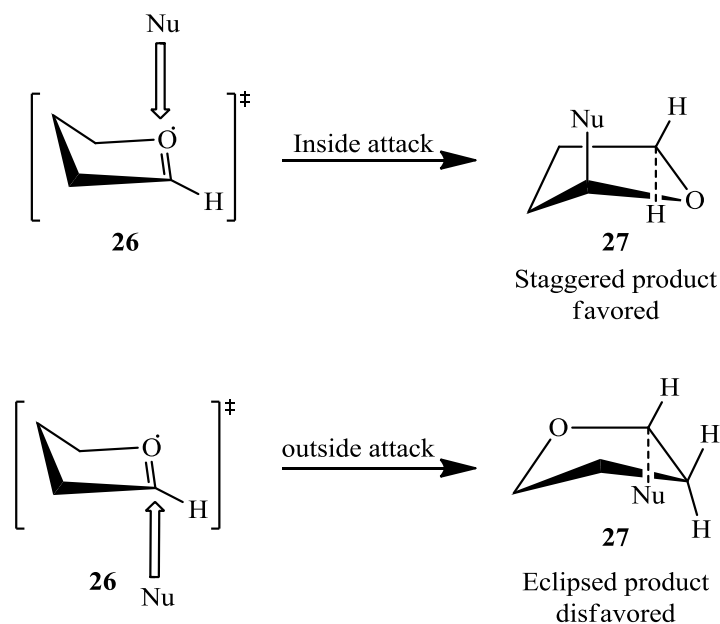
Scheme 10: Woerpel's stereoselectivity and glycosylation reaction

The glycosylation reaction involves nucleophilic displacement at the anomeric center. As the reaction takes place at the secondary carbon atom with the use of weak nucleophiles (sugar acceptors), it often follows a unimolecular S_N1 mechanism. In most cases, an activator (catalyst) assisted departure of the anomeric leaving group results in the formation of the glycosyl cation. The only possibility to intramolecularly stabilize glycosyl cation formed from the glycosyl donor bearing a non-participating group is by resonance from O-5 that results in oxocarbenium ion (Scheme 11). The anomeric carbon of either resonance contributors is sp^2 hybridized; hence, the nucleophilic attack would be almost equally possible from either the top (*trans*, *β*- for the D-glucosides) or the bottom face (*cis, α-*) of the ring. Even though the α-product is thermodynamically favored because of the so-called anomeric effect [36], a substantial amount of the kinetic *β*-linked product is often obtained owing to the irreversible character of glycosylation of complex *α* glycones. Various factors

such as temperature, protecting groups, conformation, solvent, promoter, steric hindrance or leaving groups may influence the glycosylation outcome [37, 38].
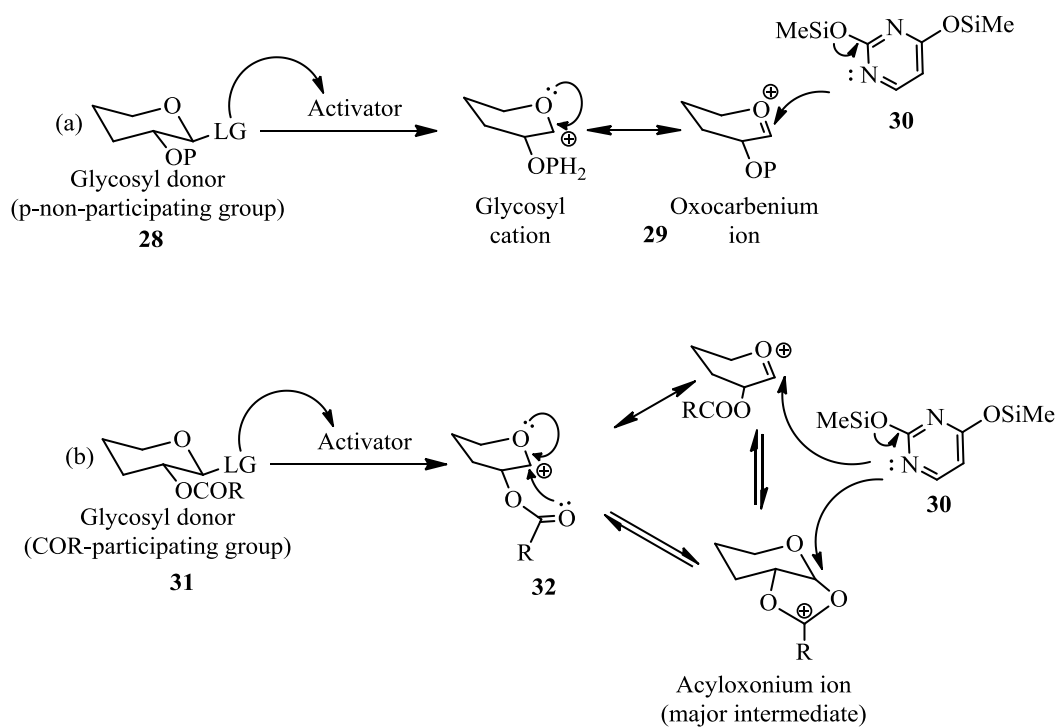
Scheme 11: General glycosylation reaction mechanism

As noted above, it is a general in carbohydrate synthesis that stereoselective preparation of 1,2-*cis* glycosides is more demanding than that of 1,2-*trans* glycosides. The formation of 1,2-*trans* glycosides is strongly favored by the neighboring-group participation (generation of intermediate acyloxonium ion). Typically, the use of a participating substituent at *C*-2 is sufficient to warrant stereoselective 1,2-*trans* glycosylation. One of the factors affecting the stereochemical outcome of glycosidation of glycosyl donors bearing a nonparticipating substituent at *C*-2 is the anomeric effect, which favors α-glycoside formation. However, because of the irreversible character of glycosylation, the role

of the anomeric effect is controlling the orientation of the new glycosidic bond. Although variation of reaction conditions or structural elements of the reactants may lead to excellent 1,2-*cis* stereoselectivity, no successful comprehensive method for 1,2-*cis* glycosylation has been discovered.

In this study, we focus on studying glycosylation reactions where furanoses was used as glycosyl donors; the most common furanoses are ribose and 2-deoxyribose. The acceptor that participates in this reaction can be nucleobase.

1.5.2 Stereoselectivity and Riboside

In comparison to their pyranosyl six-membered ring, furanosides are relatively rare. Nevertheless, furanose presence in a variety of glycostructures from bacteria, parasites and fungi makes this type of glycosidic linkage an important synthetic target [39, 40].

1.5.2.1 *N*- Riboside

The synthesis of 1,2-*trans* furanosides is relatively straightforward and, similar to that of pyranosides, can be reliably achieved with the use of glycosyl donors bearing a participating group at *C*-2. In contrast, the construction of 1,2-*cis* glycofuranosidic linkage is difficult, because the stereocontrol in glycofuranosylation cannot be added by the anomeric effect owing to the conformational flexibility of the five-membered ring. In fact, both stereoelectronic and steric effects favor the formation of 1,2-*trans* glycofuranosides. Despite some recent progress, stereoselective synthesis of 1,2-*cis* glycofuranosides has been one of the major challenges of synthetic chemistry. General glycosylation methods, involving glycosyl fluorides [41], trichloroacetimidates [39], and thioglycosides [42] along

with less common and indirect techniques [43-45], were applied to 1,2-*cis* furanosylation. More recently, a notable improvement in stereoselectivity of 1,2-*cis* furanosylation was achieved by using glycosyl donors in which the ring has been locked into a single conformation. These examples include 2,3-anhydro [46, 47], 3,5-*O*-(di-*tert*-butylsilylene) [46] and 3,5-*O*-tetraisopropyldisiloxanylidene [48] protected bicyclic glycosyl donors.

The goal of Guindon and co-workers' was to get high 1′,2′-*cis* stereoselective *N*-glycosylation of different furanoses by kinetic control [49]. In the synthesis of 1′,2′-*cis*-nucleoside, the nucleophilic base had to attack the furanose from the most hindered side. The stereoselectivity was controlled by the neighboring group participation. The silylated base moieties (thymine and cytosine) were reacted with benzoylated furanose **33** (Scheme 12) offering α-thymidine **35** and α-5-methylcytidine **37** in a good yield.
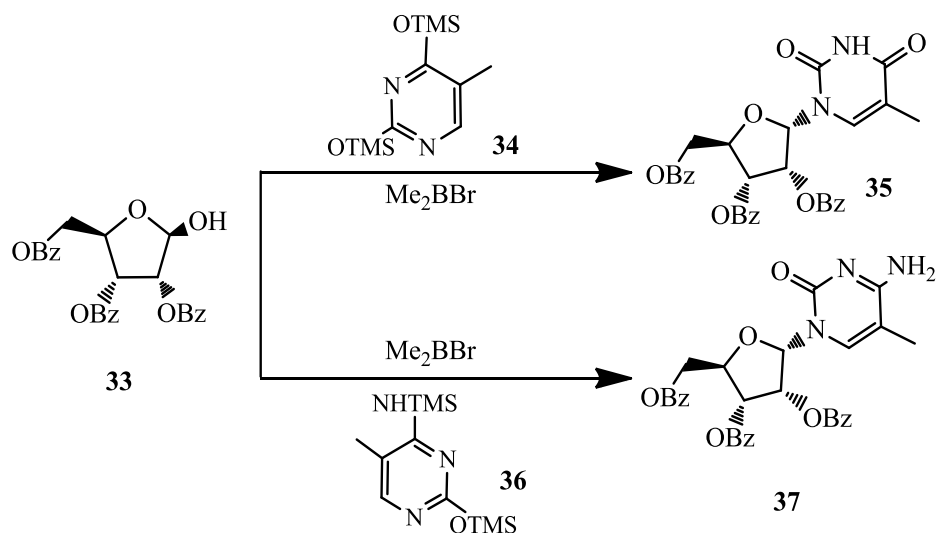
Scheme 12: Synthesis of α-5-methylcytidine **35** and α-thymidine **37**

The synthesis of *N*-riboside reaction could be also affected by the leaving group of the sugar moiety. Scheme 13 illustrates the synthesis of 1,2-*cis*-nucleosides based on silylation method. Glycosylation of 2,4-bis(trimethylsily)cytosine **38** with 1,2,3,5-tetra-*O*-acetyl-*α,β*-D-ribofuranose **39** in acetonitrile in the presence of tin(IV)chloride leads to N^1-*β*-nucleoside **40** in 68% (Scheme 13) [50] (Scheme 13).
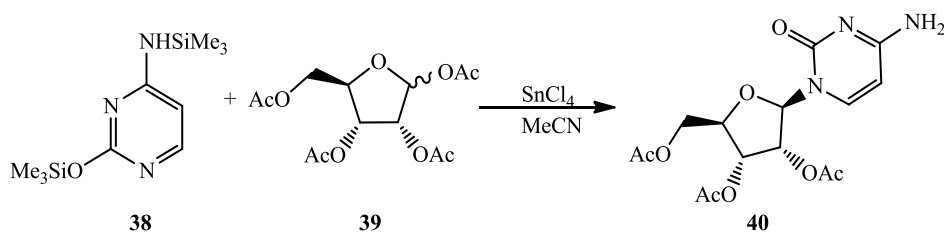
Scheme 13: *N*-Glycosylation of ribofuranosides **40**

Elgemeie and co-workers reported [51] the Ring annulation of 1-deoxy-1-hydraziny1-2,3-*O*-isopropylidene-D-ribose **42** with tetracyanoethylene **41** gave 5-amino-1-(2,3-*O*-isopropylidene-*β*-D-ribofranosyl)-pyrazole-3,4-dicarbonitrile **43**, which, on deisopropylidination, afforded 5-amino-1-(*β*-D-ribofuranosyl)pyrazole-3,4-dicarbonitrile **44** (Scheme 14).
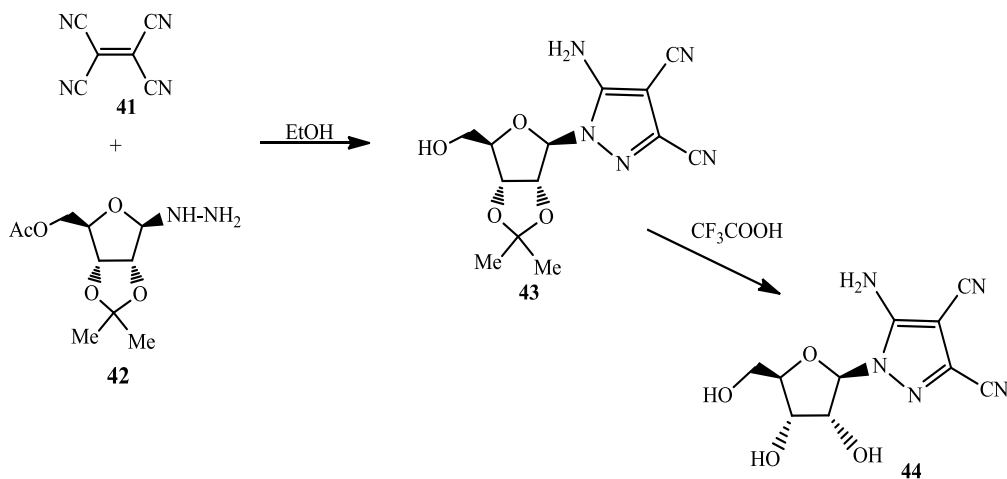
Scheme 14: **S**ynthesis of ribofuranosides **44**

In addition, Elgemeie's group [51] illustrated also the glycosylation of diethyl pyrazole-3,4-dicarboxylate **45** with 1-*O*-acety1-2,3,5-tri-*O*-benzoyl-D-ribofuranose **46** which gave predominantly the *β*-nucleoside **47**. Hydrolysis of **47** by methanolic ammonia furnished 1-*β*-D-ribofuranosylpyrazole-3,4-dicarboxamide **48** (Scheme 15).
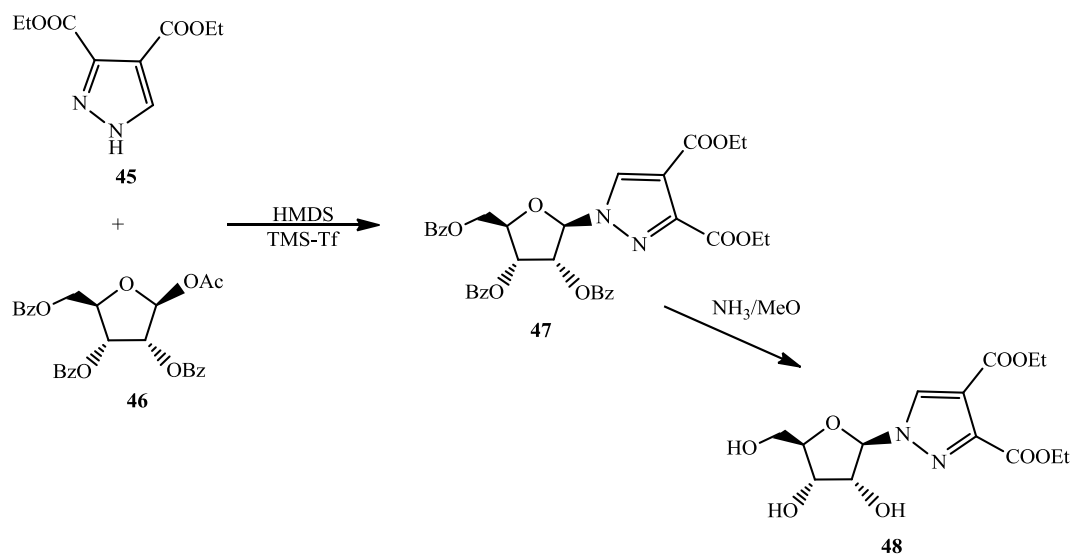
Scheme 15: Synthesis of pyrazole riboside **48**

Matsumoto reported [52] that the deisopropylidenation of 5-amino-1-(2ʹ,3ʹ-*O*-isopropylidene-*β*-D-ribofuranosyl)pyrazole-4-carbonitrile **49** gave 5-amino-1-(*β*-D-ribofuranosyl)-pyrazole-4-carbonitrile **50**, and conventional hydrolysis of **50** afforded compound **51**. Acetylation of **50** gave **52**. Non aqueous diazotization of **52** with isoamyl nitrite in dibromomethane or diiodomethane gave the corresponding C5-bromo and C5-iodo derivatives, which subsequently were transformed into 5-bromo-1-(*β*-D-ribofuranosyl)pyrazole-4-carboxamide **55** and the 5-iodo analog **54**. A similar nonaqueous diazotization of compound **52** in dichloromethane afforded after deamination and hydrolysis product **55** (Scheme 16).
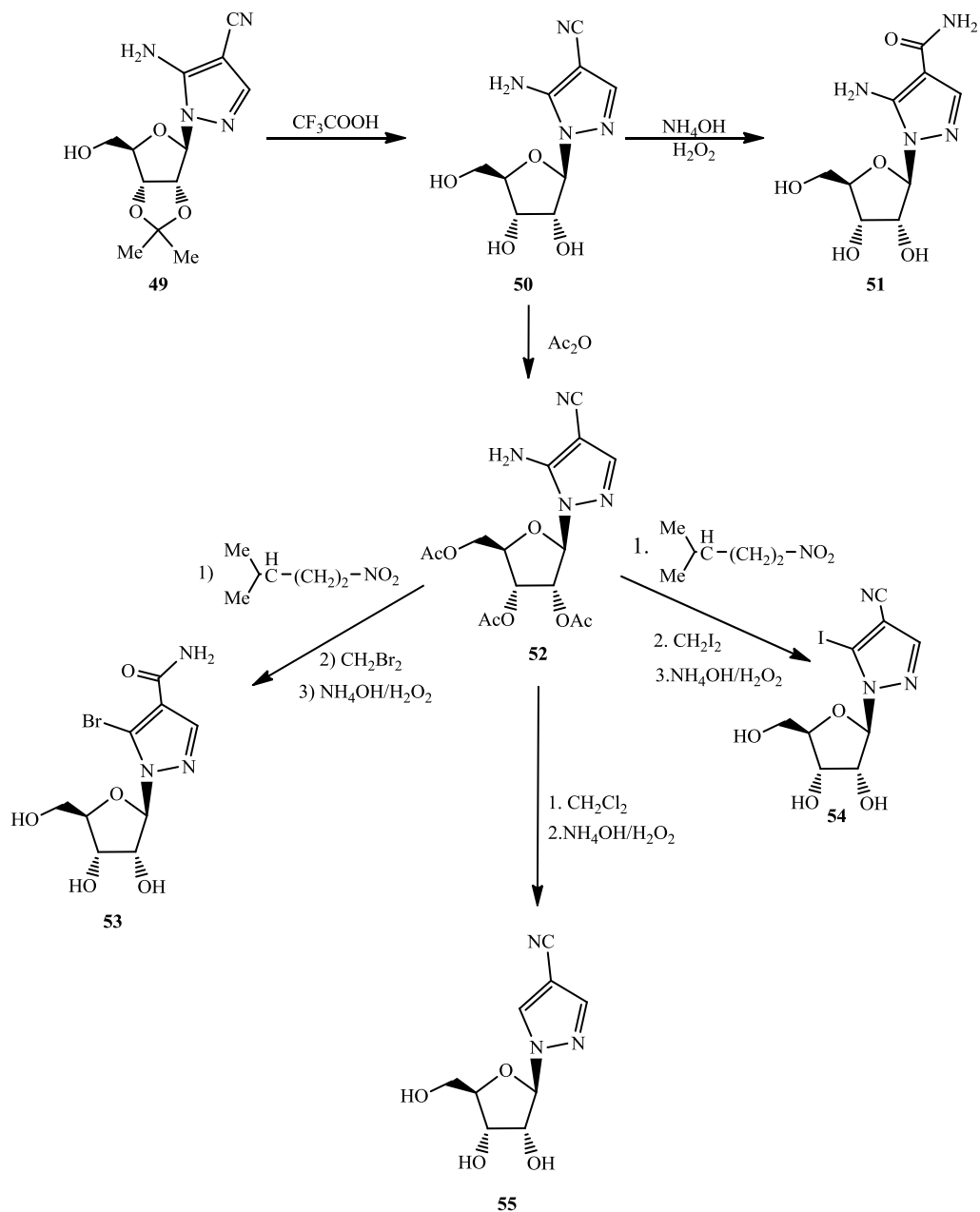
Scheme 16: Synthesis of pyrazole ribosides **52-55**

Scheme 17 shows the synthesis of pyrimidine ribosides **58** from 1,2,3,5-tetra-*O*-acetyl-*β*-D-ribofuranose **39** and silylated 5-substituted uracils **56** by using solid-supported oxazolium perchlorate **57** [53] (Scheme 17).
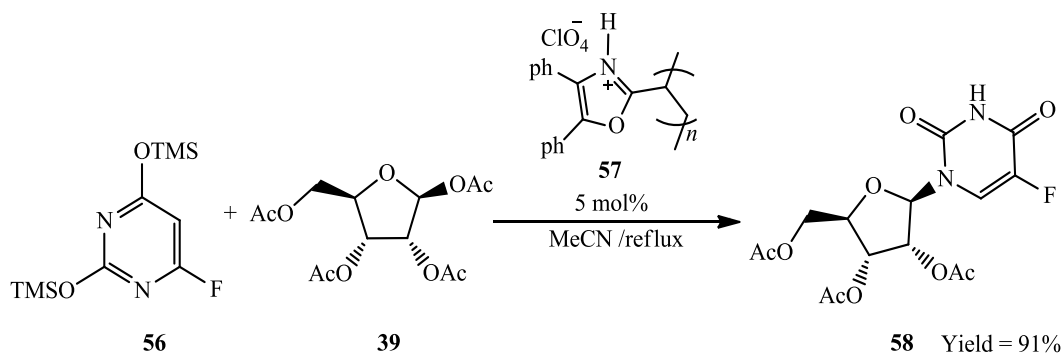
Scheme 17: Synthesis of *β-N*-Riboside derivatives **58**

Hayashi and co-workers [54] studied the synthesis of *α-*and *β*-nucleosides **61a-c** from the reaction of pyrimidinone derivative **59a-c** with protected ribose **60**. Firstly they investigated the affect of Lewis acids (Me$_3$SiOT*f*, SnCl$_4$, and BF$_3$·OEt$_2$) and (OAc and F) as leaving groups from the sugar moiety **60**. The resulted *N*-nucleosides **61a-c** demonstrate that *α*-ratio was reduced when the amount of Lewis acid was increased, for example; BF$_3$·OEt$_2$ has higher effect when more than 3.7 equivalents were used. This concludes that *α* to *β* ratio was controlled by Lewis acid. The *β*-selectivity could be also affected by the reaction time and temperature; as higher temperature increase the amount of *α*-selectivity; while *β*-selectivity increases at longer reaction time (Scheme 18).

Similar reaction conditions were used to produce the *β-N*-ribosieds **64a-c** in good yields and excellent *β*-selectivity. However, the silylation reagent in this reaction was not necessary as with **59** because **62** derivatives are more nucleophilic compared to the **59** derivatives (Scheme 19).

Scheme 18: Synthesis of *N*-Nucleoside
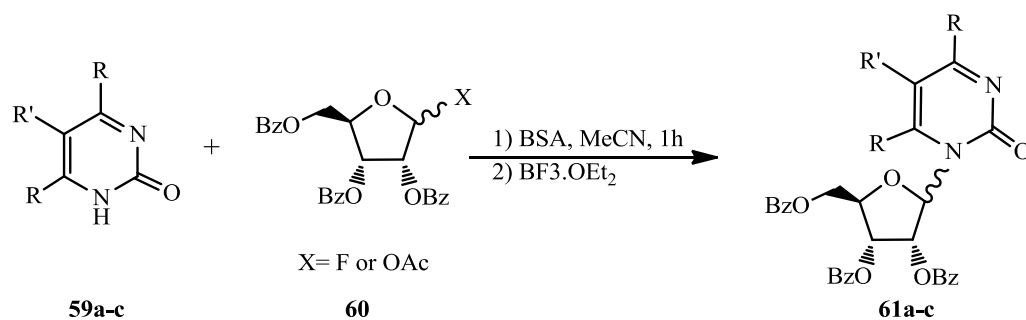
Entry	X	Time (h)	R	R'	Product	Yield (%)	α:β
1			Ph	CO₂Et	**61a**	84	12:88
2	F (α:β = 50:50)	2	Me	CO₂Et	**61b**	90	30:70
3			Ph	H	**61c**	93	10:90
4			Ph	CO₂Et	**61a**	62	0:100
5	β-OAc	3	Me	CO₂Et	**61b**	34	0:100
6			Ph	H	**61c**	46	0:100

Scheme 19: Synthesis of *β-N*-Nucleoside

Entry	R	R'	Product	Yield (%)	α:β
1	Ph	CO₂Et	**64a**	78	β
2	Me	CO₂Et	**64b**	66	β
3	Ph	H	**64c**	47	β

The synthetic methods to *α*-ribonucleosides still unfamiliar. Yet, Brown and co-worker had successfully synthesized *α*-indoline and *α*-5,6-dimethylindoline nucleosides [55]. They coupled unprotected indoline **65** with ribose **66** in ethanol or DCM for 4-7 hours, and so they obtained only *α*-isomer **67** [56] (Scheme 20).
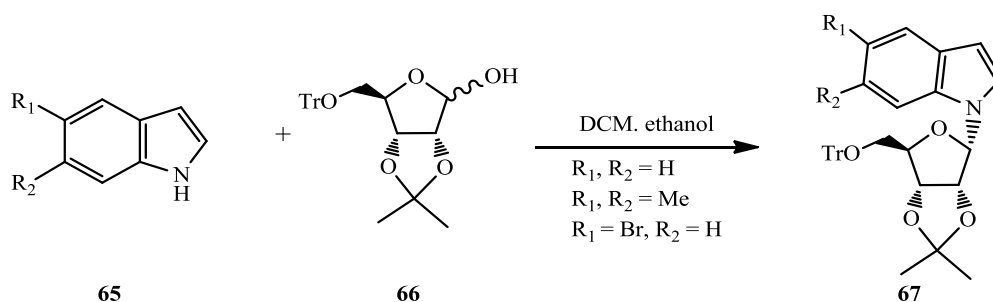
Scheme 20: Synthesis of *α*-indoline ribosides **67**

Abdou and co-workers [57] reported that the glycosylation of 6-aryl-5-cyano-2-thiouracil **68** using the silyl method forming *β-N*-ribosisde **69** (Scheme 21).
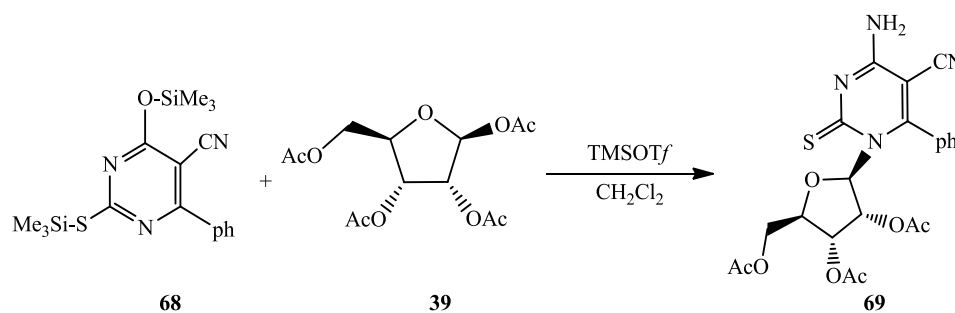
Scheme 21: Glycosylation of 2-thiopyrimidine

Researchers used 3-methoxy-2-pyridyloxide and 2-thiopyridylcarbonate as leaving groups of ribosyl derivatives **70** and **71** to produce the *N*-riboside **72** (Scheme 22). Ribosyl derivatives **70** and **71** were treated with silylated uracil, thymine, cytosine and 6-chloropurine moieties in the presence of TMS triflate or silver triflate, the reactions were highly stereoselective, giving *α-N*-ribonucleosides **72** over 90% [58].
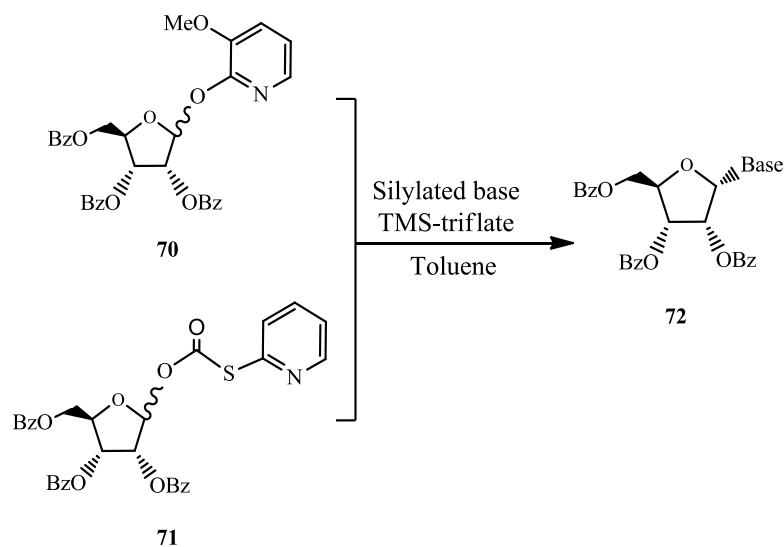
Scheme 22: *N*-Glycosylation of ribofuranosides **70** and **71**

1.5.2.2 *O*- Riboside

Chanteloup and co-worker [59] reported the synthesis of 2'-*O*-alkyl ribonucleosides **74** under Vorbrüggen condition using protected ribose **73** and silylated base. The glycosylation occurred fast giving *β-O*-nucleoside **74** with good yield and high stereoselectivity (ratio = 95:5) (Scheme 23).
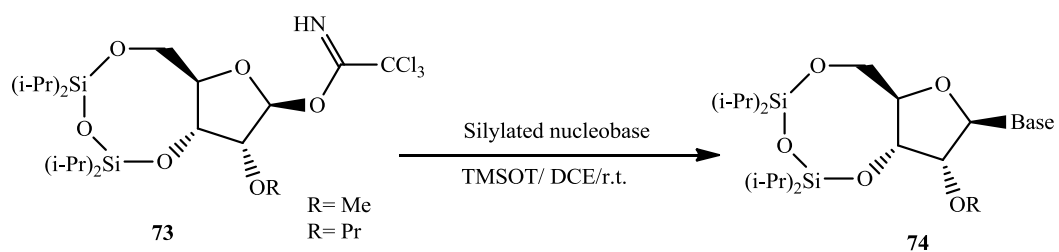
Scheme 23: Synthesis of *β*-Nucleoside

1.5.3 Synthesis of 2-Deoxynucleosides

In order to study the affect of sugar moiety of nucleosides in the biological activities; the ribose was replaced by 2-deoxy ribose. 2-Deoxyribonucleosides are biologically active as they have have anti-cancer [60] and anti-HIV activities [61]. The development of reliable methods for stereoselective synthesis of both α- and β-2-deoxynucleosides has become an important area of research of drugs and glycomimetics [58]. Synthesize and separate both of α- and β-isomers consider as notable challenge as the direct glycosylation often results in the formation of anomeric mixtures. Similar to that of conventional glycosylation, the solvent and promoter effects play important stereodirecting roles in the synthesis. Absence of O-2 acyl group on the sugar moiety makes the stereoselectivity of deoxynucleosides more challenge to control. Therefore, the resulted products are regularly mixtures of α- and β-isomers in deoxynucleoside synthesis. To overcome this challenge; three methods have been proposed by researchers: (1) O-3 acyl group involvement [62]; (2) Intramolecular Vorbrüggen method [63] within which the nucleophlic base first coupled with O-5, then it was forced to attack the anomeric carbon from β-side; (3) Reductive cleavage of $2´$-O-thiocarbonyl group of ribonucleosides [64,65]. Following are examples of these three methods.

As mentioned earlier, the synthesis of $2´$-deoxy-ribonucleosides usually leads to producing a mixture of α- and β-isomers due to the absence of $2´$-O group in the sugar moiety. Therefore, researchers developed some methods to synthesis a single isomer. Marzabadi and co-workers [62] succeeded in synthesizing $2´$-deoxy-β-ribonucleosides as single product by using deferent protecting groups at 3-O position in the sugar moiety. Compound **77** is an example which resulted from the reaction of

a silylated base **75** with an *N*-acetyl protection at the sugar *O*-3 **76**. The *N*-acetyl protection group at the sugar *O*-3 works as electron donor and stabilizes the oxocarbenium intermediate during a 1′,3′-participation mechanism (Scheme 24).
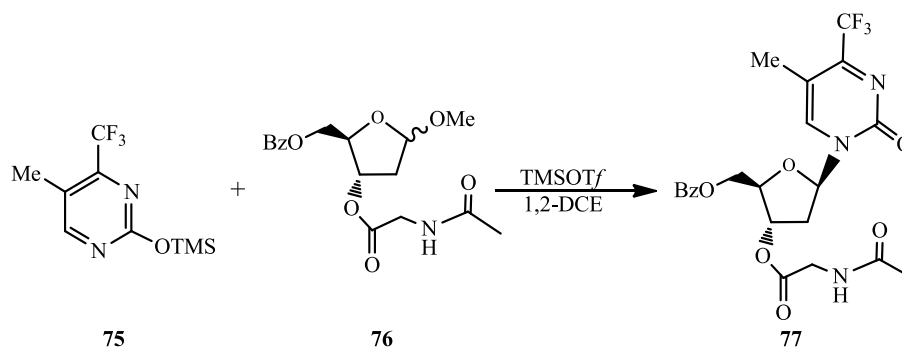
Scheme 24: Synthesis of *β*-deoxynucleosides

Marzabadi and co-workers also studied the affect of different seventeen C-3′ protecting groups. Protecting groups having S and P atoms at C-3′ gives low *β*-selectivity while the benzoyl group at the same position gives *α*-selectivity. Sugar moieties with halides **78** could block the α-side **79** which give the highest *β*-selectivity **80** (Scheme 25).
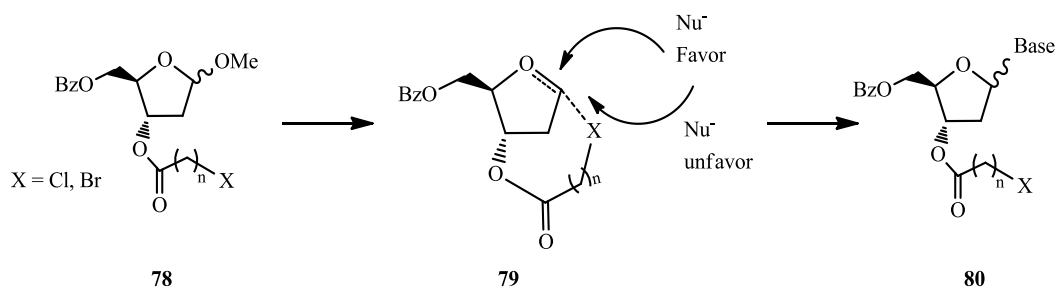
Scheme 25: 1′,3′-neighboring group participation

Robins and co-workers planned to synthesize a derivative of one of very biologically active compounds; 2-chloro-2′-deoxyadenosine (CdA) **84**. They synthesized it with higher *β*-stereoselectivity (≈ 70%) from the reaction btween sugar moieties with halides **81** and 2-chloro-6-imidazyl purine derivative **82** [65]**.** This compound is used to treat hairy cell leukemia [67] and other neoplasms [68]. Earlier; the CdA was prepared using enzymatic glycosyl transfer methods [66, 69] (Scheme 26).
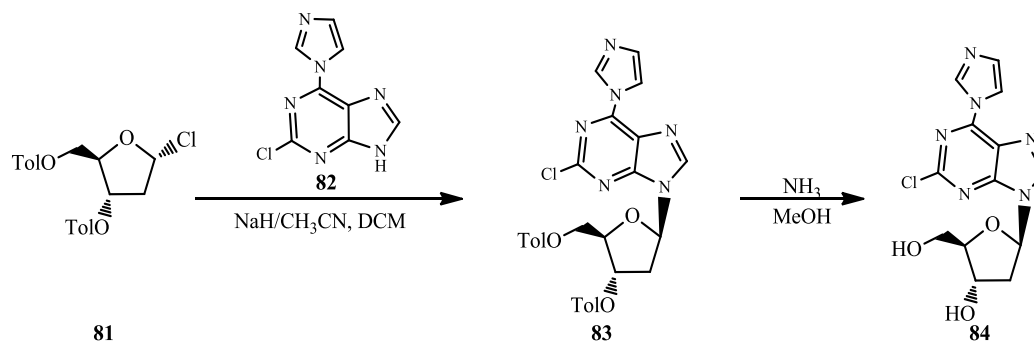
Scheme 26: Synthesis of *β-N*-deoxynucleosides

Jung and co-worker synthesized 2-deoxypyrimidine with high *β*-selectivity using intramolecular Vorbrüggen reaction [63]. They suggested that if the activated base is attached to the *O*-5 position of 2-deoxyribose, then the nucleophilic base will attack the anomeric center from the *β*-side. First the activated base coupled with the D-ribose **85** forming the expected prodect **88** (87%) and its hydrolysis product **89** (91%). Followed by sugare acetylation then base silylation and finally roduce **92** in good yield 90% which was hydrolyzed and give *β*-isomer of **93** as single product (yield ≈ 40%) (Scheme 27).
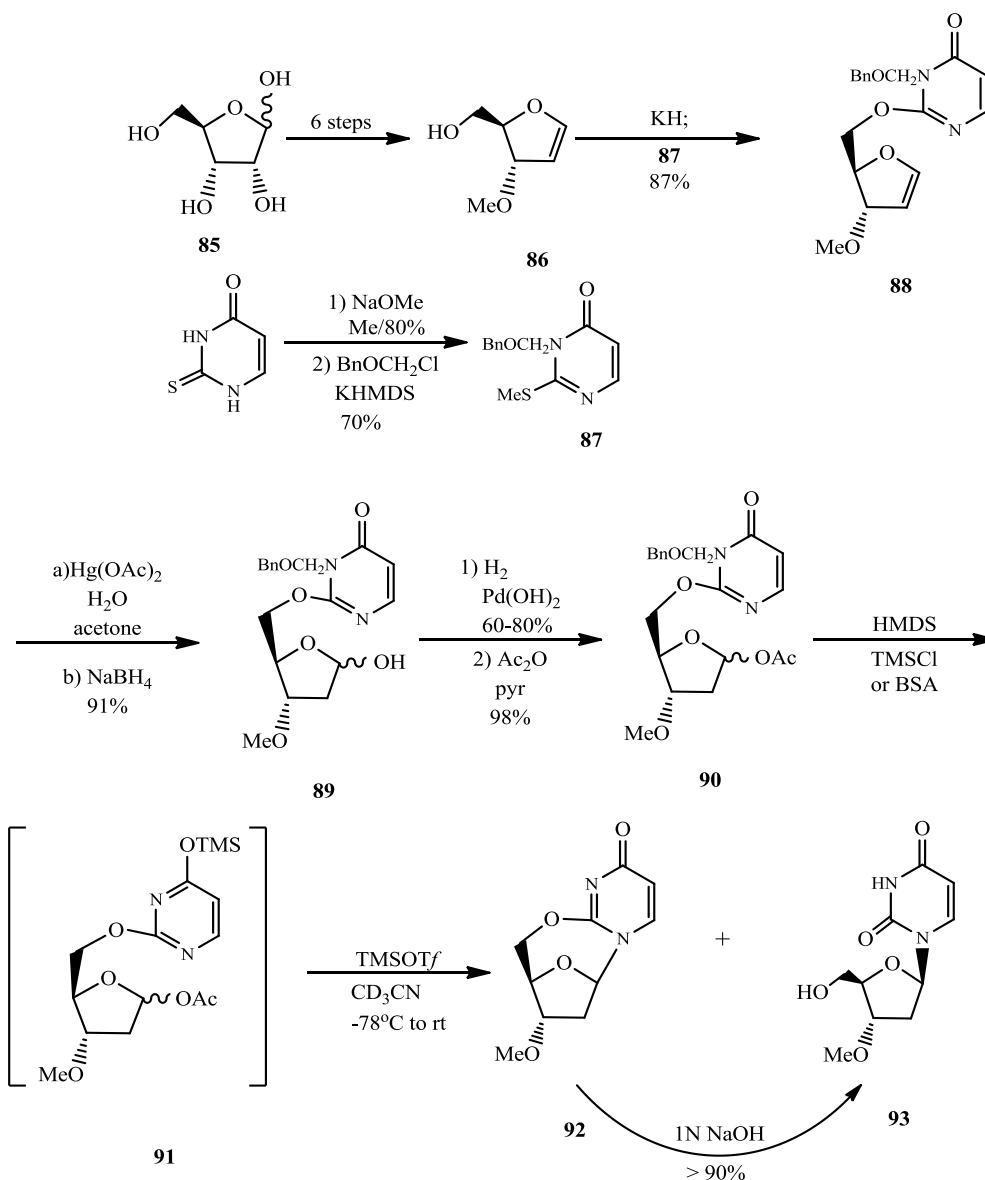
Scheme 27: Synthesis of *β*-deoxyriboside using intramolecular Vorbrüggen reaction

Sugimura's groups also synthesized *β*-deoxyriboside **96** from silylated pyrimidine base **94** and protected deoxyfuranosides **95** using *N*-bromosuccinimide (NBS) which enhances the *β*-stereoselectivity [70] (Scheme 28). Scheme 29 shows condensation of disilylated symtriazines **97** with 3,5-di-*O-* *p*-toluoyl-deoxyribofuranosyl chloride **98** in a amixture of acetonitrile and 1,2-dichloroethane with the aid of SnCl$_4$ as a catalyst leads to a mixture of *α*- and *β*-anomers of *N$_1$*-

nucleosides **99** [71]. Nucleoside yield amounted to 70% at the ratio $\alpha{:}\beta$ = 1:1. It has been found that after stirring the reaction mixture components at -25°C, the α-anomer is first formed. Subsequently, the β-anomer is formed slowly with simultaneous heating of the reaction mixture to +25°C (Scheme 29).
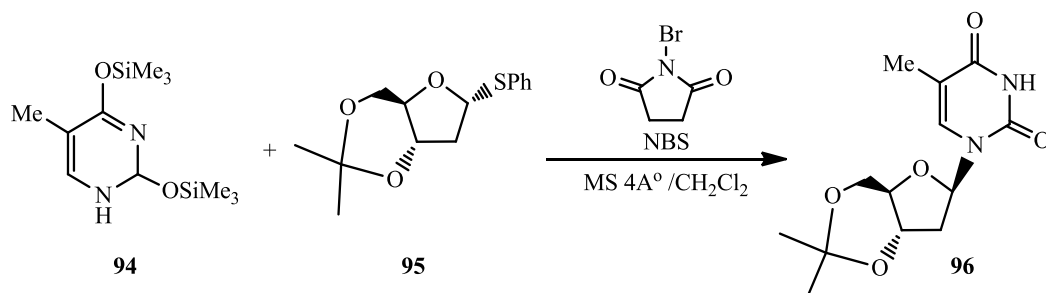
Scheme 28: Synthesis of β-deoxyriboside using NBS
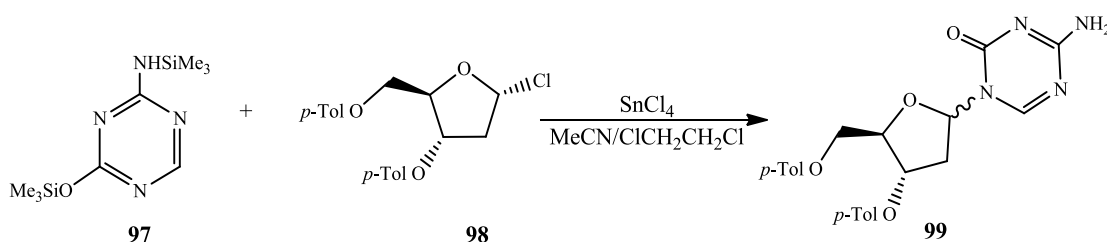
Scheme 29: Synthesis of α- and β-N-nucleosides

Zhang and co-workers [72] showed that the indole 2′-deoxyribonucleosides **102** were accomplished efficiently in one pot reaction between 3-cyano indole derivatives base **100** and protected deoxyribofuranosyl chloride **101** (Scheme 30).
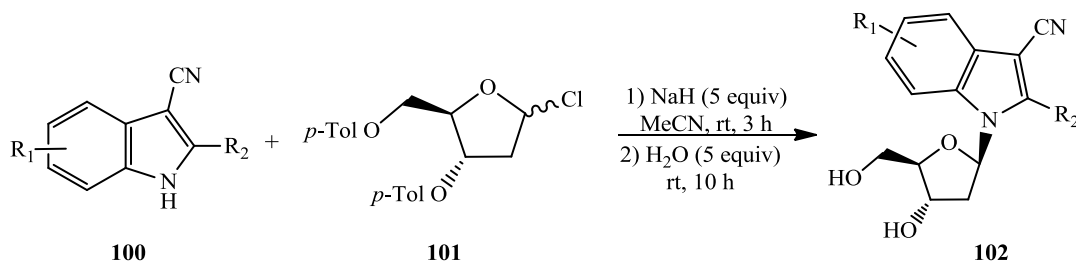
Scheme 30: Preparation of indole 2′-deoxyribonucleosides

1.6 Biological Properties of Pyrazoles

Pyrazole and its derivatives represent one of the most active classes of compounds, which exhibit broad spectrum of pharmacological activities such as antimicrobial [73], anticonvulsant [74], anticancer [75], analgesic [76], anti-inflammatory [77], antitubercular [78], ardiovascular [79] (Figure 3).
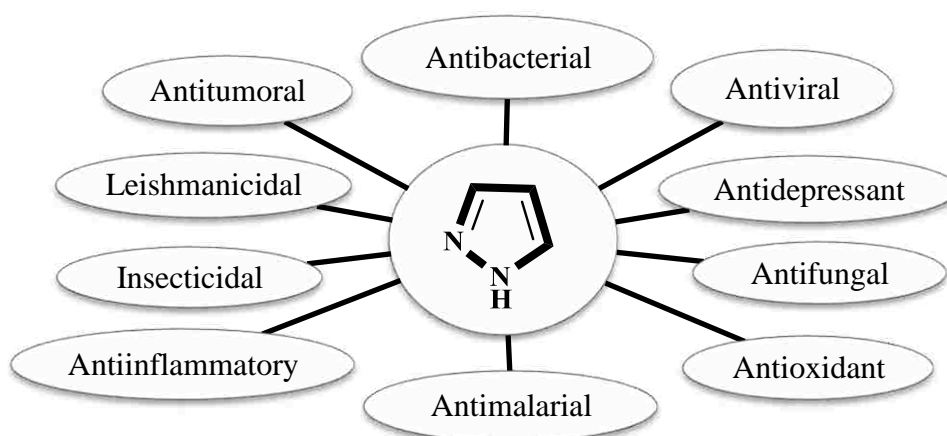
Figure 3: Pharmacological and biological activities of Pyrazolone

1.6.1 Pyrazoles as Antimicrobials

Rana and co-workers synthesized pyrazolines **103** and **104** and evaluated them for in-*vitro* against Mycobacterium tuberculosis H37Rv (Mtb H37Rv) strains; the compounds displayed potent activity (MIC = 12.5 and 0.63 repectevely) [80]. In addition, Horrocks' group synthesized 3-(4-chlorophenyl)-4-substituted pyrazole **105** and tested for activity against Mtb H37Rv strain and it shows significant antimycobacterial activity [81] (Figure 4).

103	**104**	**105**
MIC (μM) = 12.5	MIC (μM) = 0.63	MIC (μM) = 0.50
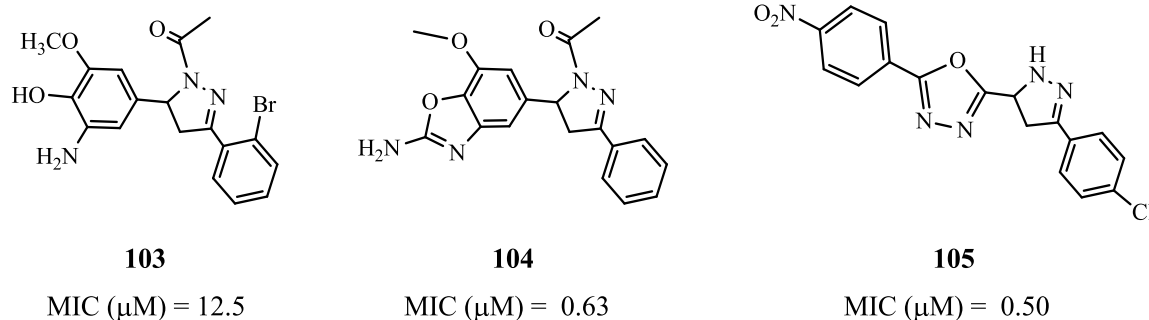
Figure 4: Prazolones **103**-**105** as antibacterial agents

1.6.2 Pyrazoles as Anticancer Agents

Xiao H. and co-workers [82] synthesized a series of pyrazole derivative reported as potent cytotoxicity against some tumour cells. Compound **106** had the strongest effectiveness against four human tumor cells including human liver cancer cell line (Hep G2), human ovary carcinoma cell (OVCAR3), keratin-forming tumor cell line (KB) and breast adenocarcinoma cells (MDR) (Figure 5).

IC_{50} = (3.24 ± 0.28) μg/mL in HepG2;
IC_{50} = (2.58 ± 0.61) μg/mL in OVCAR3;
IC_{50} = (3.81 ± 0.02) μg/mL in KB;
IC_{50} = (3.45 ± 0.03) μg/mL in MDR

106
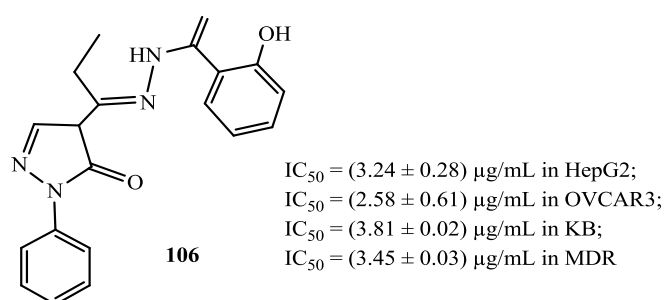
Figure 5: Prazolone has anticancer activity

Peng-cheng and co-workers [83] synthesized a series of pyrazole derivatives that may function as inhibitors of epidermal growth factor receptor (EGFR) and kinases have been evaluated. The Compound **108** showed high antiproliferative

activity against MCF-7 with IC_{50} 0.08 μM, which was comparable to the positive control erlotinib IC_{50} 0.02 μM. (Figure 6).

IC_{50} = 0.02 μM

107

IC_{50} = 0.08 μM

108
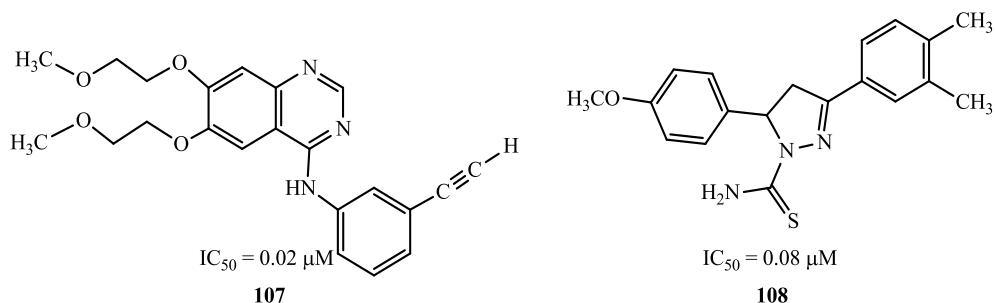
Figure 6: IC_{50} for some prazolones have anticancer activity

1.6.3 Pyrazole Nucleosides as Anticancer Agents

Stefano M. and co-workers [84] synthesized pyrezole nucleosides and tested for their antitumor activities. Compounds were tested *in vitro* for antiproliferative activity against fibroblast-like cells. Compounds bearing a bromine **109** or iodine **110** atom at position 4 of the pyrazole ring showed a potent cytostatic activity against all the T-cell lines tested (IC_{50} range = 4-50 μM) (Figure 7).

109   **110**
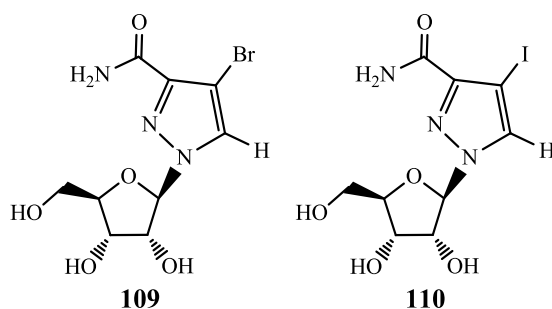
Figure 7: Some pyrazole nucleosides have anticancer activity

Palmarisa F. and co-workers [85] used *C*-nucleoside thiophenfurin **111** as a reference compound. They valuated its ability to inhibit the growth of human myelogenous leukemia K562 cells. Tumor cell proliferation was evaluated by incubating the cells continuously with either the compound or saline for 48 h. Thiophenfurin proved to be toxic to cell growth as its $IC5_0 = 4.6$ µM (Figure 8).

111
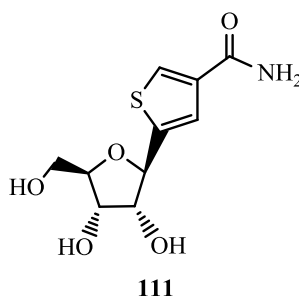
Figure 8: Thiophenfurin *C*-nucleoside as anticancer agent

1.7 DNA and Molecular Recognition

Nucleic acids are the vital components of life. They are defined as macromolecules or polymers of nucleotides. Nucleic acids are classified into two classes, deoxyribonucleic acid (DNA) and ribonucleic acid (RNA). DNA carries the genetic information used in developing and functioning of all known living organisms such as the information needed to construct proteins and RNA molecules. RNA plays the main role in the transcribing of the genetic information from DNA into proteins [86].

Nucleotide is the building blocks of DNA. It consists of phosphate group connected to 2-deoxyribose sugar forming DNA backbone which in turn connected to nitrogen base (adenine (A), guanine (G), cytosine (C) and thymine (T)). Two chains of polynucleotides, known as complementary strands, can be held together by

hydrogen bonds and form the double helix secondary structure of DNA. This structure was described for the first time by James Watson and Francis Crick in 1953 [86]. DNA in cells mostly takes one of three secondary structures; B-form, A-form and random coil. DNA structure depends on the DNA sequence and solution conditions [87].

In the double helix DNA, two strands of nucleotides twist around each other where adenine in a strand is held to thymine in the complementary strand by two hydrogen bonds while guanine is held to cytosine by three hydrogen bonds as shown in Figure 9. These hydrogen bonds are known as Watson-Crick hydrogen bonds [86]

A.T Base Pair   G.C Base Pair
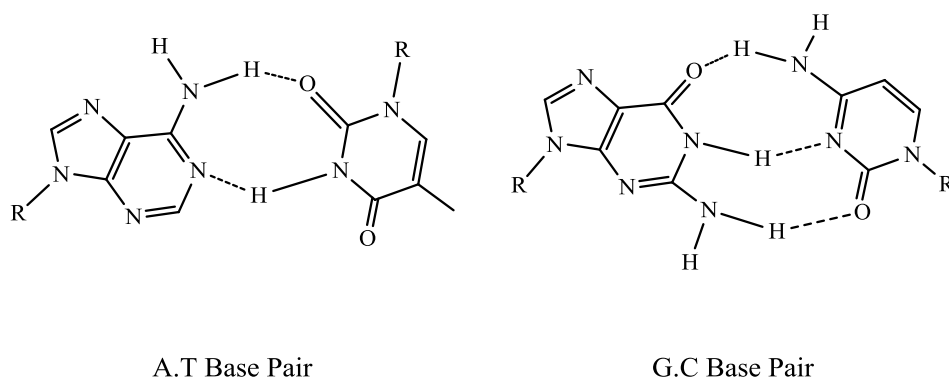
Figure 9: Hydrogen bonding in the A·T and C·G Watson-Crick DNA base pairs

Double stranded DNA can take several conformations; B-form which is the most common DNA secondary structure with right-handed double helical and minor and major grooves. Less common forms are A-form and Z-form where both of which adopt a double-helical structure as shown in Figure 10. A-form is more compact than B-DNA and exists in dehydrated and crowded environments. The Z-form shows lefthanded helicity and exists in specific conditions such as high salted solutions [86].

The discovery of the double helix DNA paved the way for the growing research on nucleic acids and their therapeutic applications.

A. A-DNA	B. B-DNA	C. Z-DNA
Twist = 33°	Twist = 36°	Twist = -30°
Rise = 2.56 Å	Rise = 3.38 Å	Rise = 3.7 Å
Roll = 6°	Roll = 0°	Roll = 0°
Inclin. = 21°	Inclin. = -6.0°	Inclin. = -6.2°
x-Dis. = -4.5 Å	x-Dis. = 0.23 Å	x-Dis. = 3.0 Å
P-Tw = -7.5°	P-Tw = -4.4°	P-Tw = -4.4°
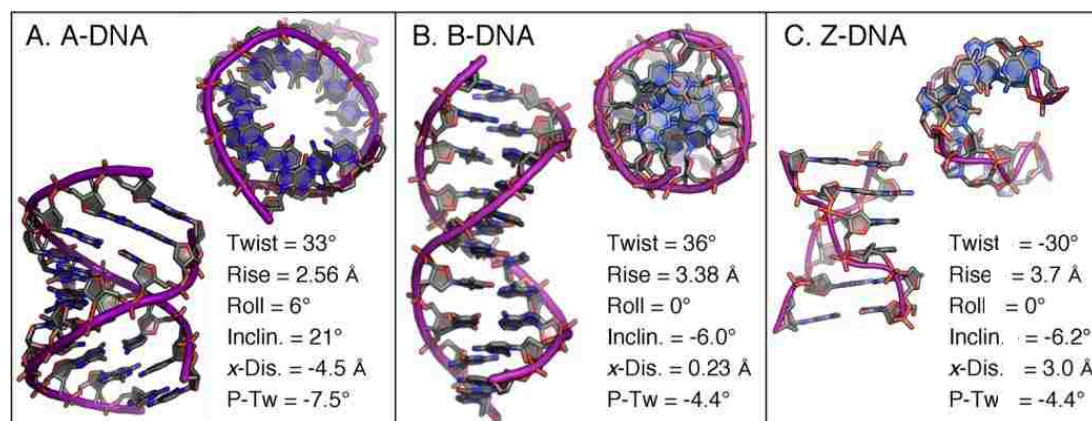
Figure 10: The helical structure A. A-DNA, B. B-DNA and C. Z-DNA [88]

It is common that DNA is the target of many anti-cancer drugs and antibiotics. The main function of these drugs is to interact with DNA in order to block gene transcription or inhibit DNA replication [89]. Many of the currently used chemotherapeutic agents such as cisplatin, mitomycin C and daunomycin have shown efficacy against some cancers. However, they bind to DNA non-specifically and cause a wide variety of side effects including secondary cancer formation. Designing small molecules with high specificity to particular DNA secondary structures might improve cancer-specific targeting and decrease the side effects [90]. The recent advances in molecular biology, biotechnologies and chemistry provide more important information concerning the oligonucleotide structures and enzyme active sites as well as receptor binding sites. Such information together with computational simulations gives chemists the tools to design and synthetize specific and effective drugs. However, the lack of selectivity of most of the common drugs

leads to the possibility of interacting with more than one target which may result in side effects. To overcome the undesired side effects, there is a need to improve the molecular recognition properties of the commonly used molecules to develop new and more potent drugs [89]. Understanding the molecular mechanism by which chemotherapeutic agents bind to nucleic acids is a fundamental issue in modern drug design. Currently, developing drugs with improved molecular recognition is one of the most expanding research areas because of its medical significance and for its expected minimum side effects. The expanding knowledge of cancer biology together with molecular recognition is considered as a useful tool for designing drugs with high selectivity towards cancer cells. The growing attention towards supramolecular structures during recent years is due to their probable involvement in cancer therapy [89].

Pyrazolones and pyrazolone nucleosides has been recognized to have anti-microbial and chemotherapeutic antitumor effects. Studies reported that trifluoromethyl nucleosides induce cell apoptosis via different mechanisms. For example, mechanism of action of some nucleosides with the topoisomerase II inhibitor, Etoposide results in biochemical evidence of apoptosis in a range of cell types [91]. The mechanism of action of initiation of apoptosis is unclear but succeeding proceedings in all of these cell types include cleavage of DNA [92-94]. Another proposed mechanism of action of some synthetic nucleosides suggested inducing apoptosis via mitochondrial pathway to encourage cell cycle arrest and allows the DNA to repair or induce apoptosis if the damage is severe and cannot be controlled [95]. Therefore, this work aimed to exam the stability of DNA in presence of the newly sunthesized pyrazolines and pyrazolines nucleosides.

1.8 Molecular Docking and Interaction between DNA and Small Molecules

DNA plays an important role in cellular processes, including cell division (DNA replication) and protein synthesis (Transcription and translation). Most of the anticancer therapies are involved in the interaction of drugs with DNA. The intercalation and groove binding are the two important modes of binding of drug with DNA. Both covalent and non-covalent types of interactions are possible in these two binding modes. Small molecules that can bind between nucleic acid base pairs are categorized as intercalators. These molecules contain planar heterocyclic groups which stack between adjacent DNA base pairs, which results decrease in the DNA helical twisting and lengthening of the DNA. On the other hand, groove binding does not induce large conformational changes in DNA and may be considered similar to standard lock and key models for ligand macromolecular binding. Such molecules bind to both major and minor groove of nucleic acid. Minor groove binders are crescent in shape and they complement the shape of minor groove [96].

The role of computational molecular docking in educational, research, and drug discovery is evolving at a rapid rate which used to address real-world research problems. Therefore, understanding protein and ligand interactions is fundamental to treat disease and avoid toxicity in biological organisms. The fundamental problems in drug discovery are based on the process of molecular recognition by small molecules. The binding specificity of DNA-small molecule is identified mainly by studying the hydrogen bonding and polar interactions. As these small molecules can act as effective therapeutic agents against many diseases, there is a need to have the detailed mechanistic insights on how they interact with DNA.

Molecular docking programs are designed to accomplish two simultaneous tasks: 1) to identify the optimal binding orientation for a ligand within the binding cavity of the receptor, and 2) to score the resulting ligand binding interaction, providing a rank order that ideally predicts experimental results. Docking engines, such as DOCK [97] and AutoDock [98], calculate the optimal ligand binding orientation by minimizing the energy of interaction between molecules. Molecular docking results are evaluated by visual inspection of ligand pose or quantitatively using a scoring algorithm. Scoring algorithms may be incorporated into the docking engine, or accessed through third-party software, such as XScore and Medusa Score [99]. Both XScore and Medusa score have been shown to improve binding energy rankings over AutoDock when evaluated against a database of Protein Data Bank (PDB) benchmark standards. XScore is frequently cited as being used to re-rank AutoDock output and serves as the basis for AutoDock Vina [100]

Docking engines calculate the Gibbs free energy of binding (ΔG) between a ligand and a receptor, which is fundamental to the understanding of complex systems in biochemistry and molecular biology. The calculation of ΔG is based on estimates of the 3 total energy of intermolecular forces of attraction including van der Waals interactions, hydrogen bonding, and electrostatic interactions. Ligands are ranked by the calculated ΔG value; lower ΔG values correspond to more favorable ligand binding, where higher ΔG values are less favorable (Figure 11).
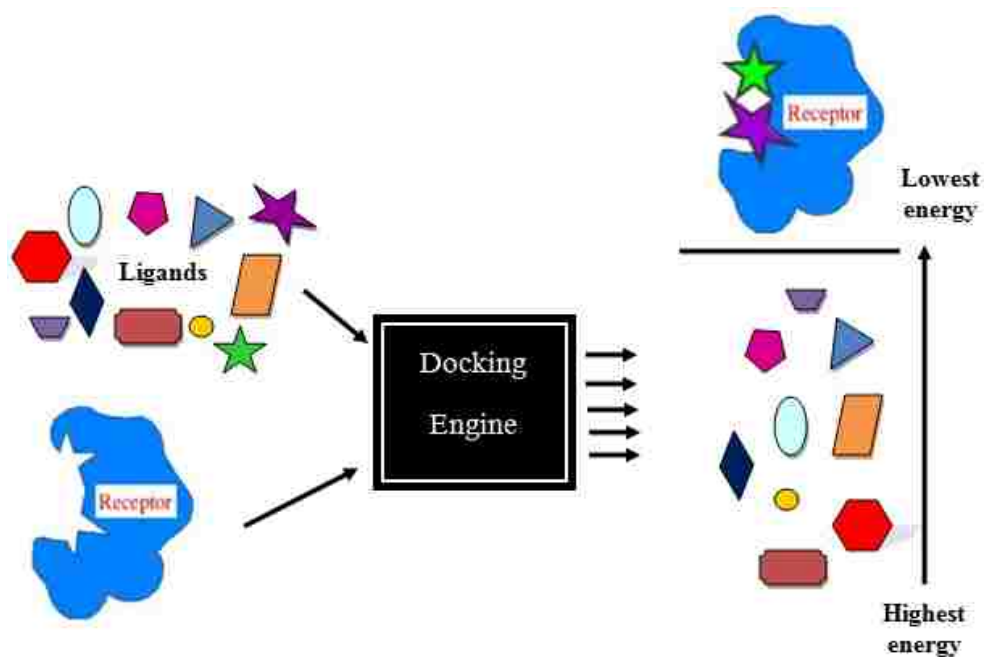
Figure 11: Depiction of high throughput virtual screening: multiple ligands are docked to a receptor and ranked by energy estimate

All structures, including proteins, can exist in functionally different conformational states based on their inter- and intra-molecular interactions. Molecular and biophysical experiments can account for the net effects of structural interactions in a molecule or for a system of molecules, but they are unable to physically isolate all molecular structures or practically manage the evaluation for all of available structures in biology. Computational techniques that simulate molecular interactions can assist in expanding coverage for structures that are unresolved through experiments, but the sheer number of molecules and potential conformational states associated with macromolecular structures presents a sampling challenge for the reproducibility and reliability of simulations. In order to efficiently sample conformational space for even a single macromolecule, simulations rely on approximations of covalent and noncovalent molecular interactions and geometrical

structural features that are believed to be relevant for capturing the energetic and thermodynamic properties of molecules. Continued research is needed to improve these approximations through a better understanding of biologically relevant inter- and intra-molecular interactions. Also, more efficient sampling methods are needed that can quickly and accurately identify conformational states of structures that are related to functions of biological interest. The function of a protein depends on its structure which can be affected by interactions with other molecules, especially small chemicals.

Despite much success in the field of structure-based discovery, current molecular modeling techniques need to be improved in order for the field to reach its anticipated potential of describing in detail how any given biological function arises from molecular structures and their interactions. It is unlikely that all structures and interactions will ever be completely modeled using experimental methods due to the vast number of structures, physical limitations of studying some important structures, and complexity of understanding increasingly higher-orders of structure. Predictive computational methods that simulate molecular interactions can aid experiments in the number of structural interactions that can be studied.

Chapter 2: Organic Synthesis and Structural Analysis

2.1 Introduction

3-Pyrazolone is a five member ring containing two nitrogen atoms and one ketonic group in its structure (Figure 12). 3-Pyrazolone and its derivatives are used for the synthesis of analgesic, anti-inflammatory, anti-pyretic, muscle relaxing, anti-convulsant, anti-diabetic and anti-tumor active drugs. Peak plasma concentration of the pyrazolone derivatives in the human body occur after 1 to 1.5 hours of oral administration. Pyrazolones are advantageous in medical studies since they act as pharamcophores of numerous compounds, are known to possess diverse pharmacological properties and they are easy to prepare [1].
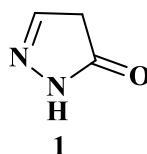
Figure 12: Structure of 3-pyrazolone

Pyrazolone and its derivatives can be synthesized by different procedures and can be considered as intermediate compound for the synthesis of various cyclic compounds of very high biological activity. In this study, pyrazolone nucleosides and its brnzoyl derivatives were synthesized and their structures were characterized using spectroscopic techniques. Infrared spectroscopy (IR) is generally used to determine the functional groups. NMR and Mass spectroscopy were also used to help to identify the chemical structure.

In this section, the syntheses procedures of different groups of pyrozolone derivatives are discussed, followed by discussion about their reaction mechanisms. Subsequently, the changes in the structure of these compounds are determined and resulting formula evaluated.

2.2 Experimental Part

All Melting points were determined in open capillary tubes and are uncorrected. TLC silica gel-G plates of 0.5 mm thickness and spots were located by UV. Column chromatography was performed on Kieselgel 60. IR spectra were recorded by Shimadzu FT-IR-8400 instrument using KBr disk method. The ^{1}H and ^{13}C-NMR spectra were recorded on Varian NMR 400 MHz spectrometer. Chemical shifts are expressed δ (ppm) scale using the solvent peak as internal reference and coupling-constant values are given in Hz. Elemental analysis of synthesized the starting compounds was carried out on Leco Model CHN-600 elemental analyzer and the results are in agreements with the structures assigned. Mass spectroscopy of synthesized the starting compounds was carried out us LC/Ms from water company. Xevo TQD coupled with Acquity UPLC H class 2.1 x 50 mm column. HPLC: Agilent 1200 series.

2.2.1 Synthesis of 5-trifluoromethyl-2,4-dihydropyrazol-3-one 112

Method A: Conventional Method

A mixture of ethyl-4,4,4-trifluoro-3-oxobutanoate (100 mmol, 14.6 mL) and hydrazine hydrate (100 mmol, 4.86 mL) in ethanol (150 mL) was refluxed for 18 hours. The precipitated formed was filtered, washed with cold ethanol then dried.

Method B: Microwave-assisted Reaction

A mixture of ethyl-4,4,4-trifluoro-3-oxobutanoate (50 mmol, 7.50 ml) and hydrazine hydrate (50 mmol, 2.50 mL) in ethanol (5.0 mL) and sulfuric acid (H_2SO_4) (1.00 mL) were placed on microwave then various conditions were applied.

5-Trifluoromethyl-2,4-dihydropyrazol-3-one (**112**): Off-white crystals. Yield 96 % (method A); **mp** = 208 – 209 °C; **IR [KBr, cm^{-1}]**: 3286 (N-H), 1750 (C=O). **^{1}H-NMR [400Hz, DMSO-d_6]**: (δ, ppm) 5.64 (s, 1H, CH), 11.22 (s, 1H, OH, exchangeable with D_2O), 12.81 (s, 1H, NH, exchangeable with D_2O); **^{13}C-NMR [100Hz, DMSO-d_6]**: (δ, ppm) 124.2 (C-4), 127.1(C-6), 129.9 (C-5), 174 (C-3). **Anal. Calcd.** for $C_4H_3F_3N_2O$: C, 31.59; H, 1.99; N, 18.42; Found: C, 31.75; H, 1.86; N, 18.18.

2.2.2 General procedure for the synthesis of 4-arylhydrazono-5-trifluoromethyl-2,4-dihydropyrazolones 113a-i

A solution of sodium nitrate (0.01 mol, 0.85 g) in water (10 mL) was added drop wise with stirring to a solution of amine hydrochloride salt in water (2 mL) at 0 °C. The mixture was added drop wise with stirring to a cold solution of 5-trifluoromethyl-2,4-dihydropyrazol-3-one (**112**, 10 mmol, 1.52 g) in ethanol (25 mL) containing sodium acetate (10 mmol, 0.82 g). The reaction mixture was allowed to stir at room temperature for 2 hr. The solid was filtrated; washed with cold H_2O (2 x 5 mL), dried and crystallized from ethanol yielding compounds **113a-i**.

4-(3'-Fuorophenylhydrazono)-5-trifluoromethyl-2,4-dihydropyrazol-3-one (**113a**): Red crystals; yield 99 %; **mp** = 211 – 213 °C; **IR [KBr, cm^{-1}]:** 3459 (NH/OH), 1633 (C=C). **^{1}H-NMR [400Hz, DMSO-d_6]:** (δ, ppm) 7.09 (s, 1H, aromatic), 7.47 (m, 3H, aromatic), 12.69 (s, 1H, NH); **^{13}C-NMR [100Hz, DMSO-d_6]:** δ 104.1 (C-2'), 112.9

(C-6'), 113.1 (C-4'), 118.2 (C-6), 123.7 (C-4), 131.5 (C-5'), 143.1 (C-1'), 158.6 (C-5), 161.4 (C-3), 163.7 (C-3'); **Anal. Calcd.** for $C_{10}H_6F_4N_4O$: C, 43.81; H, 2.21; N, 20.43. Found: C, 42.46; H, 2.11; N, 19.90.

4-(4'-Fluorophenylhydrazono)-5-trifluoromethyl-2,4-dihydropyrazol-3-one **(113b):** Dark Orange crystals; yield 93 %; **mp** = 217 – 218 °C; **IR [KBr, cm^{-1}]:** 3463 (NH/OH), 1637 (C=C). **^{1}H-NMR [400Hz, DMSO-d_6]:** (δ, ppm) 7.33 (m, 2H, aromatic), 7.66 (m, 2H, aromatic), 12.63 (s, 1H, NH); **^{13}C-NMR [100Hz, DMSO-d_6]:** δ 116.5 (2 C, C-2', C-6'), 118.9 (2 C, C-3', C-5'), 121.1 (C-6), 128.9 (C-4), 137.8 (C-4'), 158.7 (C-5), 159.3 (C-1'), 161.7 (C-3); **Anal. Calcd.** for $C_{10}H_6F_4N_4O$: C, 43.81; H, 2.21; N, 20.43. Found: C, 44.175; H,2.21; N, 20.81.

4-(3'-Trifluoromethylphenylhydrazono)-5-trifluoromethyl-2,4-dihydropyrazol-3-one **(113c):** Yellow crystals; yield 99 %; **mp** = 221 – 222 °C; **IR [KBr, cm^{-1}]:** 3419 (NH/OH), 1674 (C=O). **^{1}H-NMR [400Hz, DMSO-d_6]:** (δ, ppm) 7.98 (s, 1H, aromatic), 7.89 (d, 1H, aromatic, J = 12.0 Hz), 7.70 (t, 1H, Ar-H, J = 8.0 Hz), 7.63 (d, 1H, aromatic, J = 8.0 Hz), 12.69 (s, 1H, NH); **^{13}C-NMR [100Hz, DMSO-d_6]:** (δ, ppm) 114.0 (C-5'), 118.7 (C-4'), 120.8 (C-6'), 122.9 (C-2'), 124.6 (C-3'), 125.6 (C-4), 130.6 (CF$_3$), 131.4 (C-1'), 137.3 (CF$_3$), 142.6 (C-5), 158.0 (C-3). **Anal. Calcd.** for $C_{11}H_6F_6N_4O$: C, 40.75; H, 1.87; N, 17.28. Found: C, 41.12; H, 1.84; N, 17.55.

4-(3'-Chlorophenylhydrazono)-5-trifluoromethyl-2,4-dihydropyrazol-3-one **(113d):** Pale yellow crystals; yield 94 %; **mp** = 238 – 240 °C; **IR [KBr, cm^{-1}]:** 3458 (NH/OH), 1642 (C=C). **^{1}H-NMR [400Hz, DMSO-d_6]:** (δ, ppm) 7.68 (s, 1H, aromatic), 7.58 (d, 1H aromatic, J = 8.0 Hz), 7.48 (t, 1H, aromatic, J = 8.0 Hz), 7.31 (d, 1H, aromatic, J = 8.0 Hz), 12.69 (s, 1H, NH); **^{13}C-NMR [100Hz, DMSO-**

d_6]: (δ, ppm) 116.0 (C-6'), 117.1 (C-2'), 121.5 (C-4'), 124.4 (C-5'), 126.5 (C-3'), 131.9 (C-4), 134.6 (C-1'), 137.2 (CF$_3$), 143.2 (C-5), 159.1 (C-3); **Anal. Calcd.** for C$_{10}$H$_6$ClF$_3$N$_4$O: C, 41.33; H, 2.08; N, 19.28. Found: C, 40.96; H, 2.00; N, 19.16.

4-(4'-Chlorophenylhydrazono)-5-trifluoromethyl-2,4-dihydropyrazol-3-one **(113e):**
Yellow crystals; yield 93 %; **mp** = 226 – 228 °C; **IR [KBr, cm^{-1}]:** 3437 (NH/OH), 1618 (C=C). **^{1}H-NMR [400Hz, DMSO-d_6]:** (δ, ppm) 7.50 (m, 2H, aromatic), 7.60 (m, 2H, aromatic), 12.63 (s, 1H, NH); **^{13}C-NMR [100Hz, DMSO-d_6]:** (δ, ppm) 119.0 (2C-2',6'), 121.5 (C-4'), 123.9 (C-4), 130.1 (2C-3',5'), 131.0 (C-1'), 137.2 (CF$_3$), 140.6 (C-5), 159.2 (C-3); **Anal. Calcd.** for C$_{10}$H$_6$ClF$_3$N$_4$O: C, 41.33; H, 2.08; F, 19.61; N, 19.28. Found: C, 41.73; H, 2.11; N, 19.12.

4-(2',4'-Dichlorophenylhydrazono)-5-trifluoromethyl-2,4-dihydropyrazol-3-one
(113f): Yellow crystals; yield 90 %; **mp** = 239 – 241 °C; **IR [KBr, cm^{-1}]:** 3411 (NH/OH), 1616 (C=C). **^{1}H-NMR [400Hz, DMSO-d_6]:** (δ, ppm) 7.73 (m, 1H, aromatic), 8.03 (m, 2H), 8.45 (t, 1H, aromatic), 12.92 (s, 1H, NH); **^{13}C-NMR [100Hz, DMSO-d_6]:** (δ, ppm) 117.7 (C-6'), 121.3 (C-2'), 122.5 (C-4'), 126.3 (C-5'), 129.7 (C-3'), 130.0 (C-4), 130.9 (C-1'), 136.7 (CF$_3$), 152.8 (C-5), 160.1 (C-3); **Anal. Calcd.** for C$_{10}$H$_5$Cl$_2$F$_3$N$_4$O: C, 36.95; H, 1.55; N, 17.24. Found: C, 37.53; H, 1.64; N, 16.99.

4-(3'-Nitrophenylhydrazono)-5-trifluoromethyl-2,4-dihydropyrazol-3-one **(113g):**
Pale yellow crystals; yield 98 %; **mp** = 251 – 254 °C; **IR [KBr, cm^{-1}]:** 3438 (NH/OH), 1681 (C=O). **^{1}H-NMR [400Hz, DMSO-d_6]:** δ 7.58 - 7.85 (m, 4H, aromatic), 12.67 (s, 1H, NH, exchangeable with D$_2$O); **^{13}C-NMR [100Hz, DMSO-d_6]:** (δ, ppm) 111.96 (C-2'), 120.8 (C-4'), 121.4 (C-6'), 123.3 (C-5'), 125.0 (C-4),

131.5 (C-1'), 136.9 (CF$_3$), 143.2 (C-3'), 149.0 (C-5), 158.8 (C-3); **Anal. Calcd.** for

C$_{10}$H$_6$F$_3$N$_5$O$_3$: C, 39.88; H, 2.01; N, 23.25. Found: C, 39.88; H, 2.19; N, 22.74.

4-(4'-Bromophenylhydrazono)-5-trifluoromethyl-2,4-dihydropyrazol-3-one **(113h):**

Dark red crystals; yield 86 %; **mp** = 214 – 216 °C**; IR [KBr, cm^{-1}]:** 34673 (NH/OH),

1641 (C=C). **^{1}H-NMR [400Hz, DMSO-d_6]:** (δ, ppm) 7.54 (d, 2H, aromatic, *J* = 8.8

Hz), 7.63 (d, 2H, aromatic, *J* = 8.8 Hz), 13.68 (s, 1H, NH); **^{13}C-NMR [100Hz,**

DMSO-d_6]: (δ, ppm) 118.8 (C-4'), 119.2 (2C-2,'6'), 121.5 (C-4), 124.0 (C-1'), 133.0

(2C-3',5'), 137.1 (CF$_3$), 141.0 (C-5)**,** 152.2 (C-3); **Anal. Calcd.** for C$_{10}$H$_6$BrF$_3$N$_4$O:

C, 35.84; H, 1.80; N, 16.72. Found: C, 35.87; H, 1.88; N, 16.41.

4-[2´-(Pyrene-2''-yl)hydrazono]-5-(trifluoromethyl)-4H-pyrazol-3-ol **(113i):** Dark

violet crystals; yield 94 %; **mp** = 256 – 258 °C; **IR [KBr, cm^{-1}]:** 3435 (NH/OH),

2253 (C=N); **^{1}H-NMR [400Hz, DMSO-d_6]:** (δ, ppm) 8.12 (t, 1H, aromatic, *J* = 8.0

Hz), 8.20 (s, 2H, aromatic), 8.37 (m, 6H, aromatic), 12.79 (s, 1H, NH); **^{13}C-NMR**

[100Hz, DMSO-d_6]: (δ, ppm) 113.7 (aromatic C), 126.9 (C-4), 126.2, 126.8, 127.0,

127.5, 128.0,130.1, 131.0 (aromatic-Cs), 131.6 (CF$_3$), 161.4 (C-5)**,** 172.7 (C-3);

Anal. Calcd. for C$_{20}$H$_{11}$F$_3$N$_4$O: C, 63.16; H, 2.92; N, 14.7. Found: C, 47.25; H, 5.66;

N, 11.54.

2.2.3 General procedure for the synthesis of 3-(2'',3'',5''-tri-*O*-acetyl-*β*-ribofuranosyloxy)-4-(araylhydrazono)-5-trifluoromethyl-2,4-dihydropyrazol-3-one 116a,b

A mixture of 4-arylhydrazono-5-trifluoromethyl-2,4-dihydropyrazol-3-ones

113 (3.0 mmol), ammonium sulfate (3.0 mmol, 0.4 g), in hexamethyldisilazane

(HMDS) (25 mL) was refluxed for 6 hours under nitrogen. The excess of HMDS

evaporated under reduced pressure. A mixture of the silylated pyrazolone and

1,2,3,5-tetra-*O*-acetyl-*β*-D-ribofuranose (**115**, 3.0 mmol, 0.95 g) was dissolved in dry

CH$_2$Cl$_2$ (25 mL), and Trimethylsilyl trifluoromethanesulfonate (TMSOTf) (1.1 mmol, 0.2 mL) was added dropwise at (0 - 5 ^{o}C). The reaction mixture was stirred for 4 hours at room temperature, then CH$_2$Cl$_2$ (100 mL) was added. The organic layer washed with saturated aqueous solution of NaHCO$_3$ (50 mL) and water (3 × 30 mL), dried over anhydrous (Na$_2$SO$_4$), and evaporated under reduced pressure. The residue was purified using a silica gel column chromatography (ethylacetate: hexane; 3:7) to separate the *O*-isomer **116a,b**.

3-(2'',3'',5''-Tri-O-acetyl-β-ribofuranosyloxy)-4-(3'-fluorophenylhydrazono)-5-trifluoromethyl-2,4-dihydropyrazol-3-one (**116a**): Yield 67 %; **mp** = 130 – 131 °C; **IR [KBr, cm^{-1}]:** 3475 (NH/OH), 1750 (acetoxy carbonyl, C=O). **^{1}H-NMR [CDCl$_3$, 400 MHz]:** (δ, ppm) 2.12 (s, 3H, CH$_3$), 2.13 (s, 3H, CH$_3$), 2.16 (s, 3H, CH$_3$), 3.71 (t, 1H, H-5''b, J = 8.0 Hz), 4.19 (dd, 1H, H-4'', J = 4.8, 12 Hz), 4.44 (dd, 1H, H-5''a, J = 3.6, 15.6 Hz), 5.71 (t, 1H, H-3'', J = 8.0 Hz), 5.90 (m, 1H, H-2''), 6.01 (d, 1H, H-1'', J = 4 Hz), 7.23 (m, 1H, aromatic), 7.46 (m, 2H, aromatic), 7.63 (d, 1H, aromatic, J = 8 Hz), 9.85 (s, 1H, NH); **^{13}C-NMR [CDCl$_3$, 100 MHz]:** (δ, ppm) 20.5, 20.5, and 20.8 (3 CH$_3$), 62.9 (C-5''), 71.0 (C-3''), 74.0 (C-2''), 80.9 (C-4''), 90.2 (C-1''), 107.7 (C-2'), 118.6 (C-6'), 120.4 (C-4'), 123.6 (C-4), 130.7 (C-5'), 132.9 (CF$_3$), 152.3 (C-1'), 153.8 (C-5), 162.0 (C-3), 164.5 (C-3'), 169.3, 169.5, and 170.7 (Three acetoxy carbonyl carbon); **LC-MS/MS** (C$_{21}$H$_{20}$F$_4$N$_4$O$_8$): m/z 533, 35 % (M$^+$), 298, 15 % (acetyl sugar: C$_{11}$H$_{15}$O$_8$$^{•+}Na^+$) , 296, 53 % (C$_{10}H_5F_4N_4O^{•+}Na^+$).

3-(2'',3'',5''-Tri-O-acetyl-β-ribofuranosyloxy)-4-(3'-chlorophenylhydrazono)-5-trifluoromethyl-2,4-dihydropyrazole (**116b**): Yield 69 %; **mp** = 151 – 152 °C; **IR [KBr, cm^{-1}]:** 3418 (NH/OH), 1749 (acetoxy carbonyl, C=O). **^{1}H-NMR [CDCl$_3$, 400 MHz]:** (δ, ppm) 2.11 (s, 3H, CH$_3$), 2.12 (s, 3H, CH$_3$), 2.13 (s, 3H, CH$_3$), 4.20 (dd,

1H, H-5″b, J = 4.8, 12.4 Hz), 4.41 (m, 1H, H-4″), 4.46 (dd, 1H, H-5″a, J = 3.2, 12.4 Hz), 5.71 (t, 1H, H-3″, J = 5.6 Hz), 5.91 (dd, 1H, H-2″, J = 3.6, 4.8 Hz), 6.01 (d, 1H, H-1″, J = 3.2 Hz), 7.45 (m, 2H, aromatic), 7.73 (m, 1H, aromatic), 7.80 (m, 1H, aromatic), 9.80 (s, 1H, NH); **^{13}C-NMR [CDCl$_3$, 100 MHz]:** (δ, ppm) 20.5, 20.5, and 20.8 (3 CH$_3$), 63.0 (C-5″), 71.1 (C-3″), 74.0 (C-2″), 80.9 (C-4″), 90.3 (C-1″), 117.6 (C-2′), 121.6 (C-6′), 121.9 (C-4′), 123.7 (C-5′), 130.4 (C-4), 131.6 (C-1′), 135.5 (C-5), 138.6 (CF$_3$), 151.7 (C-4), 153.8 (C-3′), 169.3, 169.5, and 170.7 (three acetoxy carbonyl carbons); **LC-MS/MS** (C$_{21}$H$_{20}$ClF$_3$N$_4$O$_8$): m/z 571, 100 % (M$^+$Na$^+$), 290, 30 % (C$_{11}$H$_{16}$O$_7^+$), 259, 80 %, (acetyl sugar: C$_{11}$H$_{15}$O$_7^{•+}$).

2.2.4 General procedure of synthesis 2-(2″,3″,5″-Tri-O-acetyl-β-ribofuranosyloxy)-4-(Araylhydrazono)-5-trifluoromethyl-2,4-dihydropyrazol-3-one 117a-g

A mixture of 4-arylhydrazono-5-trifluoromethyl-2,4-dihydropyrazol-3-ones **3** (3.0 mmol), ammonium sulfate (3.0 mmol, 0.4 g), in hexamethyldisilazane (HMDS) (25 mL) was refluxed for 6 hours under nitrogen. The excess of HMDS evaporated under reduced pressure. A mixture of the silylated pyrazolone and 1,2,3,5-tetra-O-acetyl-β-ribofuranose (**115**, 3.0 mmol, 0.95 g) was dissolved in dry CH$_2$Cl$_2$ (25 mL), and Lewis catalyst (1.1 mmol) was added dropwise at room temperature. The reaction mixture was stirred for 18 hours, then CH$_2$Cl$_2$ (100 mL) was added, washed with saturated aqueous solution of NaHCO$_3$ (50 mL) and water (3×30 mL). The organic layer separated, dried over anhydrous (Na$_2$SO$_{4)}$, and evaporated under reduced pressure. The residue was purified using a silica gel column chromatography (ethylacetate: hexane; 3:7) to separate the N-isomers **117a-g**.

2-(2″,3″,5″-Tri-O-acetyl-β-ribofuranosyl)-4-(3′-fluorophenylhydrazono)-5-trifluoromethyl-2,4-dihydropyrazole **(117a):** Yield 80 %; **mp** = 160 – 161 °C; **IR**

[KBr, cm⁻¹]: 3433 (NH/OH), 1749 (acetyl C=O), 1680 (C=O). **¹H-NMR [CDCl₃, 400 MHz]:** (δ, ppm) 2.09 (s, 3H,CH₃), 2.10 (s, 3H, CH₃), 2.11 (s, 3H, CH₃), 4.15 (dd, 1H, H-5″b, J = 4.4, 12 Hz), 4.33 (m, 1H, H-4″), 4.44 (dd, 1H, H-5″a, J = 2.8, 12 Hz), 5.53 (t, 1H, H-3″, J = 4.8 Hz), 5.70 (t, 1H, H-2″, J = 4.4 Hz), 5.99 (d, 1H, H-1″, J = 4 Hz), 6.98 (m, 1H, aromatic), 7.18 (m, 1H, aromatic), 7.27 (m, 1H, aromatic), 7.39 (m, 1H, aromatic), 13.48 (s, 1H, NH); **¹³C-NMR [CDCl₃, 100 MHz]:** (δ, ppm) 20.5, 20.6, and 20.6 (3 CH₃), 62.9 (C-5″), 70.7 (C-3″), 72.5 (C-2″), 79.7 (C-4″), 84.4 (C-1″), 104.1 (C-2'), 112.7 (C-6'), 114.3 (C-4'), 123.3 (C-5'), 131.2 (C-4), 138.7 (CF₃), 141.8 (C-1'), 157.8 (C-5), 162.3 (C-3), 164.8 (C-3'), 169.5, 169.6, and 170.7 (three acetoxy carbonyl carbons); **LC-MS/MS** ($C_{21}H_{20}F_4N_4O_8$): m/z 555, 48 % (M⁺Na), 532, 100 % (M⁺), 296, 17 % (base: $C_{10}H_5F_4N_4O^{•+}Na^+$). 259, 75 % (acetyl sugar: $C_{11}H_{15}O_8^{•+}$).

***2-(2″,3″,5″-Tri-O-acetyl-β-ribofuranosyl)-4-(3'-chlorophenylhydrazono)-5-trifluoromethyl-2,4-dihydropyrazole* (117b):** Yield 65 %; **mp** = 165 – 166 °C; **IR [KBr, cm⁻¹]:** 3413 (NH/OH), 1749 (acetyl C=O), 1678 (C=O); **¹H-NMR [CDCl₃, 400 MHz]:** (δ, ppm) 2.10 (s, 3H,CH₃), 2.11 (s, 3H, CH₃), 2.12 (s, 3H, CH₃), 4.16 (dd, 1H, H-5″b, J = 4.8, 12 Hz), 4.34 (m, 1H, H-4″), 4.44 (dd, 1H, H-5″a, J = 3.2, 5.6 Hz), 5.53 (dd, 1H, H-3″, J = 5.6, 4.8 Hz), 5.70 (t, 1H, H-2″, J = 4.4 Hz), 5.99 (d, 1H, H-1″, J = 4.4 Hz), 7.24 (m, 1H, aromatic), 7.33 (m, 1H, aromatic), 7.35 (m, 1H, aromatic), 7.49 (m, 1H, aromatic), 13.48 (s, 1H, NH); **¹³C-NMR [CDCl₃, 100 MHz]:** (δ, ppm) 20.5, 20.6, and 20.6 (3 CH₃), 68.1 (C-5″), 70.8 (C-3″), 72.5 (C-2″), 79.7 (C-4″), 84.4 (C-1″), 115.0 (C-2'), 116.7 (C-6'), 123.4 (C-4'), 127.4 (C-5'), 128.8 (C-4), 130.9 (C-1'), 135.9 (C-5), 139.1 (CF₃), 141.2 (C-3), 157.8 (C-3'), 169.4, 169.6,

and 170.6 (three acetoxy carbonyl carbon); **LC-MS/MS** ($C_{21}H_{20}ClF_3N_4O_8$): m/z 571, 100 % (M^+Na^+), 290, 32 % ($C_{10}H_5ClF_3N_4O^+$). 259, 85 % (acetyl sugar: $C_{11}H_{15}O_8^{\bullet+}$).

***2-(2'',3'',5''-Tri-O-acetyl-β-ribofuranosyl)-4-(3'-trifluoromethyl-phenylhydrazono)-5-trifluoromethyl-2,4-dihydropyrazol-3-one* (117c):** Yield 84 %; **mp** = 140 – 141 °C; **IR [KBr, cm^{-1}]:** 3415 (NH/OH), 1749 (acetyl C=O), 1682 (C=O). **^{1}H-NMR [CDCl$_3$, 400 MHz]:** (δ, ppm) 2.10 (s, 3H, CH$_3$), 2.11 (s, 3H, CH$_3$), 2.12 (s, 3H, CH$_3$), 4.16 (dd, 1H, H-5''b, *J* = 4.4, 12 Hz), 4.34 (m, 1H, H-4''), 4.44 (dd, 1H, H-5''a, *J* = 3.2, 12 Hz), 5.53 (t, 1H, , H-3'', *J* = 5.6 Hz), 5.70 (dd, 1H, H-2'', *J* = 4.4, 5.2 Hz), 6.01 (d, 1H, H-1'', *J* = 4.4 Hz), 7.56 (m, 2H, aromatic), 7.68 (d, 2H, aromatic), 13.60 (s, 1H, NH); **^{13}C-NMR [CDCl$_3$, 100 MHz]:** (δ, ppm) 20.5, 20.5, and 20.6 (3 CH$_3$), 62.9 (C-5''), 70.8 (C-3''), 72.5 (C-2''), 79.8 (C-4''), 84.5 (C-1''), 113.6 (C-2'), 119.7 (C-6'), 120.4 (C-4'), 123.7 (C-5'), 124.6 (C-1'), 130.6 (C-5), 132.4 (CF$_3$), 138.7 (CF$_3$), 140.7 (C-3'), 157.7 (C-4), 169.7, 169.6, and 170.7 (three acetoxy carbonyl carbons); **LC-MS/MS** ($C_{22}H_{20}F_6N_4O_8$): m/z 585, 10 % (M^++1), 282, 100 % (acetyl sugar: $C_{11}H_{15}O_7^{\bullet} + Na^+$).

***2-(2'',3'',5''-Tri-O-acetyl-β-ribofuranosyl)-4-(4'-fluorophenylhydrazono)-5-trifluoromethyl-2,4-dihydropyrazole* (117d):** Yield 78 %; **mp** = 130 – 131 °C; **IR [KBr, cm^{-1}]:** 3426 (NH/OH), 1749 (acetyl C=O); 1676 (C=O). **^{1}H-NMR [CDCl$_3$, 400 MHz]:** (δ, ppm) 2.10 (s, 3H, CH$_3$), 2.10 (s, 3H, CH$_3$), 2.11 (s, 3H, CH$_3$), 4.15 (dd, 1H, H-5''b, *J* = 4.8, 12.4 Hz), 4.33 (m, 1H, H-4''), 4.44 (dd, 1H, H-5''a, *J* = 3.2, 12.4 Hz), 5.54 (t, 1H, , H-3'', *J* = 6.6 Hz), 5.70 (m, 1H, H-2''), 6.001 (d, 1H, H-1'', *J* = 4.0 Hz), 7.15 (m, 2H, aromatic), 7.46 (m, 2H, aromatic), 13.63 (s, 1H, NH); **^{13}C-NMR [CDCl$_3$, 100 MHz]:** (δ, ppm) 20.5, 20.6, and 20.6 (3 CH$_3$), 62.9 (C-5''), 70.8 (C-3''), 72.6 (C-2''), 79.7 (C-4''), 84.5 (C-1''), 116.9 (C-2'), 117.1 (C-6'), 118.4 (C-3'),

118.5 '(C-5'), 122.6 (C-4), 138.4 (C-1'), 138.6 (C-6, CF$_3$), 157.9 (C-5'), 160.4 (C-4'),

162.9 (C-3), 169.5, 169.6, and 170.7 (three acetoxy carbonyl carbons); **LC-MS/MS**

for (C$_{21}$H$_{20}$F$_4$N$_4$O$_8$): m/z 554, 38% (M$^+$Na$^+$), 533, 100 % (M$^+$), 296, 8 %

(C$_{10}$H$_5$F$_4$N$_4$O$^{•+}$Na$^+$), 282, 98 %, (C$_{11}$H$_{15}$O$_8$$^{•+}Na^+$), 259, 25 % (acetyl sugar:

C$_{11}$H$_{15}$O$_8$$^•$).

2-(2'',3'',5''-Tri-O-benzoyl-β-ribofuranosyl)-4-(4'-chlorophenylhydrazono)-5-

trifluoromethyl-2,4-dihydropyrazol-3-one **(117e):** Yield 66 %; **mp** = 160 − 162 °C;

IR **[KBr, cm^{-1}]:** 3416 (NH/OH), 1724 (benzoyl carbonyl C=O), 1680 (C=O). **^{1}H-**

NMR [CDCl$_3$, 400 MHz]: (δ, ppm) 4.62 (m, 1H, H-4″), 4.74 (m, 2H, H-5″a,b), 6.02

(t, 1H, H-3″, *J* = 5.6 Hz), 6.13 (dd, 1H, H-2″, *J* = 3.6, 5.6 Hz), 6.26 (d, 1H, H-1″, *J* =

3.6 Hz), 7.39 (m, 10H, aromatic), 7.54 (m, 3H, aromatic), 7.96 (m, 4H, aromatic),

8.09 (m, 2H, aromatic, 13.59 (s, 1H, NH); **^{13}C-NMR [CDCl$_3$, 100 MHz]:** (δ, ppm)

63.6 (C-5″), 71.4 (C-3″), 73.5 (C-2″), 79.7 (C-4″), 85.17 (C-1″), 117.9 (2C-C-2', 6'),

123.0 (C-4), 128.4-128.7 (7 C- aromatic), 129.7-129.8 (10 C- aromatic), 130.1 (2C-

C-3', 5'), 133.1 (C-1'), 133.6 (C-4), 138.7 (CF$_3$), 157.8 (C-5), 165.1, 165.2, and

166.3 (three benzoyl carbonyl carbons), 168.1 (C-3); **LC-MS/MS** (C$_{36}$H$_{26}$ClF$_3$N$_4$O$_8$):

m/z 757, 5 % (M$^+$Na$^+$), 735, 20 % (M$^+$), 445, 28 % (benzoyl Sugar C$_{26}$H$_{21}$O$_7$$^{•+}$).

2-(2'',3'',5''-Tri-O-acetyl-β-ribofuranosyloxy)-4-(3'-nitrophenylhydrazono)-5-

trifluoromethyl-2,4-dihydropyrazol-3-one **(117f):** Yield 69 %; **mp** = 122 − 123 °C;

IR [KBr, cm^{-1}]: 3464 (NH/OH), 1749 (acetyl C=O), 1684 (C=O); **^{1}H-NMR**

[CDCl$_3$, 400 MHz]: (δ, ppm) 2.11 (s, 3H, CH$_3$), 2.11 (s, 3H, CH$_3$), 2.13 (s, 3H,

CH$_3$), 4.16 (dd, 1H, H-5″b, *J* = 4.0, 12 Hz), 4.35 (m, 1H, H-4″), 4.44 (dd, 1H, H-5″a,

J = 3.2, 3.6 Hz), 5.52 (t, 1H, H-3″, *J* = 5.6 Hz), 5.69 (dd, 1H, H-2″, *J* = 3.6, 12.4

Hz), 6.01 (d, 1H, H-1″, *J* = 4.4 Hz), 7.65 (t, 1H, aromatic, *J* = 8.0 Hz), 7.82 (m, 1H,

aromatic), 8.12 (m, 1H, aromatic), 8.28 (t, 1H, aromatic, J= 2.4 Hz), 13.53 (s, 1H, NH); **^{13}C-NMR [CDCl$_3$, 100 MHz]:** (δ, ppm) 20.5, 20.5, and 20.6 (3 CH$_3$), 62.9 (C-5"), 70.7 (C-3"), 72.5 (C-2"), 79.8 (C-4"), 84.5 (C-1"), 111.6 (C-2'), 120.3 (C-6'), 121.4 (C-4'), 121.9 (C-5'), 124.4 (C-4), 130.9 (C-1'), 138.7 (CF$_3$), 141.3 (C-5), 149.3 (C-3), 157.7 (C-3'), 169.5, 169.6, and 170.6 (three acetoxy carbonyl carbons); **LC-MS/MS** (C$_{21}$H$_{20}$F$_3$N$_5$O$_{10}$): m/z 582, 34 % (M$^+$Na$^+$), 560, 52 % (M$^+$), 304, 22 % (C$_{10}$H$_5$F$_3$N$_5$O$_3$$^{\bullet+}$), 296, 23 %, (acetyl sugar: C$_{11}$H$_{15}$O$_8$$^{\bullet+}Na^+$).

***2-(2",3",5"-Tri-O-acetyl-β-ribofuranosyl)-4-(4'-bromophenylhydrazono)-5-trifluoromethyl-2,4-dihydropyrazol-3-one* (117g):** Yield 53 %; **mp** = 153 – 154 °C; **IR [KBr, cm^{-1}]:** 3467 (NH/OH), 1747 (acetyl C=O), 1672 (C=O). **^{1}H-NMR [CDCl$_3$, 400 MHz]:** (δ, ppm) 2.10 (s, 3H, CH$_3$), 2.11 (s, 3H, CH$_3$), 2.12 (s, 3H, CH$_3$), 4.16 (dd, 1H, H-5″b, J = 4.4, 4.8 Hz), 4.34 (m, 1H, H-4"), 4.44 (dd, 1H, H-5"a, J = 3.2, 3.6 Hz), 5.53 (t, 1H, H-3", J = 5.6 Hz), 5.70 (t, 1H, H-2", J = 4.4 Hz), 6.001 (d, 1H, H-1", J = 4.4 Hz), 7.36 (dd, 2H, aromatic, J = 3.2, 3.6 Hz), 7.57 (dd, 2H, aromatic, J = 2.0, 2.4 Hz), 13.54 (s, 1H, NH); **^{13}C-NMR [CDCl$_3$, 100 MHz]:** (δ, ppm) 20.5, 20.5, and 20.6 (3 CH$_3$), 62.9 (C-5"), 70.7 (C-3"), 72.6 (C-2"), 79.7 (C-4"), 84.4 (C-1"), 118.1 (C-2'), 118.2 (C-6'), 120.2 (C-4), 120.9 (C-1'), 123.1 (C-5'), 132.9 (C-3'), 133.0 (C-5'), 139.2 (CF$_3$), 149.5 (C-4'), 157.8 (C-3), 169.5, 169.6, and 170.7 (three acetoxy carbonyl carbons); **LC-MS/MS** (C$_{21}$H$_{20}$BrF$_3$N$_4$O$_8$): m/z 617, 8% (M$^+$Na$^+$), 592, 10% (M$^+$), 336, 10% (C$_{10}$H$_6$BrF$_3$N$_4$O$^+$), 282, 100% (C$_{11}$H$_{15}$O$_8$$^{\bullet+}Na^+$).

2.2.5 General procedure for de-protection of compounds 118 a-c

A mixture of triethylamine, water and methanol (1:1:1) (15 mL) was added to the acetylated ribonucleosides analogues **118a-c** (50.0 mg). The mixture was stirred overnight at room temperature and the solvents were evaporated under

reduced pressure. The residue was crystallized from 50 mL ethanol to give **118a-c** in

yield 84%, 92% and 93% respectively.

2-(β-D-Ribofuranosyl)-4-(3'-trifluoromethyl-phenylhydrazono)-5-trifluoromethyl-

***2,4-dihydropyrazol-3-one* (118a):** Yield 84 %; **mp** = 149 – 152 ^{o}C; **IR [KBr, cm^{-1}]:**

3434 (NH/OH), 1678 (C=O); **^{1}H-NMR [CDCl$_3$, 400 MHz]:** 3.11 (m, 3-OH,

exchangeable with D$_2$O), 3.73 (d, 1H, H-5″b, J = 12.0 Hz), 3.89 (d, 1H, H-5″a, J =

11.6 Hz), 4.19 (s, 1H, H-4″), 4.49 (s, 1H, H-3″), 4.69 (s, 1H, H-2″), 5.89 (d, 1H, H-

1″, J = 2.4 Hz), 7.53 (m, 2H, aromatic), 7.63 (d, 1H, aromatic, J = 7.2 Hz), 7.67 (s,

1H, aromatic), 11.07 (s, 1H, NH, exchangeable with D$_2$O); **^{13}C-NMR [CDCl$_3$, 100**

MHz]: (δ, ppm) 63.0 (C-5″), 71.6 (C-4″), 73.8 (C-3″), 85.6 (C-2″), 88.0 (C-1″),

113.6, 117.6, 119.7, 121.9 (aromatic Cs), 123.9 (C-3'), 124.7 (aromatic C), 130.6

(C4), 132.5 (CF$_3$), 138.6 (CF$_3$), 140.6 (C-5), 157.9 (C-3). **LC-MS/MS**

(C$_{16}$H$_{14}$F$_6$N$_4$O$_5$): m/z 457, 98 % (M$^+$), 322, 38 % (C$_{11}$H$_4$F$_6$N$_4$O$^+$), 140, 100 %

(C$_7$H$_9$FN$_2^+$), 134, 15 % (C$_5$H$_{10}$O$_4^+$).

2-(β-D-Ribofuranosyl)-4-(4'-chlorophenylhydrazono)-5-trifluoromethyl-2,4-

***dihydropyrazol-3-one* (118b):** Yield 92 %; **mp** = 151 – 152 ^{o}C; **IR [KBr, cm^{-1}]:**

3414 (NH/OH); 1669 (C=O) **^{1}H-NMR [CDCl$_3$, 400 MHz]:** (δ, ppm) 3.10 (m, 3-OH,

exchangeable with D$_2$O), 3.72 (d, 1H, H-5″b, J = 12.8 Hz), 3.90 (d, 1H, H-5″a, J =

10.8 Hz), 4.18 (m, 1H, H-4″), 4.50 (m, 1H, H-3″), 4.72 (m, 1H, H-2″), 5.89 (d, 1H,

H-1″, J = 4.8 Hz), 7.12 (m, 2H, aromatic), 7.48 (m, 2H, aromatic), 11.73 (s, 1H, NH,

exchangeable with D$_2$O); **^{13}C-NMR [100Hz, DMSO-d$_6$]:** (δ, ppm) 64.4 (C-5″), 71.9

(C-4″), 73.9 (C-3″), 78.4 (C-2″), 84.7 (C-1″), 119.9 (aromatic C), 122.2 (C4), 129.1

(2C, aromatic Cs), 129.8 129.1 (2C, aromatic Cs), 134.2 (CF$_3$), 165.1 (C5), 166.0

(C3), **LC-MS/MS** ($C_{15}H_{14}ClF_3N_4O_5$): m/z 423, 8 % (M^+), 404, 100 % ($C_{15}H_{12}ClF_3N_4O_4^{2\bullet+}$), 292. 48 % ($C_{10}H_6ClF_3N_4O^+$), 132, 25 % ($C_5H_8O_4^+$).

2-(β-D-Ribofuranosyl)-4-(3'-nitrophenylhydrazono)-5-trifluoromethyl-2,4-dihydropyrazol-3-one (**118c**): Yield 93 %; **mp** = 146 – 147 $^{\circ}$C; **IR [KBr, cm^{-1}]:** 3434 (NH/OH), 1670 (C=O); **^{1}H-NMR [CDCl$_3$, 400 MHz]:** (δ, ppm) 3.10 (m, 3-OH, exchangeable with D_2O), 3.74 (dd, 1H, H-5″b, J = 2.8, 2.8 Hz), 3.90 (dd, 1H, H-5″a, J = 2.4, 2.8 Hz), 4.20 (m, 1H, H-4″), 4.51 (m, 1H, H-3″), 4.72 (t, 1H, H-2″, J = 5.2 Hz), 5.90 (d, 1H, H-1″, J = 5.2 Hz), 7.65 (m, 1H, aromatic), 7.81 (dd, 1H, aromatic, J = 1.2, 1.2 Hz), 8.13 (dd, 1H, aromatic, J = 1.6, 2.0 Hz), 8.30 (t, 1H, aromatic, J = 2.0 Hz), 11.81 (s, 1H, NH, exchangeable with D_2O); **^{13}C-NMR [CDCl$_3$, 100 MHz]:** (δ, ppm) 62.9 (C-5″), 71.6 (C-4″), 73.8 (C-3″), 85.6 (C-2″), 88.0 (C-1″), 111.7, 117.5, 121.5, 121.9 (aromatic Cs), 124.6 (C4), 130.9 (aromatic C), 138.5 (CF$_3$), 141.3 (aromatic Cs), 149.3 (C5), 157.9 (C3). **LC-MS/MS** ($C_{15}H_{14}F_3N_5O_7$): m/z 456, 20 % (M^+Na^+), 433, 100 % (M^+), 302, 30 % ($C_{10}H_6F_3N_5O_3^+$), 133, 10 % ($C_5H_9O_4^{\bullet+}$).

2.2.6 Synthesis of 1,3,5-tri-*O*-acetyl-2-deoxyribofuranose 121

2-Deoxy-D-ribose (0.04 mol, 5.0 g) was dissolved in pyridine (14.0 mL). The solution was cooled to 0 °C and then acetic anhydride (12.5 mL) was added slowly. After the addition was complete, the solution was stirred at the room temperature for ~25 h. Thereafter, 10 volumes of a saturated solution of NaHCO$_3$ were added to the reaction mixture at 0 °C, and then the product was extracted with chloroform. The organic phase was washed with 1 M HCl (100 mL × 3 times), saturated solution of NaHCO$_3$ (100 mL × 1 time), and water (100 mL × 1 time) successively. After being dried and filtered, a yellow syrup was obtained. After several hours, a white solid

was precipitated from the syrup at the room temperature. The solid was filtered and washed with isopropyl ether (100 mL), and then 1,3,5-tri-*O*-acetyl-2-deoxy-ribofuranose (yield 13 %) was obtained. The filtrate was concentrated and it gave a yellow syrup, which was stored at room temperature and yielded a single crystals after several days (yield 67 %).

2.2.7 General procedure for the synthesis of deoxyribonucleoside derivatives 122a-c and 123a-c

To a solution of 4-arylhydrazono-5-trifluoromethyl-2,4-dihydropyrazol-3-ones **113** (1.0 mmol) in hexamethyldisilazine (HMDS) (6.0 mL), and anhydrous ammonium sulfate (1.0 mmol, 0.132g) was added. The mixture was refluxed for 3 hours under nitrogen, and the excess of HMDS was evaporated under vacuum to dryness. The residue was dissolved in dry acetonitrile (2.0 mL) and the resulted solution was evaporated under vacuum to remove the excess HMDS. A cold solution of 1,3,5-tri-*O*-acetyl-2-deoxy-D-ribofuranose (0.001 mol, 0.26 g) in acetonitrile (2.0 mL) was added to the silyl base (1.0 mmol) in acetonitrile (4.0 mL) at 0 $^{\circ}$C. To the previous mixture, $SnCl_4$ (1.0 mmol, 0.12 mL) in acetonitrile (2.0 mL) was added with stirring in ice (0 - 5 $^{\circ}$C). Then the mixture stirred at room temperature for four hours. The reaction mixture was quenched by chloroform (25 mL), the organic layer washed with saturated aqueous solution of sodium bicarbonate (50 mL) and water (3 x 30 mL). Then was dried over anhydrous sodium sulfate, filtered, and the solvent was removed under reduced pressure. The residue purified on column chromatography (ethyl acetate : hexane, 2:8, 3:7 then 4:6) to produce *O*-isomers **122a-c** and *N*-isomers **123a-c**.

3-(3'',5''-Di-O-acetyl-2''-β-deoxyribofuranosyloxy)-4-(3'-fluorophenylhydrazono)-5-trifluoromethyl-2,4-dihydropyrazol-3-one (**122a**): Yield 53 %; **mp** = 137 − 138 ^{o}C; **IR [KBr, cm^{-1}]:** 3414 (NH/OH), 2922 (sp^3-CH stretch), 1741 (acetoxy group), 1463 (CH$_2$ bending), 1373 (CH$_3$ bending); **^{1}H-NMR [CDCl$_3$, 400 MHz]:** (δ, ppm) 2.05 (s, 3H, CH$_3$), 2.10 (dd, 1H, H-2''b, J = 2.8, 3.2 Hz), 2.15 (s, 3H, CH$_3$), 2.67 (m, 1H, H- 2″a), 3.94 (m, 2H, H-5''a,b), 5.11 (m, 1H, H-4″), 5.66 (m, 1H, H-3″), 5.83 (dd, 1H, H-1″, J = 2.8, 8.8 Hz), 6.98 (m, 1H, aromatic), 7.18 (m, 1H, aromatic), 7.28 (m, 1H, aromatic), 7.40 (m, 1H, aromatic), 13.56 (s, 1H, NH); **^{13}C-NMR [CDCl$_3$, 100 MHz]:** (δ, ppm) 20.9 (CH$_3$), 21.1 (CH$_3$), 29.7 (C-2″), 66.1 (C-5″), 67.1 (C-4″), 68.6 (C-3″), 78.5 (C-1″), 103.8, 112.7, 114.5, 123.5, 131.2 aromatic Cs, 138.2 (CF$_3$), 141.7 (C4), 157.6 (C5),162.3 (C3), 164.3 (C-aromatic), 170.0, 170.6 (two acetoxy carbonyl carbons); **LC-MS/MS** (C$_{22}$H$_{20}$F$_6$N$_4$O$_8$): m/z 497, 32% (M$^+$Na$^+$), 475, 97 % (M$^+$), 274, 8 % (C$_{10}$H$_6$F$_4$N$_4$O$^+$), 201, 27 % (acetyl sugar: C$_9$H$_{13}$O$_5$$^{•+}$). 288, 100 % (C$_{15}H_{14}F_4N_4O_2$$^+$).

3-(3'',5''-Di-O-acetyl-2''-β-deoxyribofuranosyloxy)-4-(3'-trifluoromethyl-phenylhydrazono)-5-trifluoromethyl-2,4-dihydropyrazol-3-one (**122b**): Yield 55 %; **mp** = 135 − 136 ^{o}C; **IR [KBr, cm^{-1}]:** 3411 (NH/OH), 2920 (sp^3-CH stretch), 1735 (acetoxy group), 1461 (CH$_2$ bending), 1372 (CH$_3$ bending); **^{1}H-NMR [CDCl$_3$, 400 MHz]:** (δ, ppm) 2.05 (s, 3H, CH$_3$), 2.10 (d, 1H, H-2''b, J = 9.6), 2.15 (s, 3H, CH$_3$), 2.67 (m, 1H, H- 2″a), 3.93 (m, 2H, H-5''a,b), 5.11 (m, 1H, H-4″), 5.66 (m, 1H, H-3″), 5.83 (dd, 1H, H-1″, J = 3.2, 3.2 Hz), 7.57 (m, 2H, aromatic), 7.66 (m, 1H, aromatic), 7.69 (m, 1H, aromatic), 13.64 (s, 1H, NH); **^{13}C-NMR [CDCl$_3$, 100 MHz]:** (δ, ppm) 20.9 (CH$_3$), 21.1 (CH$_3$), 29.7 (C-2″), 66.2 (C-5″), 67.1 (C-4″), 68.6 (C-3″), 78.6 (C-1″), 104.1, 112.7, 114.2, 123.4 (aromatic Cs), 131.2 (C4), 138.2

(CF$_3$), 141.8 (C-aromatic), 145.5 (CF$_3$), 157.6 (C5),162.4 (C3), 164.9 (C-aromatic), 170.1, 170.6 (two acetoxy carbonyl carbons); **LC-MS/MS** (C$_{20}$H$_{18}$F$_6$N$_4$O$_6$): m/z 547, 100 % (M$^+$Na$^+$), 525, 32.4 % (M$^+$), 325, 10 % (C$_{11}$H$_5$F$_6$N$_4$O$^+$), 201, 50 % (C$_9$H$_{13}$O$_5$$^{•+}$).

3-(3'',5''-Di-O-acetyl-2''-β-deoxyribofuranosyloxy)-4-(3'-nitrophenylhydrazono)-5-trifluoromethyl-2,4-dihydropyrazol-3-one **(122c):** Yield 49 %; **mp** = 136 − 138 ^{o}C; **IR [KBr, cm^{-1}]:** 3411 (NH/OH), 2924 (sp^3-CH stretch), 1740 (acetoxy group), 1461 (CH$_2$ bending), 1375 (CH$_3$ bending); **^{1}H-NMR [CDCl$_3$, 400 MHz]:** (δ, ppm) 2.05 (s, 3H, CH$_3$), 2.10 (m, 1H, H-2"b), 2.15 (s, 3H, CH$_3$), 2.67 (m, 1H, H- 2″a), 3.94 (m, 2H, H-5"a,b), 5.10 (m, 1H, H-4″), 5.66 (m, 1H, H-3″), 5.83 (dd, 1H, H-1″, *J* = 2.8, 3.2 Hz), 7.65 (t, 1H, aromatic, *J* = 8.0 Hz), 7.81 (m, 1H, aromatic), 8.12 (m, 1H, aromatic), 8.27 (t, 1H, aromatic, *J* = 2.0 Hz), 13.62 (s, 1H, NH); **^{13}C-NMR [CDCl$_3$, 100 MHz]:** (δ, ppm) 20.8 (CH$_3$), 21.0 (CH$_3$), 31.2 (C-2″), 63.5 (C-5″), 66.5 (C-4″), 76.5 (C-3″), 91.8 (C-1″), 111.6, 117.6, 121.4, 121.8, 124.5 (aromatic Cs), 130.9 (C4), 138.0 (CF$_3$), 141.3 (C-aromatic), 149.3 (C5), 157.8 (C3), 169.8, 169.9 (two acetoxy carbonyl carbons); **LC-MS/MS** (C$_{19}$H$_{18}$F$_3$N$_5$O$_8$): m/z 502, 100 % (M$^+$), 201, 20 % (C$_9$H$_{13}$O$_5$$^{•+}$).

2-(3'',5''-Di-O-acetyl-2''-β-deoxy-ribofuranosyl)-4-(3'-fluorophenylhydrazono)-5-trifluoromethyl-2,4-dihydropyrazol-3-one **(123a):** Yield 47 %; **mp** = 160 − 162 ^{o}C; IR **[KBr, cm^{-1}]:** 3431 (NH/OH), 2919 (sp^3-CH stretch), 1742 (acetoxy group), 1679 (C=O), 1462 (CH$_2$ bending), 1375 (CH$_3$ bending); **^{1}H-NMR [CDCl$_3$, 400 MHz]:** (δ, ppm) 2.04 (m, 1H, H-2"b), 2.05 (s, 3H, CH$_3$), 2.20 (s, 3H, CH$_3$), 2.87 (q, 1H, H-2″a), 3.83 (d, 1H, H-5"b, *J* = 13.2 Hz), 4.13 (d, 1H, H-5"a, *J* = 13.2 Hz), 5.15 (m, 1H, H-4″), 5.21 (s, 1H, H-3″), 5.50 (d, 1H, H-1″, *J* = 10.8 Hz), 6.98 (m, 1H,

aromatic), 7.18 (m, 2H, aromatic), 7.28 (m, 1H, aromatic), 7.40 (m, 1H, aromatic),
13.54 (s, 1H, NH, exchangeable with D_2O); **^{13}C-NMR [CDCl$_3$, 100 MHz]:** (δ, ppm)
(δ, ppm) 20.8 (CH_3), 21.0 (CH_3), 29.7 (C-2″), 63.5 (C-5″), 66.6 (C-4″), 76.5 (C-3″),
77.2 (C-1″), 103.8, 112.7, 114.5, 123.4 (aromatic Cs), 131.2 (C4), 138.4 (CF_3), 141.8
(C-aromatic), 157.9 (C5),162.4 (C3), 164.9 (C-aromatic), 169.8, 169.9 (two acetoxy
carbonyl carbons); **LC-MS/MS** ($C_{22}H_{20}F_6N_4O_8$): m/z 497, 38 % (M^+Na^+), 475, 100
% (M^+), 275, 20 % ($C_{10}H_6F_4N_4O^+$), 201, 33 % ($C_9H_{13}O_5^{•+}$).

***2-(3″,5″-Di-O-acetyl-2″-β-deoxy-ribofuranosyl)-4-(3'-trifluoromethyl-
phenylhydrazono)-5-trifluoromethyl-2,4-dihydropyrazol-3-one*** **(123b):** Yield 45 %;
mp = 139 − 140 ^{o}C; IR [KBr, cm^{-1}]: 3442 (NH/OH), 2922 (sp^3-CH stretch), 1743
(acetoxy group), 1683 (C=O), 1462 (CH_2 bending), 1370 (CH_3 bending); **^{1}H-NMR
[CDCl$_3$, 400 MHz]:** (δ, ppm) 2.00 (m, 1H, H-2″b), 2.04 (s, 3H, CH_3), 2.20 (s, 3H,
CH_3), 2.87 (q, 1H, H- 2″a), 3.83 (d, 1H, H-5″b, J = 13.6 Hz), 4.13 (t, 1H, H-5″a, J =
13.2 Hz), 5.15 (d, 1H, H-4″, J = 11.6 Hz), 5.20 (s, 1H, H-3″), 5.52 (d, 1H, H-1″, J =
10.0 Hz), 7.53 (m, 2H, aromatic), 7.66 (m, 1H, aromatic, J = 7.6 Hz), 7.70 (m, 1H,
aromatic), 13.56 (s, 1H, NH); **^{13}C-NMR [CDCl$_3$, 100 MHz]:** (δ, ppm) 20.8 (C5″-
CH_3), 21.1 (C3″- CH_3), 29.7 (C-2″), 63.0 (C-5″), 64.3 (C-4″), 74.5 (C-3″), 76.0 (C-
1″), 113.5, 119.6, 127.8 (aromatic Cs), 130.6 (C4), 132.4 (CF_3), 140.8 (C-aromatic),
147.2 (CF_3), 158.0 (C), 158.1 (C3), 169.3, 170.5 (two acetoxy carbonyl carbons);
LC-MS/MS ($C_{22}H_{20}F_6N_4O_8$): m/z 47, 100 % (M^+Na^+), 525, 53 % (M^+), 325, 10 %
($C_{11}H_5F_6N_4O^+$), 5201, 38 % (acetyl sugar: $C_9H_{13}O_5^{•+}$).

***2-(3″,5″-Di-O-acetyl-2″-deoxy-ribofuranosyl)-4-(3'-nitrophenylhydrazono)-5-
trifluoromethyl-2,4-dihydropyrazol-3-one*** **(123c):** Yield 51 %; **mp** = 177 − 178 ^{o}C;
IR [KBr, cm^{-1}]: 3435 (NH/OH), 2921 (sp^3-CH stretch), 1743 (acetoxy group), 1682

(C=O), 1474 (CH$_2$ bending), 1374 (CH$_3$ bending); **^{1}H-NMR [CDCl$_3$, 100 MHz]:** (δ, ppm) 2.01 (m, 1H, H-2″b), 2.05 (s, 3H, CH$_3$), 2.20 (s, 3H, CH$_3$), 2.87 (q, 1H, H-2″a), 3.84 (d, 1H, H-5″b, *J* = 12.8 Hz), 4.15 (dd, 1H, H-5″a, *J* = 1.6, 2.0 Hz), 5.16 (m, 1H, H-4″), 5.21 (s, 1H, H-3″), 5.51 (dd, 1H, H-1″, *J* = 2.0, 2.4 Hz), 7.64 (t, 1H, aromatic, *J* = 8.0 Hz), 7.80 (m, 1H, aromatic), 8.12 (m, 1H, aromatic), 8.29 (t, 1H, aromatic, *J* = 2.4 Hz), 13.63 (s, 1H, NH); **^{13}C-NMR [CDCl$_3$, 100 MHz]:** (δ, ppm) 20.7 (CH$_3$), 20.8 (CH$_3$), 30.9 (C-2″), 63.6 (C-5″), 66.5 (C-4″), 68.1 (C-3″), 81.2 (C-1″), 111.6, 121.4, 121.8, 128.8, 130.8 aromatic Cs, 132.4 (C-4), 138.0 (CF$_3$), 141.4 aromatic C, 149.3 (C-5), 157.8 (C-3), 167.7, 169.8 (two acetoxy carbonyl carbons); **LC-MS/MS** (C$_{19}$H$_{18}$F$_3$N$_5$O$_8$): m/z 502, 100 % (M$^+$), 201, 29 % (C$_9$H$_{13}$O$_5$$^{•+}$).

2.2.8 Synthesis of *O*- and *N*-benzoyl of 5-trifluoromethyl-2,4-dihydropyrazolone

General Procedures

4-Arylhydrazono-5-trifluoromethyl-2,4-dihydropyrazol-3-ones **113** (1.0 mmol) was dissolved in methylene chloride (5.0 mL) at 0 °C. The arayl chloride (2.0 mmol) was added dropwise into the solution with stirring at 0 °C. The reaction mixture was allowed to stir at room temperature for 24 hours. To the reaction mixture, hexane (25 mL) was added dropwise until a yellow precipitate was formed. The precipitate was then filtered off and dried.

4-[2-(3'-Fluorophenyl)hydrazono]-5-(trifluoromethyl)-4H-pyrazol-3-yl-4″-fluorobenzoate **(124a):** Yield 77.5 %; **mp** = 183 − 184 °C; **IR [KBr, cm^{-1}]:** 3438 (NH/OH), 1733(C=O); **^{1}H-NMR [CDCl$_3$, 400 MHz]:** (δ, ppm) 7.03 (m, 1H, aromatic), 7.19 (m,3H, aromatic), 7.29 (m, 1H, aromatic), 7.44 (m, 1H, aromatic), 7.97 (m, 2H, aromatic), 13.67 (s, 1H, NH, exchangeable with D$_2$O); **^{13}C-NMR [CDCl$_3$, 100 MHz]:** (δ, ppm) 104.3, 113.1, 115.5, 115.7, 117.5, 120.2, 121.9, 127.3,

131.4, 131.5, 133.5 (aromatic Cs), 141.5 (CF$_3$), 158.5 (C-5), 162.4 (C-3), 164.0 (C=O), 164.8 (C-F), 167.1 (C4"). **LC-MS/MS** (C$_{17}$H$_9$F$_5$N$_4$O$_2$): m/z 419, 29 % (M$^+$Na$^+$), 396, 10 0% (M$^+$), 124, 15 % (C$_7$H$_5$FO$^+$).

4-[2-(4'-Fluorophenyl)hydrazono]-5-(trifluoromethyl)-4H-pyrazol-3-yl-4''-fluorobenzoate (124b): Yield 80 %; **mp** = 182 – 183 °C; **IR [KBr, cm^{-1}]:** 3411 (NH/OH), 1727 (C=O); **^{1}H-NMR [CDCl$_3$, 100 MHz]:** (δ, ppm) 7.18 (m, 4H, aromatic), 7.50 (m, 2H, aromatic), 7.98 (m, 2H, aromatic), 13.80 (s, 1H, NH, exchangeable with D$_2$O); **^{13}C-NMR [CDCl$_3$, 100 MHz]:** (δ, ppm) 115.5, 115.7, 117.1, 117.3, 118.8 118.9, 127.4, 133.5. 133.6 (aromatic Cs), 136.2 (C-4), 140.5 (CF$_3$), 158.5 (C-5), 160.7 (C- 4'), 163.2 (C-1'), 164.2 (C-3), 164.6 (C=O), 167.1 (C-4"). **LC-MS/MS** (C$_{17}$H$_9$F$_5$N$_4$O$_2$): m/z 419, 22 % (M$^+$Na$^+$), 396, 100 % (M$^+$), 275, 32 % (C$_{10}$H$_6$F$_4$N$_4$O$^+$), 124, 10 % (C$_7$H$_5$FO$^+$).

4-[2-(3'-Trifluoromethoxyphenyl)hydrazono]-3-(trifluoromethyl)-4-4H-pyrazol-3-yl-4''-fluorobenzoate **(124c):** Yield 96 %; **mp** = 185 – 186 °C; **IR [KBr, cm^{-1}]:** 3400 (NH/OH), 1731 (C=O); **^{1}H-NMR [CDCl$_3$, 400 MHz]:** (δ, ppm) 7.18 (t, 2H, aromatic, *J* = 7.2 Hz), 7.62 (m, 4 H, aromatic), 7.96 (m, 2H, aromatic), 3.71 (s, 1H, NH); **^{13}C-NMR [CDCl$_3$, 100 MHz]:** (δ, ppm) 113.8, 115.5, 115.7, 120.0, 122.3, 124.3, 127.2, 130.7 aromatic Cs, 133.4 (CF$_3$), 140.4 (CF$_3$), 158.4 (C-5), 164.0 (C-3), 164.6 (C=O), 167.2 (C4"). **LC-MS/MS** (C$_{18}$H$_9$F$_7$N$_4$O$_2$): m/z 469, 18 % (M$^+$Na$^+$), 447, 100 % (M$^+$), 323, 5 % (C$_{11}$H$_5$F$_6$N$_4$O$^{•+}$), 123, 8 % (C$_7$H$_4$FO$^{•+}$).

4-[2-(3'-Trifluoromethoxyphenyl)hydrazono]-3-(trifluoromethyl]-4-4H-pyrazol-3-yl-4''-(trifluoromethoxy)benzoate **(124d):** Bright yellow; yield 97 %; **mp** = 197 – 198 °C; **IR [KBr, cm^{-1}]:** 3435 (NH/OH), 1730 (C=O); **^{1}H-NMR [CDCl$_3$, 400 MHz]:** (δ, ppm) 7.33 (d, 2H, aromatic, *J* = 8.8 Hz), 7.64 (m, 3H, aromatic), 7.73 (s,

1H, aromatic), 8.00 (d, 2H, aromatic, J = 8.8 Hz), 13.73 (s, 1H, NH); **^{13}C-NMR [CDCl$_3$, 100 MHz]:** (δ, ppm) 113.8, 119.9, 120.0, 120.2 (2C) (aromatic Cs), 122.3 (CF$_3$), 124.4, 124.5 (aromatic Cs), 130.8 (CF$_3$), 132.6, 132.9 (aromatic Cs), 140.4 (CF$_3$), 152.9 (C-5), 158.4 (C-3), 163.9 (C=O). **LC-MS/MS** (C$_{19}$H$_9$F$_9$N$_4$O$_3$): m/z 536, 18 % (M$^+$Na$^+$), 513, 55 % (M$^+$), 324, 100 % (C$_{11}$H$_6$F$_6$N$_4$O$^+$), 189, 12 % (C$_8$H$_4$F$_3$O$_2$$^{\bullet+}$).

4-[2-(4'-Fluorophenyl)hydrazono]-3-(trifluoromethyl)-4-4H-pyrazol-3-benzoate

(124e): Orang; yield 79 %; **mp** = 227 – 229 °C; **IR [KBr, cm^{-1}]:** 3416 (NH/OH), 1733 (C=O); **^{1}H-NMR [DMSO-d_6, 400 MHz]:** (δ, ppm) 7.31 (m, 2H, , aromatic), 7.51 (m, 2H, aromatic), 7.62 (m, 1H, aromatic), 7.70 (q, 2H, aromatic), 7.83 (m, 2H aromatic), 12.64 (s, 1H, NH); **^{13}C-NMR [DMSO-d_6, 100 MHz]:** (δ, ppm) 117.1 118.5,119.9, 121.2, 122.2, 128.7 (2C), 130.5 (2C), 132.8 (aromatic Cs), 133.5 (C-4), 138.6 (C-1´), 140.6 (CF$_3$), 156.6 (C-4´) 160.0 (C-5), 162.5 (C-3), 165.6 (C=O). **Anal. Calcd** for C$_{17}$H$_{10}$F$_4$N$_4$O$_2$: C, 53.98; H, 2.66; N, 14.81; Found: C, 54.23; H, 2.76; N, 15.05.

4-[2-(3'-Nitrophenyl)hydrazono]-3-(trifluoromethyl)-4-4H-pyrazol-3-benzoate

(124f): Yellow; yield 90 %; **mp** = 216 – 217 °C; **IR [KBr, cm^{-1}]:** 3432 (NH/OH), 1725 (C=O), **^{1}H-NMR [DMSO-d_6, 400 MHz]:** (δ, ppm) 7.54 (m, 1H, aromatic), 7.71 (m, 2H, aromatic), 7.85 (d, 1H, aromatic, J = 7.6 Hz), 8.04 (m, 4H, aromatic), 8.45 (s, 1H, aromatic), 12.75 (s, 1H, NH); **^{13}C-NMR DMSO-d_6, 100 MHz]:** (δ, ppm) 111.8, 117.4, 120.1, 121.9, 122.1, 123.2, 128.3 (2C), 130.6 (2C), 131.1, 133.7 (aromatic Cs), 140.7 (CF$_3$), 141.1 (C-3´), 149.3 (C-5), 158.4 (C-3), 165.1 (C=O). **LC-MS/MS** (C$_{17}$H$_{12}$F$_3$N$_5$O$_4$): m/z 407, 25 % (M$^+$), 406, 100 % (C$_{17}$H$_{11}$F$_3$N$_5$O$_4$$^{\bullet+}$), 302, 10 % (C$_{10}H_7F_3N_5O_3$$^{\bullet+}$), 105, 15 % (C$_7H_5O^{\bullet+}$).

4-(2-(3'-Nitrophenyl)hydrazono)-5-(trifluoromethyl)-pyrazoyl-4''-fluorobenzoate

(124g): Yellow; yield 96 %; **mp** = 189 – 190 °C; **IR [KBr, cm⁻¹]:** 3473 (NH/OH), 1733 (C=O), **¹H-NMR [CDCl₃, 400 MHz]:** (δ, ppm) 7.19 (m, 2H, aromatic), 7.68 (t, 1H, aromatic, J = 8.0 Hz), 7.81 (m, 1H, aromatic), 7.97 (m, 2H, aromatic), 8.17 (m, 1H, aromatic), 8.33 (t, 1H, aromatic, J = 2.0 Hz), 13.72 (s, 1H, NH); **¹³C-NMR [CDCl₃, 100 MHz]:** (δ, ppm) 111.8, 115.6, 115.8 117.3, 122.0, 123.0, 127.1, 131.5, 133.5, (aromatic Cs), 133.6, (C-4), 140.7 (CF₃), 141.0 (C-1'), 149.3 (C-3'), 158.3 (C-5), 163.8 (C-3), 164.7 (C-4''), 167.2 (C=O). **LC-MS/MS** ($C_{17}H_{11}F_4N_5O_4$): m/z 425, 25 % (M⁺), 424, 88 % ($C_{17}H_{10}F_4N_5O_4^{•+}$), 362, 100 % ($C_{17}H_{13}F_3N_4O_2^{+}$), 406, 100 % ($C_{17}H_{11}F_3N_5O_4^{•+}$), 302, 10 % ($C_{10}H_7F_3N_5O_3^{•+}$), 105, 15 % ($C_7H_5O^{•+}$).

4-(2-(4'-Bromophenyl)hydrazono)-3-(trifluoromethyl)-4,5-dihydro-1H-pyrazol-5-yl

benzoate **(124h):** Dark orange; yield 82 %; **mp** = 260 – 261 °C; IR [KBr, cm⁻¹]: 3411(NH/OH), 1738 (C=O); **¹H-NMR [DMSO-*d₆*, 400 MHz]:** (δ, ppm) 7.54 (m, 2H, aromatic), 7.65 (m, 5H, aromatic), 7.85 (m, 2H, aromatic), 12.65 (s, 1H, NH); **¹³C-NMR [DMSO-*d₆*, 100 MHz]:** (δ, ppm) 119.8, 119.9. 122.8, 128.6 (2C), 129.0, 129.7, 130.4 (2C), 132.7, 133.0 (aromatic Cs), 133.4 (C-4), 140.6 (CF₃), 141.2 (C-1'), 156.4 (C-5), 165.5 (C-3), 167.8 (C=O). **Anal. Calcd** for $C_{17}H_{10}BrF_3N_4O_2$: C, 46.49; H, 2.30; N, 12.76; Found: C, 46.80; H, 2.45; N, 13.07.

2.2.9 Synthesis of (*N²*-Benzoyl)-4-(3'-arylhydrazono)-5-trifluoromethyl pyrazolone 127a-d

Synthesis of Benzohydrazide 125

A mixture of hydrazine hydrated (1.0 mmol, 0.03 g) and pyridine (1.0 ml) were stirred in methylene chloride (20 mL) at 0 °C for 15 min. Benzoyl chloride (2.0 mmol, 0.23 ml) was added dropwise into the reaction mixture with stirring. The reaction mixture was continuously stirring at room temperature until the reaction

mixture was judged complete by the TLC (ethyl acetate : hexane, 3:7). To this reaction mixture, hexane (10 mL) was added dropwise until a white precipitate formed. The precipitate was filtered off and dried; yield 94 %; **mp** = 112-114 ^{o}C; **^{1}H-NMR [DMSO-d_6, 400 MHz]**: (δ, ppm) 8.81 (s, H, NH), 6.88 (d, 2H, C-3), 6.55 (m, 1H, C-5), 6.49 (m, 2H, C-4), 3.52 (s, 2H, NH$_2$); **^{13}C-NMR [DMSO-d_6, 100 MHz]**: (δ, ppm) 127.4 (C-3), 128.8 (C-4), 131.5 (C-5), 167.0 (C-1).

Synthesis of N^2-benzoyl- 5-trifluoromethylpyrazolone 126

2-*N*-benzoyl-5-trifluoromethyl pyrazolone **126** was obtained by the reaction of ethyl 4,4,4-trifluoro-3-oxobutanoate (0.1 mol, 21.41 mL) with benzohydrazide **125** (0.1 mol, 13.61 g) in ethanol (150 mL) and refluxed for 18 hours. The precipitat was filtered, washed with cold ethanol then air dried to offered white crystals; yield 90%. **mp** = 127-128°C; **^{1}H-NMR [DMSO-d_6, 400 MHz]**: (δ, ppm) 3.91 (s, 2H, CH$_2$), 7.52 (t, 2H, aromatic), 7.62 (m, 1H, aromatic), 7.77 (m, 2H, aromatic), 11.55 (s, 1H, OH); **^{13}C-NMR [DMSO-d_6, 100 MHz]:** (δ, ppm) 14.36 (C-4), 119.9 (C-6), 122.6 (C-2"), 128.9 (C-3"), 129.0 (C-4"), 132.7 (C-5"), 133.2 (C-5), 167.0 (C-1")

Synthesis of N^2-Benzoyl-4-(3'-arylhydrazono)-5-trifluoromethylpyrazolone 127a-c

A solution of sodium nitrite (0.01 mol, 0.85 g) in water (10.0 mL) was added dropwise with stirring to a solution of aniline hydrochloride in water (2.0 mL) at 0 ^{o}C. The above mixture was added dropwise with stirring to a cold solution of compound **126** (0.01 mol, 2.39 g) in ethanol (25 mL) and sodium acetate (10.0 mmol, 0.82 g). The reaction mixture was stirred at room temperature for 3 hr. The solid was filtrated; washed with cold H$_2$O (2 x 5 mL), dried and crystallized from ethanol yielding compounds **127a-c**.

N²-Benzoyl)-4-(3'-trifluoromethylphenylhydrazono)-5-trifluoromethylpyrazolone

(**127a**): Yield 95 %; **mp** = 205 – 209 °C **IR [KBr, cm⁻¹]**: 3438 (NH/OH), 1727 (C=O), 1538 (C=C); **¹H-NMR[DMSO-*d₆*, 400 MHz]:** (δ, ppm) 7.39 (m, 5H, aromatic), 7.50 (m, 4H, aromatic), 12.71 (s, 1H, NH); **¹³C-NMR [DMSO-*d₆*, 100 MHz]:** (δ, ppm) 117.6, 117.8, 120.5, 122.8, 124.8, 128.3, 129.4 (aromatic Cs), 129.7 (C4) , 130.1, 131.1, 131.9, 133.3 (aromatic Cs), 136.5 (CF₃), 139.6 (C-5), 157.6 (C-3), 164.9 (C=O), **Anal. Calcd** for $C_{18}H_{10}F_6N_4O_2$: C, 50.48; H, 2.35; N, 13.08; Found: C, 50.79; H, 2.66; N, 13.39.

(N²-Benzoyl)-4-[2-(2',4'-dichlorophenyl)hydrazono]-3-(trifluoromethyl)-1H-pyrazolone (**127b**): Yield 93 %; **mp** = 209 – 211 °C, **IR [KBr, cm⁻¹]**: 3415 (NH/OH), 1732 (C=O), 1542 (C=C); **¹H-NMR[DMSO-*d₆*, 400 MHz]:** (δ, ppm) 7.56 (m, 3H, aromatic), 7.76 (m, 3H, aromatic), 12.92 (s, 1H, NH); **¹³C-NMR [DMSO-*d₆*, 100 MHz]:** (δ, ppm) 117.6, 122.6, 123.2, 125.0, 128.3, 128.6, 129.4, 129.7 (C-4), 130.1, 131.1, 131.8 (aromatic Cs), 133.4 (CF₃), 136.1 (C-5), 157.6 (C-3), 164.9 (C=O); **Anal. Calcd** for $C_{17}H_9Cl_2F_3N_4O_2$: C, 47.57; H, 2.11; N, 13.05; Found: C, 48.17; H, 2.71; N, 13.65.

(N²-Benzoyl)-4-(3'-nitrophenylhydrazono)-5-trifluoromethylpyrazolone (**127c**) **:** Yield 89 %; **mp** = 223 – 225 °C; **IR (KBr, cm⁻¹)**: 3412 (NH/OH), 1725 (C=O), 1660 (C=O); **¹H-NMR[DMSO-*d₆*, 400 MHz]:** (δ, ppm) 7.60 (m, 2H, aromatic), 7.73 (m, 1H, aromatic), 7.87 (m, 6H, aromatic), 12.93 (s, 1H, NH); **¹³C-NMR [DMSO-*d₆*, 100 MHz]:** (δ, ppm) 112.5, 118.3, 121.0, 123.1, 129.0 (2C), 129.6, 129.7, 130.6 (2C) (aromatic Cs), 131.6 (C-4), 132.3, 133.9, 136.6 (aromatic Cs), 139.7 (CF₃), 140.1 (C-5), 158.1(C-3), 165.1 (C=O); **Anal. Calcd** for $C_{17}H_{10}F_3N_5O_4$: C, 50.38; H, 2.49; N, 17.28; Found: C, 50.74; H, 2.85; N, 17.64.

2.3 Results and Discussion

Fluorinated pyrazolones and their nucleoside derivatives are mainly an interesting field in chemistry and medicine science. Introducing mono-fluorine atom or trifluoromethyl group in place of hydrogen atoms often enhance the biological activity of the aglycone [101]. Therefore, efforts for designing new pyrazolone nucleosides substituted with fluorine in different positions have been achieved using two sugar moieties such as D(+)ribose and D(+)-2-deoxyribose. Pyrazolone derivatives **113a-i** prepared according to the literature method [102] with improving the overall yield as outlined in Scheme 31 and then allowed to react with various activated sugar derivatives under various experimental conditions to produce noval pyrazolone nucleosides **116-123**.

2.3.1 Synthesis of 5-trifluoromethyl-2,4-dihydropyrazol-3-ones 113a-i
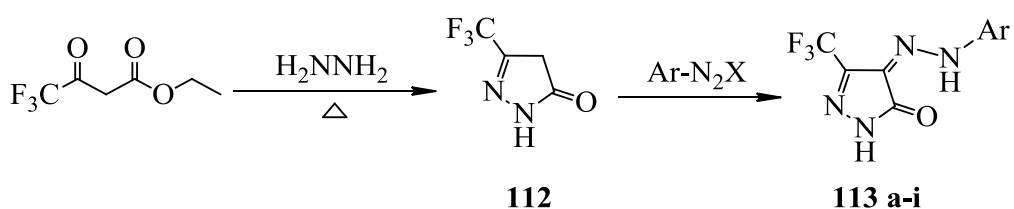
Scheme 31**:** Synthesis of 4-arylhydrazono-5-trifluoromethyl-2,4-dihydropyrazol-3-ones **113 a-i**

2,4-dione and hydrazine to produce 5-trifluoromethyl-2,4-dihydropyrazol-3-one **112**. In the first step, hydrazine as nucleophile attacks the more electropositive center followed by 5-exo trig cyclization to form the final product **112**. The mechanism in (Scheme 32) explains the reaction between trifluoromethyl

Table 1: The synthesized 4-arylhydrazono-5-trifluoromethyl-2,4-dihydropyrazol-3-ones yiels compared with the literature ones

Entry	Ar	mp (^{o}C)	Yield %	lit. mp (^{o}C)	lit. yield %
112	-	208-209	96.3	207-208	15
113a	3'-fluorophenylhy	211-213	99.3	201-203	78
113b	4'-fluorophenyl	217-218	93.0	212-214	75
113c	3'-trifluoromethylphenyl	221-222	99.6	218-220	85
113d	3'-chlorophenyl	238-240	94.0	New	-
113e	4'-chlorophenyl	226-228	93.0	220-221	94
113f	2',4'-dichlorophenyl	239-241	90.0		78
113g	3'-nitrophenyl	251-254	98.0		75
113h	4'-bromophenyl	214-216	86.0	New	85
113i	2-(pyren-2-yl)	256-258	94.0	New	-
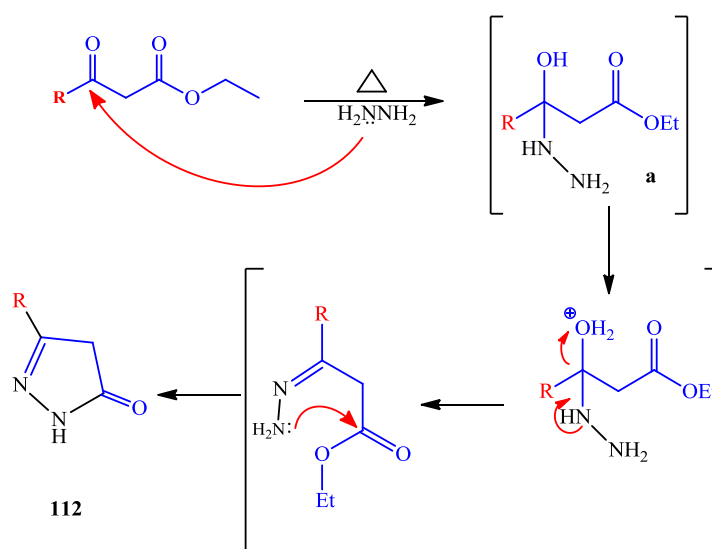
Scheme 32: Suggested mechanism for the synthesis of 5-trifluoromethyl-2,4-dihydropyrazol-3-one

Microwave mediated organic reactions are typically environment friendly, safe, and rapid as compared to conventional methods. CEM Microwave reactor was used to synthesize 5-trifluoromethyl-2,4-dihydropyrazol-3-one **112** with various conditions as shown in Table 2.

Table 2: Microwave conditions used to synthesized 5-trifluoromethyl-2,4-dihydropyrazol-3-one **112**

Entry	Mixing Temp (^{o}C)	MW Temp (^{o}C)	Reaction Period (min)	Yield %
1	rt	75	5	0
2	rt	75	10	19
3	rt	75	12	26
4	rt	75	15	31
5	rt	75	30	33
6	rt	75	35	34
7	0-5	75	30	32
8	0-5	150	60	39
9	0-5	75	60	42
10	rt	75	60	45
11	rt	150	60	51

The structure of 5-trifluoromethyl-2,4-dihydropyrazol-3-one **112** and the obtained azopyrazolones have been confirmed according to their spectroscopic data analysis.
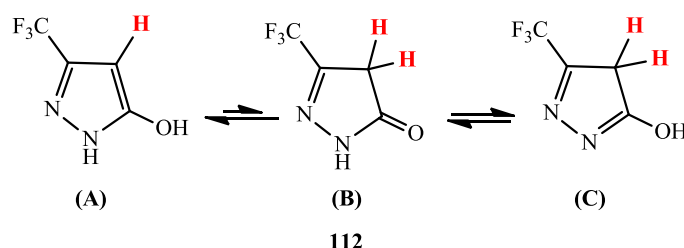
Scheme 33: Resonance structures of 5-trifluoromethyl-2,4-dihydropyrazol-3-one **112**

5-Trifluoromethyl-2,4-dihydropyrazol-3-one **112** shown in Scheme 33 is existing in form **A** in polar aprotic solvents according to ^{1}H-NMR (400 MHz, DMSO-d_6) data (Figure 13). The ^{1}H-NMR analysis in DMSO-d_6 showed H-4 as a singlet at δ 5.66 ppm. In addition, two protons appeared at δ 11.25 ppm and δ 12.84 ppm exchangeable with D_2O were assigned to NH and OH protons, respectively. To confirm the existing of both isomers **B** and **C**, the ^{1}H-NMR was carried out in D_2O

(Figure 14). The ^{1}H-NMR showed two signals at δ 2.67 ppm and δ 3.06 ppm corresponding to the methylene protons **112 B** (Figure 13, 14).
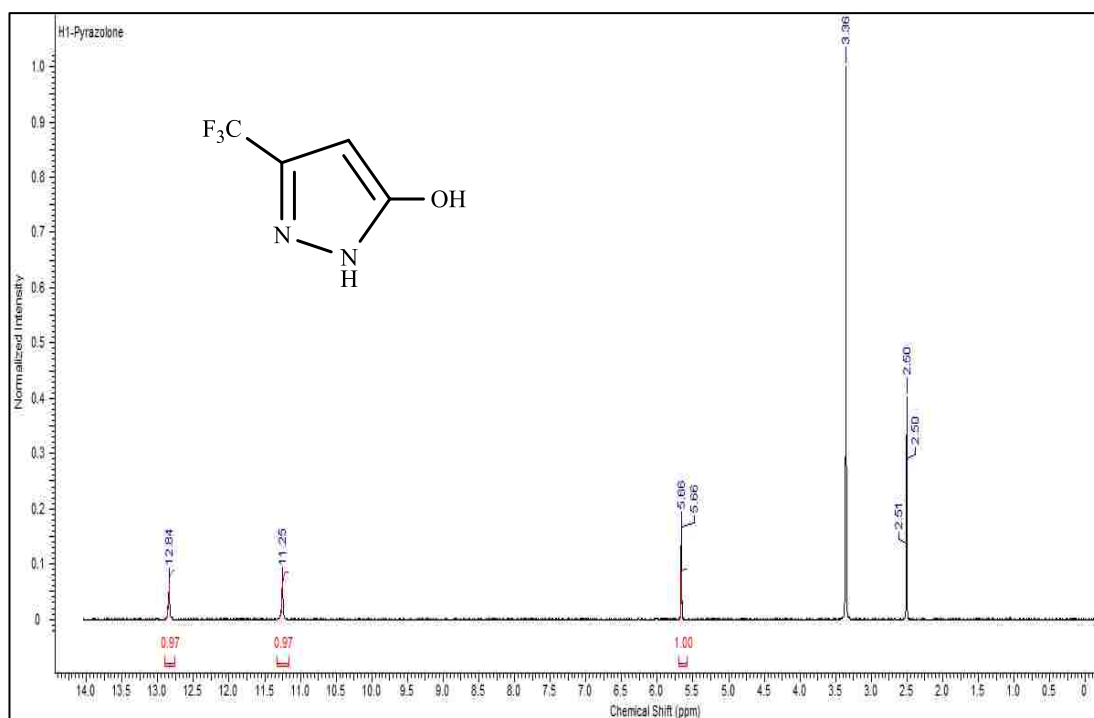
Figure 13: ^{1}H-NMR Spectrum for 5-trifluoromethyl-2,4-dihydropyrazol-3-one **112** in DMSO-d_6
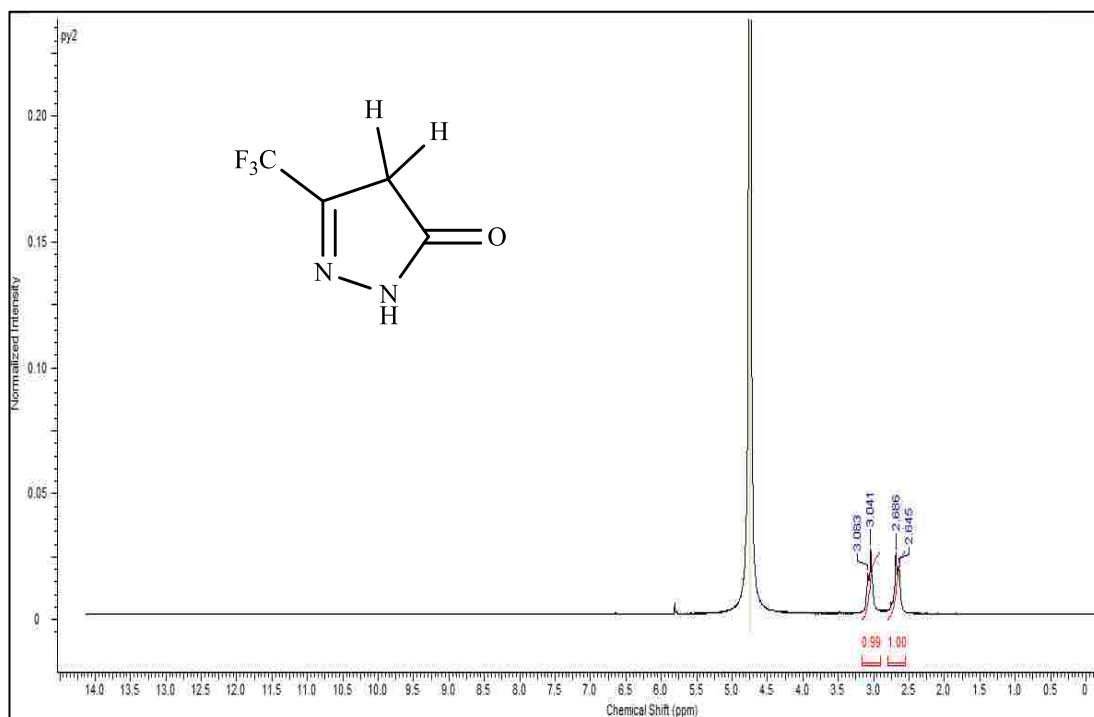
Figure 14**:** ^{1}H-NMR Spectrum for 5-trifluoromethyl-2,4-dihydropyrazol-3-one **112** in D_2O

4-Arylhydrazono-5-trifluoromethyl-2,4-dihydropyrazol-3-ones **113a-i** were synthesized by diazotization reaction of **112** using aryldiazonium salt which was conducted by using a well-developed methodology [103] and the desired azo dyes **113a-i** were obtained in high yield 94 % (Scheme 34).

The general synthetic mechanism of alryl hydrazone is shown in Scheme 34. The diazodization step was carried out in acidic condition with stirring at $0 - 5^{o}C$. Three structures are in equilibrium **112 A-C**, under an acidic condition, pyrazolone **112B** was activated then allowed to react with arydiazonium salt to afford the final products **113a-i**.
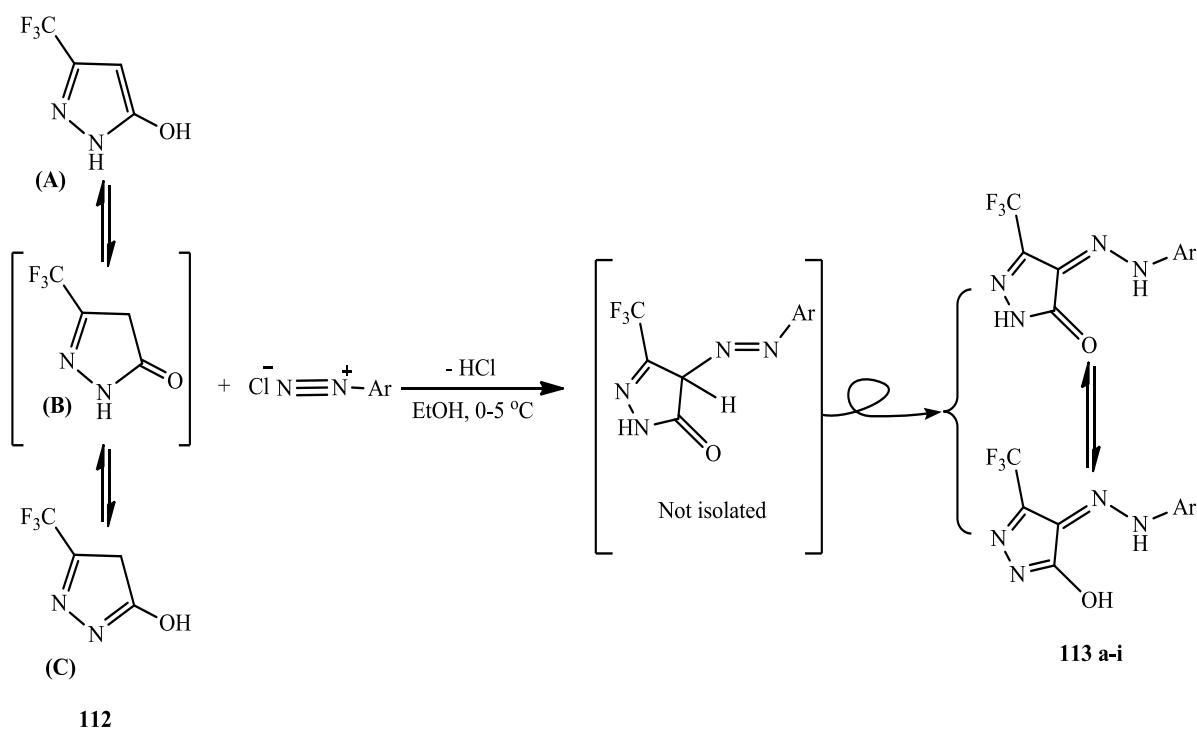
Scheme 34: Suggested mechanism for the synthesis of 5-trifluoromethyl-2,4-dihydropyrazol-3-ones **113 a-i**

To confirm the correct structure of the final products, spectroscopic analysis of 4-(3'-fluorophenylhydrazono)-5-trifluoromethyl-2,4-dihydropyrazol-3-one **113a**, was used. FT-IR assigned the functional groups such as the appearance of broad peak at ν 3421 cm^{-1} prove the existing of hydroxy group. The peak at ν 1635 cm^{-1} assigns for C=C while the peak at ν 1558 cm^{-1} assigns for C=N; and the peak at 1384 cm^{-1} assign for O-H bending in plan (Figure 15).
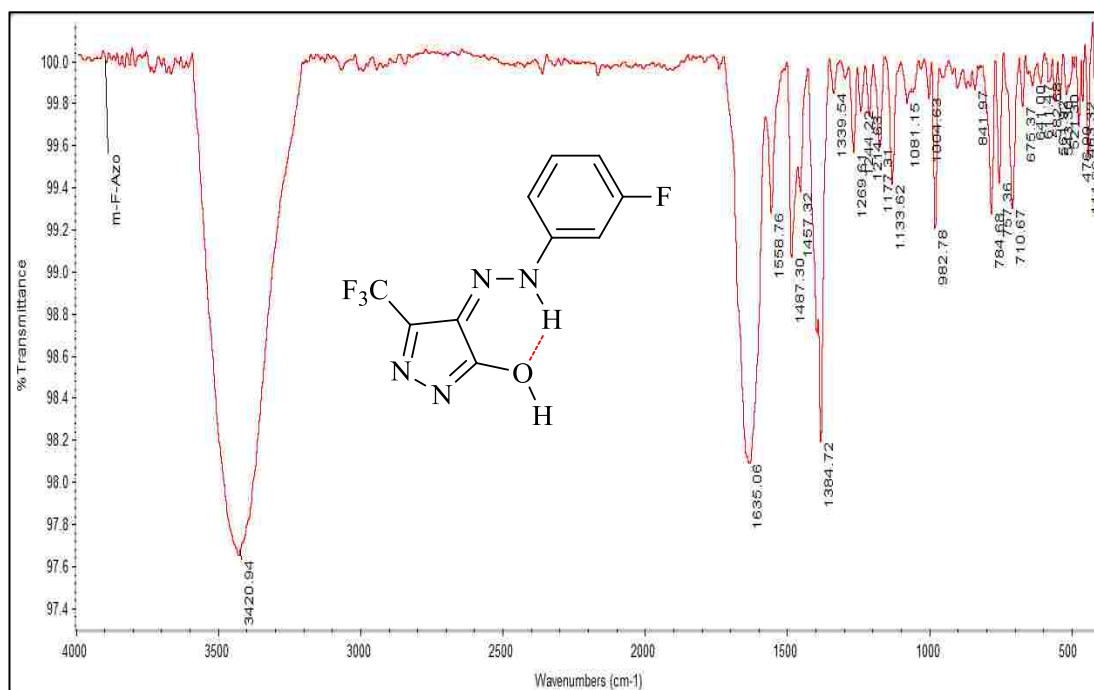
Figure 15: IR Spectrum of 4-(3'-fluorophenylhydrazono)-5-trifluoromethyl-2,4-dihydropyrazol-3-one **113a**

^{1}H-NMR (400 MHz, DMSO-d_6) was used to confirm the suggested structure. For example, compound **113a** shows a singlet at δ 7.10 ppm assigned for one aromatic proton at 2'-position while other aromatic protons resonate at 4',5' and 6' positions as multiplets at δ 7.45 - 7.54 ppm integrated to three protons. ^{1}H-NMR shows sharp singlet resonates at δ 12.67 ppm corresponding to one proton NH; the disappearance of the second imino-proton can be explained due to the formation of

hydrogen-bond with oxygen at C-3 (Figure 16). The ^{13}C-NMR spectrum (100 MHz, DMSO-d_6) of compound **113a** gave the correct number of carbons on the right chemical shift for each carbon (Figure 17).
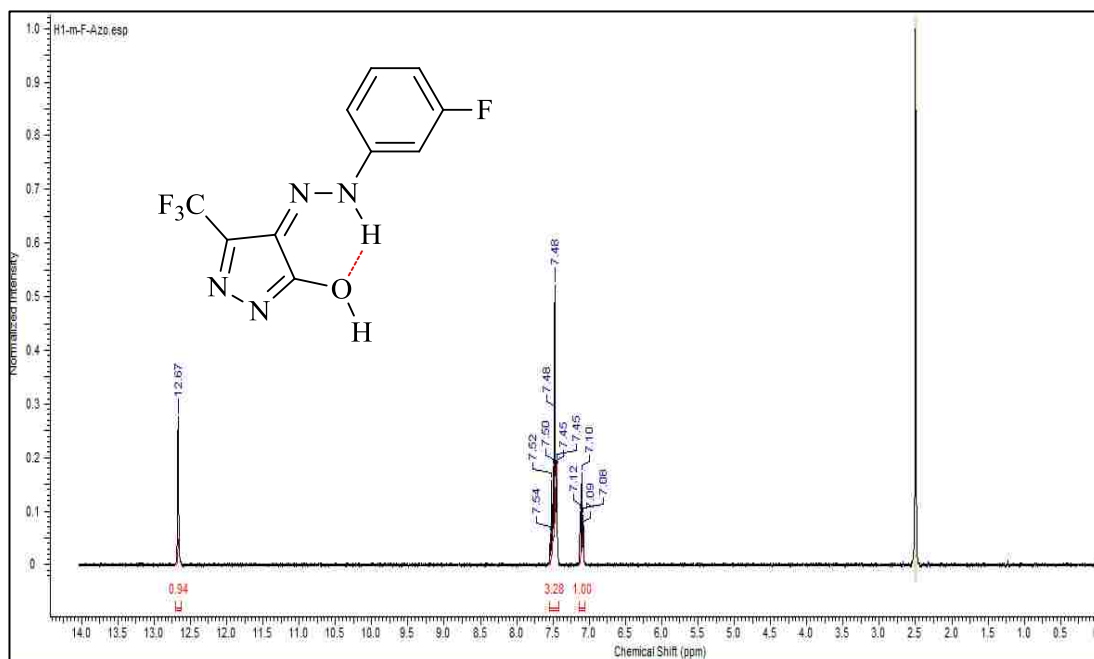
Figure 16: ^{1}H-NMR spectrum for 4-(3'-fluorophenylhydrazono)-5-trifluoromethyl-2,4-dihydropyrazol-3-one **113a** in DMSO-d_6
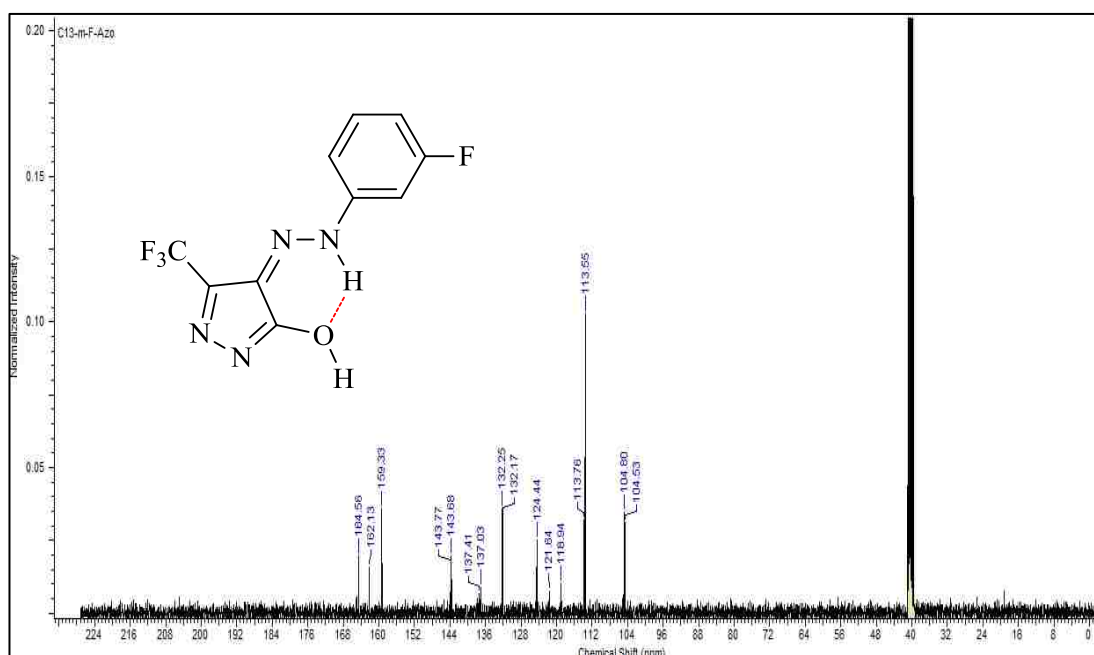
Figure 17: ^{13}C-NMR Spectrum for 4-(3'-fluorophenylhydrazono)-5-trifluoromethyl-2,4-dihydropyrazol-3-one **113a** in DMSO-d_6

2.3.2 Synthesis of Pyrazolinone Ribosides

To achieve our goal in enhancing the bioavailability of the pyrazolinone moieties, ribose derivatives introduced to two different nucleophlic centers in the pyrazolone ring. The silyl-method is used to activate the pyrazolone ring, while the ribose was used as 1-acetyl analog that activated by Lewis acid catalyst. The sensitivity of both silyl pyrazolone and sugar needs dry conditions to achieve the final products **116** and **117**. Hexamethyldisilazane (HMDS) was found a suitable silylating agent to activate the pyrazolone in the form of 3-trimethylsilyloxy pyrazoline **114** intermediate while ten (IV) chloride or trimethylsilyl trifluoromethanesulfonate (TMSOTf) was used as a catalyst in two solvents (CH$_3$CN, CH$_2$Cl$_2$). The activated ribose allowed to react with the silyl intermediate (**114**) to afford the target products **116** and **117** (Scheme 35). The synthesis of *O-* and *N-* isomer was controlled by the reaction time. The silyl intermediate **114** reacts with an activated surge in either dry acetonitrile or methylene chloride for 4 hours at room temperature. The reaction afford *O-* and *N-* nucleosides, isolated and identified as 3-(2",3",5"-tri-*O*-acetyl-*β*-D-ribofuranosyloxy)-4-(3'-fluorophenylhydrazono)-5-trifluoromethyl-2,4-dihydropyrazoline (**116a**) and **2**-(2",3",5"-tri-*O*-acetyl-*β*-D-ribofuranosyl)-4-(3'-fluorophenylhydrazono)-5-trifluoromethyl-2,4-dihydropyrazole **117a** in yield 66% and 34% respectively. The mechanism of the reaction can be explained as follow: the silyl group increases the electron-density at the neighboring oxygen atom, that attacks to the acyl oxonium ion from the *β*-face producing the 3-(2",3",5"-tri-*O*-acetyl-*β*-D-ribofuranosyloxy)-4-(arylhydrazono)-5-trifluoromethyl-2,4-dihydropyrazoline **116** or by increasing the electron-density around *N*-3 that attacks the activated sugar from the *β*-face as well to form the *N*-isomer **117** (Scheme 35).
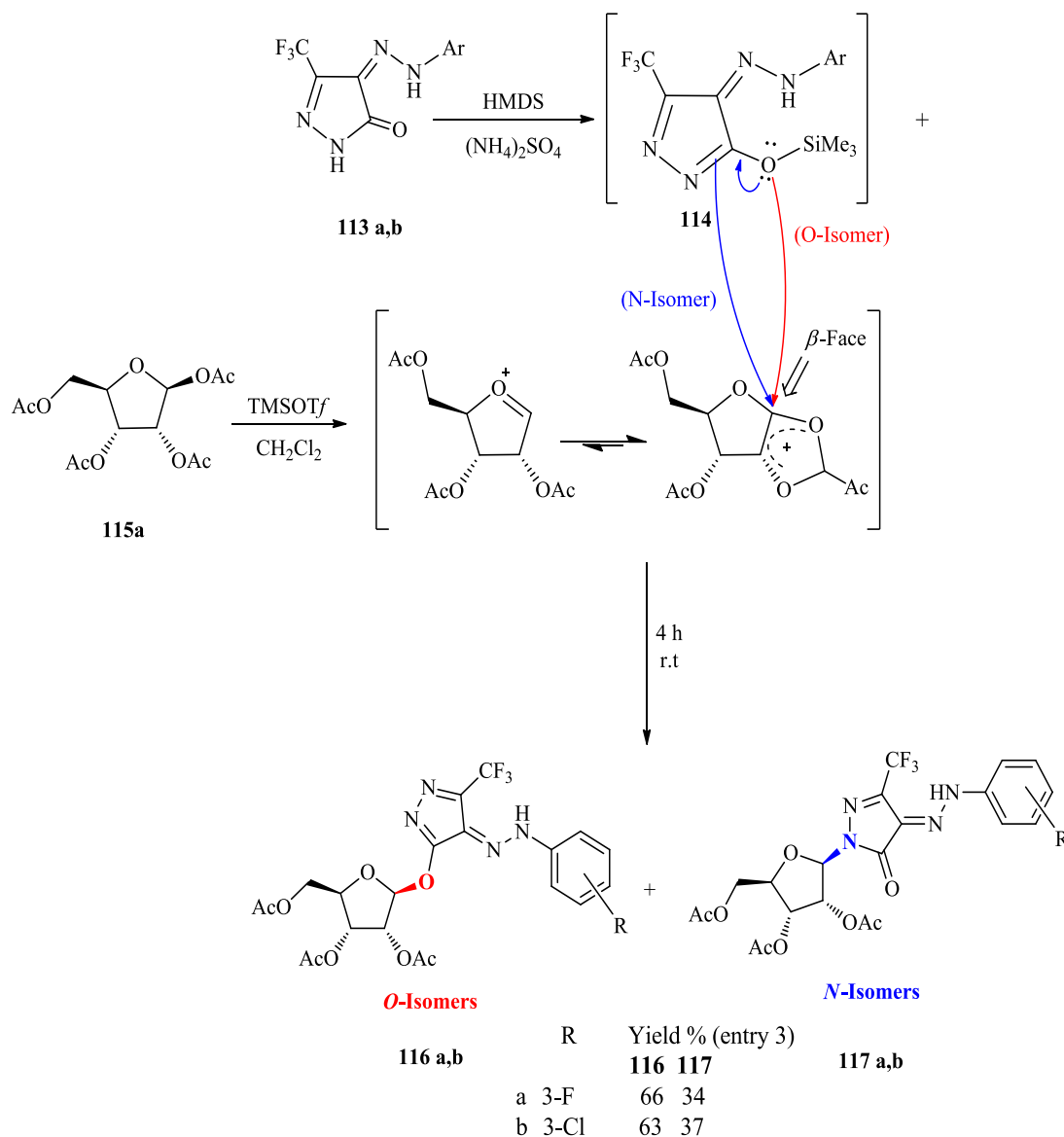
Scheme 35: Synthesis of *O*- and *N*- Pyrazolone Ribosides

The structure of *O*-ribose products **116a,b** were confirmed using FT-IR, ^{1}H-NMR, ^{13}C-NMR and LC-MS. The IR confirmed the formation of 3-(2",3",5"-tri-*O*-acetyl-*β*-D-ribofuranosyloxy)-4-(3'-fluorophenylhydrazono)-5-trifluoromethyl-2,4-dihydropyrazoline **116a** by the appearance of a new sharp signal at ν = 1751 cm^{-1} assigined to the acetyl ester at the sugar moiety while no signals observed at ν = 1640-1690 cm^{-1} related to the carbonyl imid of pyrazoline. NMR data also confirmed

the suggested structures. For example,^{1}H-NMR (400 MHz, CDCl₃) showed new three signals at δ 2.12, 2.13, and 2.16 ppm corresponding to three methyl groups, while ribose anomeric proton appeared as a doublet at δ 6.01 ppm integrated to one proton with coupling constant J = 4.0 Hz confirmig the diaxial oriantation in β-form. While other sugar protons H-5"a , 4", 5"b, 3", and 2", resonate at δ 3.71, 4.19, 4.44, 5.71, 5.90 ppm respectively. The aromatic protons of **116a** appeared as multiplets at 6.98-7.39 ppm (Figure 18).

Figure 18: ^{1}H-NMR Spectrum for 3-(2",3",5"-tri-*O*-acetyl-β-D-ribofuranosyloxy)-4-(3'-fluorophenylhydrazono)-5-trifluoromethyl-2,4-dihydropyrazoline **116a**

^{13}C-NMR (100 MHz, CDCl₃) also used to confirm the correct number of carbon atoms at the correct chemical shifts. The anomeric carbon resonates at δ 90.2 ppm though C-5 appeared at δ 153.6, ppm and C-3 appeared at δ 162.0 ppm. A complete set of assigned carbons are presented in (Figure 19).
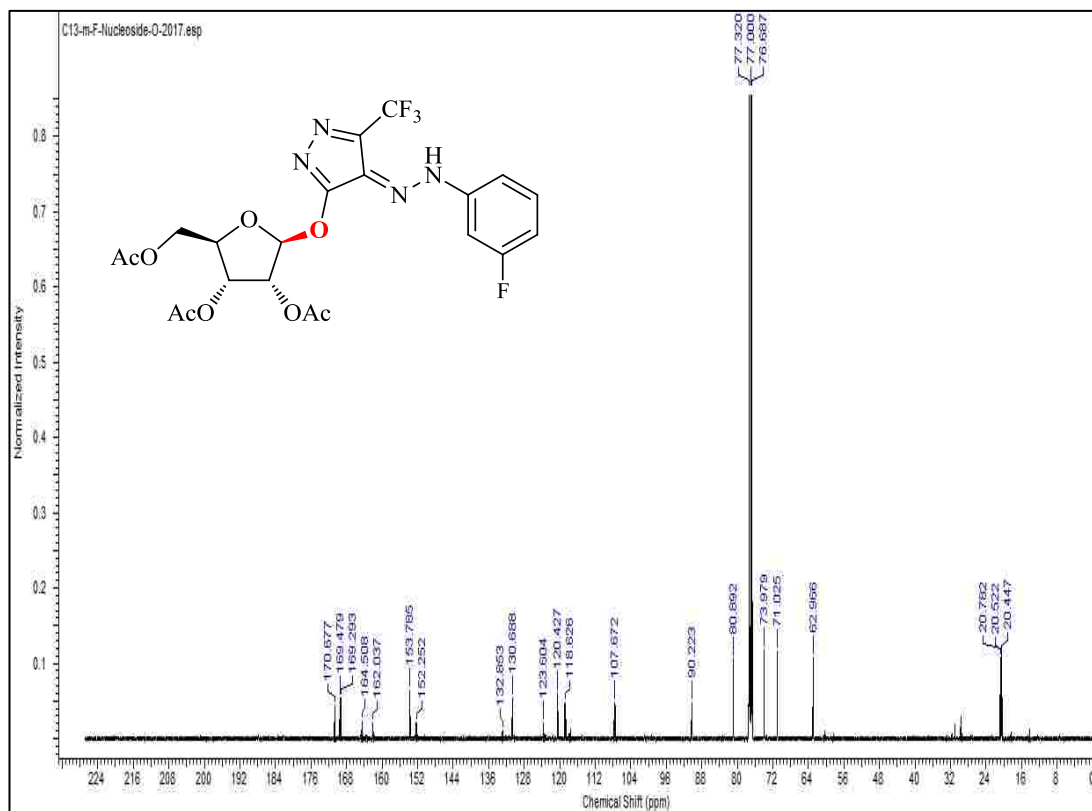
Figure 19: ^{13}C-NMR Spectrum for 3-(2",3",5"-tri-*O*-acetyl-*β*-D-ribofuranosyloxy)-4-(3'-fluorophenylhydrazono)-5-trifluoromethyl-2,4-dihydropyrazoline **116a**

Long-range heteronuclear correlation gHMBC (400 MHz, CDCl$_3$) was used to assign the ^{1}H-^{13}C interaction. Strong cross-peak interactions were found between the anomeric proton H-1" (δ 6.01 ppm) with C-2" (δ 74.0 ppm) of the sugar moiety. While H-3" (δ 5.71 ppm) showed cross-peak interaction with C-1", C-2" and C-5" at (δ 90.2, 74.0 and 62.9 ppm); respectively. H-5"a (δ 4.44 ppm) showed cross-peak interaction with C-2" (δ 74.0 ppm). While H-4" (δ 4.19 ppm) showed cross-peak interaction with both of C-3" at (δ 71.0 ppm). Both H-3" (δ 5.71 ppm) and H-4" (δ 4.19 ppm) showed a week cross-peak interactions with acetoxy carbonyl carbon of the sugar moiety at (δ 169.5 and 170.7 ppm) (Figure 20).
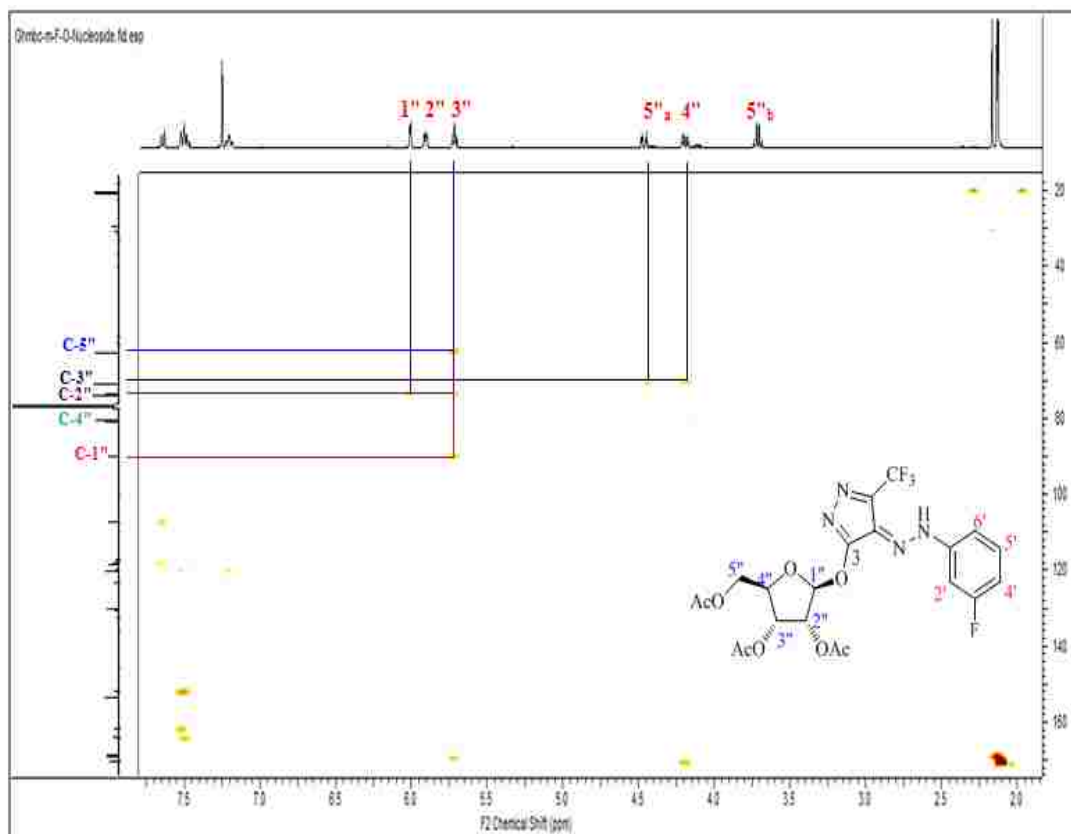
Figure 20: 2D- gHMBC Spectrum for 3-(2",3",5"-tri-*O*-acetyl-*β*-D-ribofuranosyloxy)-4-(3'-fluorophenylhydrazono)-5-trifluoromethyl-2,4-dihydropyrazoline **116a**

Mass spectroscopic was used to confirm the formation of the targeted product **116a.** The total molecular ion peak appeared at m/z 533 with 35% intensity (Figure 22). The fragment mass analysis scheme shows the pattern of fragmentation with its relative intensity (Scheme 36).

2.3.3 Solvent and Catalyst Effects

To study the effect of the solvent and/or catalyst on regioselective synthesis, a complete study was reported as shown in Table 3. Eleven different reaction conditions were carried out to study the regioselectivety of the *O-* and *N*-isomers as nucleophile counters in the pyrazoline ring. In entry 1, the conditions were optimized using TMSOT*f* as catalyst in acetonitrile for 4 h at room temperature afforded only

one isomer identified as *O*-riboside **116a** while tin (IV) chloride afforded a mixture of *O*-isomer (64%) and *N*-isomer (36%) (entry 2). While entries 3 and 4 CH$_2$Cl$_2$ was used as a solvent and both SnCl$_4$ and TMSOT*f* were used in two different experiments and in the same reaction time (4h). The two reactions (entries 3 and 4) afforded *O*-isomers as major products (66%, 60%) while *N*-isomers identified in yield (34%, 40%) respectively. In entry 5, tin (IV) chloride in CH$_2$Cl$_2$ was used for 8 hs, the reaction afforded a mixture of *O*-isomer (61%) and *N*-isomer (38%). The same reaction conditions in entry 3 repeated in doubled reaction time (8 hs) (entry 7). These reaction conditions (entry 7) were found enhancing the formation of *N*-isomer (42%). From entry 1 to 7, it was noticed that time may enhance the formation of *N*-isomers, accordingly, the reaction time was increase to 10 hs using SnCl$_4$ in CH$_2$Cl$_2$ (entry 8). The reaction afforded *N*-isomer in (57%) yield in a mixture of *O*-isomer (43%). When TMSOT*f* was used in acetonitrile at room temperature for 18 hs *N*-isomer ratio increased to (62%) (entry 9), while using SnCl$_4$ gave more ratio of *N*-isomer (67%) to *O*-isomer (33%) (entry 10). Comparing both of the reaction conditions used in both entry 8 and entry 10, it is clear to notice that acetonitile shifted the reaction toward the formation of *N*-isomers (yield $\approx$ 67%). The same reaction conditions in entries 3 and 7 repeated in longer reaction time (18 hs) (entry 11); these reaction conditions afforded only one isomer identified as *N*-riboside **117a**.

Table 3: Optimum synthesis conditions for *O*- and *N*-ribosides isomers

Entry	Condensation conditions [a]	Products	Yield of *O* (%)[b]	Yield of *N* (%)[b]
1	TMSOT*f*, MeCN, rt, 4 h	*O*-isomer (**116**)	67	ND[c]
2	SnCl$_4$, MeCN, rt, 4 h	*O/N* (**116/117**)	64	36
3	TMSOT*f*, CH$_2$Cl$_2$, rt, 4 h	*O/N* (**116/117**)	66	34
4	SnCl$_4$, CH$_2$Cl$_2$, rt, 4 h	*O/N* (**116/117**)	60	40
5	SnCl$_4$, CH$_2$Cl$_2$, rt, 8 h	*O/N* (**116/117**)	61	39
6	SnCl$_4$, MeCN, rt, 8 h	*O/N* (**116/117**)	62	38
7	TMSOT*f*, CH$_2$Cl$_2$, rt, 8 h	*O/N* (**116/117**)	58	42
8	SnCl$_4$, CH$_2$Cl$_2$, rt, 10 h	*O/N* (**116/117**)	43	57
9	TMSOT*f*, MeCN, rt, 18 h	*O/N* (**116/117**)	38	62
10	SnCl$_4$, MeCN, rt, 18 h	*O/N* (**116/117**)	33	67
11	TMSOT*f*, CH$_2$Cl$_2$, rt, 18 h	*N*-isomer (**117**)	ND	80

a Molar ratio sugar: pyrazole base: Catalyst – 1:1:1
b Isolated yield of *O*- and *N*- isomers by column chromatography.
c ND: Not Detected

In summary, solvents, catalyst and reaction times are controlled the regioselectivites of the reaction between silylated pyrazoline and the sugar moiety. Most particularly, the time is the most significant effect as it is noticed when solvents and catalyst are fixed (entries 3,7 and 11), the yield of *O*-isomer decrease dramatically while the yield of *N*-isomer increase gradually as shown in (Figure 21). This is may be attributed to the stability of *N*-isomer.
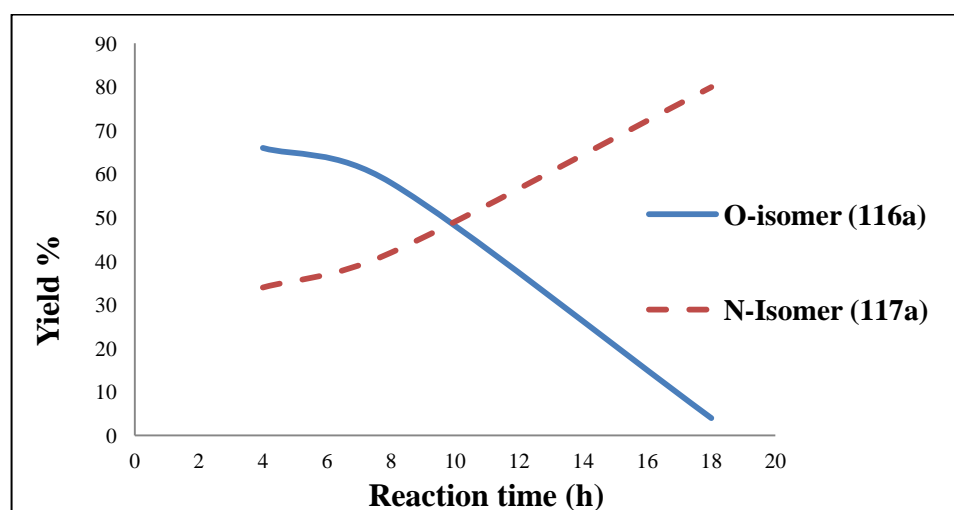
Figure 21: Effect of reaction time in controlling the regioselectivity in synthesizing **116a** and **117a** using same catalyst and solvent (TMSOT*f* and CH$_2$Cl$_2$)

Figure 22: Mass fragmentation spectrum for 3-(2'',3'',5''-tri-*O*-acetyl-*β*-D-ribofuranosyloxy)-4-(3'-fluorophenylhydrazono)-5-trifluoromethyl-2,4-dihydropyrazoline **116a**

Scheme 36: Mass fragments scheme for 3-(2",3",5"-tri-*O*-acetyl-*β*-D-ribofuranosyloxy)-4-(3'-fluorophenylhydrazono)-5-trifluoromethyl-2,4-dihydropyrazoline **116a**

2.3.4 Synthesis of Pure *N*-isomers 117c-g

Since the reaction between the silylation pyrazolone **113** and the activated sugar derivatives in the presence of Lewis acid catalyst was found to be time dependent. The reaction was repeated under an optimizing condition using dichloromethane as solvent and in presence of TMSOT*f* as catalyst for 18 hours. The reaction afforded only *N*-isomer **117c-g** (Scheme 37). The structure of the obtained product **117c-g** were confirmed spectroscopycally to insure that structures are correct as suggested. FT-IR was used to confirmed the formation of glycosidic bonds between the anomeric carbon of the sugar moiety and the N^2 of the pyrazolone. The IR-spectrum of compound **117a** showed the appearance of two main signals at ν 1680 cm^{-1} corresponding to the pyrazolone carbonyl and at ν 1749 cm^{-1} assigned to the acetoxy carbonyl carbones of the three acetyl groups allocated at C-2″, 3″ and 5″ of the ribose moiety (Figure 23). ^{1}H-NMR spectroscopy was used to confirm the suggested structures. For example ^{1}H-NMR of compound **117a** showed a slightly high filed shifting of the anomeric proton (δ 5.99 ppm) compared to the *O*-isomer (δ 6.01 ppm) **116a** which indicated the formation of *N*-glycosidic bond. While other sugar protons H-5″a , 4″, 5″b, 3″, and 2″, resonate at δ 4.15, 4.33, 4.44, 5.53, 5.69 ppm; respectively. The aromatic protons of **117a** appeared as multiplets at 6.98-7.27 ppm (Figure 24).$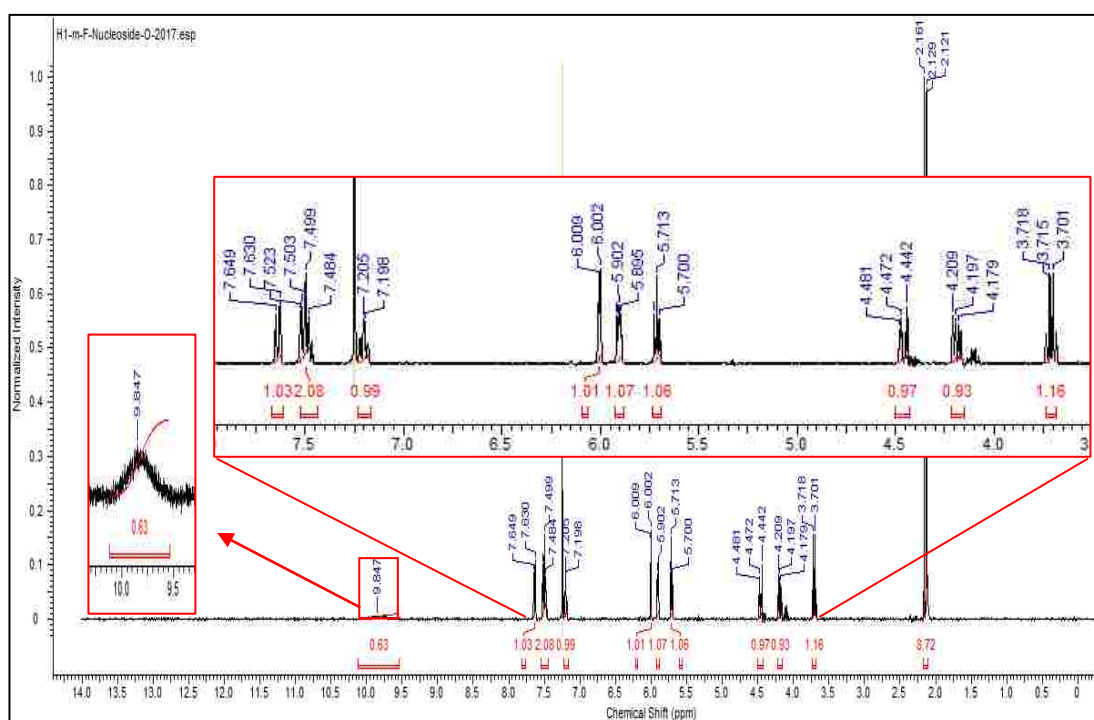^{13}$C-NMR also used to confirm the correct number of carbon atoms at the correct chemical shifts. The anomeric carbon resonates at δ 84.4 ppm while C-5 appeared at δ 157.8 ppm and C-3 appeared at δ 162.3 ppm (Figure 25).

Scheme 37: Synthesis of *N*-pyrazolinone ribosides

Compoun **117**	R	R'	Yield (%)
c	3-CF$_3$	Ac	84
d	4-F	Ac	78
e	4-Cl	Bz	66
f	3-NO$_2$	Ac	69
g	4-Br	Ac	53

The *N*-isomers **117a,b** were obtained in a mixture with **116a,b**. The pure *N*-isomer **117a,b** was separated using chromatography in yield 80%, 65%; respectively (Scheme 37). The obtained *N*-isomers **117a,b** characterized as in the next section.

The mechanism of the reaction can be explained as follow; since short reaction time afforded mixture of two isomers, the major was identified as *O*-ribosides **116a,b** and the minor is *N*-ribosides **117a,b**. The reaction was continuous under dry condition with stirring at room temperature for about 18 hours. The formation of *N*-isomer can be explained as follows: the same reaction conditions of synthesizing the mixture of *O*-and *N*-isomers, as mentioned in the previous section, are applied but the reaction time was extended up to 18 hours. The progress of the reaction was monitored by TLC (ethyl acetate: hexane, 3:7). As observed previously, the reaction initially produced the *O*-isomers. In the presence of a Lewis acid catalyst and 1-*O*-acetyl ribose derivative, rearrangement occurred to produce the *N*-isomers. The mechanism of *O*→*N* rearrangement attributed to the excess of acetyl ten tetrachloride cation and/or trimethylsilyl cation coordinate with oxygen, weaken the *O*-ribose bond. Keto-enol tatumeric increases the electron-density at nitrogen atom at

position 2 enhancing the nucleophilicity of N^2 that attacked the activated oxanium ion from β-face to form β-N-ribose isomer **117** (Scheme 38).
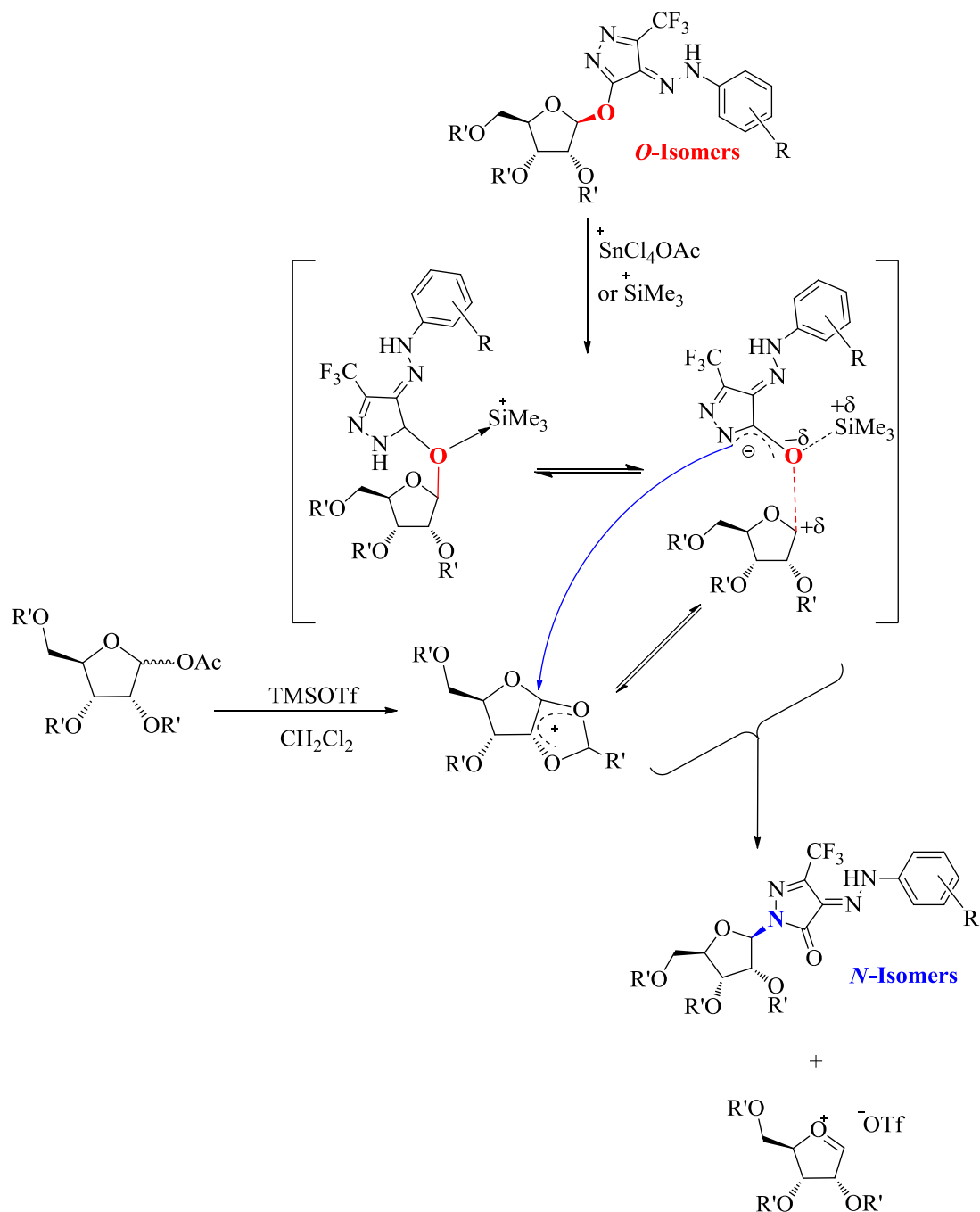
Scheme 38: Suggested mechanism of the $O \rightarrow N$ rearrangement

The formation of O- and N-ribosides **116a** and **117a**, can be analyzed using FT-IR, NMR and mass spectroscopy. For example, the IR spectra of O-riboside **116a**

and the *N*-riboside **117a** were used to distinguish between different signals appeared within ν 1640-1690 cm^{-1} corresponding to the imide-carbonyl of the pyrazoline ring.

For *O*-riboside **116a** the disappearance of the imid carbonyl at ν 1650-1690 cm^{-1} (Figure 23,A) confirms the existing of *O*-linkage, while *N*-riboside is confirmed by the existing of the imid-carbonyl at ν 1680 cm^{-1} (Figure 23, B).

On the other hand.^{1}H-NMR (400 MHz, CDCl$_3$) data was used to confirm our observation of forming *O*- and *N*-ribosides. The difference in chemical shifts of the anomeric protons in both isomers were studied, the highly shielded proton in *N*-isomer compared to highly deshielded proton in *O*–isomer gave a slightly difference in chemical shift for both products **116a**, **117a**. The anomeric proton in **116a** observed as doublet at δ 6.01 ppm while the anomeric proton in **117a** observed as doublet at δ 5.99 ppm.^{13}CNMR (100 MHz, CDCl$_3$) also confirmed the forming of *O*- and *N*-ribosides by studying the difference in chemical shift of the anomeric carbon in both isomers, the highly shielded carbon in *N*- isomer compared to highly deshielded carbon in *O*-isomer gave a difference in chemical shift for both isomers. The anomeric carbon in **116a** observed at δ 90.2 ppm while the anomeric carbon in **117a** observed at δ 84.4 ppm (Figures 24, 25).

^{19}F-NMR (376 MHz, CDCl$_3$) was used also to confirm the presences of two fluorine groups in **117a**. ^{19}F-NMR spectrum showed a singlet at δ -109.5 ppm corresponding to mono fluorobenzen. A sharp singlet appears at δ -64.5 ppm integrated to three fluorine atoms confirmig the existing of the CF$_3$ (Figure 26).
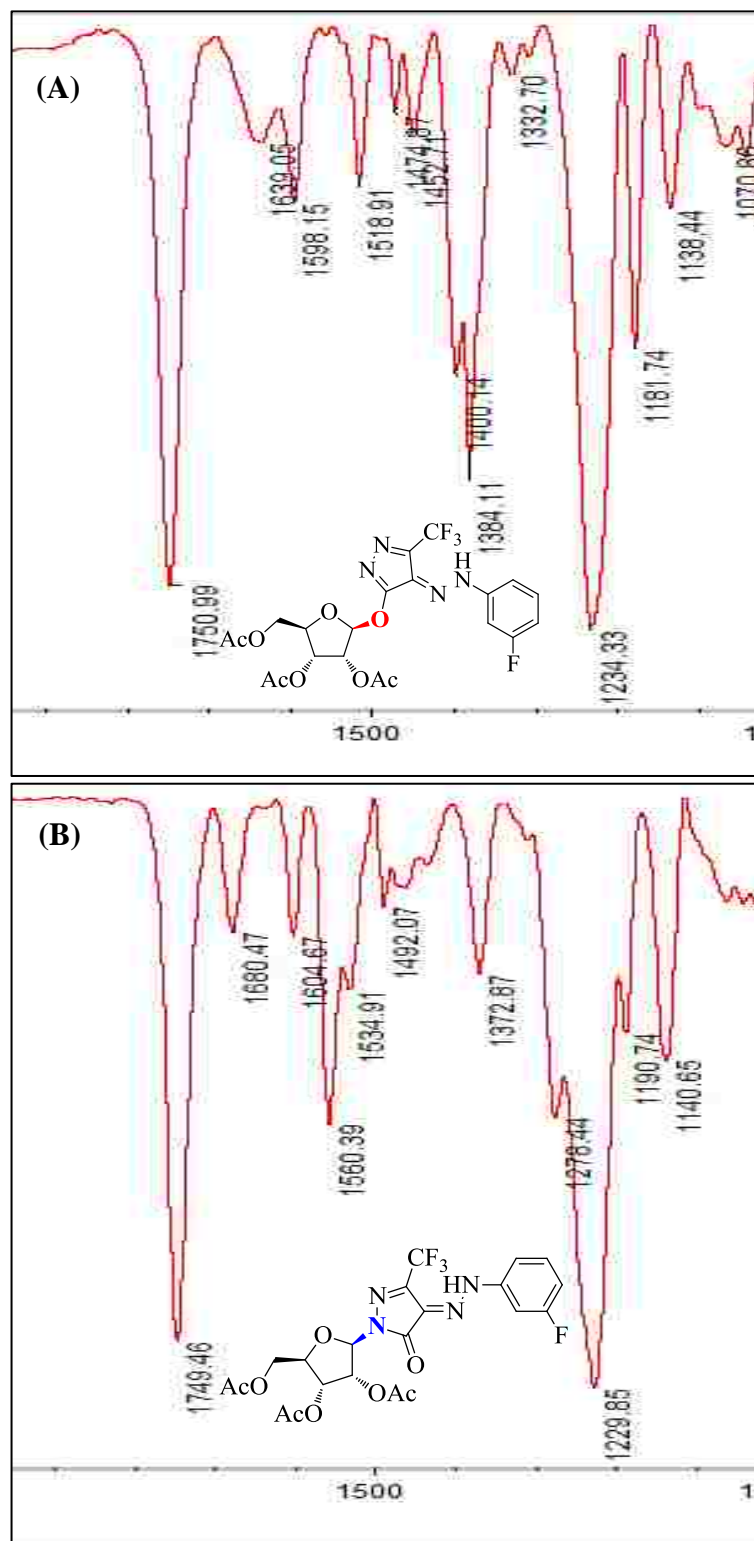
Figure 23: IR Spectra for (A) *O*-riboside **116a**, (B) *N*-riboside **117a**
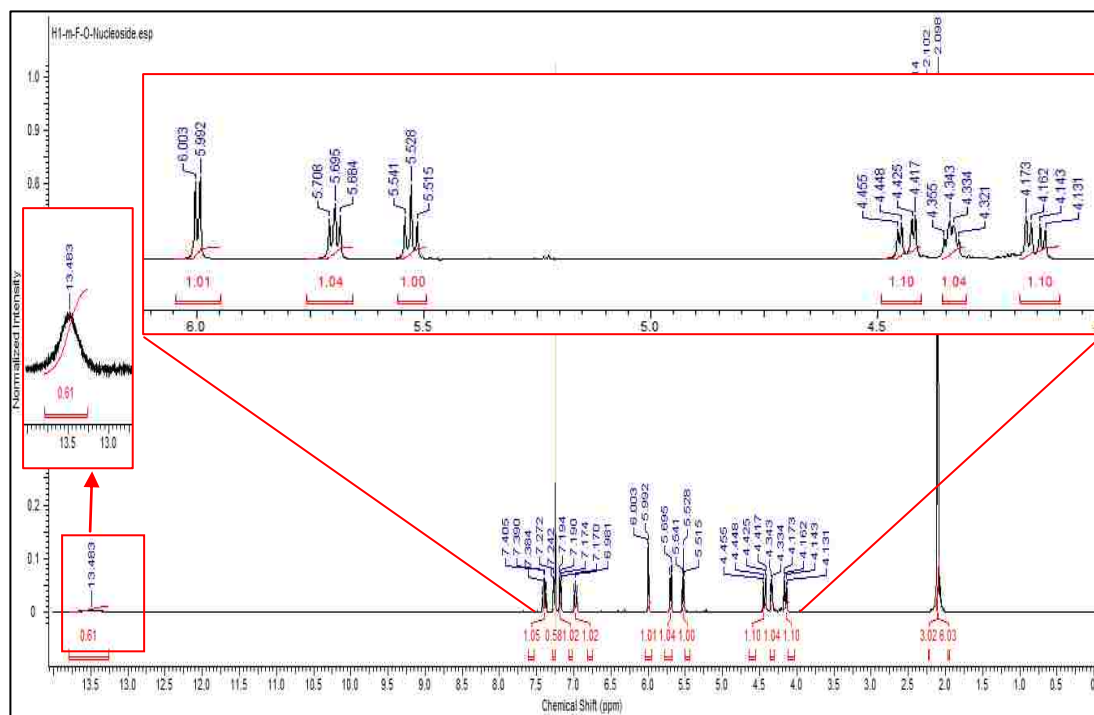
Figure 24: ¹H-NMR Spectrum for 2-(2",3",5"-tri-*O*-acetyl-*β*- ribofuranosyl)-4-(3'-fluorophenylhydrazono)-5-trifluoromethyl-2,4-dihydropyrazol-3-one **117a**
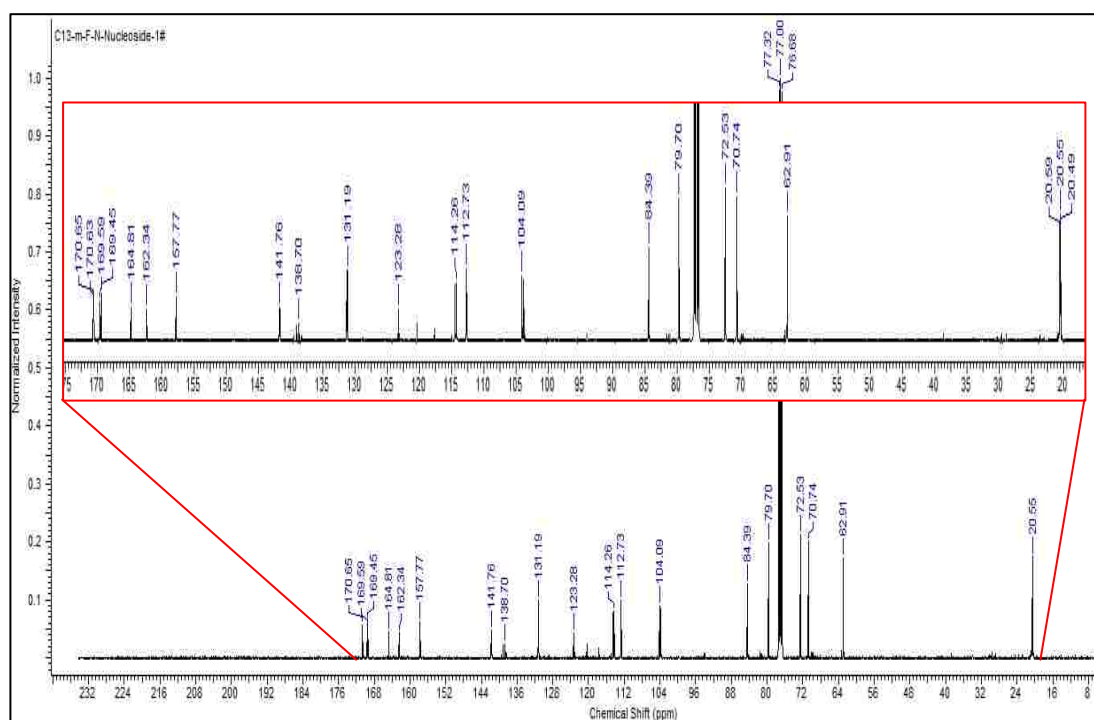


Figure 25: ¹³C-NMR Spectrum for 2-(2",3",5"-tri-*O*-acetyl-*β*- ribofuranosyl)-4-(3'-fluorophenylhydrazono)-5-trifluoromethyl-2,4-dihydropyrazol-3-one **117a.** Inset is the full spectra
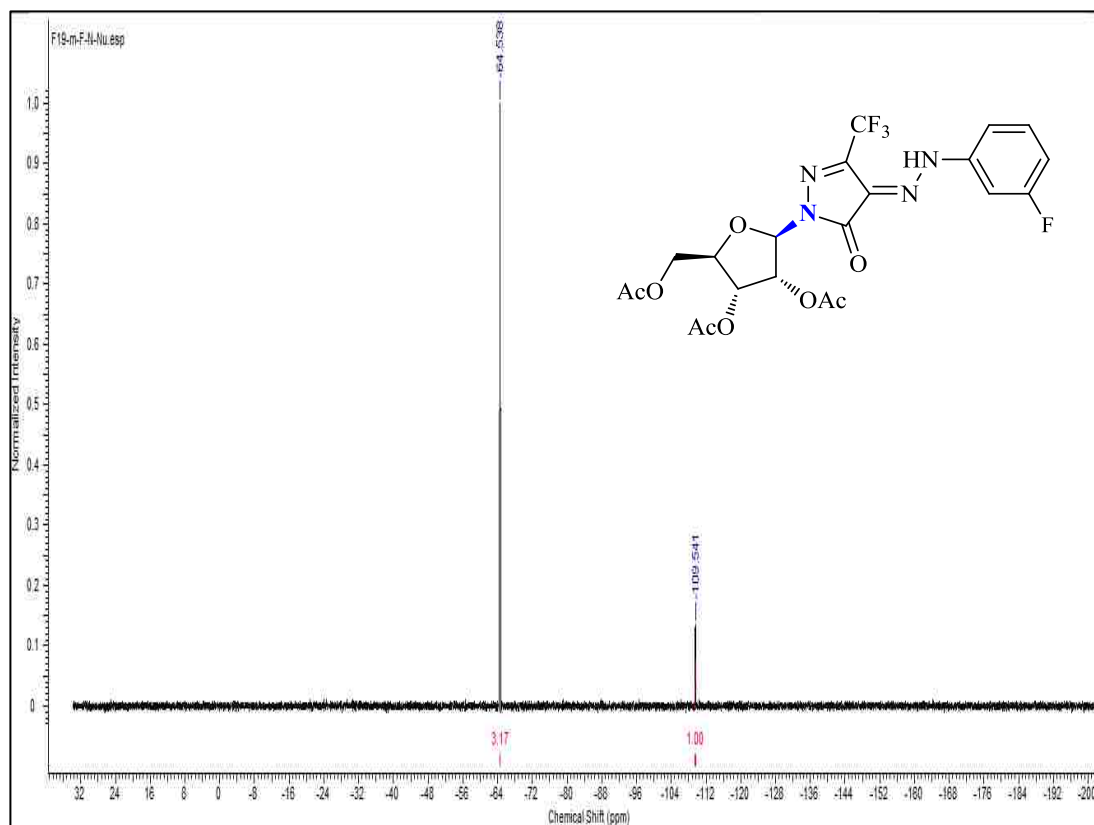
Figure 26: ^{19}F-NMR Spectrum for 2-(2'',3'',5''-tri-*O*-acetyl-*β*-ribofuranosyl)-4-(3'-fluorophenylhydrazono)-5-trifluoromethyl-2,4-dihydropyrazol-3-one **117a**

2D-COSY was obtained to assign the correct chemical shift of the sugar protons. The anomeric proton H-1'' (δ 5.99 ppm) showed across-peak interaction with H-2'' (δ 5.70 ppm). H-2'' (δ 5.70 ppm) has also a cross-peak interaction with H-3'' (δ 5.53 ppm). H-3'' (δ 5.53 ppm) has a clear cross-peak interaction with H-4'' (δ 4.33 ppm). H-4'' (δ 4.44 ppm) showed a cross-peak interaction with both of H-5''a (δ 4.44 ppm) and H-5''b (δ 4.15 ppm). While H-5''a (δ 4.44 ppm) showed strong correlation with H-5''b (δ 4.15 ppm). 2D-COSY data gave the correct order of assigned as follow: H-1'', H-2'', H-3'', H-5''a, H-4'' and H-5''b. 2D-COSY correlation also showed strong cross-peak interaction between the aromatic protons at (δ 6.98-7.39 ppm) (Figure 27).
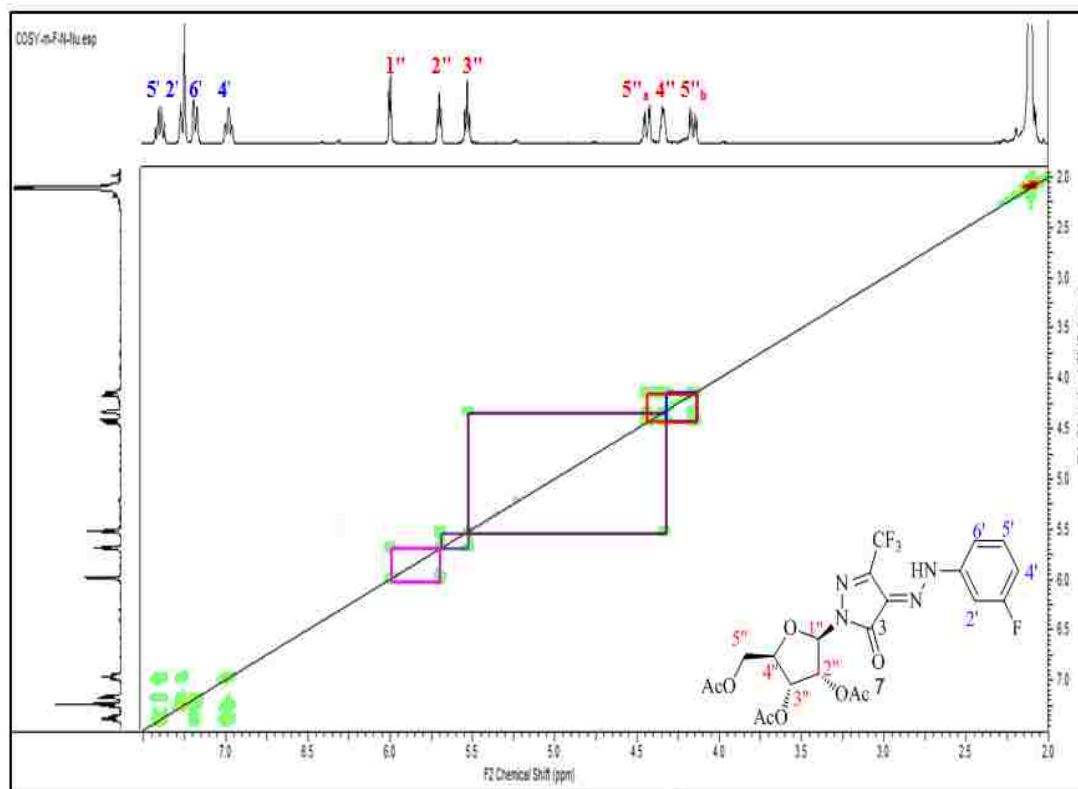
Figure 27: 2D-COSY NMR spectrum for 2-(2",3",5"-tri-*O*-acetyl-*β*-ribofuranosyl)-4-(3'-fluorophenylhydrazono)-5-trifluoromethyl-2,4-dihydropyrazol-3-one **117a**

2D-HSQC and 2D-gHMBC were used to establish the structural conformational. HSQC showed direct correlation for short range ^{1}H-^{13}C interaction. H-1″ (δ 5.99 ppm) has a correlation with C-1″ (δ 84.4 ppm), while H-2″ (δ 5.70 ppm) correlated with C-2″ (δ 72.5 ppm), H-3″ (δ 5.53 ppm) correlated with C-3″ (δ 70.7 ppm), H-4″ (δ 4.33 ppm) correlated with C-4″ (δ 79.7 ppm). While H-5a″ and H-5b″ (δ 4.44 and 4.15 ppm) showed a cross-peak interaction with C-5″(δ 62.9 ppm). In the aromatic region, H-2' at (δ 7.27 ppm) correlated with C-2' (δ 104.1 ppm). While H-4' at (δ 6.98 ppm) correlated with C-4' (δ 114.3 ppm), H-5' (δ 7.39 ppm) correlated with C-5' (δ 123.3 ppm) and H-6' (δ 7.18 ppm) correlated with C-6' (δ 112.7 ppm) (Figure 28).
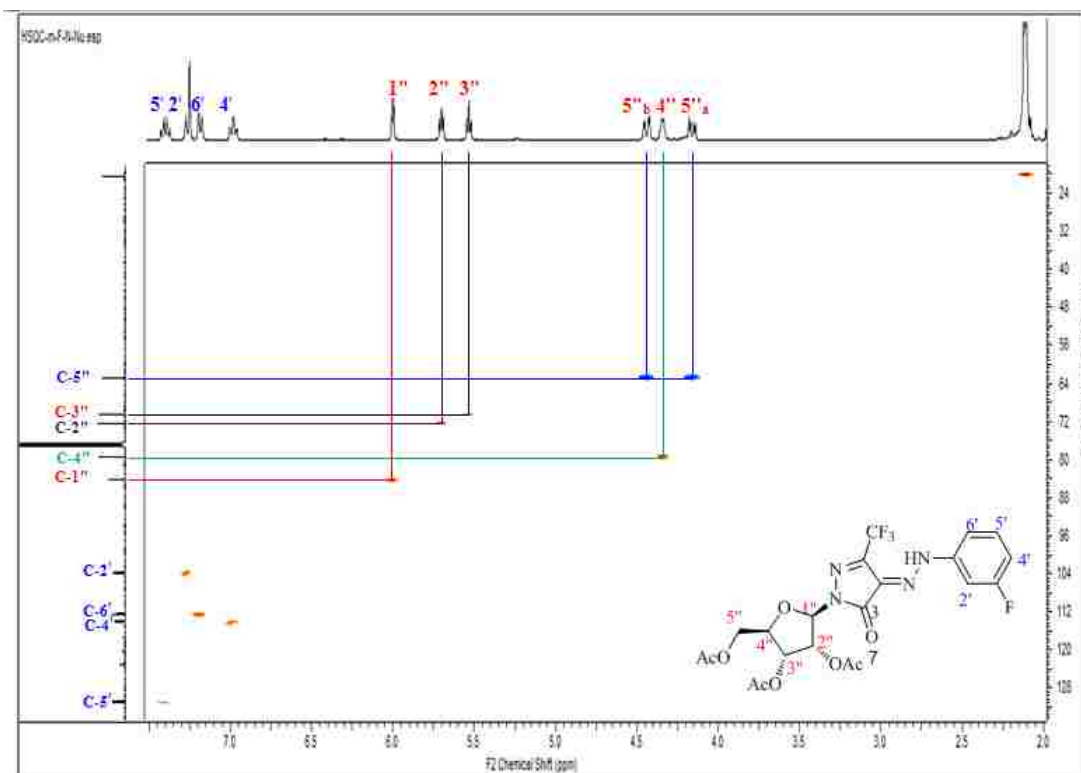
Figure 28: 2D-HSQC NMR Spectrum for 2-(2",3",5"-tri-*O*-acetyl-*β*- ribofuranosyl)-4-(3'-fluorophenylhydrazono)-5-trifluoromethyl-2,4-dihydropyrazol-3-one **117a**

Long-range heteronuclear correlation 2D-gHMBC was used to assign the [1]H-^{13}C interaction. The cross-peak interactions was found between the anomeric proton H-1″ (δ 5.99 ppm) with C-2″ (δ 72.5 ppm) of the sugar moiety. While H-2″ (δ 5.70 ppm) showed with cross-peak interactions with C-4″ (δ 79.7 ppm). H-3" (δ 5.53 ppm) showed a cross-peak interaction with C-1" and C-5" at (δ 84.4 and 62.9 ppm); respectively. Both H-5"a (δ 4.44 ppm) and H-5"b (δ 4.15 ppm) showed a cross-peak interaction with C-3" (δ 70.7 ppm) (Figure 29).

Mass spectroscopic also used to confirm the formation of 2-(2",3",5"-tri-*O*-acetyl-*β*-ribofuranosyl)-4-(3'-fluorophenylhydrazono)-5-trifluoromethyl-2,4-dihydropyrazol-3-one **117a**. The total molecular ion peak appeared at m/z 533 with

100% intensity (Figure 30). The fragment mass analysis scheme shows the pattern of

fragmentation with its relative intensity (Scheme 39).
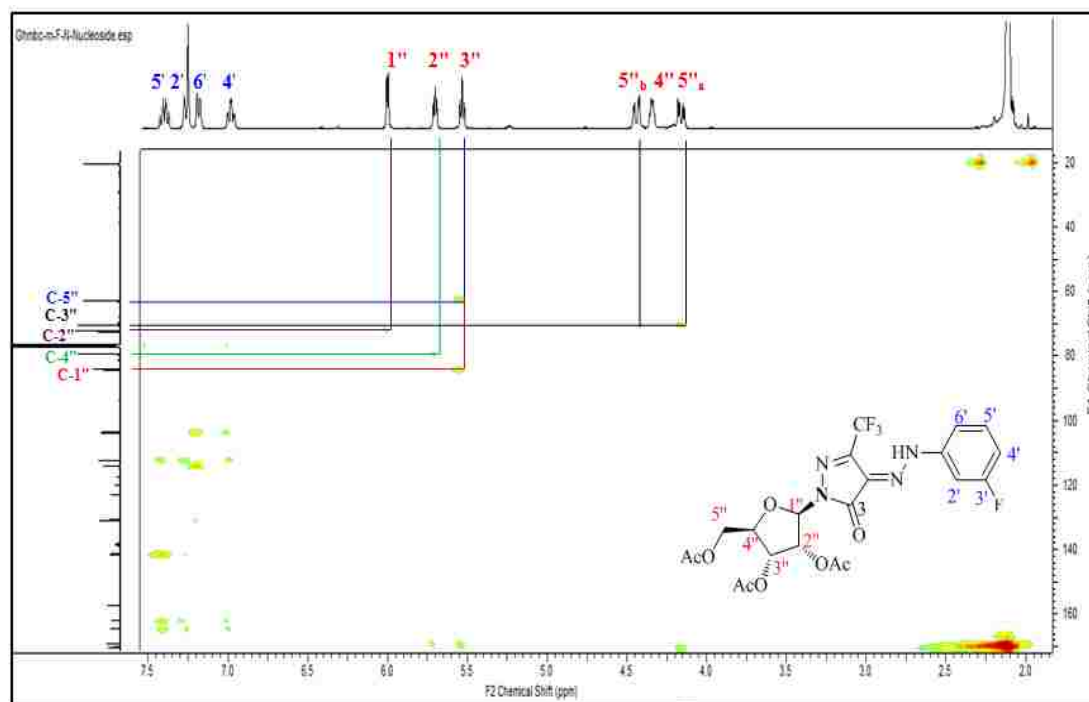
Figure 29: 2D-gHMBC NMR Spectrum for 2-(2",3",5"-tri-*O*-acetyl-*β*-ribofuranosyl)-4-(3'-fluorophenylhydrazono)-5-trifluoromethyl-2,4-dihydropyrazol-3-one **117a**
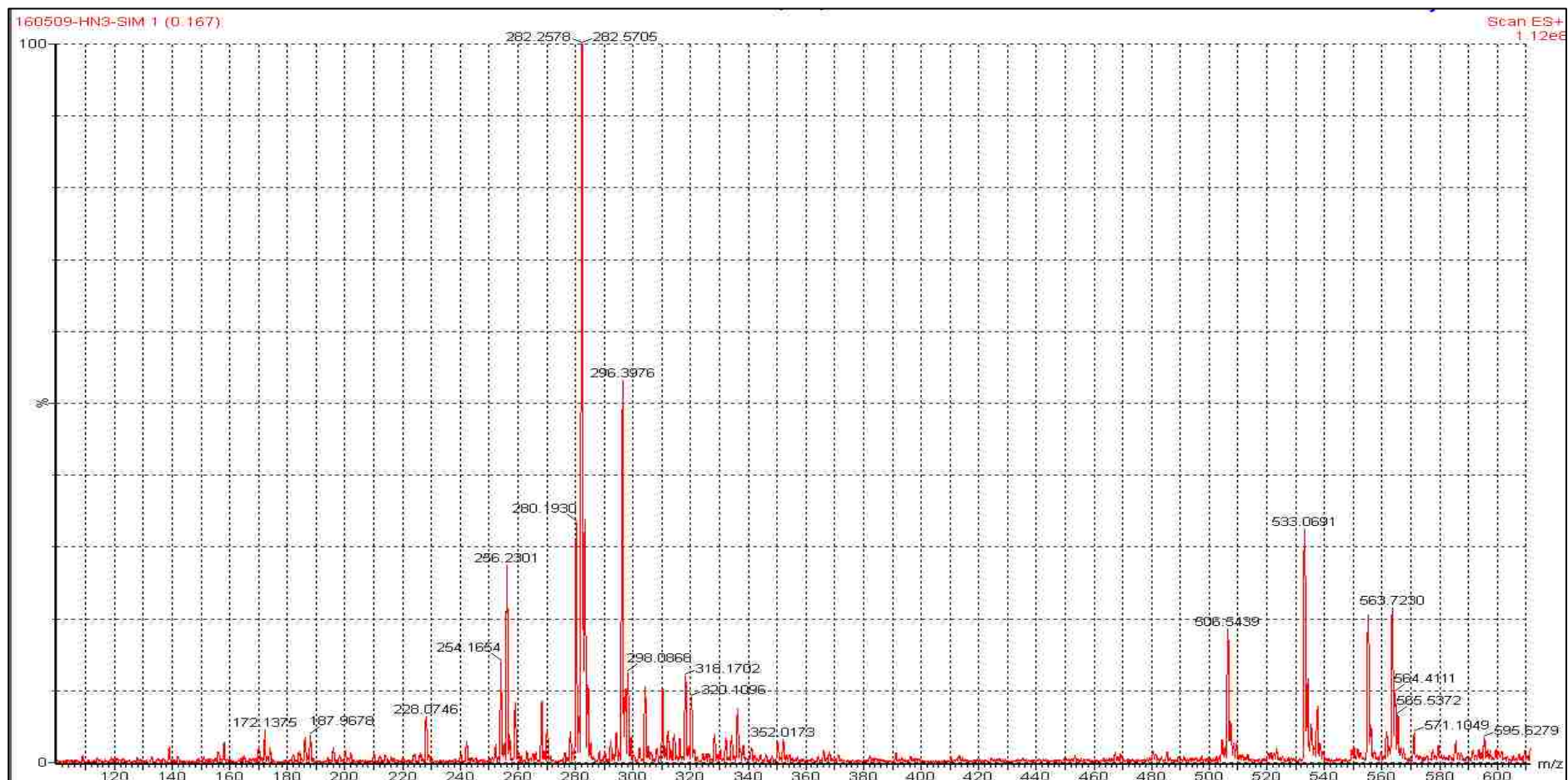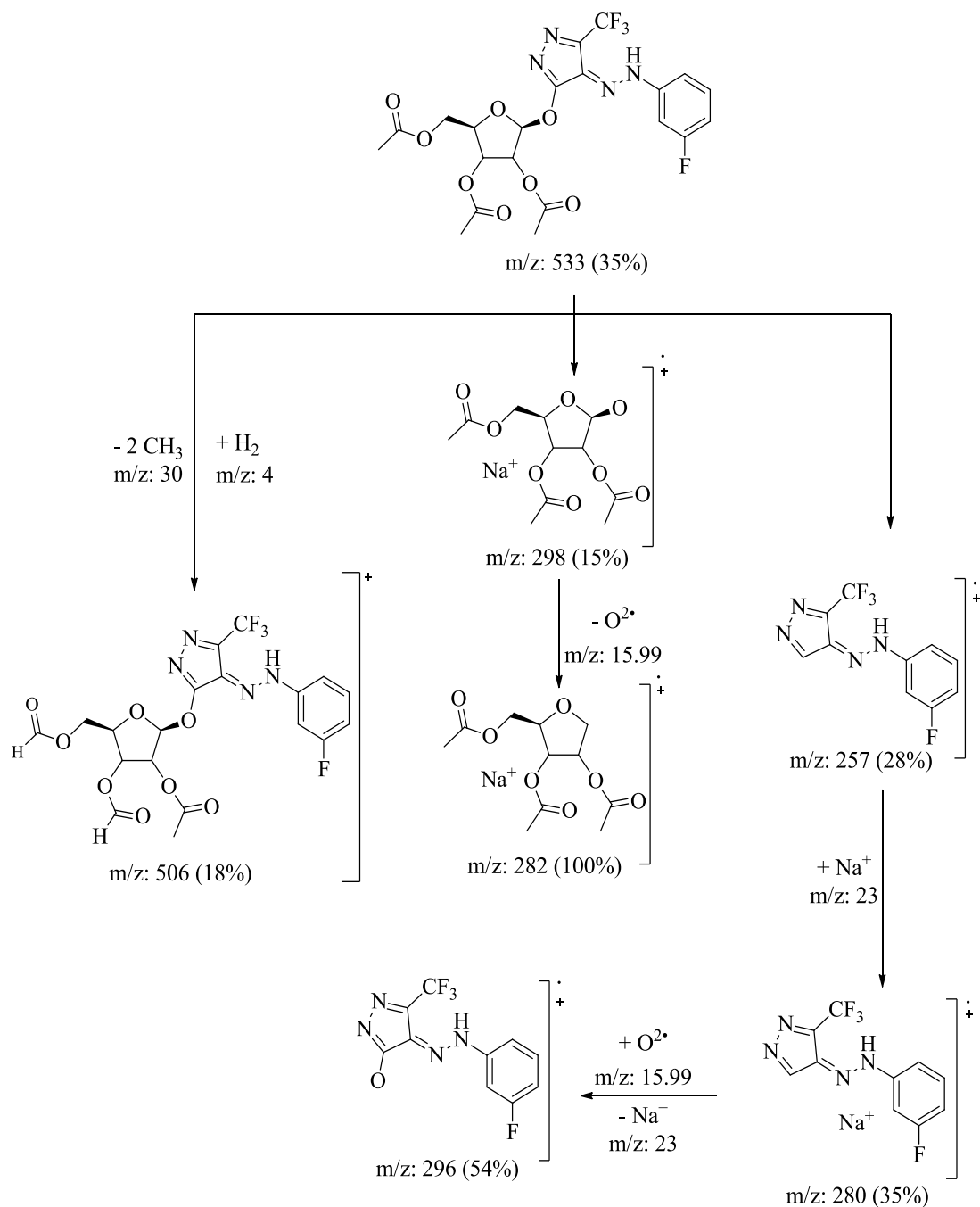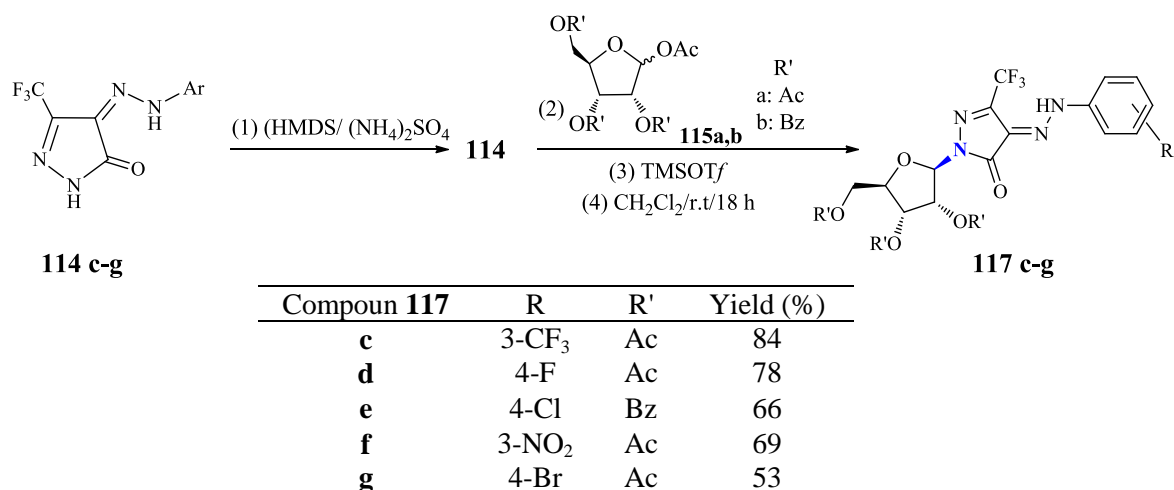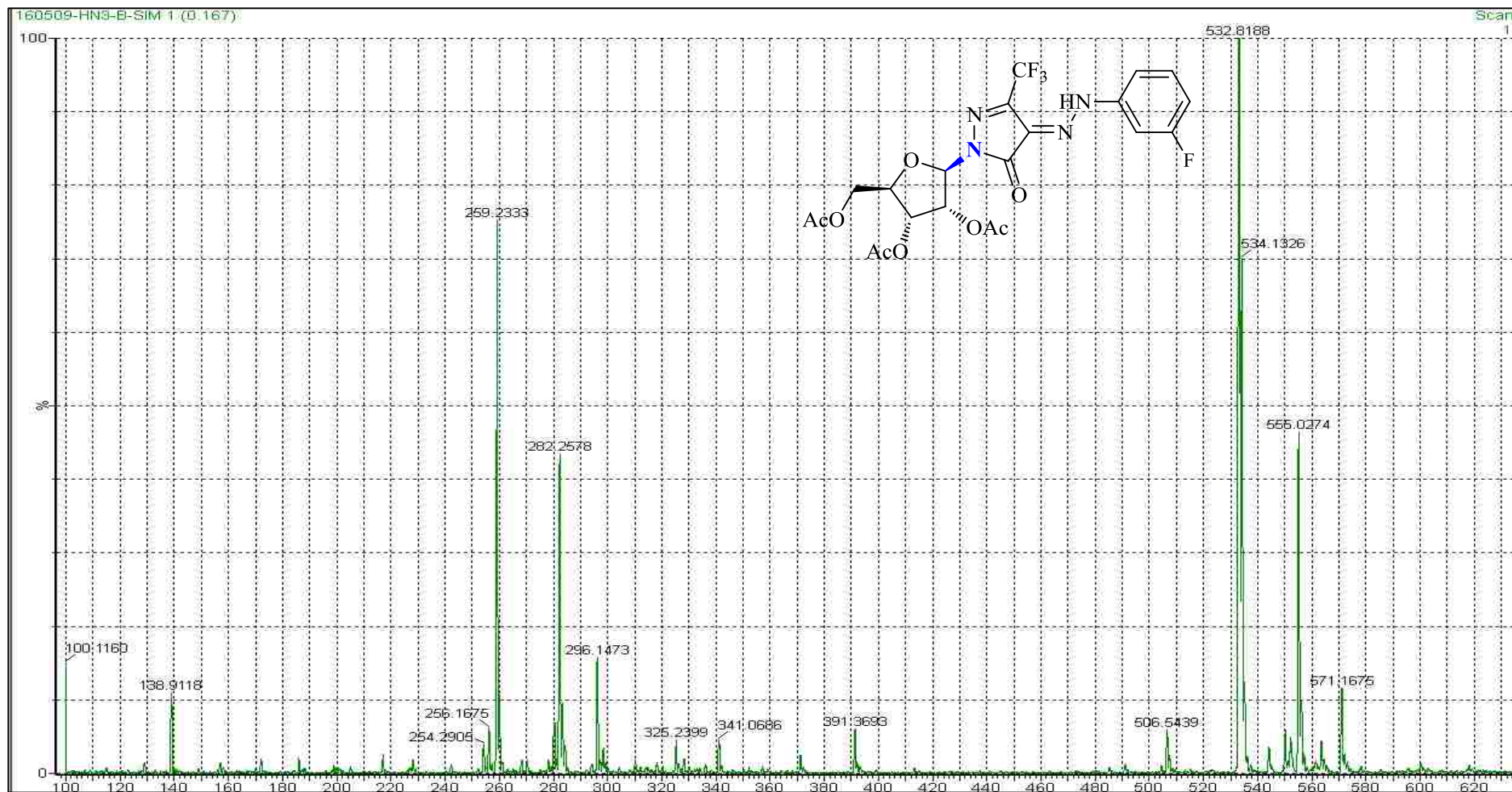
Figure 30: Mass fragmentation spectrum for 2-(2",3",5"-tri-*O*-acetyl-*β*- ribofuranosyl)-4-(3'-fluorophenylhydrazono)-5-trifluoromethyl-2,4-dihydropyrazol-3-one **117a**
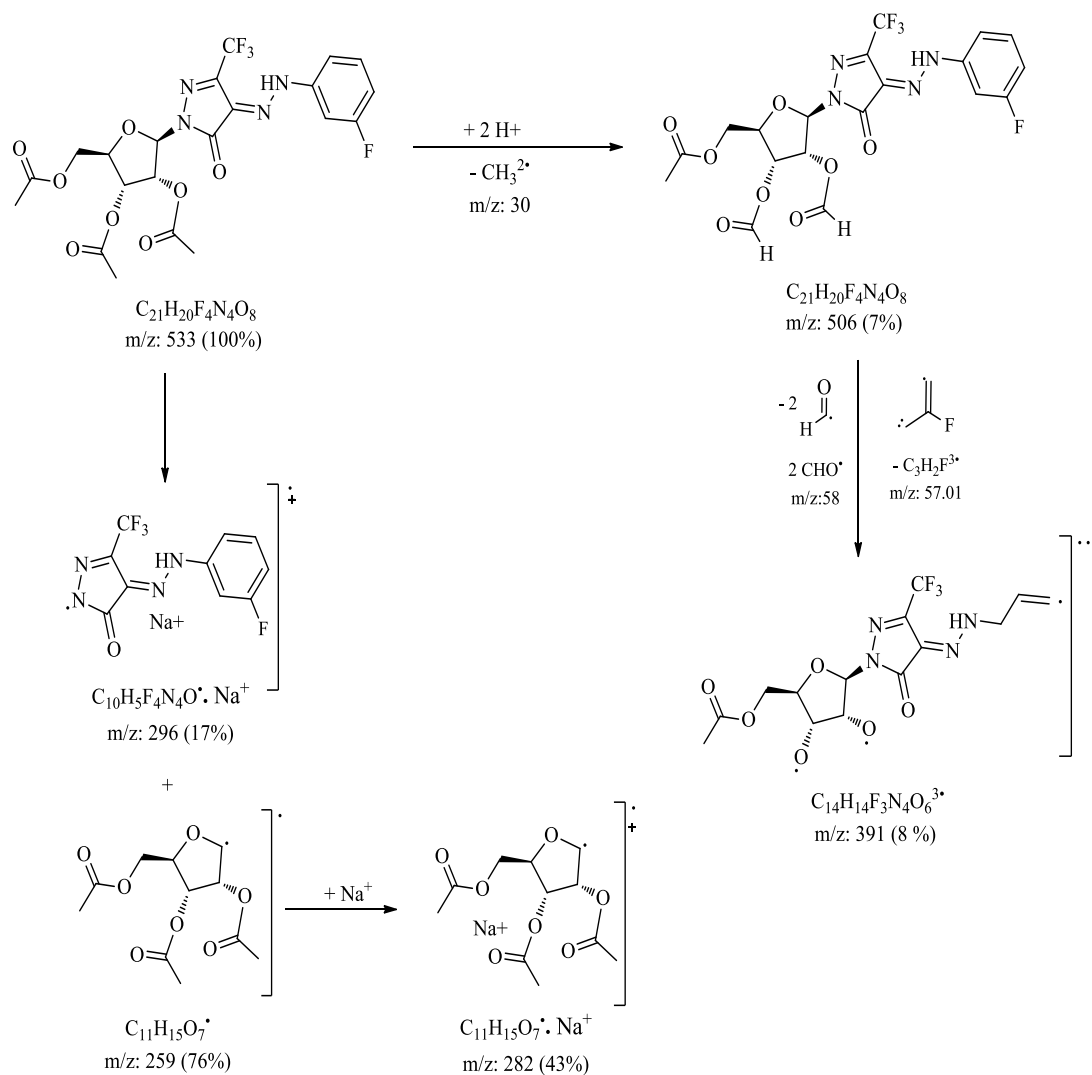
Scheme 39: Mass fragments scheme for 2-(2",3",5"-tri-*O*-acetyl-*β*- ribofuranosyl)-4-(3'-fluorophenylhydrazono)-5-trifluoromethyl-2,4-dihydropyrazol-3-one **117a**

2.3.5 Hydrolysis of *N*-Nucleosides 118a-c

Ammonolysis of the nucleosides **117c,e,f** using triethyl amin in methanol gives free nucleosides **118a-c** in 93%, 84%, 92%; respectively (Scheme 40).
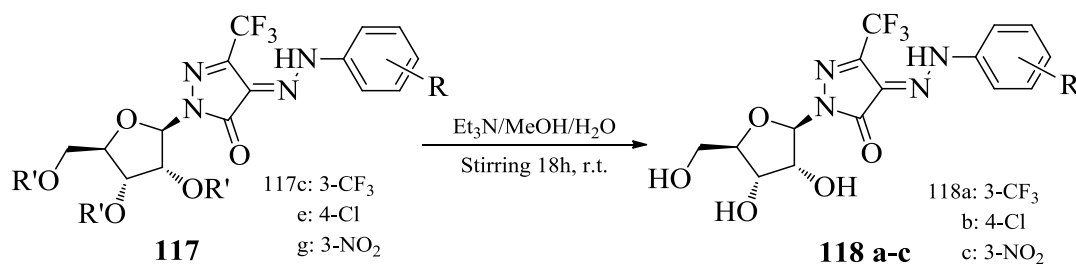
Scheme 40: Deprotection of **117c,e,g** using triethylamine in methanol and water (1:1:1)

Structures of the obtained nucleosides **118a-c** are elucidated by studying their IR, ^{1}H-NMR and ^{13}C-NMR spectra which are in accordance with the proposed structures. The IR (KBr) absorption spectrum of compounds **118c** showed a characteristic band at ν 3443 cm^{-1} due to the sugar hydroxy groups. Another strong band at ν 1670 cm^{-1} is attributed to the imide–carbonyl of the pyrazolone. Signal corresponding to three acetoxy carbonyl groups have disappeared (Figure 31).
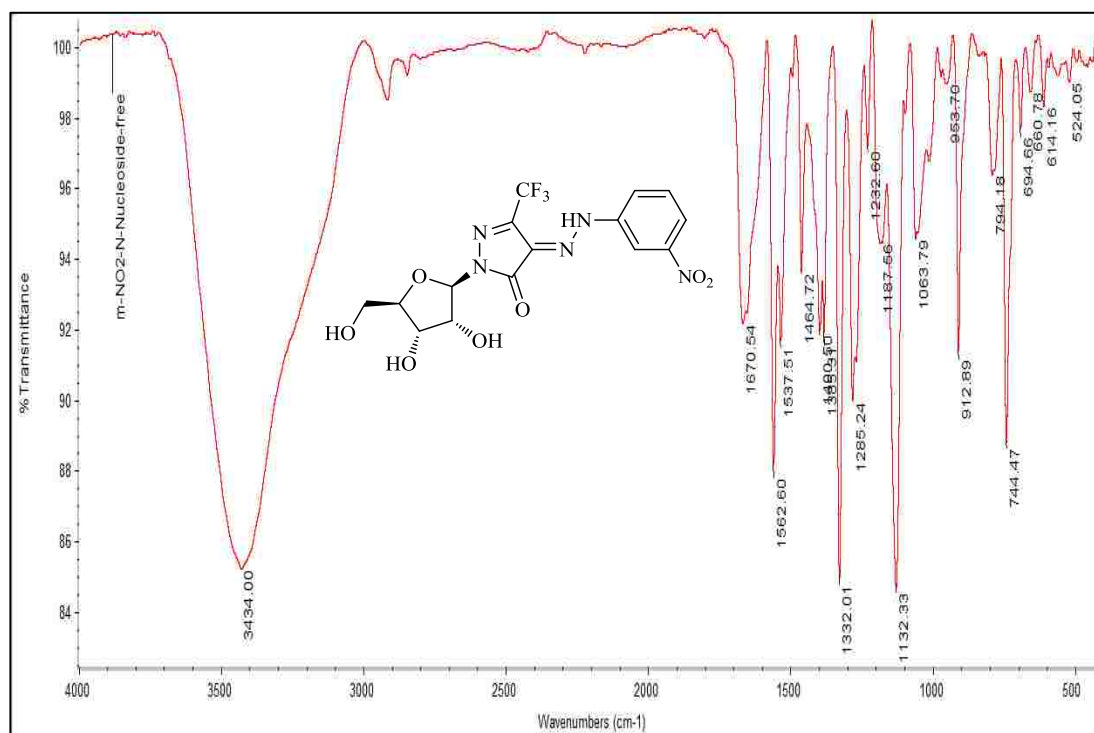
Figure 31: IR Spectrum of 3-(β-D-ribofuranosyl)-4-(3'-nitrophenylhydrazono)-5-trifluoromethyl-2,4-dihydropyrazol-3-one **118c**

The ^{1}H-NMR (400 MHz, CDCl$_3$) spectrum of compound **118c** is confirmed by the appearance of a doublet at δ = 5.89 ppm corresponding to the anomeric proton of the ribose moiety with a spin-spin coupling constant equal to 4.0 Hz corresponding to the diaxial orientation of the H-1″ and H-2″ protons indicating the formation of only one *β*-isomer. And also the appearance of peak at δ = 2.82 ppm corresponding to the three OH groups; which is exchangeable with D$_2$O. In addition to that, the three peaks of the acetyl groups at δ ≈ 2.10 ppm disappeared which also confirm the formation of the free nucleoside (Figure 32).
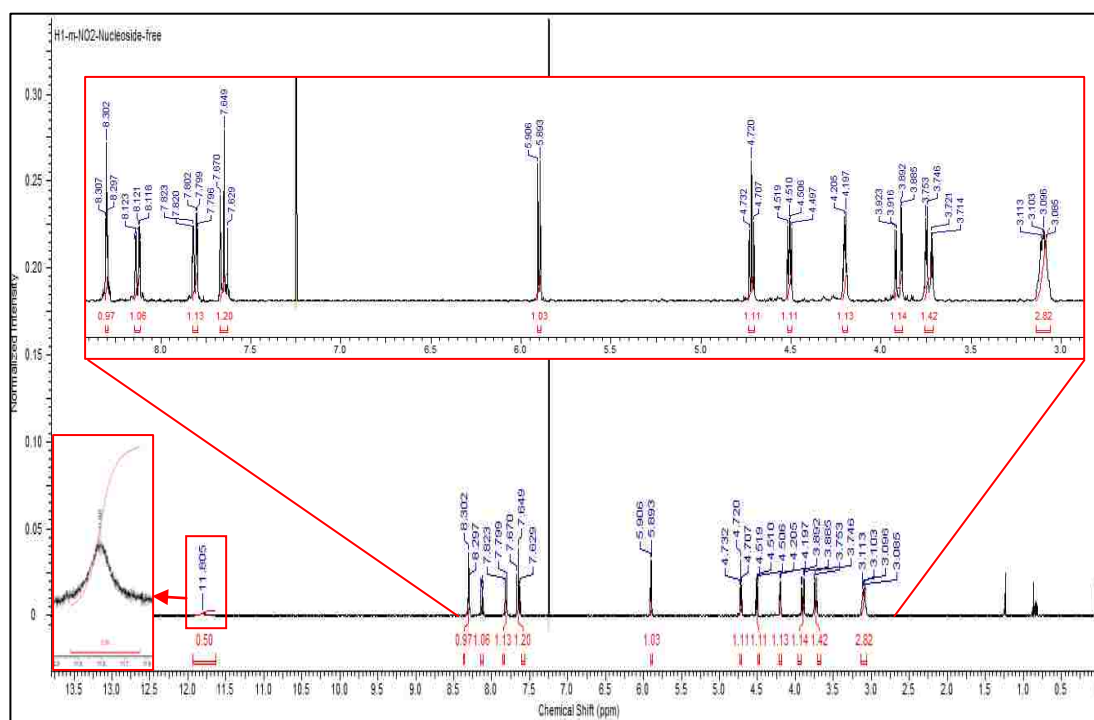
Figure 32: ^{1}H-NMR Spectrum for 3-(*β*-D-ribofuranosyl)-4-(3'-nitrophenylhydrazono)-5-trifluoromethyl-2,4-dihydropyrazol-3-one **118c**

The ^{13}C-NMR (100 MHz, CDCl$_3$) spectrum of **(118c)** is characterized by a signal at δ = 88.0 ppm corresponding to the C-1″ atom of ribose residue. No more

signals appear in the region δ ≈ 20.5 ppm corresponding to the methyl of acetoxy groups (Figure 33).
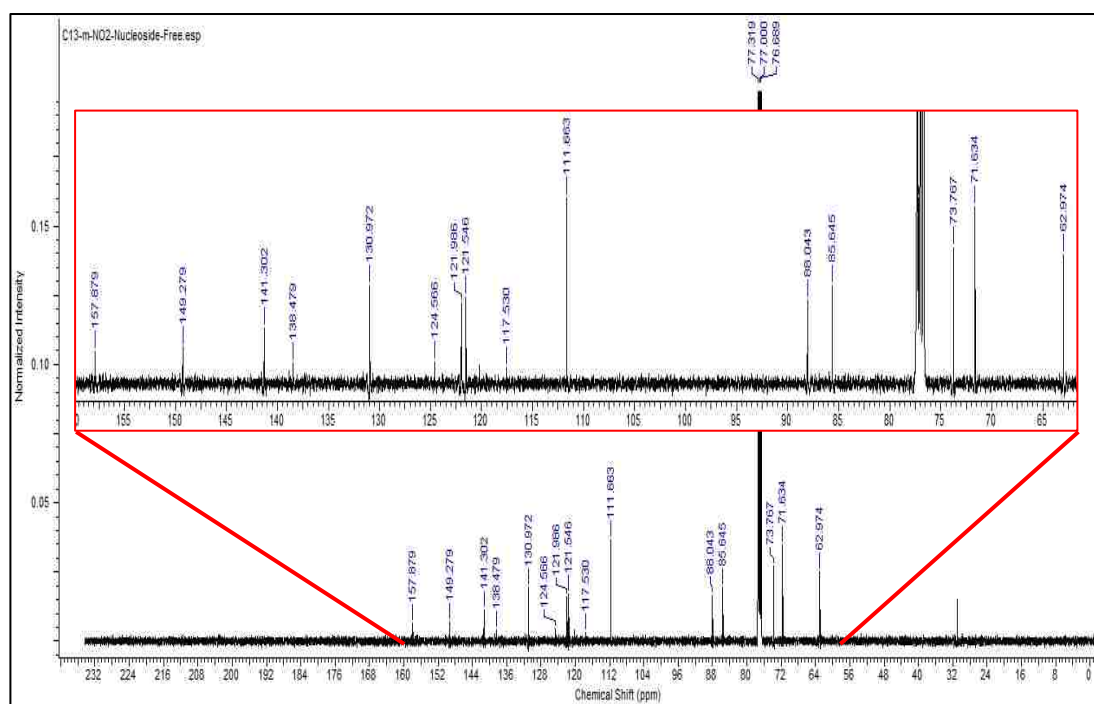
Figure 33: ^{13}C-NMR Spectrum for 3-(β-ribofuranosyl)-4-(3'-nitrophenylhydrazono)-5-trifluoromethyl-2,4-dihydropyrazol-3-one **118c**

Heteronuclear correlation ^{1}H - ^{13}C was used to support the suggested structure of 3-(β-ribofuranosyl)-4-(3'-nitrophenylhydrazono)-5-trifluoromethyl-2,4-dihydropyrazol-3-one **118c**. 2D-HSQC showed direct correlation for short range ^{1}H-^{13}C interaction. H-1″ (δ 5.90 ppm) has a correlation with C-1″ (δ 88.0 ppm), while H-2″ (δ 4.72 ppm) correlated with C-2″ (δ 85.6 ppm), H-3″ (δ 4.51 ppm) correlated with C-3″ (δ 73.8 ppm), H-4″ (δ 4.30 ppm) correlated with C-4″ (δ 71.6 ppm). While H-5a″ and H-5b″ (δ 3.90 and 3.74 ppm) showed a cross-peak interaction with C-5″ (δ 62.9 ppm). In the aromatic region. H-2' at (δ 8.30 ppm) correlated with C-2' (δ 111.7 ppm). While H-4' at (δ 8.13 ppm) correlated with C-4' (δ 121.5 ppm), H-5' (δ

7.65 ppm) correlated with C-5' (δ 130.9 ppm) and H-6' (δ 7.81 ppm) correlated with

C-6' (δ 121.9 ppm) (Figure 34)
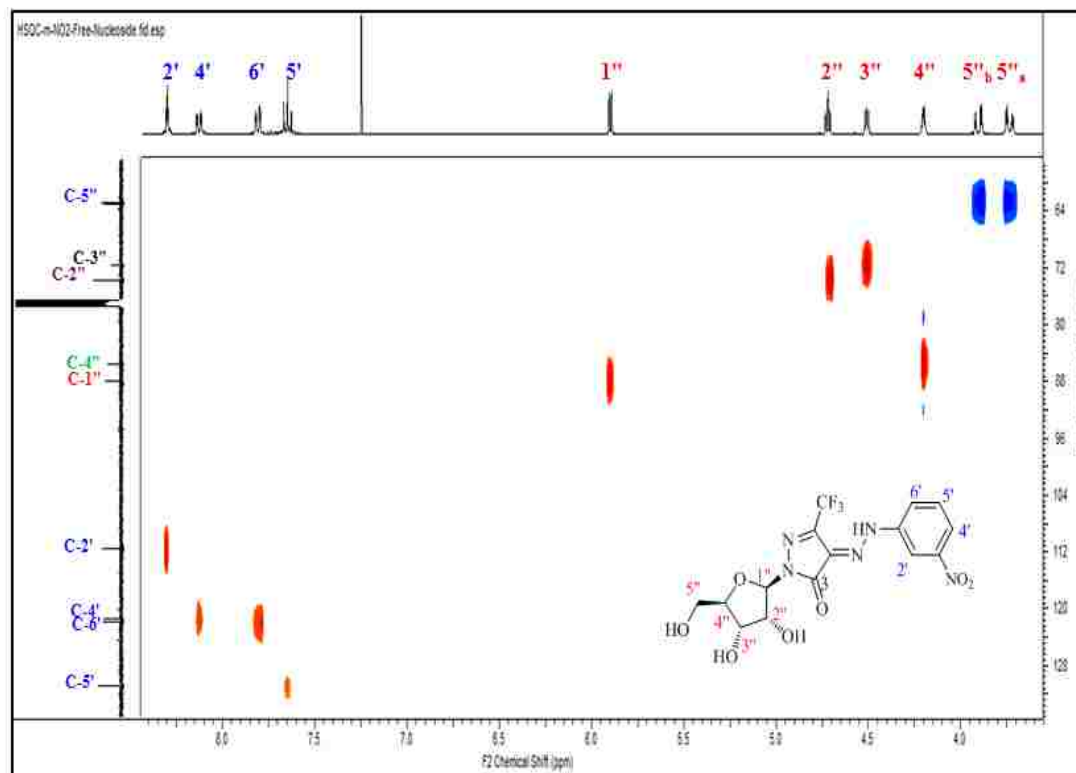
Figure 34: 2D-HSQC Spectrum for 3-(β-ribofuranosyl)-4-(3'-nitrophenylhydrazono)-
5-trifluoromethyl-2,4-dihydropyrazol-3-one **118c**

Mass spectroscopic used to confirm the formation of the free riboside **118c**.
The total molecular ion peak appeared at m/z 433 with 100% intensity (Figure 35).
The fragment mass analysis scheme shows the pattern of fragmentation with its
relative intensity (Scheme 41).
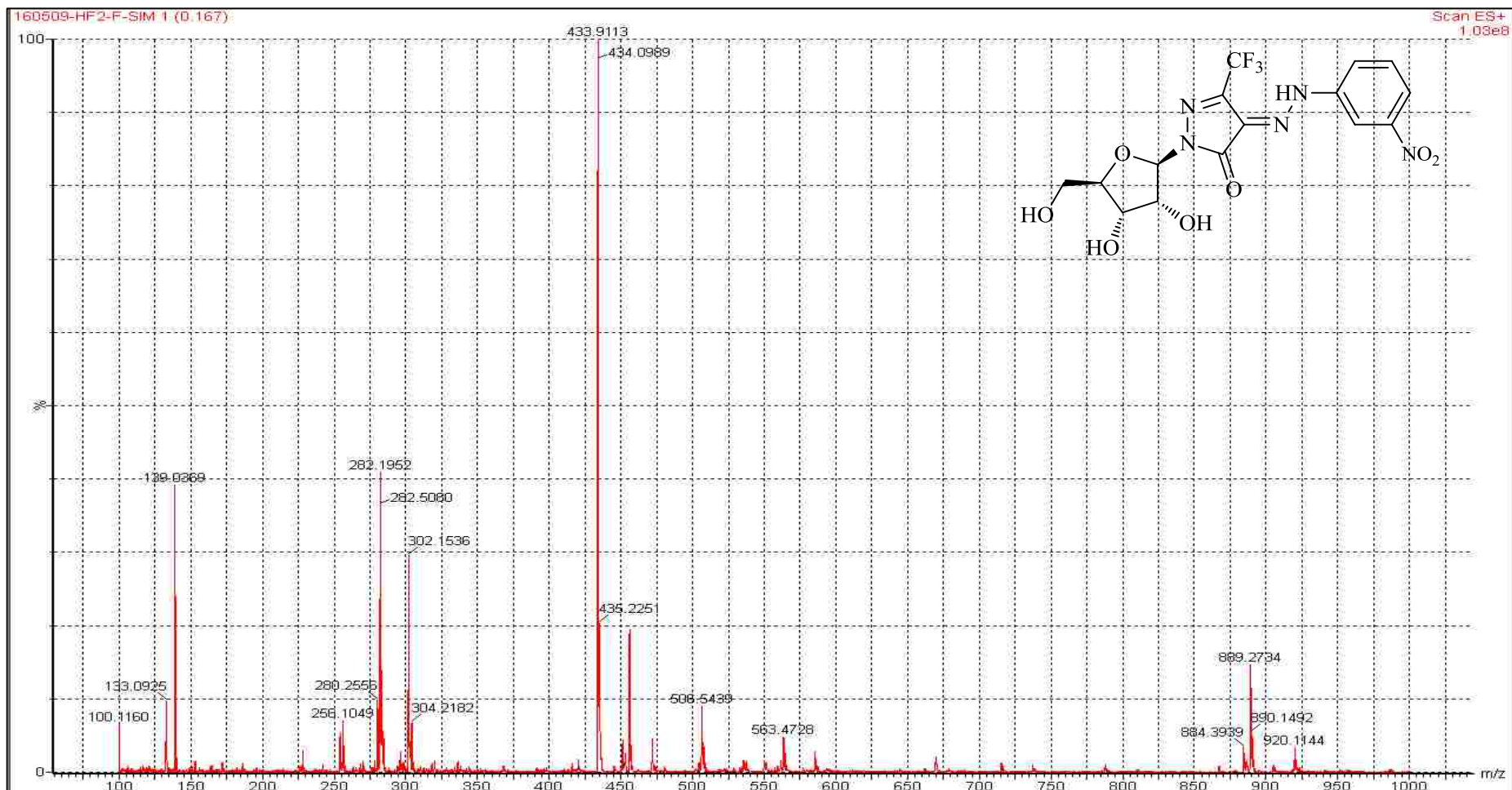
Figure 35: Mass fragmentation spectrum for 3-(β-ribofuranosyl)-4-(3'-nitrophenylhydrazono)-5-trifluoromethyl-2,4-dihydropyrazol-3-one **118c**
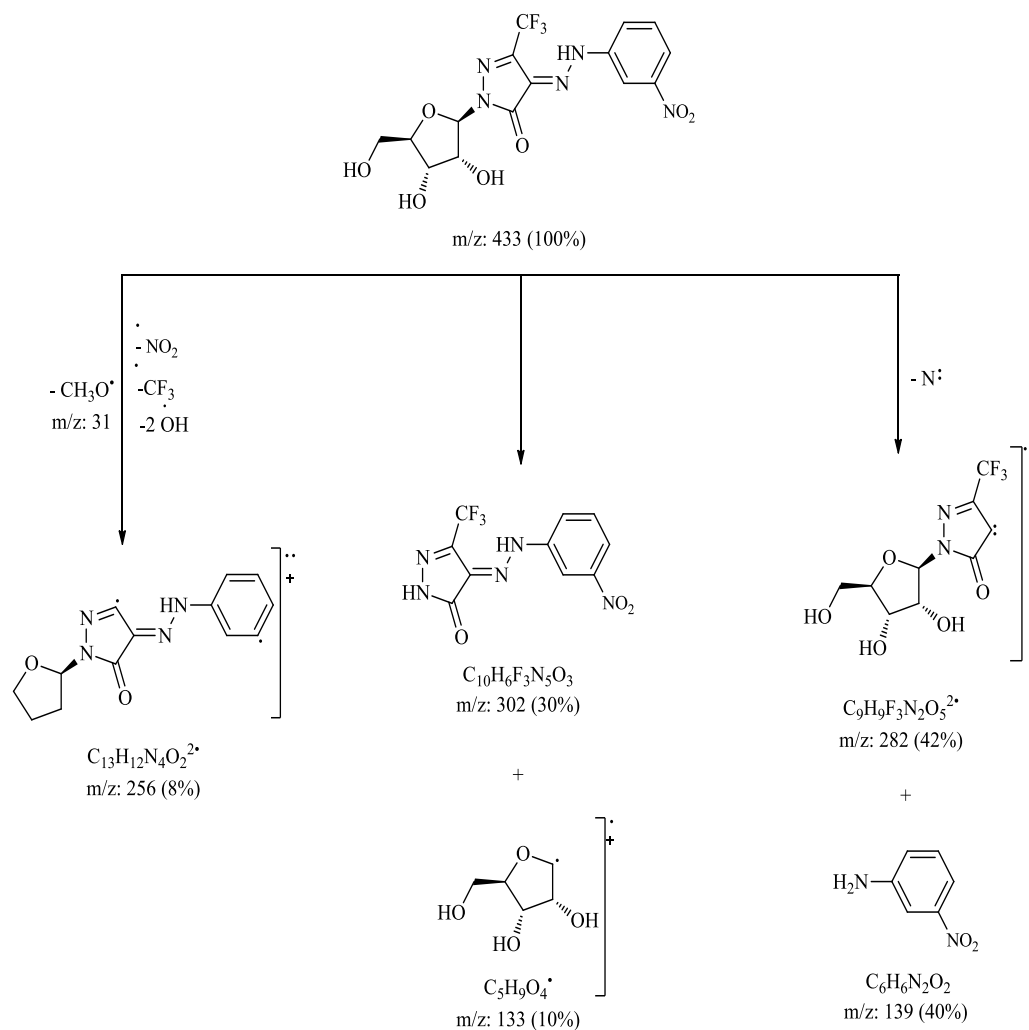
Scheme 41: Mass fragments scheme for 3-(β-D-ribofuranosyl)-4-(3'-nitrophenylhydrazono)-5-trifluoromethyl-2,4-dihydropyrazol-3-one **118c**

2.3.6 Synthesis of Deoxyribonucleoside Pyrazolones

2.3.6.1 Synthesis of 1,3,5-tri-*O*-acetyl-2-deoxyribofuranose 121

1,3,5-Tri-*O*-acetyl-2-deoxyribofuranose **121** was synthesized using 2-deoxy-D-ribose, which is commercially available from sigma-aldrich according to the method described in literature [104]. Scheme 42 shows that the acetylated deoxyribose **121** was synthesized using a well-developed methodology [105].
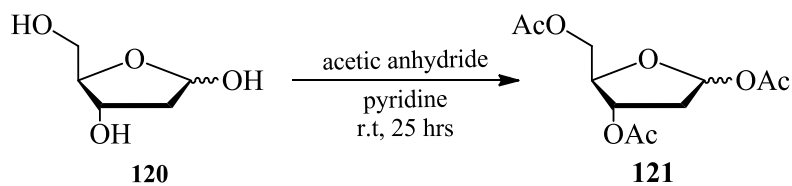
Scheme 42: Synthesis of 1,3,5-tri-*O*-acetyl-2-deoxyribofuranose

The structure of 1,3,5-tri-*O*-acetyl-2-deoxyribofuranose **121** was confirmed using spectroscopic techniqus such as FT-IR and NMR. The FT-IR was used to confirmed the presence of signal at ν 1743 cm^{-1} corresponding to the acetoxy carbonyl carbones of the three acetyl groups allocated at C-1, 3 and 5 of the deoxyribose moiety. ^{1}H-NMR (400 MHz, CDCl$_3$) spectroscopy was used to confirm the suggested structures. For example, ^{1}H-NMR spectrum of compound **121** showed the anomeric proton as triplet (δ 6.25 ppm) integrated to one proton with a coupling constant *J* = 4.0 Hz. While the remaining sugar protons H-2a, 2b, 5a,b, 4, and 3, resonate at δ 1.90, 2.26, 3.85, 4.00, 5.20, 5.30 ppm respectively (Figure 36). ^{13}C-NMR (100 MHz, CDCl$_3$) also used to confirm the correct number of carbon atoms at the correct chemical shifts. The anomeric carbon resonates at δ 91.5 ppm while C-2, 5, 4 and 3 appeared at δ 29.4, 62.7, 65.0, 66.9 ppm; respectively (Figure 36). ^{13}C-NMR also showed new three signals at δ 20.6, 20.6, and 20.8 ppm corresponding to the three methyl of the acetoxy groups at C-1, 3 and 5 (Figure 37).

2D-COSY NMR was used for clearly assigning the correlation btween protons in the sugar moiety. Figure 38 shows a cross-peak interaction between anomeric proton H-1 (δ 6.25 ppm) H-2b at (δ 1.91 ppm). A cross-peak interaction was observed between H-2 at (δ 2.26 ppm) and H-3 (δ 5.30 ppm). The 2D-COSY NMR spectrum also shows a cross-peak interaction between H-3 and H-4 (δ 5.20 ppm). Additionally a cross-peak interaction was observed between H-4 and H-5a,b (δ

4.00, 3.85 ppm). 2D-COSY data gave the correct order of assigned as follow: H-1, H-3, H-4, H-5a, H-5b, H-2a, H-2b.
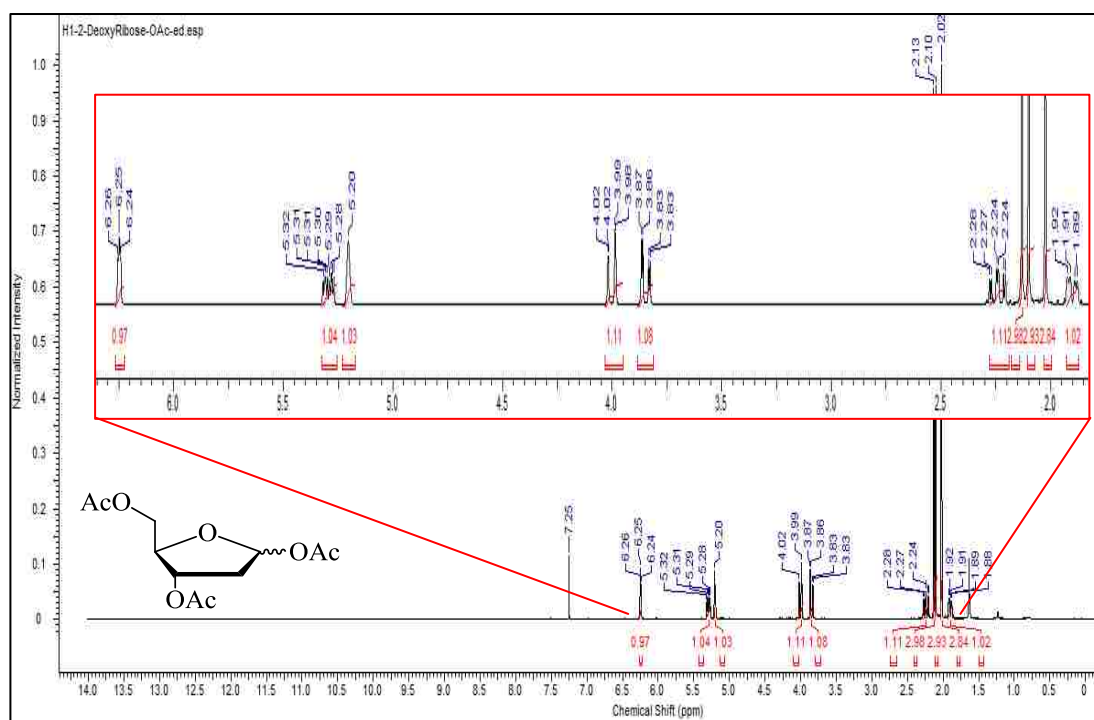
Figure 36: ^{1}H-NMR Spectrum for 1,3,5-tri-*O*-acetyl-2-deoxyribofuranose **121**
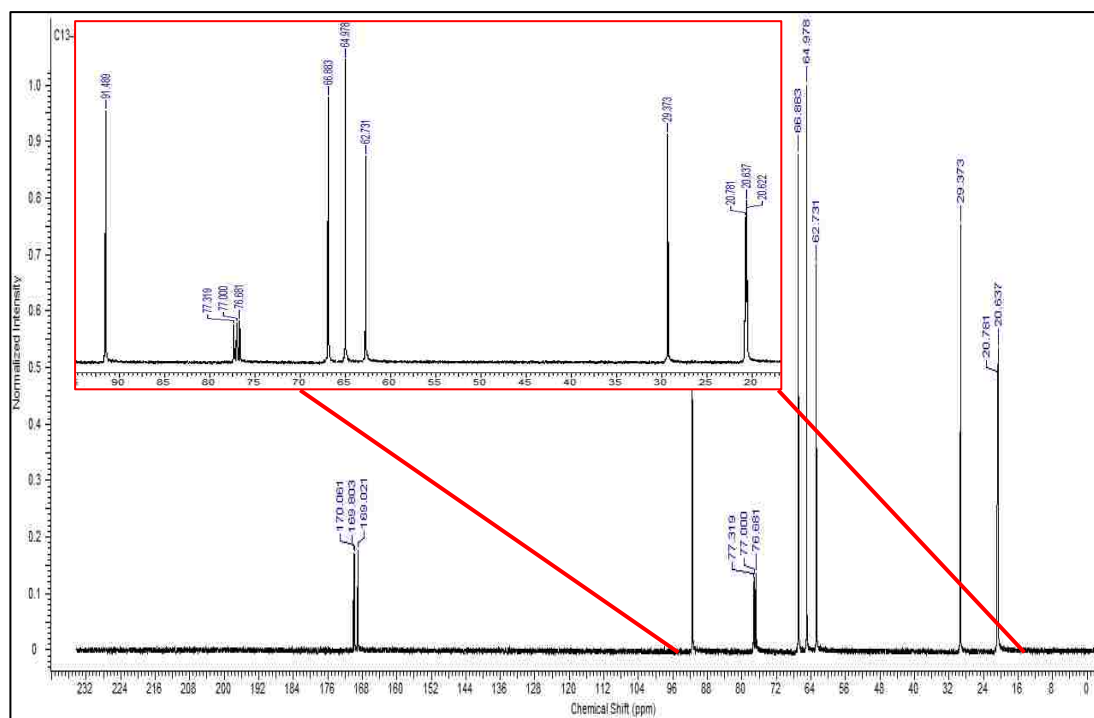
Figure 37: ^{13}C-NMR Spectrum for 1,3,5-tri-*O*-acetyl-2-deoxy-ribofuranose **121**
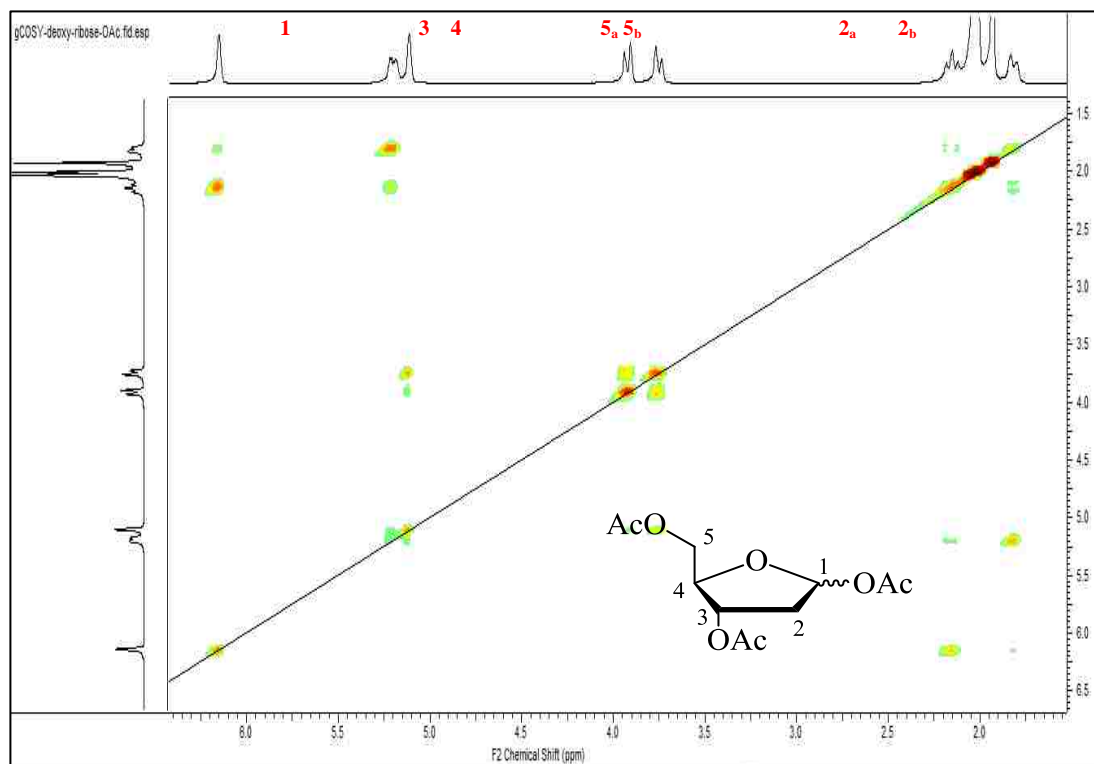
Figure 38: 2D-gCOSY Spectrum for 1,3,5-tri-*O*-acetyl-2-deoxyribofuranose **121**

2.3.6.2 Synthesis of Deoxyribonucleosides derivatives 122 and 123

Since there are insistent international demands for 2-deoxyribonucleosides as important resources of drugs [106], 1,3,5-tri-*O*-acetyl-2-deoxyribofuranose **121** introduced to two different nucleophlic centers in the pyrazolone ring. As in the ribosides synthesis, the silyl-method is used to activate the pyrazolone ring, while the sugar moiety **121** was used as 1-acetyl analog that activated by Lewis acid catalyst (Scheme 43). Hexamethyldisilazane (HMDS) was used as silylation agent to activate the pyrazolone in the form of 3-trimethylsilyloxy pyrazoline **114** intermediate (Scheme 44). While Trimethylsilyl trifluoromethanesulfonate (TMSOT*f*) was used to activate the sugar. The silyl intermediate **113** reacts with the activated surge **125** in dry methylene chloride for 8 hours at room temperature. The reaction afford *O*- and *N*-nucleosides, isolated and identified as 3-(3″,5″-di-*O*-acetyl-2″-*β*-Deoxy-

ribofuranosyloxy)-4-(3'-fluorophenylhydrazono)-5-trifluoromethyl-2,4-

dihydropyrazol-3-one **122a** and 2-(3",5"-di-*O*-acetyl-2"-*β*-Deoxy-ribofuranosyl)-4-

(3'-fluorophenylhydrazono)-5-trifluoromethyl-2,4-dihydropyrazol-3-one **123a** in

yield 53 % and 47 % ; respectively.

113 a,c,g

114a: 3-F, c:3-CF$_3$, g:3-NO$_2$

122 a-c

123 a-c

122,123

R: a 3-F, b 3-CF$_3$, C 3-NO$_2$

Scheme 43: **S**ynthesis of *O*- and *N*-Deoxy ribonucleosides derivatives of pyrazolones

The formation of only *β*-isomers can be explained based on the fact that the

HMDS enhances the nucleophlicity of both of the two nucleophlic centers of the

pyrazolone and its reaction with anthe activated sugar to afford the desired 2-

deoxynucleosides. Surprisingly, the activated deoxy sugar under these conditions

expected to produced both *α*- and *β* -isomers due to the lack of acetoxy group at 2"-

position of the 2"-deoxy analoge, while two *β*-isomers identified as *O*- and *N*-

isomers were detected. The mechanism of the reaction can be explaned as Lewis acid

substracted the acyl group from the anomeric carbon of the 2-deoxy sugar forming

oxycarbonium triflate ion pair **124-126**. The stereochemistry of the final product will

depend on the equilibrium of the oxycarbonium triflate **124,126** which preferred to

be in *α*-position **125**. The silyl base as nucleophile attacks to the oxycarbonium

triflate from β-face afforded only β-isomers **122**, **123** as mixture of *O-* and *N-*nucleosides (Scheme 44).

The structure of the obtained products **122a-c** was confirmed by using FT-IR, ^{1}H-NMR, ^{13}C-NMR and LC-MS. The IR confirmed the formation of *O-*isomer by the appearance of a new signal at $\nu = 1741$ cm[-1] assigned to the acetyl ester at the sugar moiety while no signals observed at $\nu = 1640 - 1690$ cm[-1] related to the pyrazolin-3-one. ^{1}H-NMR (400 MHz, CDCl$_3$) showed two signals at δ 2.05, 2.15 ppm corresponding to the two methyl protons of the acetoxy groups, while the 2"-deoxyribose anomeric proton appeared as a doublet of doublet at δ 5.83 ppm, integrated to one proton with coupling constant $J = 2.8, 8.8$ Hz confirmig the diaxial in β-form. While other sugar proton H-2"a, 2"b, 5a,b", 4", and 3", resonate at δ 2.10, 2.67, 3.94, 5.11, 5.66 respectively. The aromatic protons of **122a** appeared as multiplets at 6.98-7.40 ppm (Figure 39). ^{13}C-NMR (100 MHz, CDCl$_3$) also used to confirm the correct number of carbon atoms at the correct chemical shifts. The anomeric carbon resonates at δ 78.5 ppm while C-5 appeared at δ 157.6, ppm and C-3 appeared at δ 162.3 ppm (Figure 40).
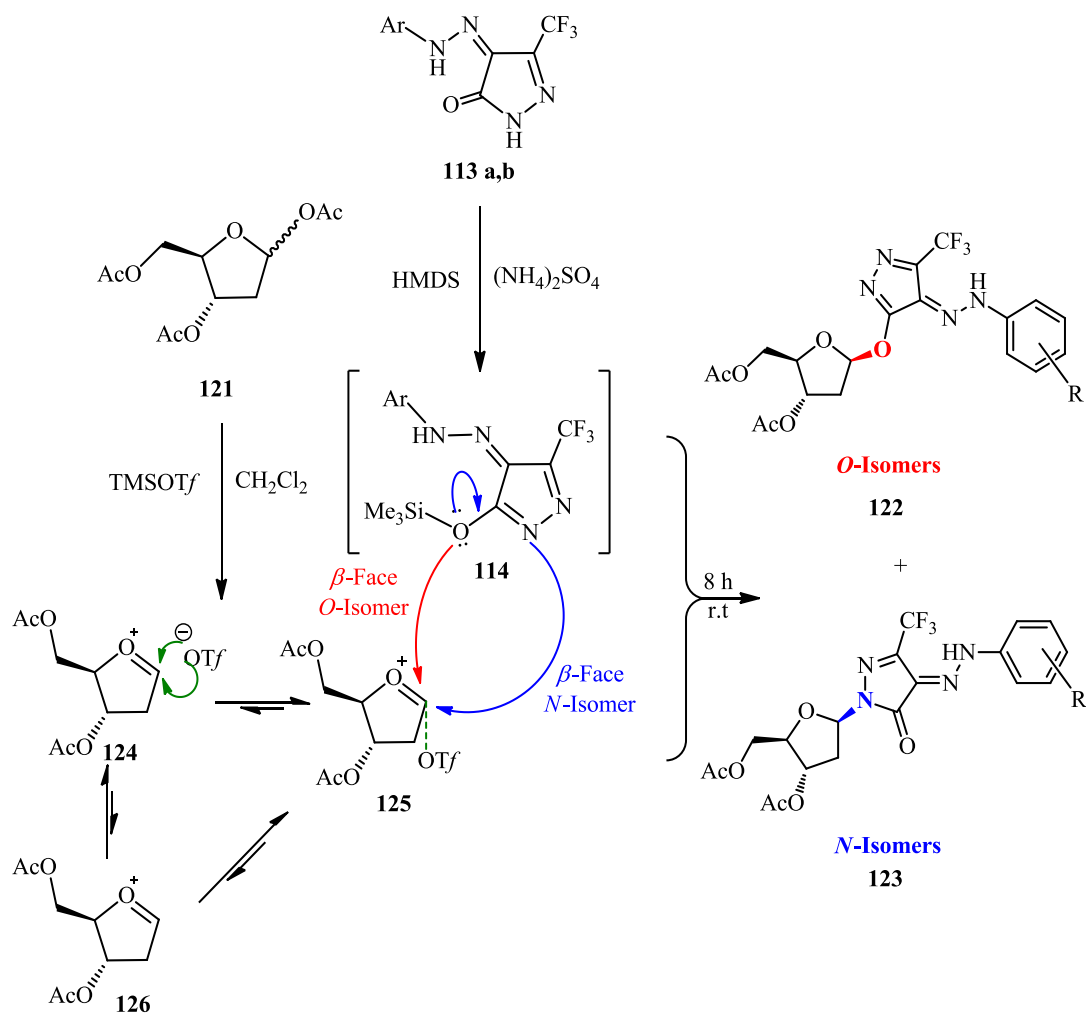
Scheme 44: Stereoselective synthesis of *O*- and *N*-β-2″-deoxyribose derivatives **122** and **123**
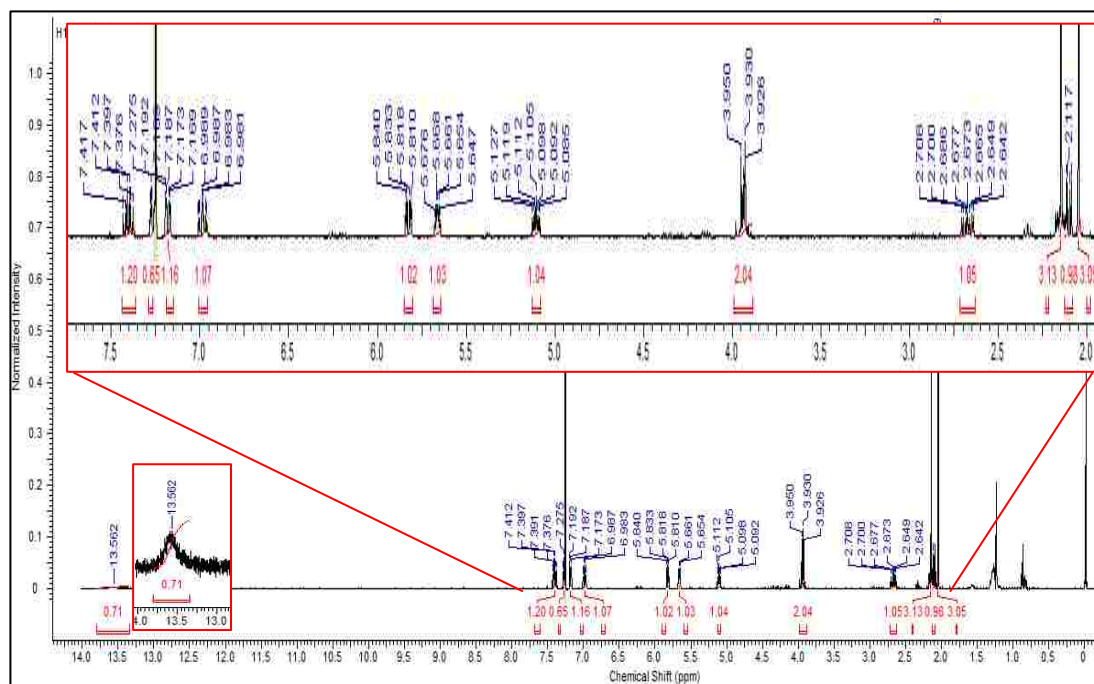
Figure 39: ^{1}H-NMR Spectrum for 3-(3'',5''-di-*O*-acetyl-2''-*β*-deoxy-ribofuranosyloxy)-4-(3'-fluorophenylhydrazono)-5-trifluoromethyl-2,4-dihydropyrazoline **122a**
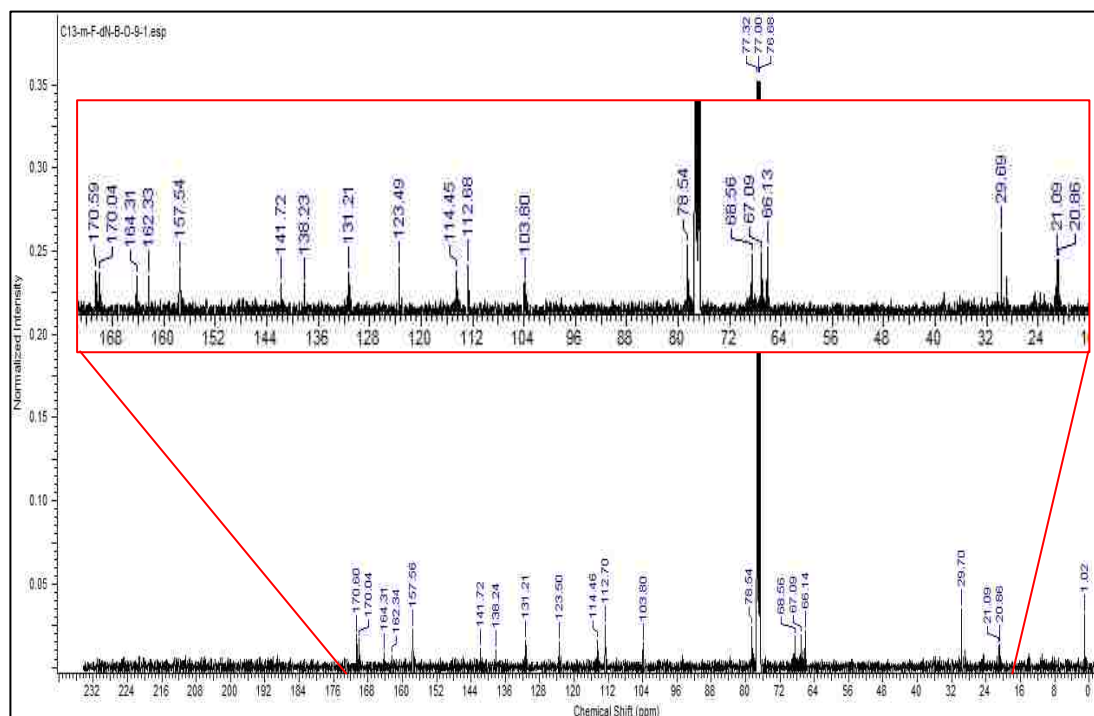

Figure 40: ^{13}C-NMR Spectrum for 3-(3'',5''-di-*O*-acetyl-2''-*β*-deoxy-ribofuranosyloxy)-4-(3'-fluorophenylhydrazono)-5-trifluoromethyl-2,4-dihydropyrazoline **122a**

2D-COSY NMR used for clearly assigning the correlation between protons in the sugar moiety. Figure 41 shows a strong cross-peak interaction between anomeric proton H-1″ δ 5.83 ppm and H-2″a at δ 2.67 ppm. H-2″a at δ 2.67 ppm has a cross-peak interaction with H-2″ b at δ 2.10 ppm. And H-2″ b at δ 2.10 ppm showed cross-peak interaction with H-3″ at δ 5.66 ppm. 2D-COSY shows also another cross-peak interaction between H-4″ at δ 5.11 ppm and H-5″a,b at δ 3.94 ppm. That confirm the correct order of sugar moiety protons assign. H-2' at δ 7.28 ppm showed no interaction with any other protons in the molecule. While both H-4' δ 6.98 ppm and H-6' δ 7.18 ppm showed a cross-peak interaction with H-5' δ 7.40 ppm (Figure 41).
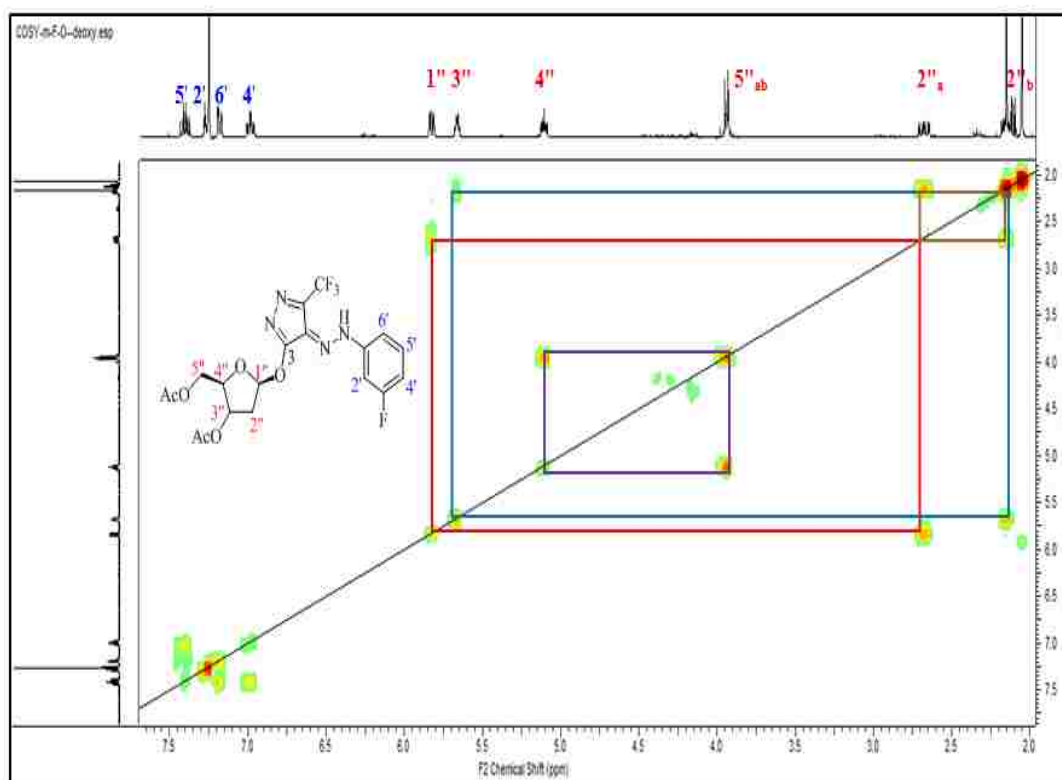
Figure 41: 2D-COSY Spectrum for 3-(3″,5″-di-*O*-acetyl-2″-*β*-deoxy-ribofuranosyloxy)-4-(3'-fluorophenylhydrazono)-5-trifluoromethyl-2,4-dihydropyrazoline **122a**

Heteronuclear correlation ¹H-¹³C was used to support the suggested structure of 3-(3″,5″-di-*O*-acetyl-2″-*β*-deoxy-ribofuranosyloxy)-4-(3'-fluorophenylhydrazono)-

5-trifluoromethyl-2,4-dihydropyrazoline **122a**. The HSQC spectrum showed the direct correlation for short range ^{1}H-^{13}C interaction. Strong cross-peak interactions were found between the anomeric proton H-1" at δ 5.83 ppm with C-1″ at δ 78.5 ppm of the sugar moiety. While the both protons at position 2″, H-2"a,b δ 2.10 and 2.67 ppm, showed cross-peak interaction with C-2″at δ 29.7 ppm, H-3" δ 5.66 ppm correlated with C-3″ at δ 68.6 ppm, H-4" δ 5.11 ppm correlated with C-4″ at δ 67.1 ppm, and the both protons at position 5″, H-5"a,b δ 3.94 ppm, correlated with C-5″ at δ 66.1 ppm. In the aromatic region, The four aromatic protons at δ 6.98, 7.18, 7.28, 7.40 ppm showed cross-peak interaction with the aromatic carbons at δ 114.5, 112.7, 103.8 and 131.2 ppm; respectively (Figure 42).
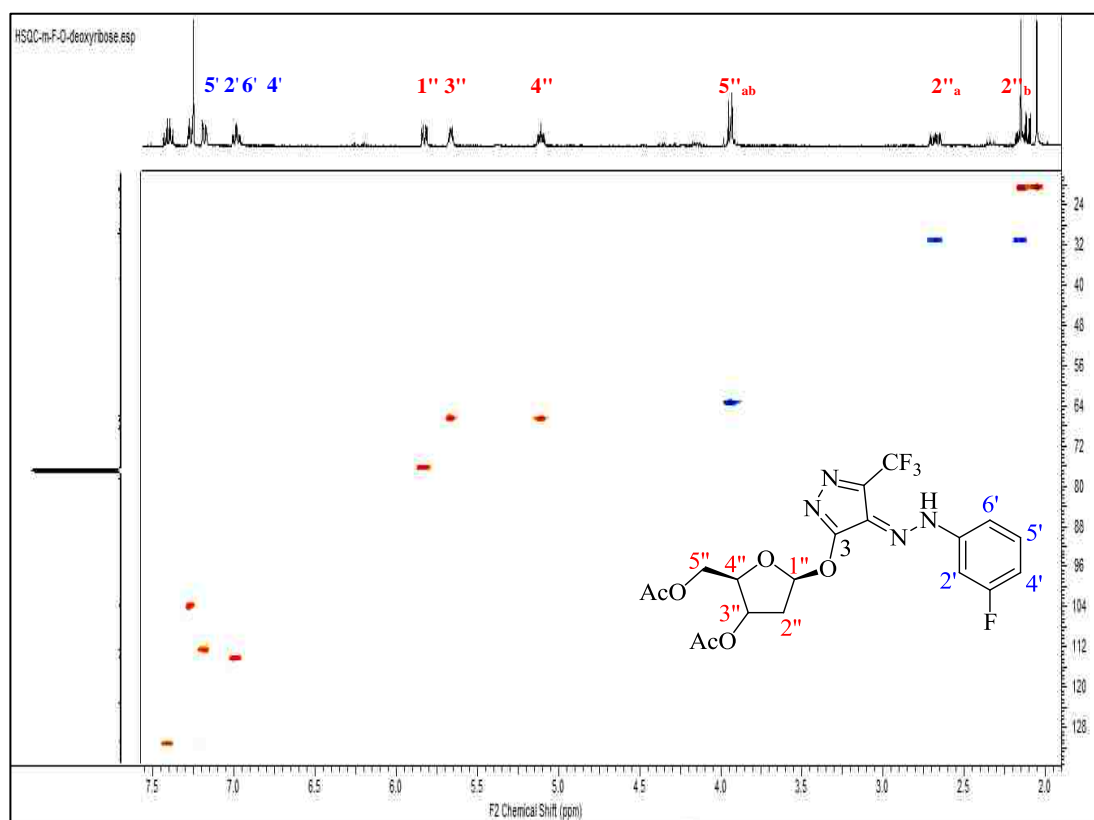
Figure 42: 2D-HSQC Spectrum for 3-(3",5"-di-*O*-acetyl-2"-*β*-deoxy-ribofuranosyloxy)-4-(3'-fluorophenylhydrazono)-5-trifluoromethyl-2,4-dihydropyrazoline **122a**

Mass spectroscopic analysis was used to confirm the fractions of the targeted product **122a**. The total molecular ion peak appeared at m/z 475 with 97% intensity (Figure 43). The fragment mass spectroscopic scheme shows the pattern of fragmentation with its relative intensity (Scheme 45).

To confirm the formation of *O*- and *N*-deoxyribosides, spectra analysis such as IR, and NMR were used. For example, the *O*-deoxyriboside **122a** compared to the *N*-deoxyribosides using IR spectroscopy analysis by comparing between signals appeared within $v = 1640\text{-}1690$ cm^{-1}. The formation of *O*-deoxyriboside leads to the disappearance of the amid carbonyl at 1640-1690 cm^{-1} (Figure 44, **A**) while the formation of *N*-deoxyribosides is confirmed by the existing of the amid-carbonyl at 1640-1690 cm^{-1} (Figure 44, **B**).

The ^{1}H-NMR (400 MHz, $CDCl_3$) data was used to confirmed the formation of both our *O*- and *N*-ribosides. Studying the difference in chemical shift of the anomeric proton in both isomers. The anomeric proton in **122a** observed as doublet of doublet at δ 5.83 ppm with coupling constant $J = 2.8$, 8.8 Hz, while the anomeric proton in **123a** observed as doublet at δ 5.50 ppm with coupling constant $J = 10.8$ Hz confirmig the diaxial in *β*-form (Figure 45). ^{13}C-NMR (100 MHz, $CDCl_3$) also confirmed the forming of *O*- and *N*-deoxyribosides by studying the difference in chemical shift of the anomeric carbon in both isomers. The anomeric carbon in **122a** observed at δ 78.5 ppm while the anomeric carbon in **123a** observed at δ 77.2 ppm due to the highly shielded *N*-atom compared to the deshieded *O*-atom (Figure 46).
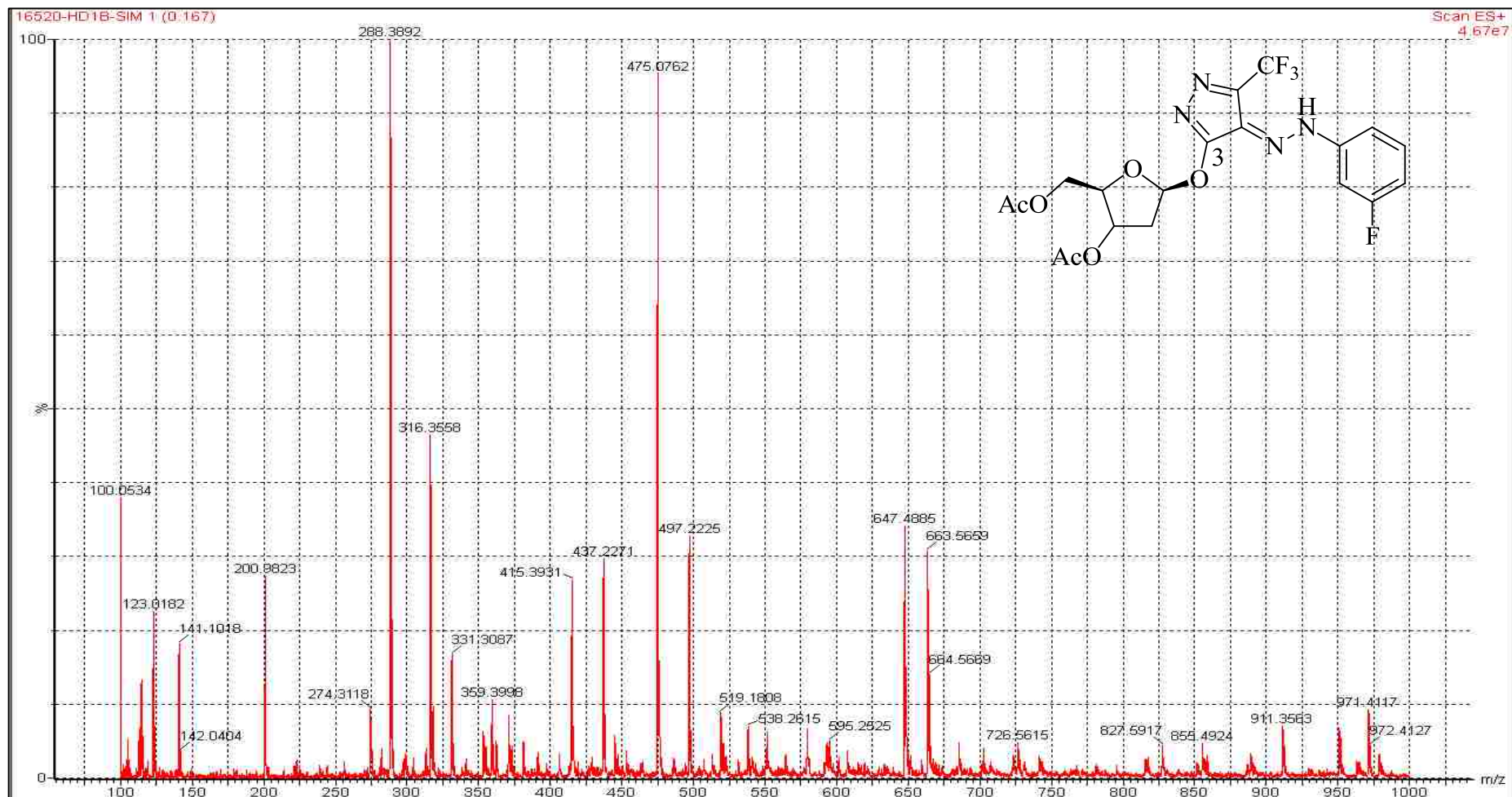
Figure 43: Mass fragmentation spectrum for 3-(3",5"-di-*O*-acetyl-2"-*β*-deoxy-ribofuranosyloxy)-4-(3'-fluorophenylhydrazono)-5-trifluoromethyl-2,4-dihydropyrazoline **122a**
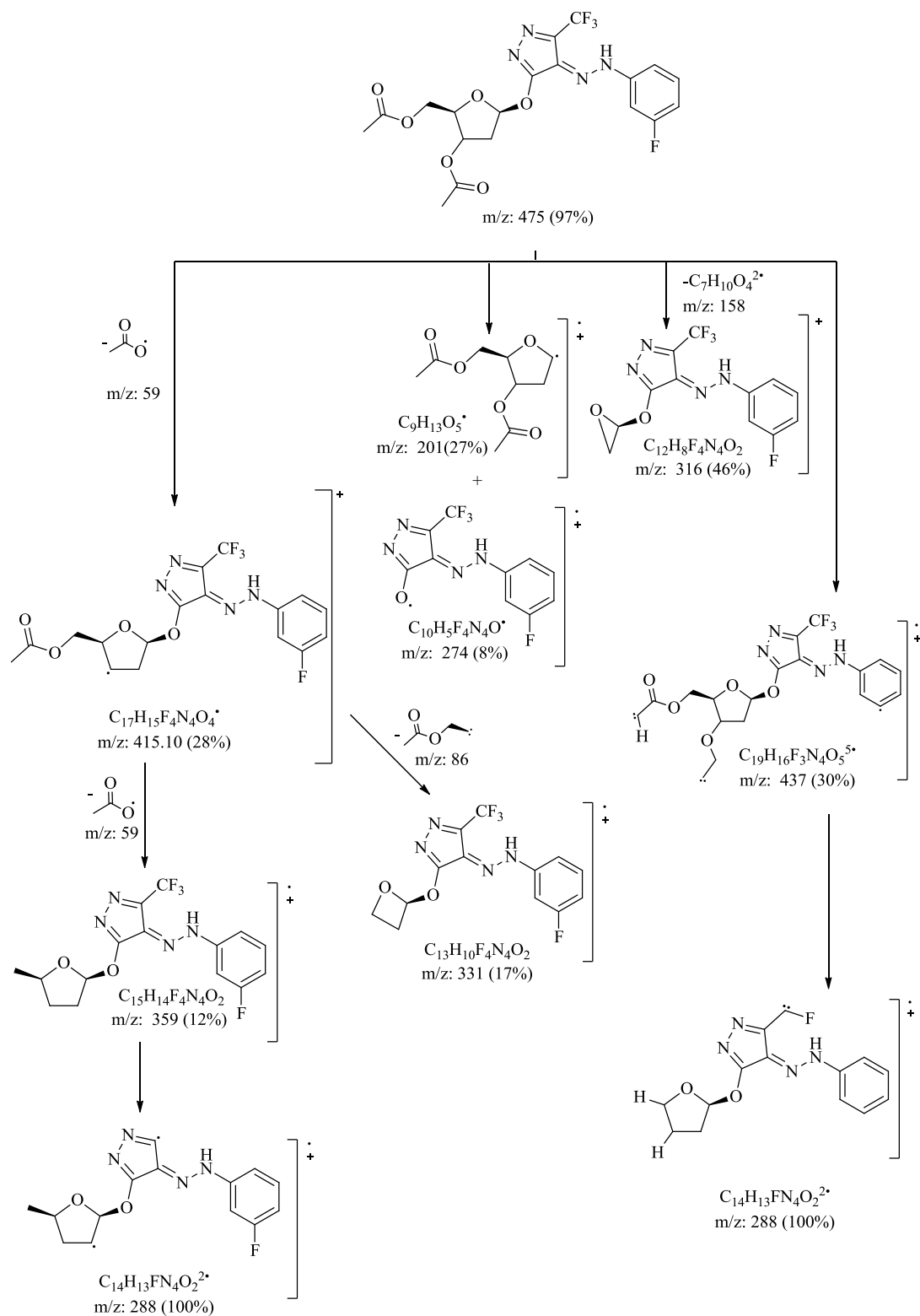
Scheme 45: Mass fragments scheme for 3-(3",5"-di-*O*-acetyl-2"-β-deoxy-
ribofuranosyloxy)-4-(3'-fluorophenylhydrazono)-5-trifluoromethyl-2,4-
dihydropyrazoline **122a**
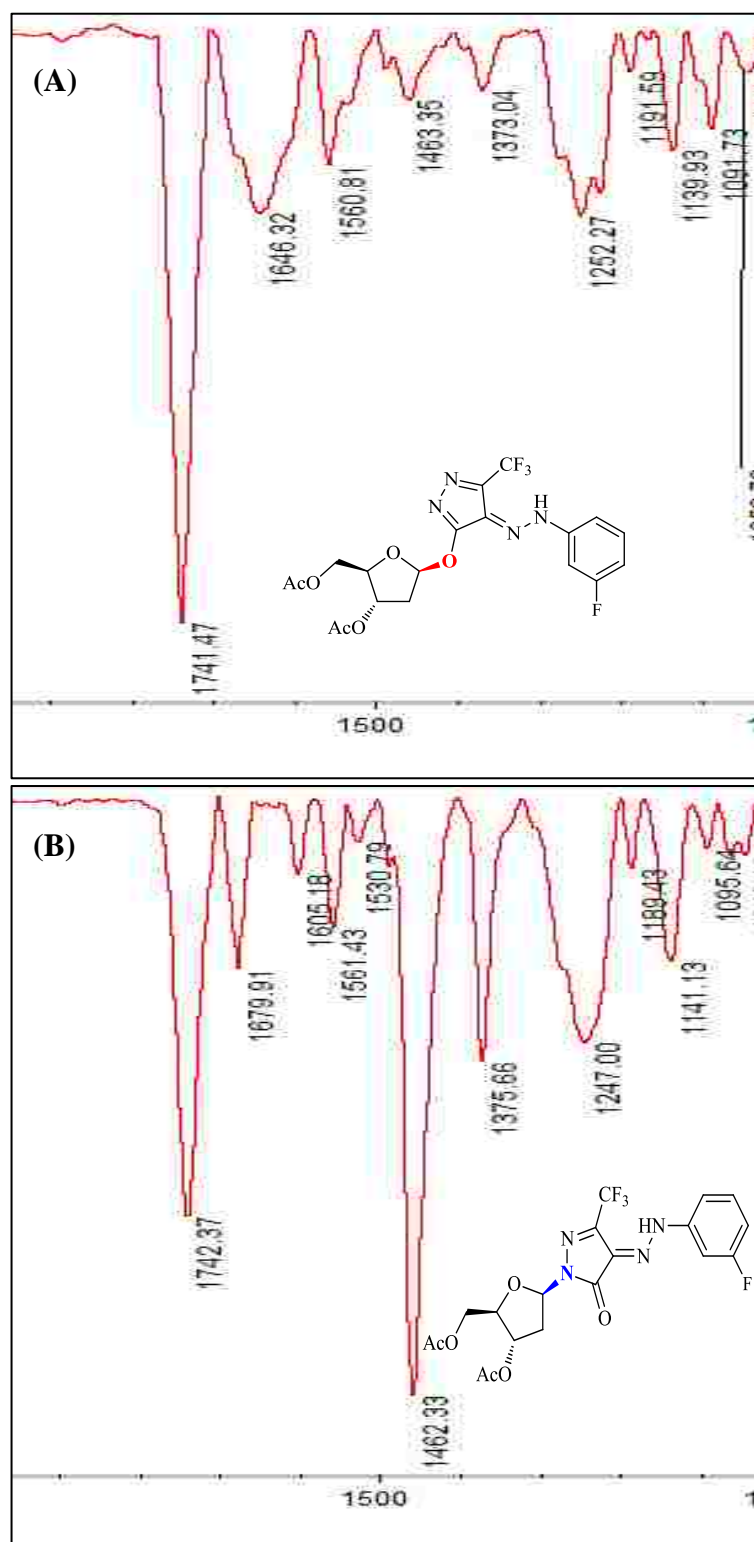
Figure 44: IR spectra for (**A**) *O*-deoxyriboside **122a**, (**B**) *N*-deoxyriboside **123a**
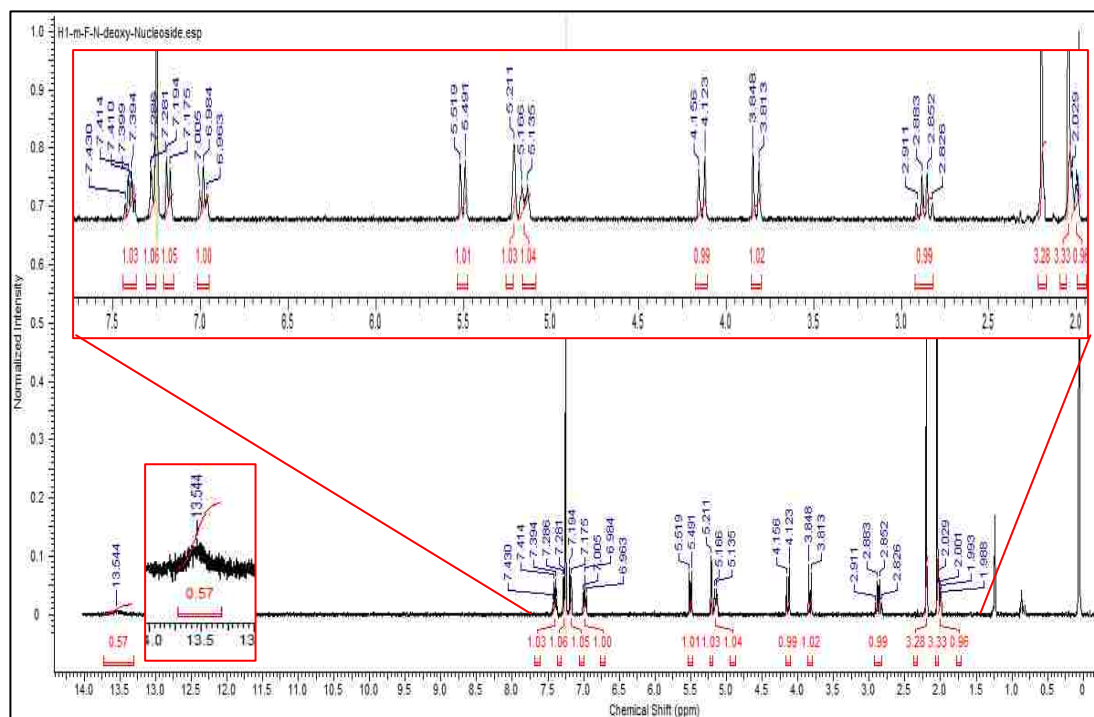
Figure 45: ^{1}H-NMR Spectrum for 2-(3",5"-di-*O*-acetyl-2"-*β*-deoxy-ribofuranosyl)-4-(3'-fluorophenylhydrazono)-5-trifluoromethyl-2,4-dihydropyrazol-3-one **123a**
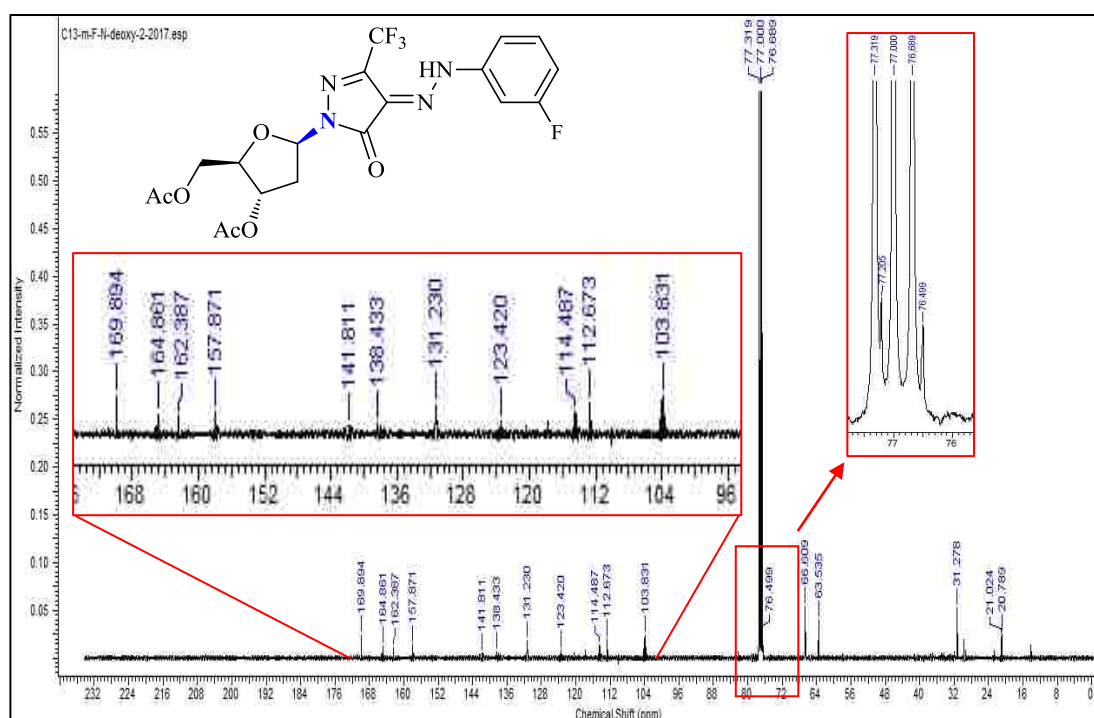
Figure 46: ^{13}C-NMR Spectrum for 2-(3",5"-di-*O*-acetyl-2"-*β*-deoxy-ribofuranosyl)-4-(3'-fluorophenylhydrazono)-5-trifluoromethyl-2,4-dihydropyrazol-3-one **123a**
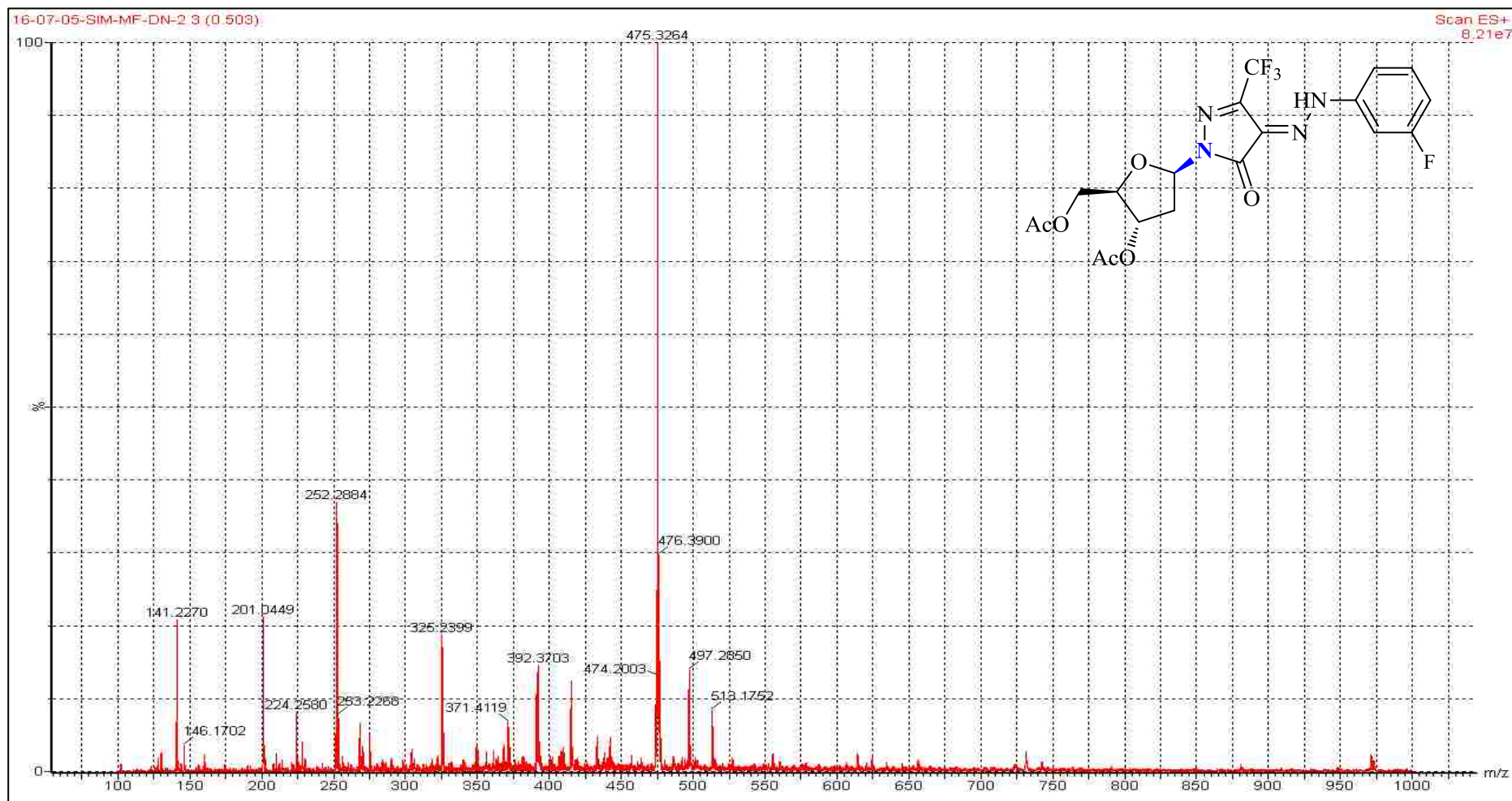
Figure 47: Mass spectrum for 2-(3",5"-di-*O*-acetyl-2"-*β*-deoxy-ribofuranosyl)-4-(3'-fluorophenylhydrazono)-5-trifluoromethyl-2,4-dihydropyrazol-3-one **123a**

Mass spectroscopic analysis was used to confirm the fractions of the targeted product **123a**. The total molecular ion peak appeared at m/z 475 with 97% intensity (Figure 47). The fragment mass spectroscopic scheme shows the pattern of fragmentation with its relative intensity (Scheme 46).
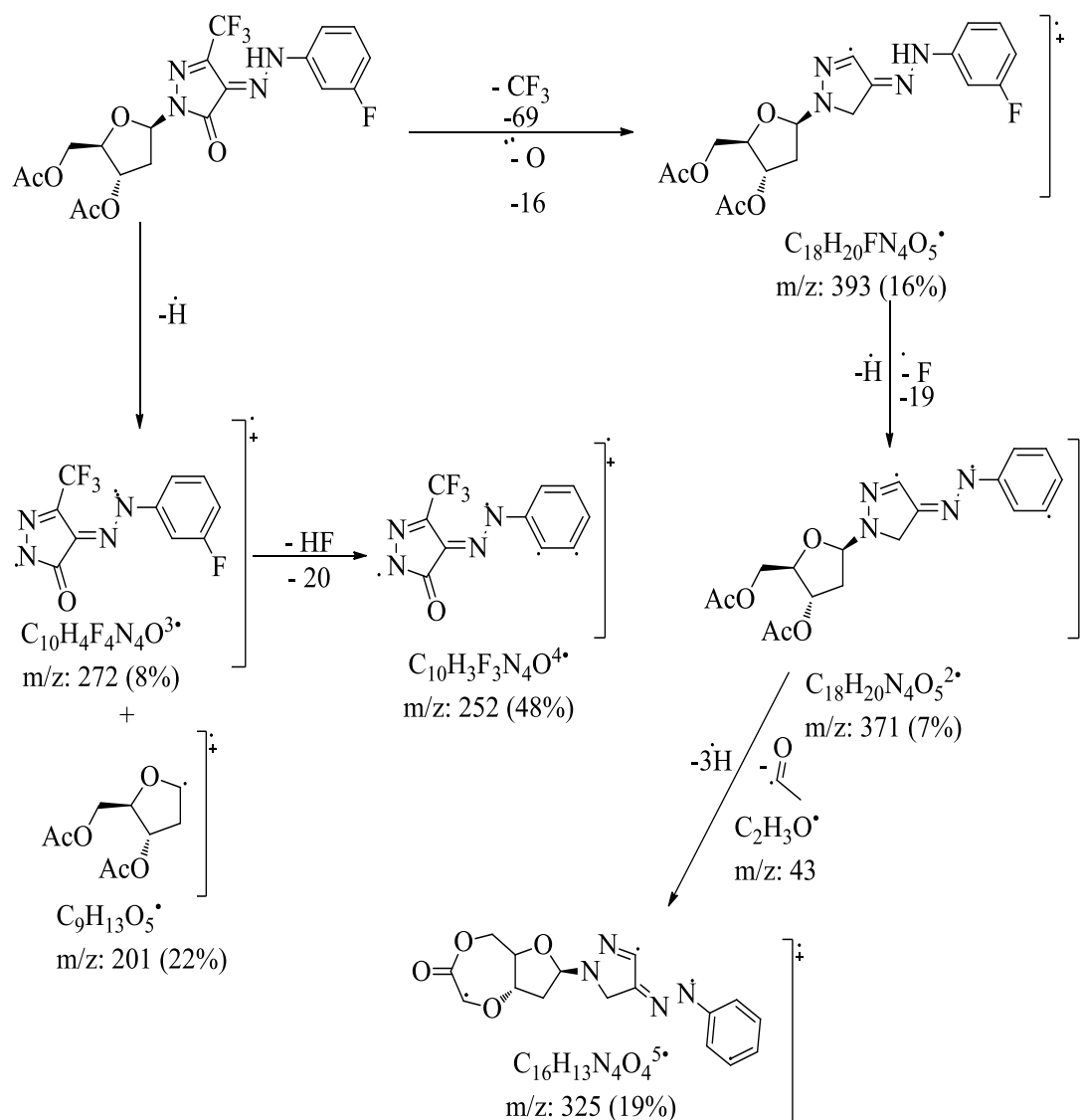
Scheme 46: Mass fragments scheme for 2-(3",5"-di-*O*-acetyl-2"-β-deoxy-ribofuranosyl)-4-(3'-fluorophenylhydrazono)-5-trifluoromethyl-2,4-dihydropyrazol-3-one **123a**

2.3.7 Synthesis of Benzolyated Pyrazolone Derivatives

To extend our study to more hydrophobic examples, brnzoyl group was choosen to interduce into pyrazolone ring using two different synthetic methods. In method 1, a simple nucleophlic substitution reaction was used to introduce the benzoyl group into the pyrazolone ring. As discussed earlier, activating pyrazolone enhanced the nucleophilicity of both O- and N^2 center of the pyrazolone ring. The reaction between the pyrazolone and benzoyl chloride afforded only one isomer identified later as benzoyl ester of the pyrazolone (Scheme 47).

Entry	R	R´
124a	3-F	4-F
124b	4-F	4-F
124c	$3-CF_3$	4-F
124d	$3-CF_3$	$4-OCF_3$
124e	4-F	H
124f	$3-NO_2$	H
124g	$3-NO_2$	4-F
127h	4-Br	H
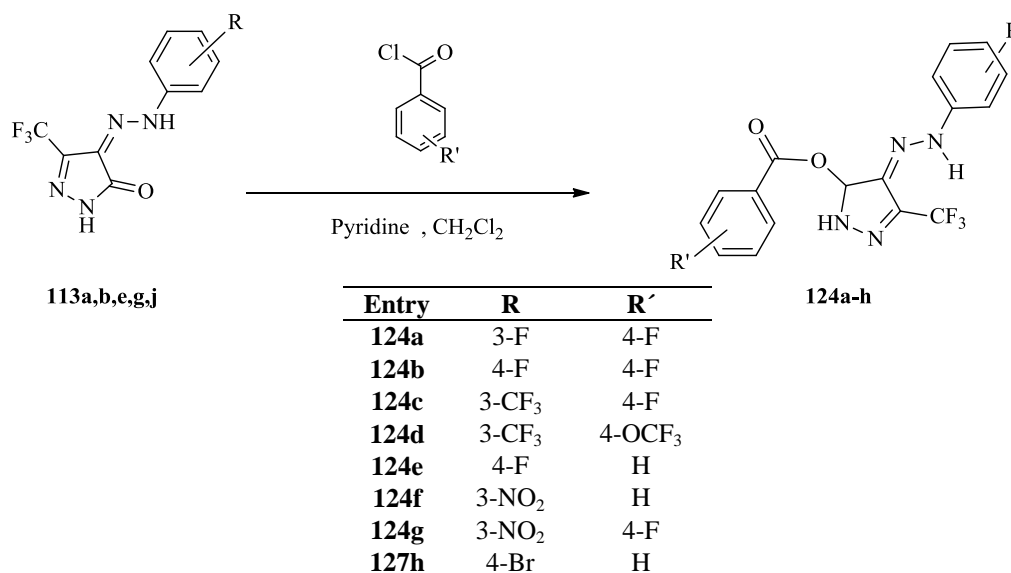
Scheme 47: Synthesis of 4-arylhydrazono-benzoyl-5-trifluoromethyl-2,4 dihydropyrazoline **124a-h**

In method 2, benzoyl group introduced directly into the hydrazine nitrogen then cyclizaed followed by diazotization to afforded the *N*-benzoyl analogue **127a-c** (Scheme 48). The structures of both *O*-benzoylation and *N*-benzoylation were confirmed.

The structure of the obtained products **124a-h** were confirmed by using FT-IR, ^{1}H-NMR, ^{13}C-NMR and LC-MS. The IR for 4-[2-(3'-nitrophenyl)hydrazono]-3-(trifluoromethyl)-4-*4H*-pyrazol-3-benzoate **124f** confirmed the formation of Pyrazolone-*O*-benzoyl by the appearance of a the sharp signal at ν = 1725 cm^{-1} assigned to the ester group formed by the bezoyl and the pyrazolone *O*-atom. While no signals observed at ν = 1640-1690 cm^{-1} related to the pyrazolin-3-one (Figure 48). ^{1}H-NMR (400 MHz, DMSO-d_6) showed all aromatic protons, as maltiplet at δ 7.54 and 7.71 ppm integrated to one and two protons repectivly. Then it showed doublet at δ 7.85 ppm with coupling constant *J* = 7.6 Hz. ^{1}H-NMR also showed a multipltet at δ 8.04 ppm integrated to one proton. Then singlet at 8.45 ppm assigned for the H-2´ (Figure 49). ^{13}C-NMR (100 MHz, DMSO-d_6) also used to confirm the correct number of carbon atoms at the correct chemical shifts. The pyrazoline carbones C-3 resonates at δ 158.8 ppm while C-5 appeared at δ 149.1 ppm. The ester carbonyl appeared at 165.6 ppm (Figure 50).

Entry	R
127a	3-CF$_3$
127b	2,4-di-Cl
127c	3-NO$_2$
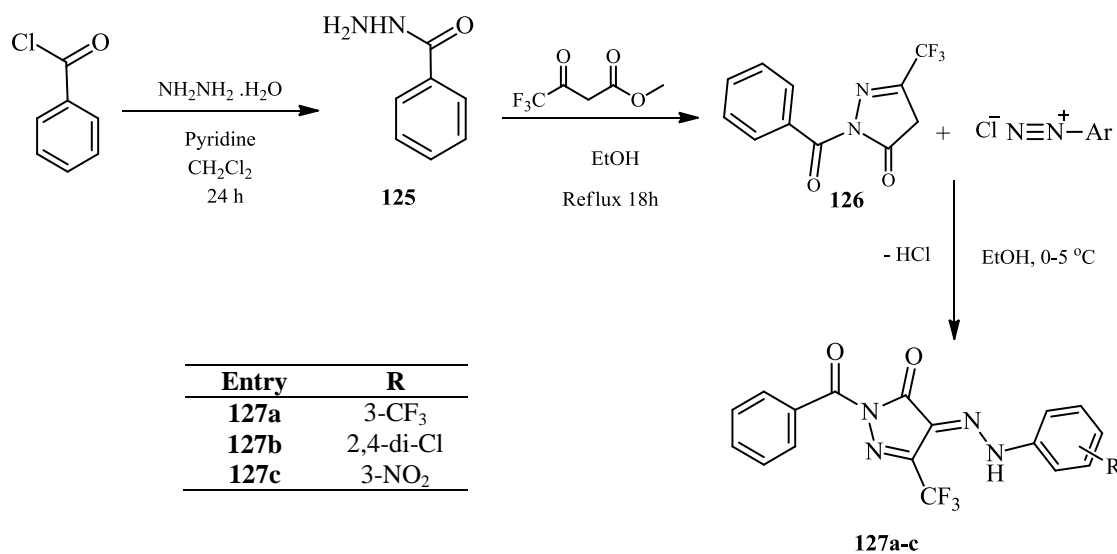
Scheme 48: Synthesis of 2-benzoyl-5-trifluoromethyl pyrazol-3-one **127a-c**
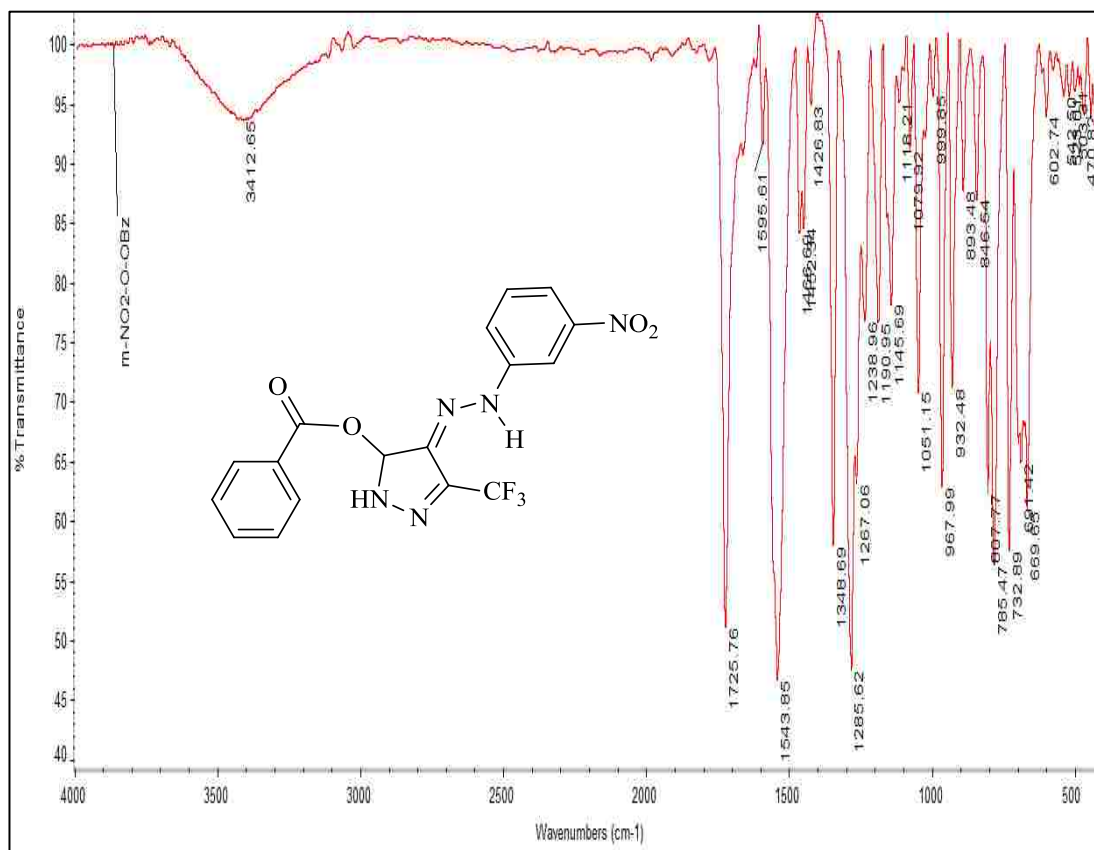
Figure 48: IR Spectrum of 4-[2-(3'-nitrophenyl)hydrazono]-3-(trifluoromethyl)-4-4*H*-pyrazol-3-benzoate **124f**
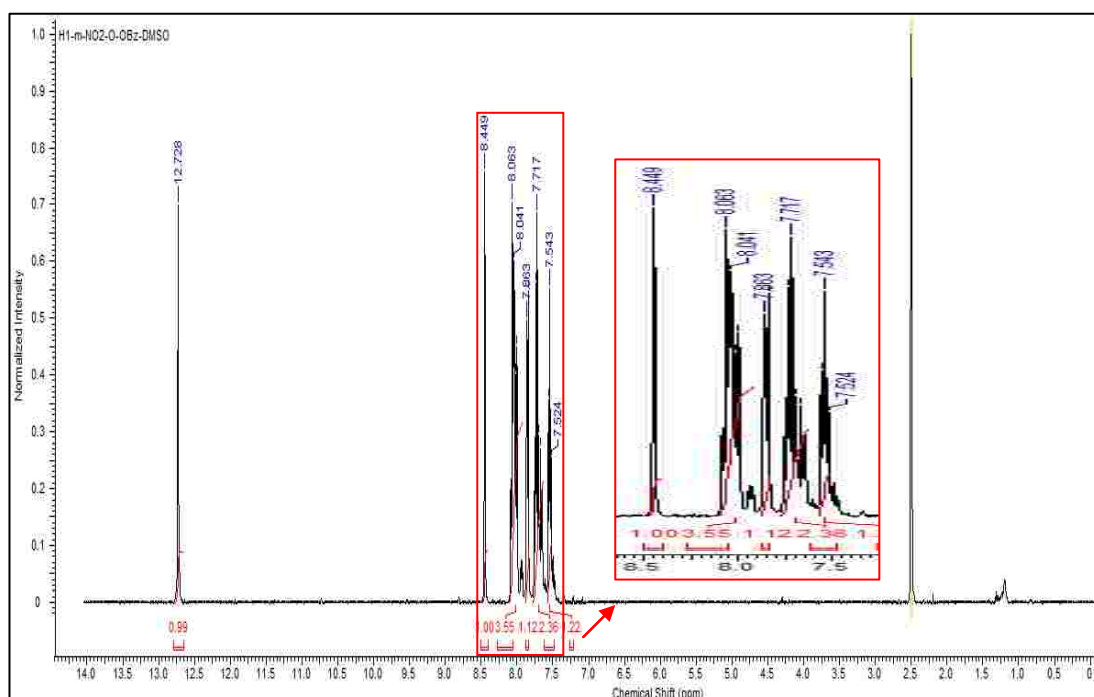
Figure 49: ^{1}H-NMR Spectrum for 4-[2-(3'-nitrophenyl)hydrazono]-3-(trifluoromethyl)-4-4*H*-pyrazol-3-benzoate **124f**
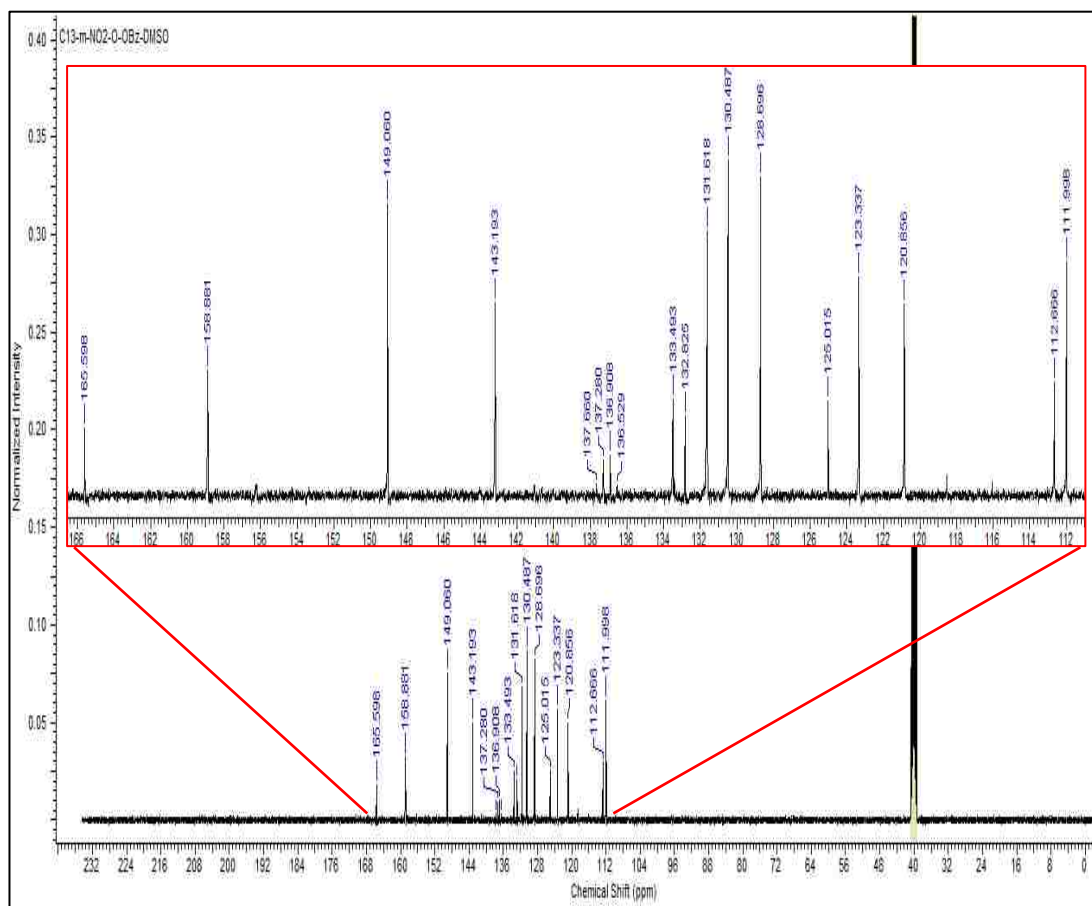
Figure 50: ¹³C-NMR Spectrum for 4-[2-(3'-nitrophenyl)hydrazono]-3-(trifluoromethyl)-4-4*H*-pyrazol-3-benzoate **124f**

The mass spectroscopic analysis was used to confirm the fractions of the targeted product **124f**. The total molecular ion peak appeared at m/z 407 with 25% intensity. The fragment mass spectroscopic scheme shows the pattern of fragmentation with its relative intensity (Scheme 49).
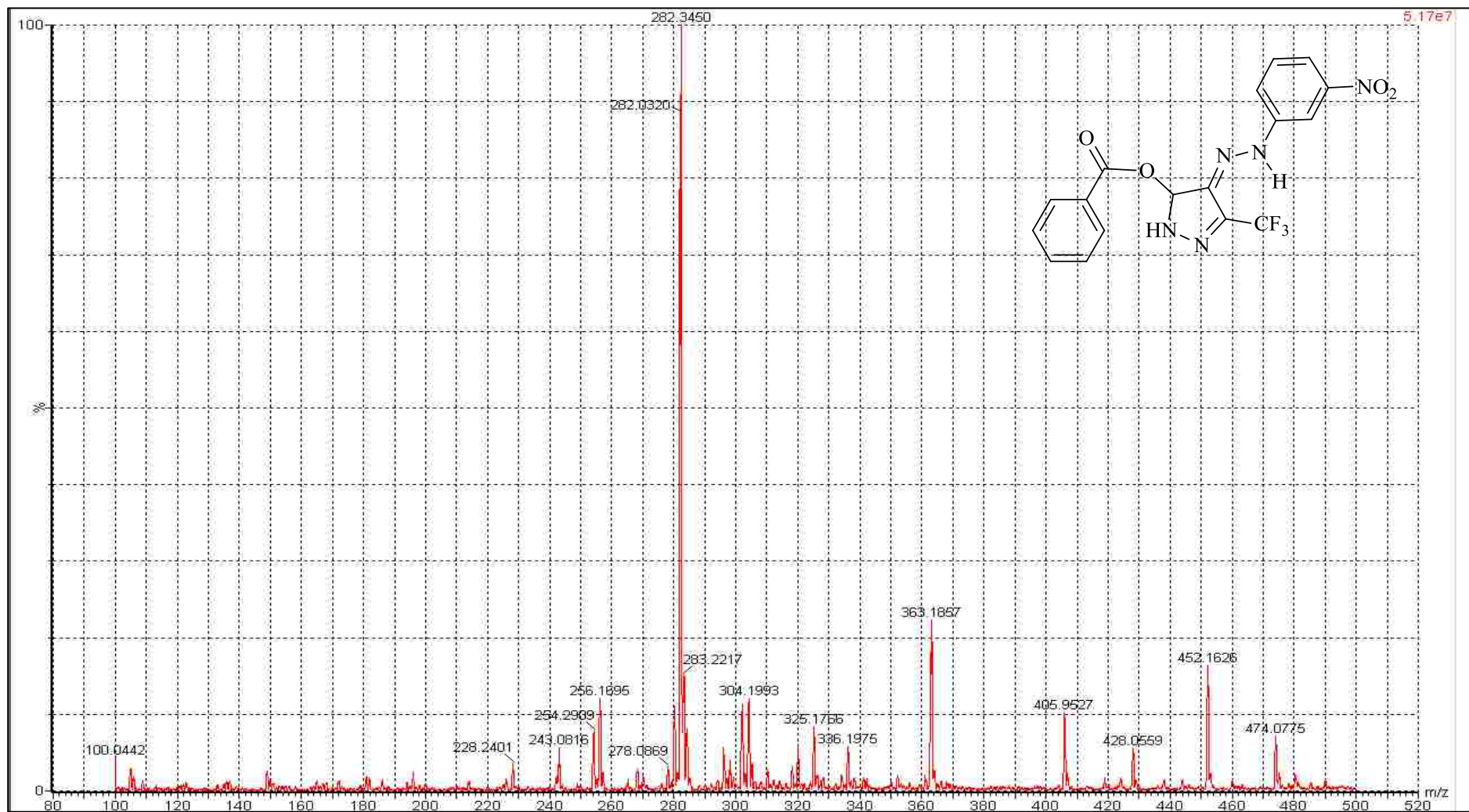
Figure 51: Mass spectrum for 4-[2-(3'-nitrophenyl)hydrazono]-3-(trifluoromethyl)-4-4*H*-pyrazol-3-benzoate **124f**
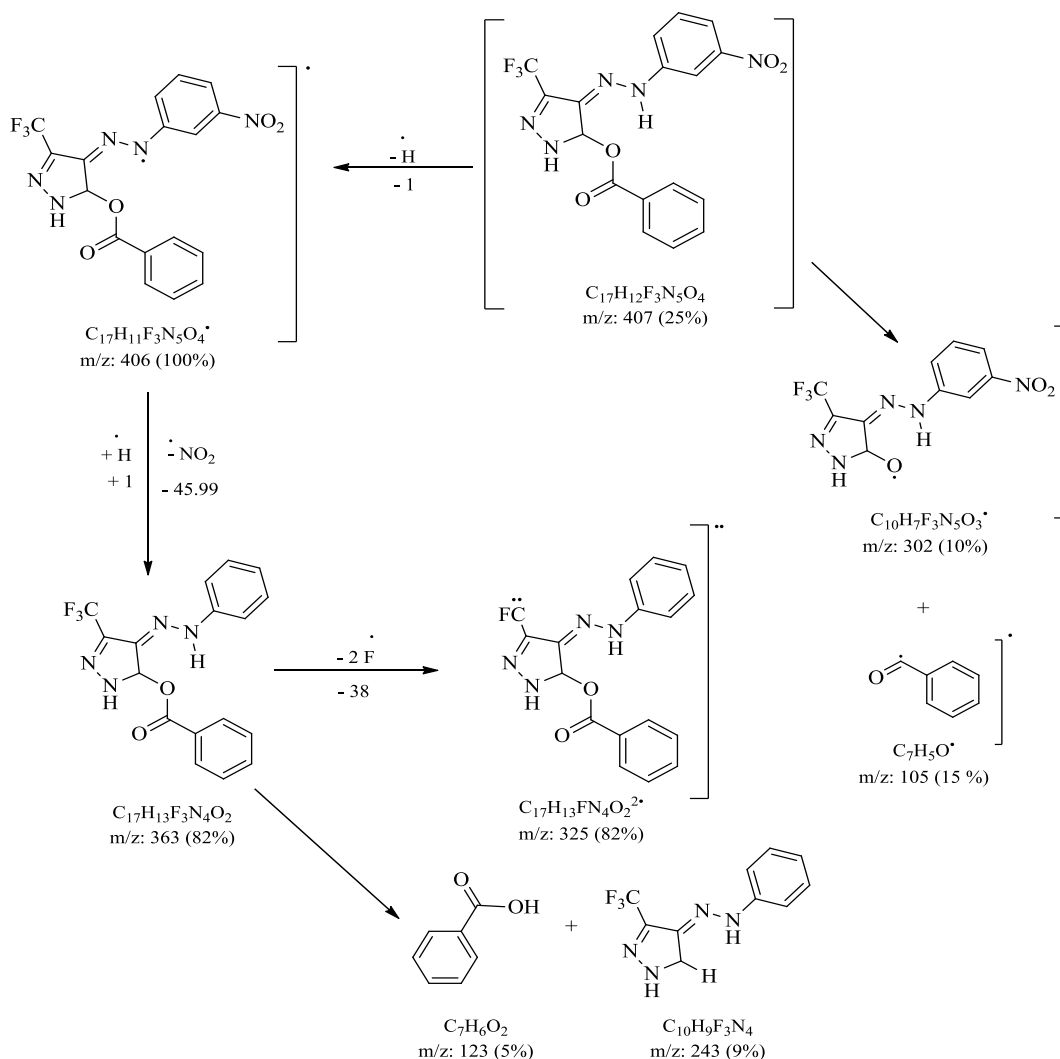
Scheme 49: Mass fragments scheme for 4-[2-(3'-nitrophenyl)hydrazono]-3-
(trifluoromethyl)-4-4*H*-pyrazol-3-benzoate **124f**

To confirm the formation of *O*- and *N*-benzoyl, spectrascopic analysis such as
IR, and NMR were used. For example, IR spectroscopy analysis was used to
compare between the *O*-isomer **124f** and the *N*-isomer **127c** using the IR signals
appeared within $\nu = 1650\text{-}1690 \text{ cm}^{-1}$. The formation of *O*-isomer **124** leads to the
disappearance of the amid carbonyl at $1650\text{-}1690 \text{ cm}^{-1}$ (Figure 52, **A**) while the

formation of *N*-isomer is confirmed by the existing of the amid-carbonyl at 1640-1690 cm^{-1} (Figure 52, **B**).

The ^{1}H-NMR (400 MHz, DMSO-d_6) data also used to confirmed the formation of both our *O*- and *N*-isomers. Studying the difference in chemical shift of the aromatic protons in both isomers. The aromatic protons in *O*-isomer **124f** observed shifted little bit to the lower filed region δ 7.54-8.45 ppm compared to the *N*-isomer **127c** which appear at δ 7.55-7.85 ppm (Figure 54).

^{13}C-NMR (100 MHz, DMSO-d_6) also used to confirmed the structure of N^2-benzoyl)-4-(3'-nitrophenylhydrazono)-5-trifluoromethyl-pyrazolone **127c** by confirm the correct number of carbon atoms at the correct chemical shifts. The pyrazoline carbone C-3 resonates at δ 158.0 ppm while C-5 appeared at δ 140.1 ppm. And the ester carbonyl appeared at 165.1 ppm (Figure 55).
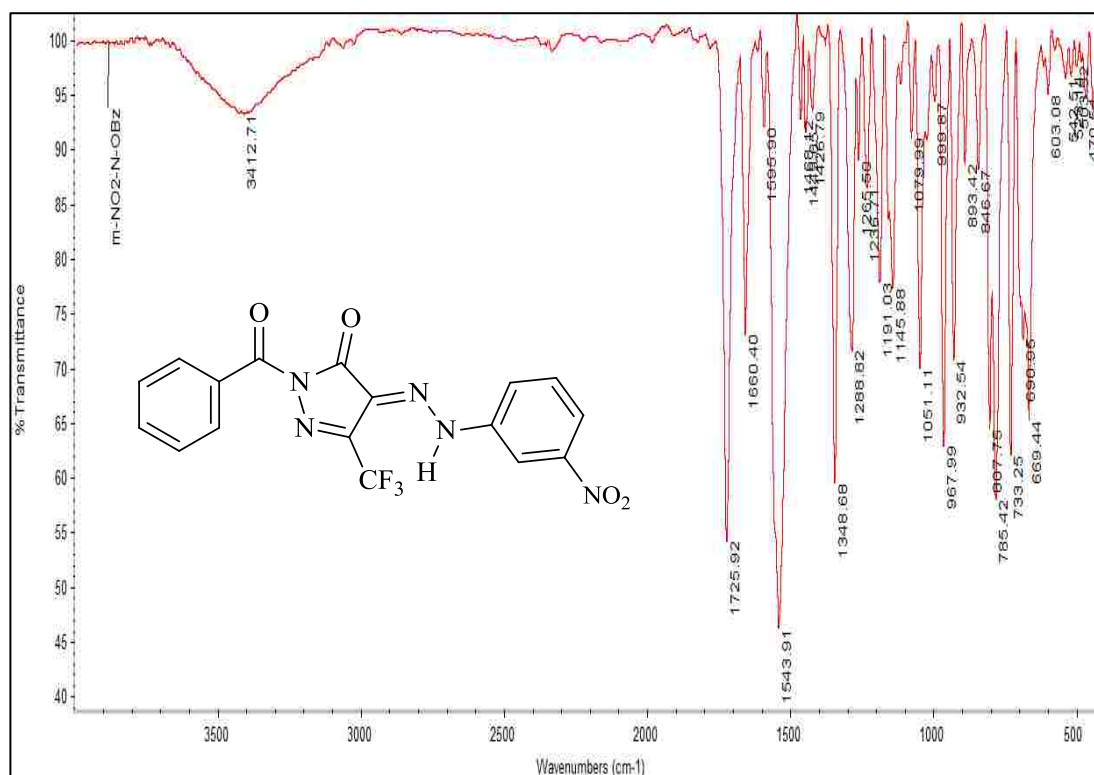
Figure 52: IR Spectrum of N^2-benzoyl)-4-(3'-nitrophenylhydrazono)-5-trifluoromethyl-pyrazolone **127c**
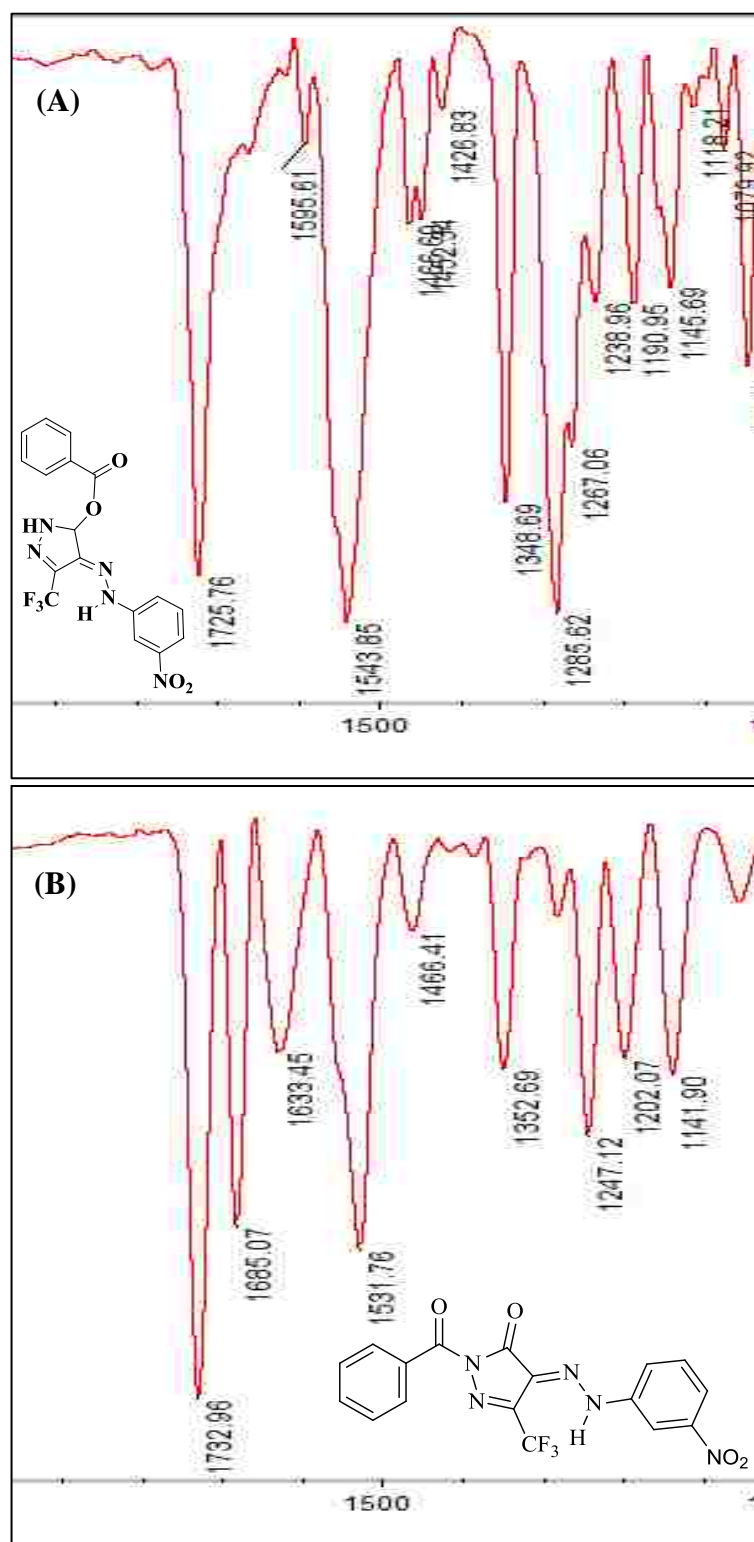
Figure 53: IR Spectra for (A) *O*-isomer **124f**, (B) *N*-isomer **127c**
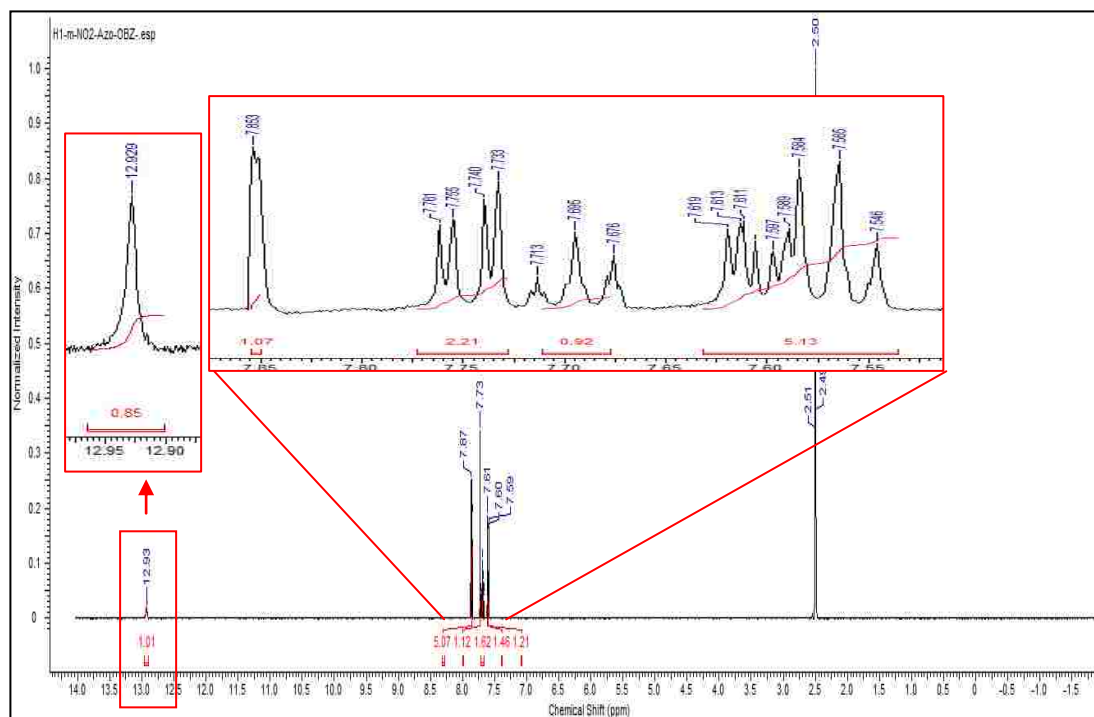
Figure 54: ^{1}H-NMR Spectrum for N^2-benzoyl)-4-(3'-nitrophenylhydrazono)-5-
trifluoromethyl-pyrazolone 1**27c**
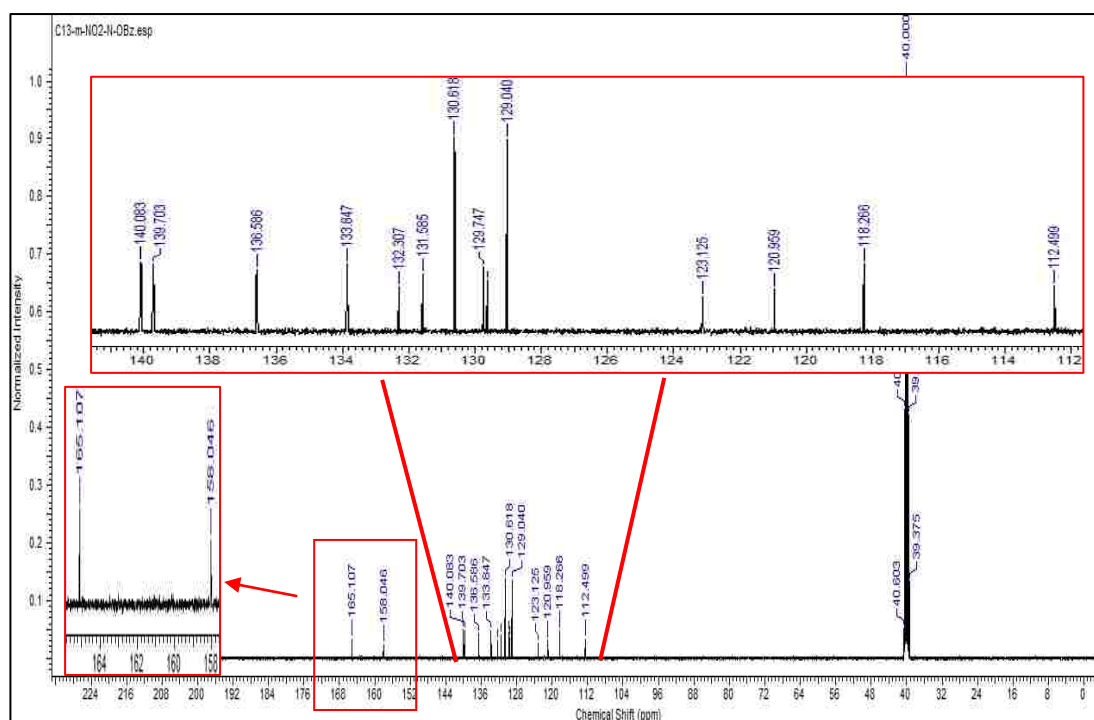
Figure 55: ^{13}C-NMR Spectrum for N^2-benzoyl)-4-(3'-nitrophenylhydrazono)-5-
trifluoromethyl-pyrazolone **127c**
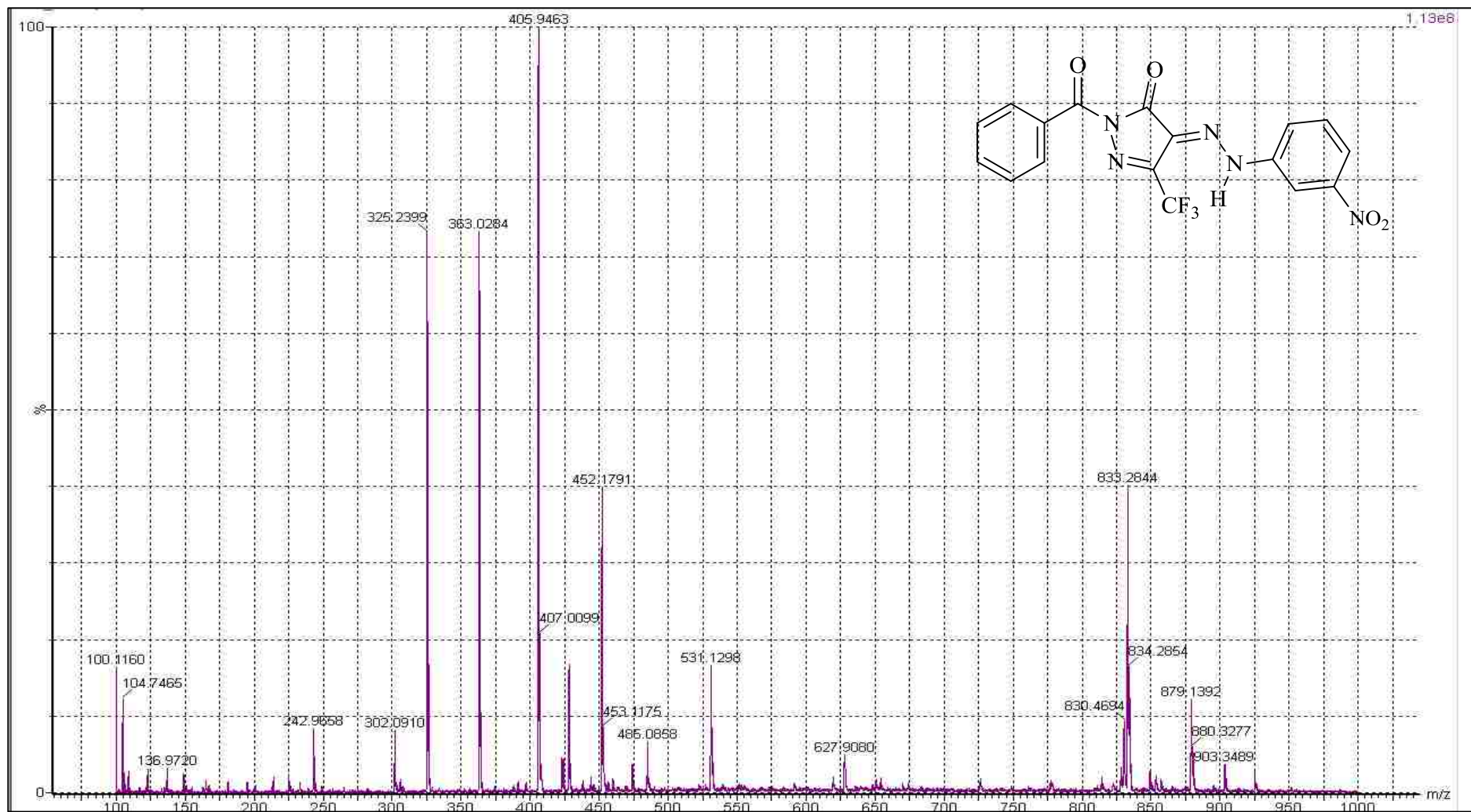
Figure 56: Mass spectrum for N^2-benzoyl)-4-(3'-nitrophenylhydrazono)-5-trifluoromethyl-pyrazolone **127c**
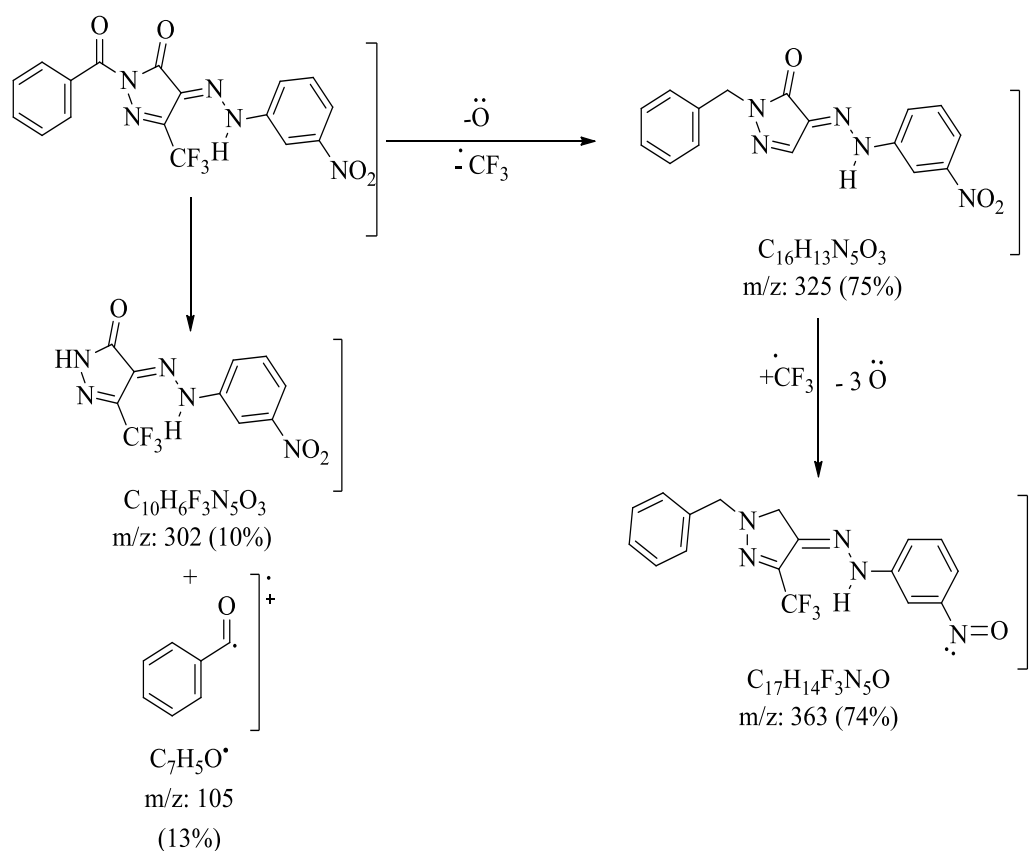
Scheme 50: Mass fragments scheme for of N^2-benzoyl)-4-(3'-nitrophenylhydrazono)-5-trifluoromethyl-pyrazolone **127c**

2.4 Summary

The main objective of the present study involved synthesis of some novel pyrazolone derivatives and to estudy their mechanisms and to confirm suggested structures. The study includes the syntheses and characterization of new pyrazolone derivatives, such as: pyrazolone riboside, deoxyriboside and benzolyated analogues. The organic synthesis contains two main parts, synthesis and structural analysis.

Initially, the synthesis of pyrazolone covered their reaction mechanisms and the spectral data analysis to confirm suggested structures of the novel derivatives.

Two isomers were successfully obtained and identified as *O-* and *N-* isomers. The structures of two isomers were confirmed using FT-IR, ^{1}H-NMR, ^{13}C-NMR and LC-MS/MS spectroscopic techniques. From the data analysis, it was stated that the reaction time regeioselective controlled the synthesized *O-* and *N-*isomers.

Chapter 3: Biological Activities

3.1 Introduction

Due to the increasing incidents of human's susceptibility to microbial and cancerous infections, attempts have been made to synthesize new heterocyclic compounds including pyrazoles to overcome the antimicrobial resistance and to minimize its side effects. Although pyrazoles have been reported to exhibit a wide range of biological activities, their potential has not been exploited to its full extent with respect to the previous reported applications. This part aimed to study the biological activities possessed by newly synthesized pyrazoles and their derivatives against common microbes as well as cancerous cells.

Some of the published results obtained from pyrazoline compound, including nucleosides, against bacterial infictions and leukemia showed promising results. The experiment was designed to be the Bauer Kirby disk susceptibility test to detect the growth of microbes and their sensitivity to the new synthezised compounds. The obtained results were reported using the minimum inhibitory concentration (MIC). In case of anti-cancer study, compounds tested against **HL60** human caucasian promyelocytic leukemia cell Line and **A-549** human non-small cell lung adenocarcinoma, then some active compounds tested against **MDA-MB- 231** human breast adenocarcinoma Cell Line and **HT29** human caucasian colon adenocarcinoma grade II Cell Line.

3.2 Experimental Part

3.2.1 Anti-fungal and Anti-bacterial Activities

3.2.1.1 Materials

Media for culturing (nutrient agar and broth) were obtained from Lab M Limited (UK). Two Gram positive bacteria (*Bacillus* and *Staphylococcus aureus*). Two Gram negative bacteria (*Escherichia coli and Proteus*) and used fungi (*Yeast*). Ceftriaxone (CEF) was used as a control antibiotic.

3.2.1.2 Methods

Some the synthesized compounds (Table 4) tested for their *in vitro* growth inhibitory activity against a panel of standard strains of pathogenic microorganism including Gram-positive and Gram-negative bacteria. Gram-positive bacteria's are*, Bacillus and Staphylococcus aureus*, Gram-negative bacteria's are *Escherichia coli and Proteus* and fungi *Yeast*. The efficacy determined by zone of inhibition values using disk diffusion technique [107]. To each plate, 20 mL of sterilized medium was added. After the agar had set, 10 % of each microorganism culture added to each plate. Sterilized Whatmann no. 1 filter paper discs (diameter 5 mm) were thoroughly moistened with the synthesized compounds of concentration 100 μg/ mL in DMSO and placed on seeded agar plates. Paper discs moistened with DMSO considered as negative control. Discs saturated with Ceftriaxone at the same concentration 100 μg/ mL used as positive control. The plates incubated at 37 °C for 18 hrs. The clear zone of inhibition around disc-paper demonstrated the relative susceptibility towards the synthesized derivatives. The MIC test method performed in series of dilutions twelve concentrations in the test medium to prepare the required concentration of the tested compounds. Each concentration was added to a growth medium in separate

test tubes. All tubes are then inoculated with the selected bacteria. Turbidity of tubes was measured by multi-channel tube (BioTeK) at 550 nm absorbance maxima. All experiments were performed in triplicate.

3.2.2 The Anticancer Activities (Viability Test Assay)

3.2.2.1 Material

Reagents: Pyrazolone analogues (Table 5) prepared by dissolving specific concentration in dimethylsulfoxide (DMSO; Sigma Aldrich Chemie GmbH Steinheim, Germany) to prepare stock solutions of each tested compound. The concentrations of the stock solutions were 2.5, 5.0, 10, 20, 30, and 40 µM (HL60 experiment), 6.5, 12.5, 25, 50 µM (A-549, MDA-MB- 231 and HT29 experiments). All solutions were stored in dark at at -20 °C.

3.2.2.2 Tissue Culture

Experiments were performed using cultured HL-60 (Human Promyelocytic Leukemia Cell Line). 0.5 mL cultured cells (3×10^5) in RBMI 1640 Medium. Human non-small cell lung adenocarcinoma A549 cells, human breast adenocarcinoma MDA-MB-231 cells, and human colorectal adenocarcinoma HT-29 cells were maintained at 37 °C in culture medium supplemented with antibiotics as described in by Mechkarska and co-others [108].

3.2.2.3 Methods

In HL60 experiment, stock solution added to the culture cells as 1:1000 dilutions to give 2.5, 5.0, 10, 20, 30, and 40 MicroMolar final concentration. Incubation time with Cells was 30 hours. After incubation, cells were washed 2 times with PBS (phoshate Buffer Saline) and incubated for 5 minutes with muse cell and

count viability kite from millipore. The Viability was analyzed using muse cell analyzer flow cytometer. The DMSO concentration in each experiment was less than 0.05%. All control contained 0.05% DMSO. Four independent experiments were performed for each concentration and for each molecule. Positive control etoposide 4, 8, and 10 MicroMolar was added to the cultured HL60 in each experiment for the active compounds.

In the A-549, MDA-MB- 231 and HT29 experiments, the cells were seeded in 96-well plates at a density of 5×10^3 cells/ well. After 24 h, all cells were treated for 24, 48 and 72 h with increasing concentrations of the synthesized compounds in triplicate. The effect of the synthesized compounds on cell viability was determined by measurement of ATP concentrations using a CellTiter-Glo Luminescent Cell Viability assay (Promega Corporation, Madison, WI, USA) [108].

3.3 Results and Discussion

3.3.1 Antifungal and Antibacterial Activities

Compounds contain pyrazole moiety are used to treat diseases such as inflammation, pain, cancer, tuberculosis, and bacterial infections [109]. Structure activity relationship conducted by Radi et al in 2010, showed that substitutes at N^2 position of pyrazole nucleus, do not impact any biological activities [110]. This section is the antibacterial and antifungal properties of N^2-pyrazole derivatives by calculating the areas of the zones of inhibition generated by each synthesized compound. Also, the minimum concentration of inhibition (MIC) can be attributed to the bactericidal or bacteriostatic activity of these compounds. The data obtained in this part will help to confirm the effectiveness of the compound as new anti-microbial candidate.

Table 4: Some the synthesized compounds used in the anti-fungal and anti-bacterial study

Compound code	R	Structure
113a	3-F	
113c	3-CF$_3$	
113d	3-Cl	
113g	3-NO$_2$	
116a	3-F	
116b	3-Cl	
117a	3-F	
117c	3-CF$_3$	
117f	3-NO$_2$	
118a	3-CF$_3$	
118c	3-NO$_2$	
122a	3-F	
122b	3-CF$_3$	
122c	3-NO$_2$	
123a	3-F	
123b	3-CF$_3$	
123c	3-NO$_2$	
124e	4-F	
124f	3-NO$_2$	
127c	3-NO$_2$	

Table 5: Some of the synthesized compounds used in the anticancer study

Compound code	R	Structure
116a	3-F	
116b	3-Cl	
117a	3-F	
117b	3-Cl	
117c	3-CF$_3$	
117d	4-F	
117e	4-Cl	
117f	3-NO$_2$	
118a	3-CF$_3$	
118b	4-Cl	
118c	3-NO$_2$	
122a	3-F	
122b	3-CF$_3$	
122c	3-NO$_2$	
123a	3-F	
123b	3-CF$_3$	
123c	3-NO$_2$	
124a	3-F, R' = 4-F	
124b	4-F, R' = 4-F	
124c	3-CF$_3$, R' = 4-F	
124d	3-CF$_3$, R' = 4-OCF$_3$	
124e	4-F, R' = H	
124f	3-NO$_2$, R' = H	
124g	3-NO$_2$, R' = 4-F	
124h	4-Br, R' = H	
127a	3-CF$_3$	
127b	2,4-Di-Cl	
127c	3-NO$_2$	

3.3.1.1 Study of Inhibition Zones

Inhibition zone is the clear zone generated around the drug-candidate, To accomplish our study, bacterial cultures on agar plates were subjected to expose to pyrazolone derivatives. The initial results of the experiment showed both of the Gram positive bacteria *Staphylococcus Aureus* and Gram negative bacteria *Escherichia Coli* were found to be inactive to word all the pyrazoles derivatives. While both of the Gram positive bacteria *Bacillus* and Gram negative bacteria *Proteus* were found affected by some of the pyrazoles derivatives.

3.3.1.1.1 Pyrazolones Inhibition Zones

To study the affect of some of our pyrazolines, the inhibition zone of the for the *Yeast* was determined and calculated for each compound compared to Ceftriaxone. The obtained data showed that compound **113c**, and **113g** were both exhibited better activities than Ceftriaxone (Table 6). Compound **113a** also showed slightly same zone of inhibition (21 mm) when it Ceftriaxone (23 mm). However **113d** didn't produced appreciable value of inhibition (14 mm). These results can be attributed to the fact that compounds having pyrazolone moieties showed the greatest activities against *Aspergillus niger*, *Aspergillus flavus, Pencillium chrysogenum* and *Fusirium moneliforme* are known pharmacophores and hence show activity against fungal infections [111]. Results collected against *Bacillus* using pyrazones **113a**, **113c**, **113d**, **113g**, **113i** showed that the most active compound is **113c**. Compound **113c** gave area of inhibition 15 mm compared to the positive control used in this experiment (Ceftriaxone, 10 mm). The results showed as well that compounds **113i**, **113d**, and **113g** were found inactive compared to the same antibiotic. To understand the difference in activity, structures of both **113a,c** compared with **113g** were

studied. The study demonstrate that, fluorine atom substituted in the phenyl group at position 3´ was found responsible in enhancing the activity compared to the chlorine atom or nitro group at the same position. These results confirmed that fluorine substituted heterocyclic compounds are owning better activities (Table 6) and Figure 56 same results were obtained when Gram-negative bacteria was used (Table 6) and (Figure 57).

Table 6: Inhibition zones values for active pyrazolones with respect to *Yeast*, *Bacillus* and *Proteus*

Compound Code	Zone of Inhibition (mm)		
	Yeast ± SD	*Bacillus* ± SD	*Proteus* ± SD
113a	21.67 ± 0.58	13.17 ± 0.29	18.50 ± 0.50
113c	**34.33 ± 0.58**	**15.00 ± 0.29**	**26.00 ± 0.29**
113d	13.67 ± 2.08	7.83 ± 0.29	9.00 ± 0.00
113g	24.33 ± 1.53	8.83 ± 0.29	24.00 ± 1.00
113i	7.00 ± 0 .50	6.50 ± 0.50	10.50 ± 0.50
DMSO	0.00 ± 0.00	0.00 ± 0.00	0.00 ± 0.00
CEF	23.00 ± 1.00	10.00 ± 1.00	16.67 ± 2.08

Values are mean of triplicate readings (mean ± SD). SD = standard deviation
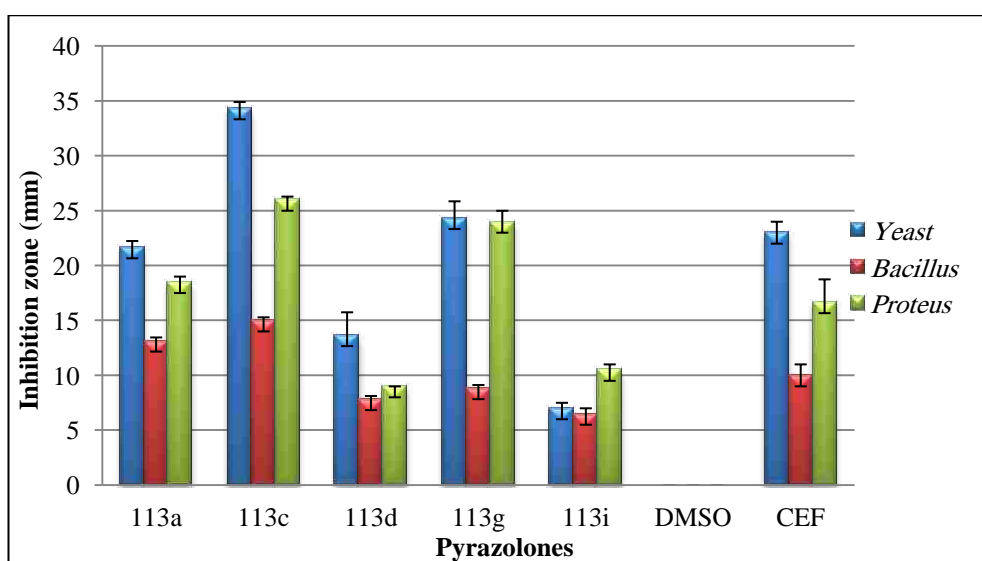
Figure 57: Comparison of inhibition zone values of some pyrazolones against *Yeast*, *Bacillus*, and *Proteus* with reference standard (CEF)

3.3.1.1.2 Pyrazoline Ribosides Inhibition Zones

The antibacterial activites of some pyrazoline nucleosides **116** and **117** were evaluated against several pathogen (Table 7). To understand the effect of furanosyl ring introduced at either N^2 or O-3 of the pyrazoline ring, accululated dara showed that the ribose moiety has no effect on the activity against different bacteria while the substituted arylhydrazo groups at pyrazoline C-4 played the major factors comparing to the positive control used in this experiment, For example, compounds **116a** and **117a,c** were found the most active compounds among all synthesized isomers with respect to position and the type of the glycosidic linkage. It was found that both of O-isomer **116a** and N-isomers **117a,c** possessed the highest antibacterial activites ahere the phynyl eing substited with fluorine atom (Table 7) and (Figure 58).

Table 7: Inhibition zone values for pyrazoline ribosides with respect to *Yeast*, *Bacillus* and *Proteus*

Compound Code	Zone of Inhibition (mm)		
	Yeast ± SD	*Bacillus* ± SD	*Proteus* ± SD
116a	22.33 ± 1.53	14.67 ± 0.58	13.83 ± 0.29
116d	18.33 ± 0.58	7.17 ± 0.29	13.00 ± 1.00
117a	21.67 ± 0.58	13.50 ± 0.50	12.50 ± 0.50
117c	**31.00 ± 1.00**	**16.50 ± 0.50**	0.00 ± 0.00
117f	11.50 ± 0.50	13.5 ± 00.50	**24.00 ± 2.00**
118a	28.33 ± 1.53	14.00 ± 0.50	14.83 ± 0.29
118c	9.67 ± 0.58	5.83 ± 0.29	7.50 ± 0.50
DMSO	0.00 ± 0.00	0.00 ± 0.00	0.00 ± 0.00
CEF	23.00 ± 1.00	10.00 ± 1.00	16.67 ± 2.08

Values are mean of triplicate readings (mean ± SD). SD = standard deviation
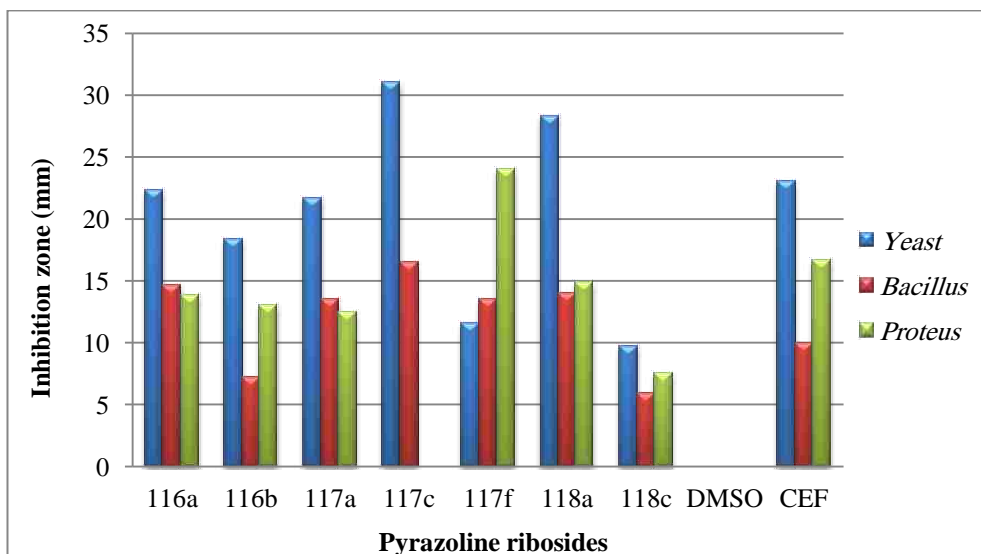
Figure 58: Comparison of inhibition zone values of some pyrazoline ribosides against *Yeast*, *Bacillus*, and *Proteus* with reference standard (CEF)

3.3.1.1.3 Pyrazoline Deoxyriboside Inhibition Zones

Pyrazoles deoxyribosides antimicrobial affect is studied by exposing the five bacterial cultures on to the following derivatives **122a-c** and **123a-c**. As other pyrazolines derivatives the gram positive bacteria *Staphylococcus aureus* and gram negative bacteria *Escherichia coli* were found to be inactive to word them, while pyrazoles deoxyribosides found have affect on both of the gram positive bacteria *Bacillus* and gram negative bacteria *Proteus*.

The affect of the pyrazoles deoxyribosides on *Yeast* where studied by recording the inhibition zone for each compound and compared them with Ceftriaxone. The findings showed that compound **123b** has better activities than Ceftriaxone (Table 8). Compound **122b** also showed same inhibition zone of Ceftriaxone (23.0 mm). On the other hand, Compounds **122c** and **123c** didn't show a significant effect on *Yeast* (1.0 mm). **123b** and **122b** also showed good results against *Bacillus* (14.17 and 15.83 mm) respectively. These inhibition zones values

are higher than that for the positive control used in this experiment (Ceftriaxone, 10.00 mm). Compounds **123a** and **123c 113c** area of inhibition (10.17 and 10.5 mm) respectively which are slightly higher than the same antibiotic. Similar results were obtained when Gram-negative bacteria was used (Table 8). These results can be justified by the fact that compounds **123b** and **122b** having trifluoromethyl as a functional group. One more time, these results established that fluorine substituted heterocyclic compounds have better activities (Table 8) and (Figure 59).

Table 8: Inhibition zone values for pyrazoles deoxyriboside derivatives with respect to *Yeast*, *Bacillus* and *Proteus*

Compound code	Zone of Inhibition (mm)		
	Yeast ± SD	*Bacillus* ± SD	*Proteus* ± SD
122a	11.50 ± 0.50	7.17 ± 0.29	7.00 ± 12.12
122b	**23.00 ± 0.50**	**14.17 ± 0.76**	**19.33 ± 0.29**
122c	1.00 ± 0.00	8.50 ± 0.50	0.97 ± 0.06
123a	18.17 ± 0.29	10.17 ± 0.29	21.00 ± 1.00
123b	**27.83 ± 0.29**	**15.83 ± 0.76**	**19.17 ± 0.29**
123c	1.00 ± 0.00	10.50 ± 0.50	0.93 ± 0.12
DMSO	0.00 ± 0.00	0.00 ± 0.00	0.00 ± 0.00
CEF	23.00 ± 1.00	10.00 ± 1.00	16.67 ± 2.08

Values are mean of triplicate readings (mean ± SD). SD = standard deviation
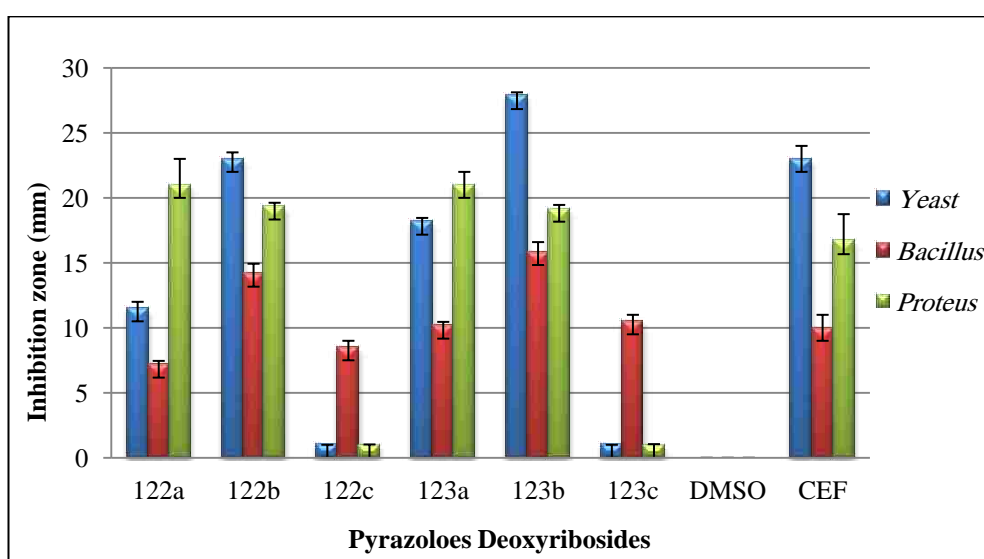
Figure 59: Comparison of zone of inhibition values pyrazoloes deoxyribosides against *Yeast*, *Bacillus*, and *Proteus* with reference standard (CEF)

3.3.1.1.4 Benzolyated Pyrazolines Inhibition Zones

Antimicrobial affect is also studied for the benzoylated pyrazoline derivatives. The same five bacterial cultures were exposing the on to the following derivatives **124a, 124g and 127c**. The benzoylated pyrazoline derivatives were found inactive gram positive bacteria *Staphylococcus aureus* and gram negative bacteria *Escherichia coli* as all other tested pyrazolines derivatives. Whereas they have affect on both of the gram positive bacteria *Bacillus* and gram negative bacteria *Proteus*.

The examined enzoylated pyrazoline derivatives affect on *Yeast* where studied also and the inhibition zones were recorded for each compound and compared with the positive control (Ceftriaxone). The results showed that the *N*-isomer **124g** has good activities in referenced to the Ceftriaxone (Table 9). Compound **124g** showed slightly close inhibition zone (17.0 mm) of Ceftriaxone (23.0 mm) against *Yeast*. While it show better activities against *Bacillus* (15.3 mm) and *Proteus* (20.0 mm) in compared to the positive control against the same bacteria cultures (10.0 and 16.7 mm) respectively. The *O*-isomer, on the other hand, **127c** doesn't show good activity ageist Yeast culture. Close to the positive control against *Bacellues* (9.8 mm) and beter than the antibiotic (CEF) against *Proteus* (17.2 mm). In general, It was found that both of *O*-isomer **124g** and *N*-isomers **127c** showed high antibacterial activates but *O*-isomer **124g** activates were higher (Table 9) and (Figure 60).

Table 9: Inhibition zone values for benzolyated pyrazolines for *Yeast*, *Bacillus* and *Proteus*

Compounds code	Zone of Inhibition (mm)		
	Yeast ± SD	*Bacillus* ± SD	*Proteus* ± SD
124a	6.17 ± 0.29	6.33 ± 1.04	10.17 ± 0.76
124g	**17.00 ± 0.50**	**15.33 ± 1.53**	**20.00 ± 1.00**
127c	8.00 ± 1.50	9.83 ± 0.29	17.17 ± 0.76
DMSO	0.00 ± 0.00	0.00 ± 0.00	0.00 ± 0.00
CEF	23.00 ± 1.00	10.00 ± 1.00	16.67 ± 2.08

Values are mean of triplicate readings (mean ± SD). SD = standard deviation
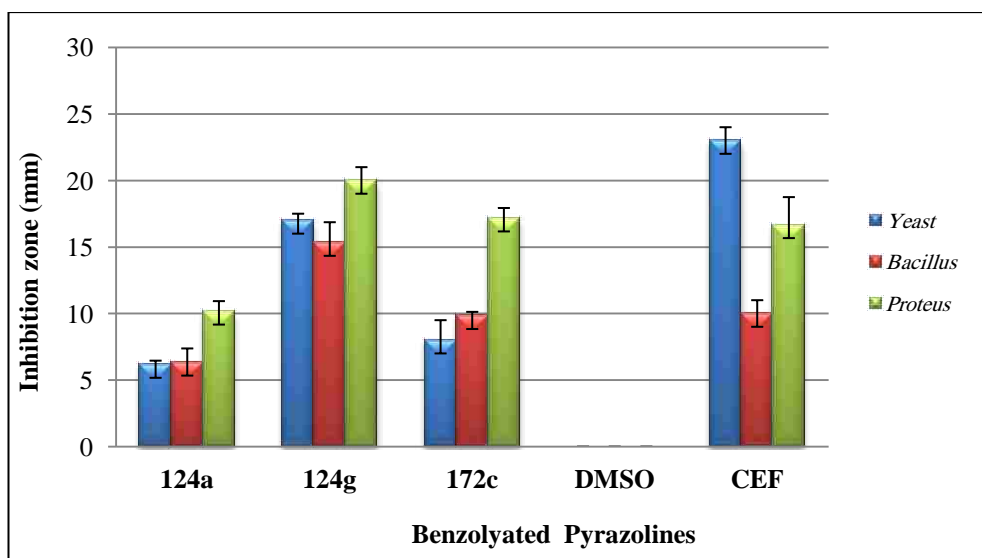
Figure 60: Comparison of zone of inhibition values of some Benzolyated Pyrazolines against *Bacillus*, *Proteus* and *Yeast* with reference standards

3.3.1.2 Minimum Inhibition Concentration

Minimum Inhibition Concentration (MIC) is the minimum concentration of a substance which is required to inhibit the growth of microorganisms in a culture. It is a measure of strength of the antimicrobial compound [16]. The strength of antimicrobial activity has an inverse relationship with MIC, higher value of MIC indicates lower strength of the compound, and low MIC values indicate towards a

strong antimicrobial activity. Ahar et al. in 2015 analyzed the in-*vitro* activity of chemically synthesized pyrazolones using this method and the MIC values for six bacteria were calculated and found to be influenced by functional groups present [17]. The MIC studies of certain compounds in this study were evaluated, against *Yeast, Bacillus* and *Proteus* to determine the potency of the synthesized compounds' antimicrobial activity.

MIC studies on some active synthesized pyrazolines during the study were carried out, and the results are given in Table 10. Among all the pyrazolones tested for their MIC values, 4-(3'-fluorophenylhydrazono)-5-trifluoromethyl-2,4-dihydropyrazol-3-one **113a** was found to have the maximum value of MIC, for all the three microbes, that is, *Yeast, Bacillus,* and *Proteus*. This indicates that a high concentration of this compound will be required to completely inhibit their growth, thus making it the least desired compound of choice for inhibiting microbial growth. Among the *Yeast, Bacillus,* and *Proteus; Proteus* required the maximum concentration of **113a**, whereas the MIC values for other two were the same. *Yeast, Bacillus* and *Proteus* were inhibited most effectively **113c**, followed by **113g** and **113d.** *Bacillus* had the least value of MIC out of all the microbes, regarding the three pyrazoles **113c**, **113g** and **113d**. This indicates that *Bacillus* is more prone to inhibition by active pyrazolone compounds.

The common active pyrazolones were subjected to chemical reactions to synthesize the riboside derivatives of the compounds, and further the MIC values for these compounds were tested, and tabulated as below. Among all the riboside pyrazolones tested for their MIC values, **117a** was found to have the maximum value of MIC, for all the three microbes. This indicates that a high concentration of this

compound will be required to completely inhibit their growth, thus making it the least desired compound of choice for inhibiting microbial growth.

As seen in Table 10, *Yeast* was inhibited most effectively by **118a**, with least concentration, among all the compounds. **116b** had comparable values of MIC, and are secondary in inhibition activity as compared to **118a**. **117a** had higher values of MIC, as compared to other compounds. Hence, these are not favored over other compounds for inhibition of growth.

The active pyrazoles derivatives were compared with MIC concentration of Ceftriaxone, (antibiotic positive control), and Amphotericin B (antifungal positive control) then tested upon the gram negative bacteria *Proteus* and *Yeast*. Comparing with The positive control helped in results validation.

As seen in Figure 61, **113c,g** exhibited the least values of MIC, showing slight increment in values as compared to the control. **113d**, **116d**, and **118c** exhibited concentrations less than 1 µg/mL, and even less than the positive controls (Ceftriaxone and Amphotericin B).

116a and **116g** have concentrations higher than 1µg/mL, with **116a** having higher value as compared to **116g**. Hence, **116g** is a better inhibitor as compared to **116a**. **113a** had MIC value greater than 2µg/mL, thus it is not a very good inhibitor of *Proteus* cultures. Among all the compounds **117a** exhibited the highest value of MIC, which makes it the least favored compound to bring about microbial inhibition.

Table 10: MIC for active pyrazolones against *Yeast*, *Bacillus* and *Proteus*

Compound Code	MIC for (μg/ml)		
	Yeast	*Bacillus*	*Proteus*
113a	1.234	1.234	2.468
113c	0.151	0.075	**0.151**
113d	0.336	0.084	0.672
113g	0.324	0.081	0.162
116a	0.364	0.728	1.456
116b	0.547	**0.034**	**0.547**
117a	**1.644**	**3.287**	**6.574**
117c	0.316	2.525	ND
117f	0.533	0.533	1.065
118a	**0.124**	0.062	**0.497**
CEF	-		2
Amphotericin B*	0.25	-	-

*Amphotericin B: antifungal
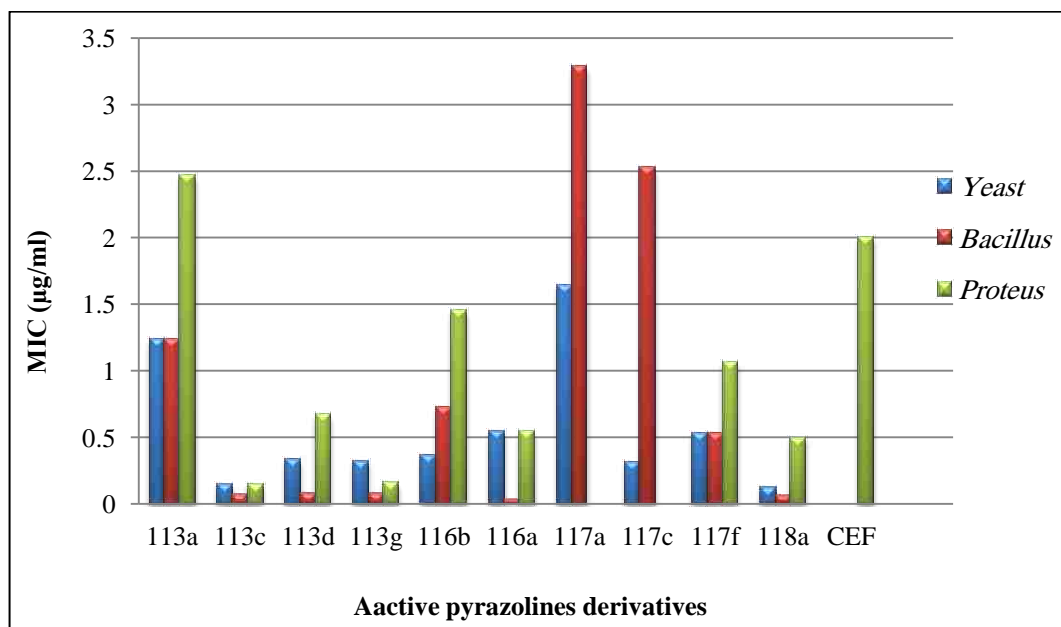
Figure 61: MIC for some active pyrazolones against *Yeast*, *Bacillus* and *Proteus* compared to the positive controls

3.3.2 Anticancer Activities (Viability Test)

3.3.2.1 Effect of the synthesized compounds on the cellular viability of HL60 Leukemia Cancer Cell Line

To examine the anticancer effect of the synthesized compounds **116a, 116b, 117a, 117b, 117c, 117d, 117e, 117f, 118a, 118b, 118c, 122a, 122b, 123a, 123b** and **124f** on Leukemia cancer cell line; the effect of various concentration of synthesized compounds on the proliferation of HL-60 were measured. The results showed a decrease in the cellular viability when the cells exposed to various concentration of different synthesized compounds **117a, 122a, 122b** and **123a** and Etoposide. Rile there is no significant effect were shown in compounds **116a, 117e, 118a, 118b** and **124f** graphs. Furthermore, treatment with 20 µM of synthesized compounds for 24, 48 and 72 hrs (Figure 62) resulted in approximately 50% decrease in the cell viability. The results confirmed that the cellular viability of the experienced compounds is a concentration- and time-dependent.

3.3.2.2 Effect of the synthesized compounds on the cellular viability of the A-549 cell line

The anticancer effect of some of the synthesized compounds **116a, 117a 117c, 117d, 117e, 117f, 117g, 118b, 118c, 122a, 124a, 124b, 124c, 124d, 124e, 124f, 124g** and **127c** were examined on A-549 cell line. The results illustrated a decrease in the cellular viability of A-549 cell line when exposed to various concentration of different synthesized compounds. Additionally, treatment with small dose (25 µM) of synthesized compounds for 24, 48 and 72 hs (Figure 63) resulted in approximately 50 % decrease in the cell viability of A-549. The exposure of A-549 to synthesized compounds decreased cellular viability in a concentration

and time-dependent manner compared to a control cells treated with vehicle (DMSO).

Effects of the experimental compounds on cell proliferation were determined by measurement of ATP concentrations using a CellTiter-Glo Luminescent Cell Viability assay. The DMSO concentration was less than 0.05% in all experimented compounds.

3.4 Summary

The present study involves extensive experiments which help to explore and understand the biological activity of the synthesized compounds. The study involved synthesis of pyrazolone compounds, and their testing for antimicrobial and anticancer activities. Both **113c** and **118c** were found to be the most effective in inhibiting the growth of all test microbes (*Yeast, Bacillus, Proteus*). Furthermore **117a, 117e, 117f, 122a, 122b, 123a, 124c, 124d, 124f** and **124g** were found the most effective as anticancer drug in different cell lines. In the subsequent section, the physical interactions of the derived compounds of pyrazolones were studied, especially with regards to their behavior with UV, fluorescence radiation and DNA.
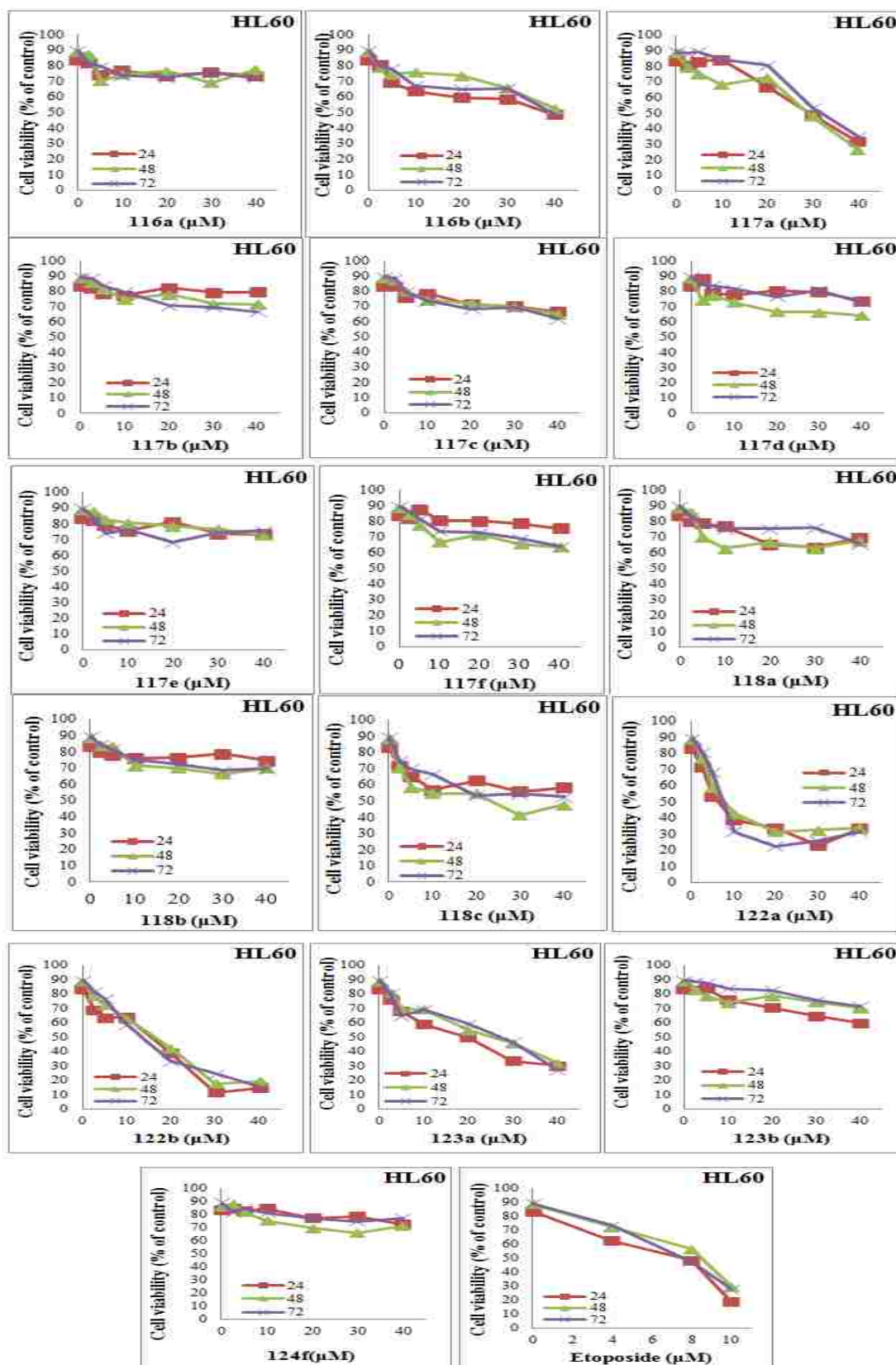
Figure 62: Cell viability of HL-60 cells with 2.5, 5.0, 10, 20, 30, and 40 μM of the synthesized pyrazolone derivatives. DMSO concentration was 0.05 % in all experimented compounds
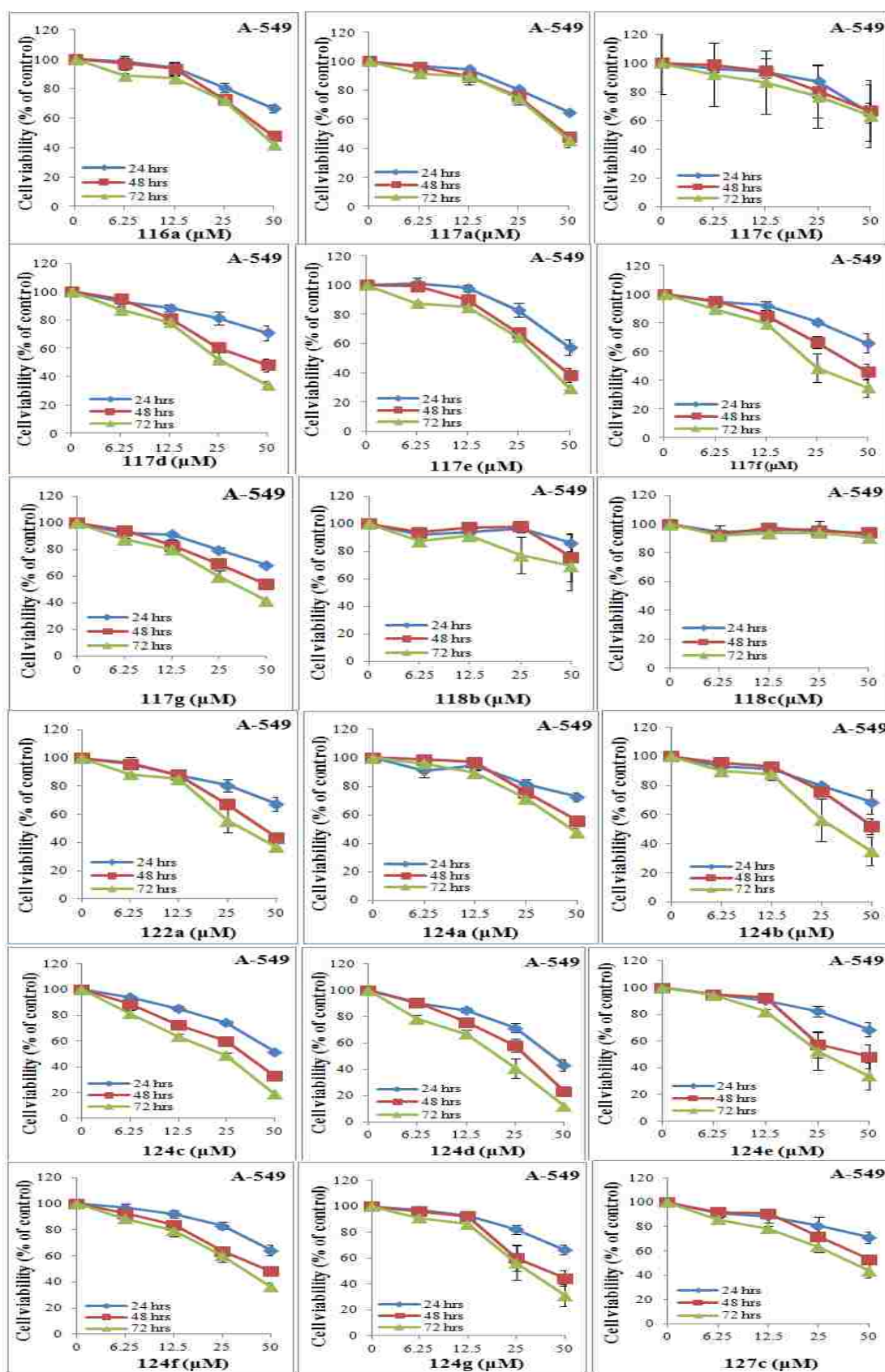
Figure 63: Cell viability of A-549 cells with 6.5, 12.5, 25 and 50 μM of the synthesized pyrazolone derivatives for 1, 2 and 3 days

Chapter 4: Physical Studies of Pyrazole and its Derivatives

4.1 Introduction

Pyrazolone compounds showed some biological applications as anti-inflammatory, anti-microbial, anti-cancer. Before any compound considered as a pharmacological agent several properties should be studied and evaluated. In this part, the physical properties of the newly synthesized pyrazolone derivatives have been studied. This study include the stability of the compounds **113g**, **117f**, **118c** and **127c** in different solvents, and the effect of a series of pHs.

Pyrazolone nucleosides have been found to have anti-bacterial and antitumor effects. Studies reported that trifluoromethyl nucleosides induce cell apoptosis via different mechanisms as mentioned in chapter 1. In this part, the direct interaction with DNA will be discussed by examing the DNA in the presence of the newly sunthesized pyrazoline nucleosides. Confirmations for the interaction of the investigated compound **118c** with duplex DNA (*ct*-DNA) were obtained using melting temperature curves, circular dichroismand titration, UV–vis spectroscopy and fluorescence spectroscopy.

4.2 Materials and Reagents

All chemicals and reagents were used without further purification. Ethylenediaminetetraacetic acid (EDTA), 99 %, potassium chloride, 99 %, tris(hydroxymethyl)aminomethane hydrochloride (Tris-HCl), 99 % and calf thymus DNA were purchased from Sigma-Aldrich.

4.3 Apparatus

Fluorescence measurements were carried in quartz cell (1.00 cm path length) using Cary Eclipse model-3 spectroflourometer equipped with a high intensity Xenon flash lamp (Varian, Austria). Absorption spectrophotometric measurements were carried out using Agilent 8453, matched with 1 cm quartz cells. CD measurements were done using Jasco J-815 spectrometer (Jasco, USA). The study of the PH effects was done using Orion-401-Plus pH meter supported with Orion glass electrode.

4.4 Small Molecules-DNA Interactions

Tris-KCl buffer solution

A 0.01 M Tris–KCl buffer solution, pH 7.4, was prepared by dissolving 10.00 mM of tris–hydroxymethylaminomethane hydrochloride (1.576 g), 1.00 mM Na_2EDTA (0.3722 g) and 100 mM KCl (7.455 g) into 1.00 L of deionized water. The pH was adjusted using the glass electrode.

Ligands' solutions

Stock solutions (0.02 M) of **113g**, **117f**, **118c** and **127c** were prepared in 100% DMSO. Solutions having concentrations of 1×10^{-3}, 5×10^{-4}, 1×10^{-4} M were prepared by appropriate dilution into 4 mL using Tris-KCl buffer, pH 7.4. DMSO was kept at 5 % in all solutions

Calf Thymus DNA (*ct*-DNA)

Calf thymus *ct*-DNA 107 mg/L (1.07×10^{-5} M) was prepared by dissolving 53.5 mg of DNA into 500 mL Tris-KCl buffer, pH 7.4, without sonication or stirring.

To prevent shearing of the large genomic DNA, the solution was gently inverted overnight at 4.00 $^\circ$C to completely solubilize the DNA. Solutions of DNA are stable for several months at 4.00 $^\circ$C in Tris–Cl buffer pH 7–8.

Melting Temperature Curves

The interaction between compounds **113g**, **117f**, and **118c** and *ct*-DNA studied using CD as follow; a 1.00 mL *ct*-DNA (1.07 x 10^{-5} M, 107 ppm) and its ligands (3.93 x 10^{-6} M) in Tris-KCl-buffer, pH 7.4 were heated up in 5.00 $^\circ$C increments in the range 25 – 95 $^\circ$C using 5 minutes as incubation time intervals to be sure that the temperature in the cuvette is similar to that of the water bath. The data collected with 1 – 2 $^\circ$C increments in temperature in the CD jump range. CD spectra were recorded in the range 200 – 400 nm against temperature

UV-Vis Study

Solution (5.0 x 10^{-5} M) of **118c** was prepared in Tris-KCl buffer, pH 7.4, 5 % by diluting 50 µL of 1 x 10^{-3} M to a final volume of 1000 µL. Successive additions of (1.07 x 10^{-5} M) DNA were added. Solutions were shacked 10 times up-down after each addition and incubated for 3 minutes at room temperature then scanned in the range 200 – 700 nm using 1500 µL cuvette, 1cm path length. Increasing incubation time to one hour was found ineffective. Therefore, 5 min incubation time was applied throughout all measurements. Titration was stopped at saturation when no change in absorbance intensity observed.

Fluorescence Study

Interactions of **118c** with *ct*-DNA were followed fluorimetrically at λ_{max} of

emission 425 nm and excited at 280 nm respectively using slits width of 10.00 nm.

Circular Dichroism Study

The interaction between **118c** and *ct*-DNA was studied. **118c** (4×10^{-6} M,

1000 µL) was prepared using Tris-KCl buffer, pH 7. then titrated with successive

amounts of the ligands' solutions (1×10^{-4} M – 1×10^{-3} M).

Solutions after each addition was shacked well, incubated for 3 minutes at

room temperature and scanned in the range 200 – 400 nm with 50 nm/min, band

width 1 nm and 3 accumulations. Increasing incubation times to one hour was found

ineffective. Therefore, 3 min was applied. Incubation time throughout all

measurements.

4.5 Results and Discussion

4.5.1 Effect of Solvents

The solvents effect on organic compounds have been studied for more than a

century [112]. Studying the effect of solvents on azo compounds using electronic

spectra (absorption and fluorescence) became an important subject for research

because it can play a significant role in the photophysics of the excited states [113].

Azo dyes are one of the important classes of colorants [112] and they are represent

over than 50% of all colorants [114]. Their photosensitivity and the superior

structuring properties are mainly due to the lability of substituents binding to the

N=N groups [115]. Furthermore, heterocyclic azo dyes have played an important role

in the development of the chemistry of dyes. The physical properties of arylazo pyrazolones are strongly related to their tautomerism. [114].

In solutions, the solvent environment cause important changes in the electro-optical properties of the azo dye compounds. Theories behind the solvent effects on the electronic spectra developed to estimate the electro-optical parameters, such as dipole electric moments electric permittivity and refractive indices. One of these methods is the solvatochromism [113]. Solvatochromism is caused by differential salvation of the ground and the first excited state of the photo-active molecule. If the ground state of the molecule is stabilized by increasing the solvent polarity; negative solvatochromism (blue shift) will result. On contrast, a positive solvatochromism (red shift) will result by stabilize the first excited state relative to the ground state [116].

The intensity, shape, and maximum absorption and/or emotion wavelength of dyes in solution depend strongly on the solvent-solute interactions and solvent properties. This effect is related to the interaction of the dye–solvent. The solvent affect could be from either non-specific (dielectric enhancement) or specific solute–solvent interactions (e.g. hydrogen-bonding). The solvent effect can be determined by Solvent polarity scale or solvatochromic parameters. Solvent polarity is a commonly used term related to the capacity of a solvent for solvating dissolved charged or neutral. The effect of solvent polarity on the absorption spectra are interpreted by means of linear solvation energy relationship (LSER) using a Kamlet–Taft Eq. (1).

$$\nu = \nu_0 + s\pi * + b\beta + a\alpha \text{------------(1)}$$

Where π* is a measure of the solvent dipolarity/polarizability, β is the scale of the solvent hydrogen bond acceptor (HBA) basicities, α is the scale of the solvent hydrogen bond donor (HBD) acidities, and ν0 is the regression value of the solute property in the reference solvent cyclohexane. The regression coefficients s, b and a in Eq. (1) measure the relative susceptibilities of the solvent-dependent solute property (absorption frequencies) to the indicated solvent parameters [117].

This study of solvent effects on the electronic (absorption and fluorescence) spectra. It is directed to describe some applications giving information about the liquid structure, including the internal forces in liquid state and also allowing estimation the molecular electro-optical parameters in the electronic excited states of the spectrally active molecules [113].

The synthesized compounds were dissolved in different solvents and the resulting effect was observed through the absorption spectra. Compounds **113g, 117f, 118c** and **127c** were analyzed using absorption and fluorescence spectroscopy. The correlation of spectral bands with the solvent systems helped in identifying the solvent which maintains the pyrazolone in its most stable state.

4.5.1.1 Solvent Effect Using UV-Visible Spectroscopy

Four solvents used (Ethyl alcohol, Methyl alcohol, DMSO, and DMF) to measure absorption bands were altered due to the physical interactions between solvent and solute molecules [28]. For compound **113g**, has a maximum absorption peak (λ_{max}) at (418 nm), mainly regard to n-π* transition. In different solvents, **113g** showed highest absorbtion in EtOH, which indicate a strong interaction between the solvent and the solute molecules. In DMSO and DMF, **113g** shows similar

interaction. While in MeOH the compound shows decreasing in its absorption compared to other solvents (Figure 64).

For compound **117f**, absorption peak in DMSO and Methanol showed small red shift. The compound showed lower absorbance with ethanol, and the DMF absorption band tend to show shift towards lower range of wavelength (Figure 64).

For compound **118c**, absorption peak in DMSO showed highest red shift thus, DMSO proved to be the most suitable solvent system (Figure 64). In experiments conducted on Azo dyes by Zakerhamidi et al, showed the suitability and stability of DMSO solvent systems, pertaining to the strong solvent solute interactions, showing red shifts [30].
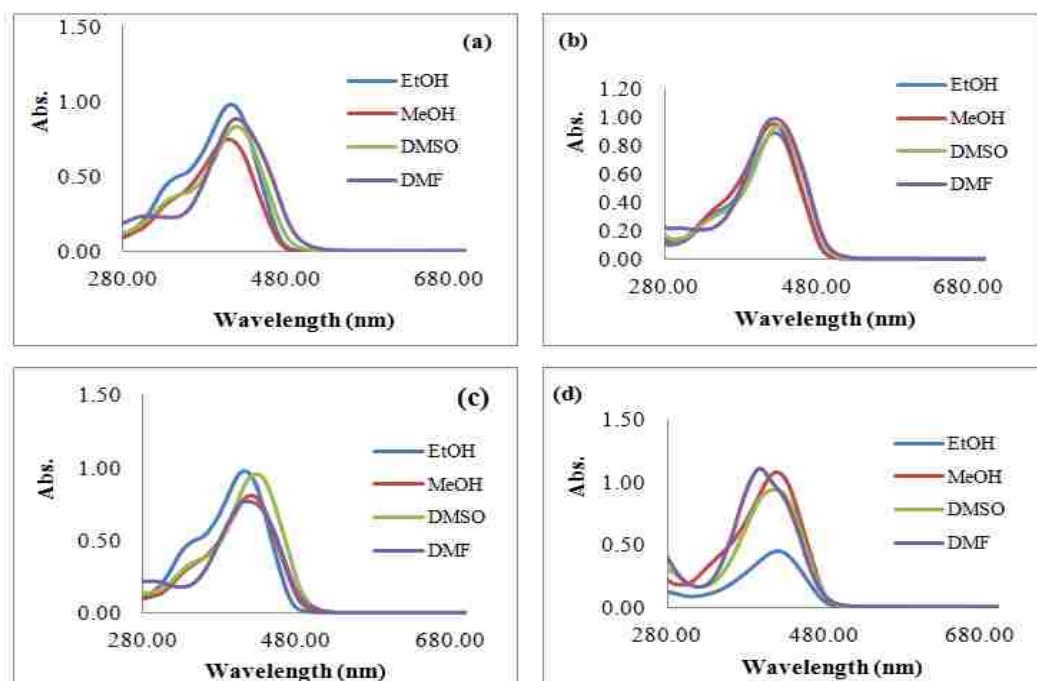
Figure 64: The absorption spectra for the synthesized compounds (a) **113g**, (b) **117f**, (c) **118c** and (d) **127c** in different solvents (EtOH, MeOH, DMSO and DMF)

Among the four solvents DMSO has the highest value of dielectric constant, followed by dimethylformamide DMF, methanol and ethanol [29]. Higher dielectric constants are due to high polarity of the solvent, which could lead to higher solvent-solute interaction [29]. Figure 65 shows the correlations of shifts in the frequency of the n-π* band with dielectric constant (D) constants.
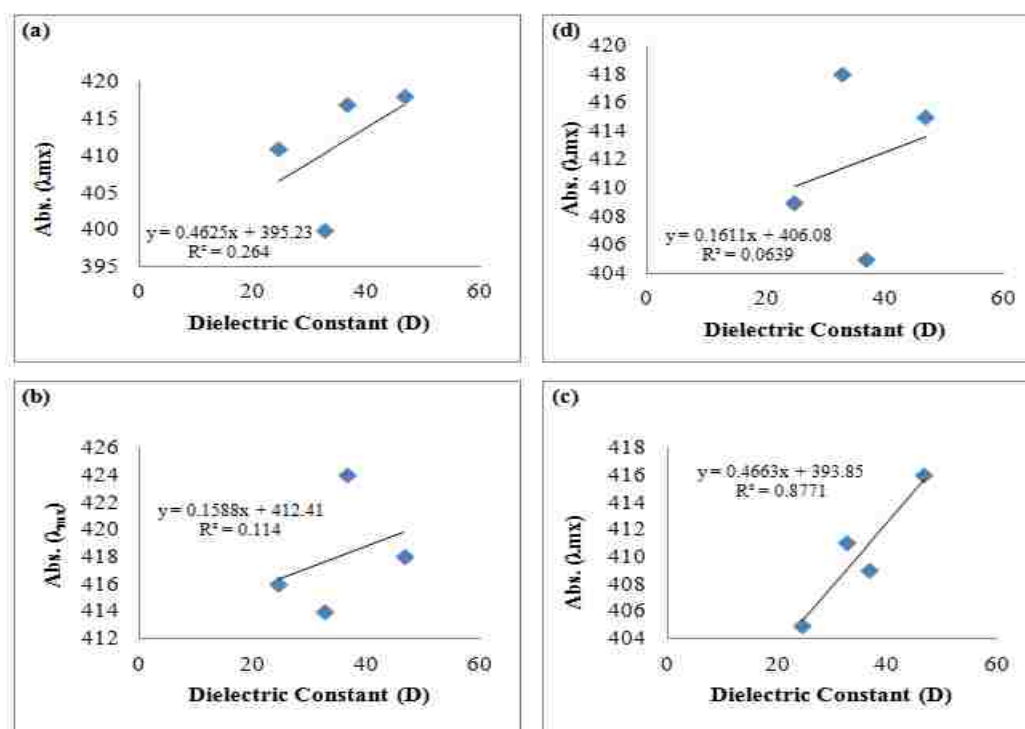
Figure 65: Solvents dielectric constant versus the absorption at λ_{max} of synthesized compounds (a) **113g**, (b) **117f**, (c) **118c**, and (d) **122c**

Table 11 shows the solvent parameters and the tested compound maxima absorption. When absorption spectra are recorded; usually, the spectral shifts are attributed to specific solute-solvent interaction in form of hydrogen bonding or solvent properties. Solvatochromic effect has been used to determine the magnitude of the solute-solvent interactions such as the polarizability/dipolarity parameter, π*, of the solvent, as well as giving information about hydrogen bond donor (HBD), α and/or acceptor (HBA), β ability of the solvent [113]. The correlations of shifts in the

frequency of the n-π* bands of all the examined compounds with the solvents parameters (π*,β and the normalized polarity parameter E_T^N) were obtained (Figure 66)

Table 11: Solvent parameters of the studied solvents and absorption maxima of the synthesized compounds. E_T^N: normalized polarity parameter of Dimroth–Reichardt; Solvent parameters of Kamlet–Taft: π*, polarity–polarizability; α, hydrogen-bond donor, and β, hydrogen-bond acceptor.

Solvent	E_T^N	Dielectric Constant (D)	π*	β	α	113g	117f	118c	127c
EtOH	0.65	24.6	0.54	0.75	0.86	411	416	405	409
MeOH	0.76	32.7	0.60	0.66	0.98	400	414	411	418
DMSO	0.44	46.7	1.00	0.76	0.00	418	418	416	415
DMF	0.39	36.7	0.88	0.69	0.00	417	424	409	405

All solvent constanst are referenced by [117]
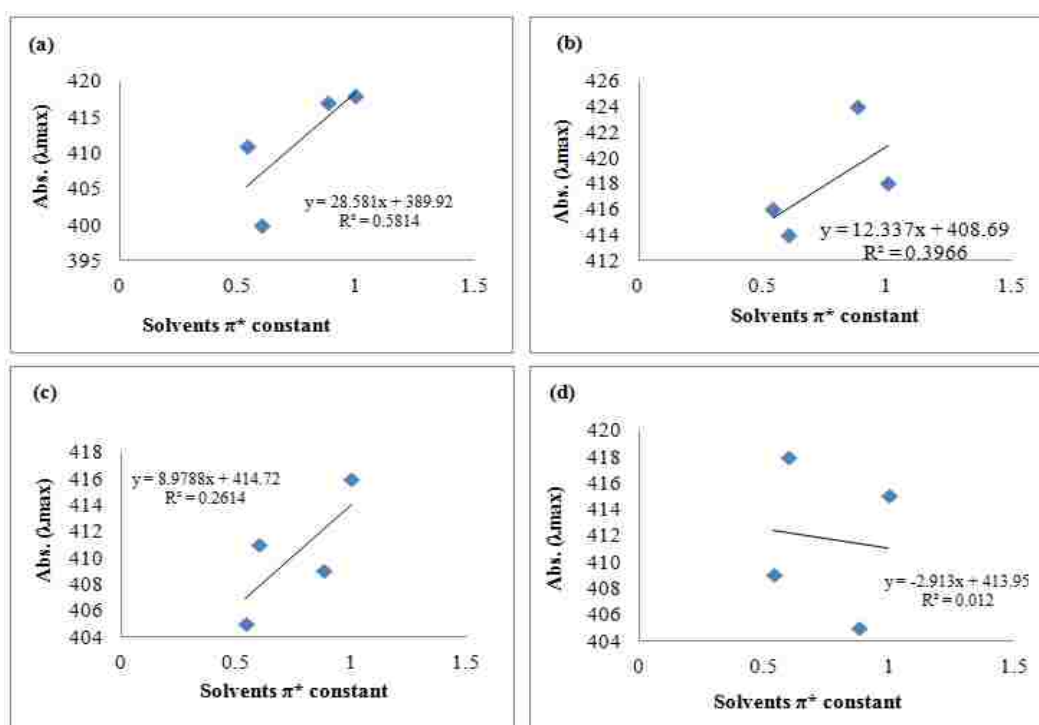
Figure 66: Solvents π* constant versus the absorption at λ_{max} of synthesized compounds (a) **113g**, (b) **117f**, (c) **118c**, and (d) **127c**
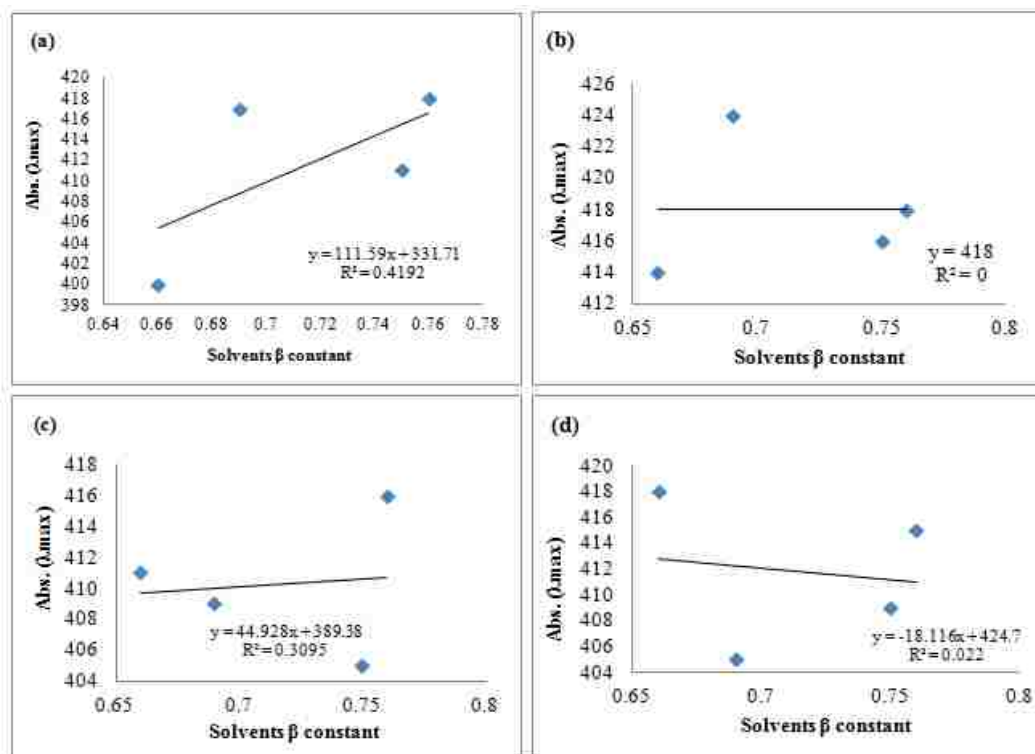
Figure 67: Solvents β constant versus the absorption at λ_{max} of synthesized compounds (a) **113g**, (b) **117f**, (c) **118c**, and (d) **127c**
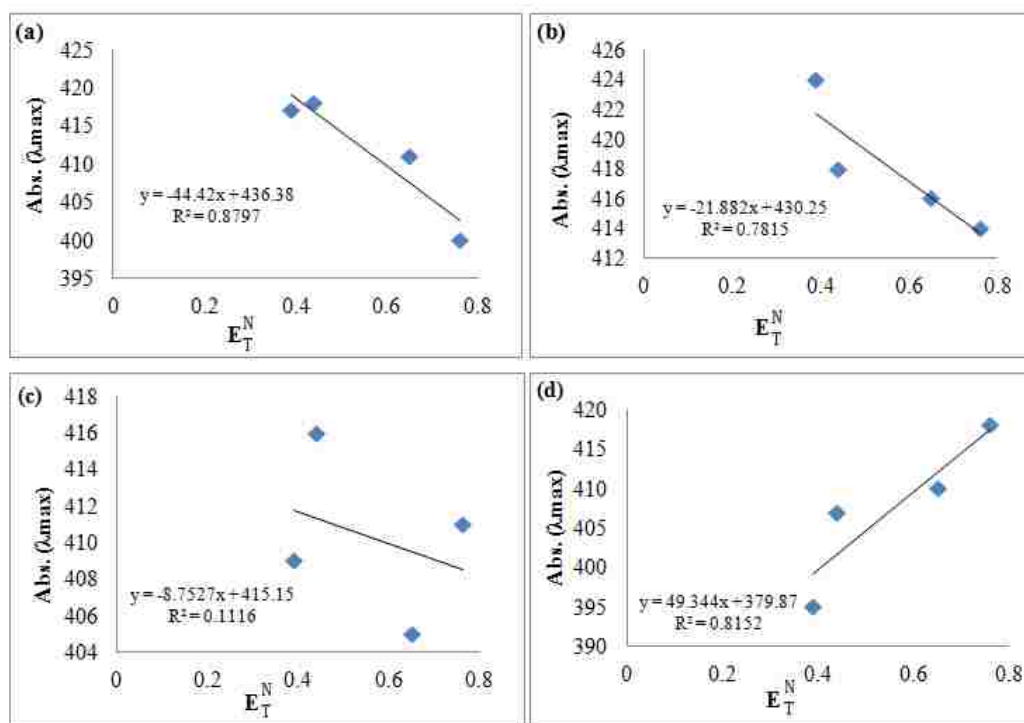
Figure 68: Solvents normalized polarity parameter (E_T^N) versus the absorption at λ_{max} of synthesized compounds (a) **113g**, (b) **117f**, (c) **118c**, and (d) **127c**

MeOH and EtOH are protic solvents, hydrogen bond donor capacity (HBD), α for MeOH is higher than in EtOH (0.98 and 0.86) respectively. In HBD interactions, during the excitation process, if the electron density move away from the basic atom, formation of the hydrogen bond opposes this movement; a blue shift is observed with an increase of the HBD capacity of the solvent. Conversely, if the charge migration occurs towards the basic atom upon excitation, a red shift is observed with the increasing HBD capacity of the solvent [118] . That is why there is blue shift of **113g** and **117f** in MeOH and EtOH in compared with **118c** and **127c.** Additionaly, the shift is higher in MeOH as it has higher hydrogen bond donor capacity.
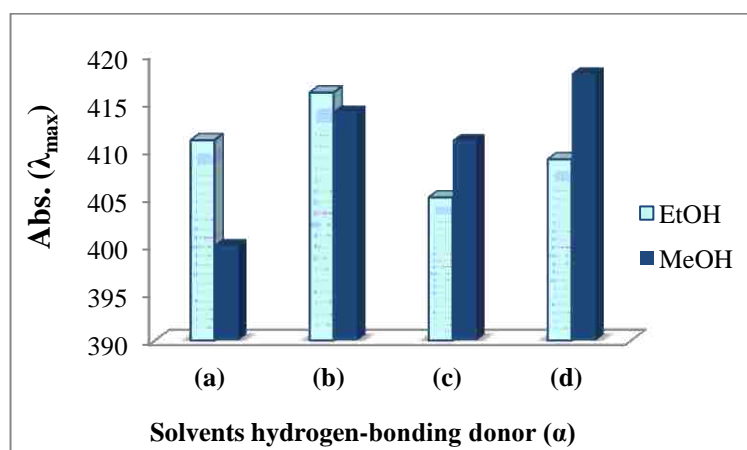
Figure 69: Solvents hydrogen-bonding donor (HBD) acidity (α) versus the absorption at λ_{max} of synthesized compounds (a) **113g**, (b) **117f**, (c) **118c**, and (d) **127c**

4.5.1.2 Solvent Effect Using Fluorescence Spectroscopy

The fluorescence spectra for the obtained products in solvents with different polarity gave information about the effect of polarity of the solvents on the profile of the spectra, which is a result of electronic interactions between the pyrazolines derivatives and the surrounding environment. Figure 70. Usually dye compounds in aprotic solvents, show a single absorption band in the visible range, whereas in protic solvents this band is considerably broadened and is split into two bands [113] as

shown by the pyrazolines azo derivatives fluorescence in EtOH. Table 14 shows

different solvent parameters and fluorescence maxima of the synthesized
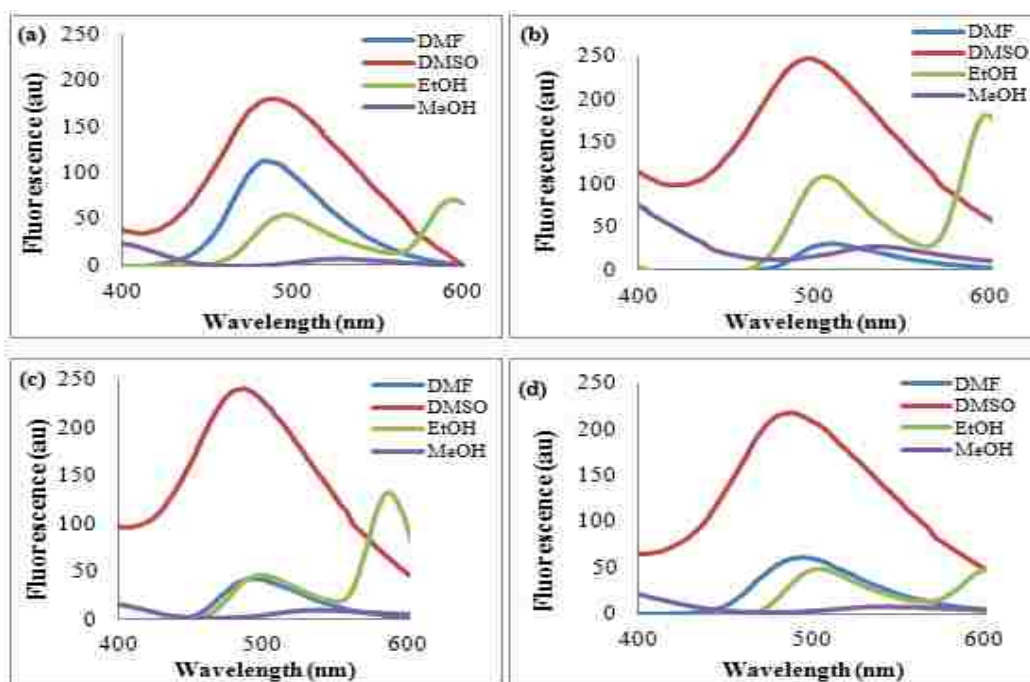
compounds.

Figure 70: Fluorescence spectra for the synthesized compounds (a) **113g,** (b) **117f,** (c) **118c** and (d) **122c** in different solvent systems (EtOH, MeOH, DMSO and DMF)

Table 12: Solvent parameters of the studied solvents and fluorescence maxima of the synthesized compounds. E_T^N: normalized polarity parameter of Dimroth–Reichardt; solvent parameters of Kamlet–Taft: π^*, polarity–polarizability; and hydrogen-bond donor

Solvent	E_T^N	Dielectric Constant (D)	π^*	α	113g	117f	118c	122c
EtOH	0.65	24.6	0.54	0.86	502 587	501 596	492 587	501 596
MeOH	0.76	32.7	0.60	0.98	535	535	542	550
DMSO	0.44	46.7	1.00	0.00	481	497	487	478
DMF	0.39	36.7	0.88	0.00	496	505	493	490

The correlations of shifts in fluorescence maxima of the synthesized

compounds band with D, and E were obtained (Figuers 71 and 72). Figure 71 shows

that the flouresence shift of the synthesized compounds are directly proportion with the solvent polarity as dielectric constant (D). When the D increases, a red shift occurred for the fluorescence maxima band of the examined compounds. This results were confirmed by the solvents normalized polarity values (E_T^N); A red shift occurred for the fluorescence maxima band of the compounds as the (E_T^N) increases (Figure 72).
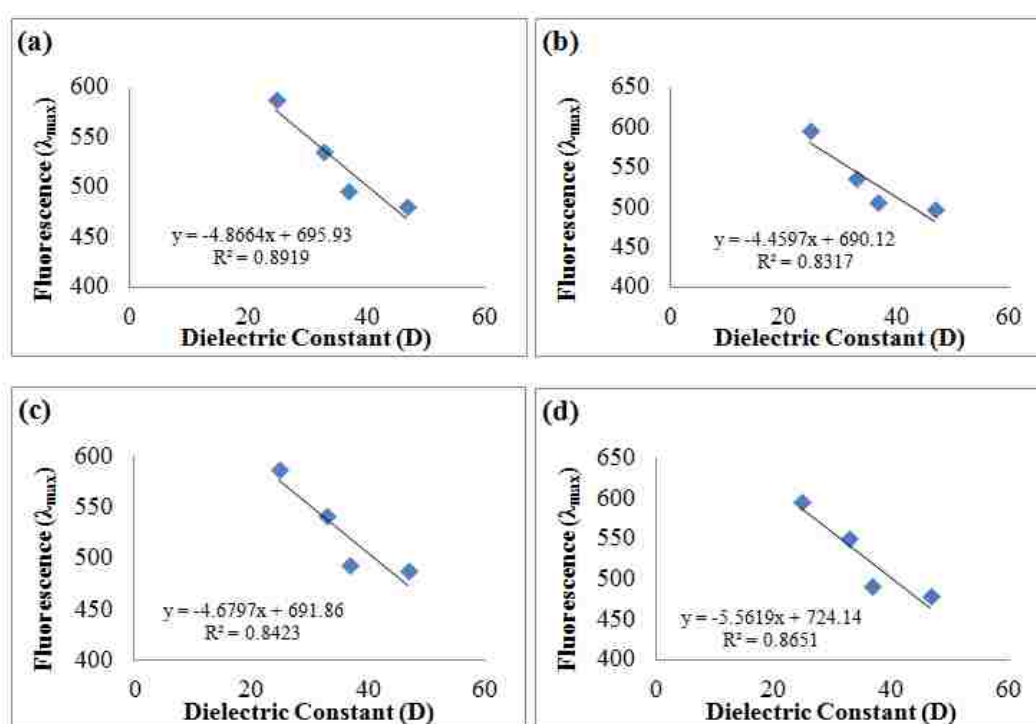
Figure 71: Solvents dielectric constant versus the fluorescence at λ_{max} of synthesized compounds (a) **113g**, (b) **117f**, (c) **118c**, and (d) **122c**

Table 13 shows that, DMSO exhibited the highest fluorescence, with least amount of quenching in all the compounds as shown in Figure 70. This may indicate that charge-transfer interactions between DMSO and the compounds occur most significantly. Methanol showed the least fluorescence with all the compounds, owing to weakest electronic interactions with the compounds. Figure 73 showed correlation

between the normalized polarity and the fluorescence. Interestingly, it shows that as the solvent polarity increase the intensity of the tested compound fluorescence decreases. While the compound intensity increases with increasing the polarizability of the solvents (Figure 74).
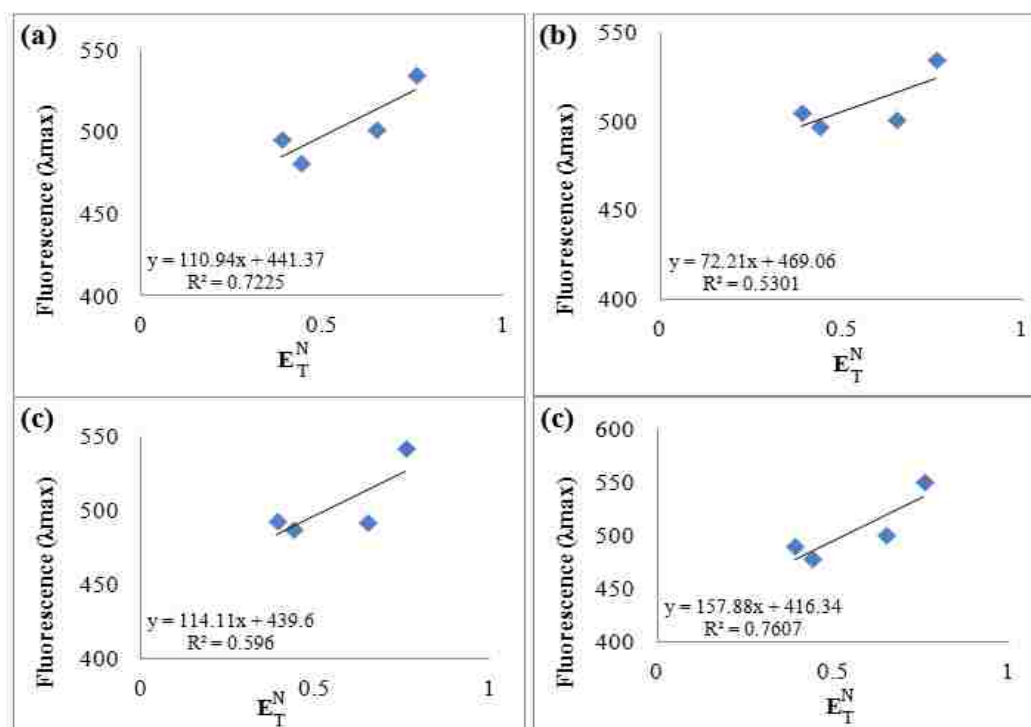
Figure 72: Solvents normalized polarity parameter (E_T^N) versus the fluorescence at λ_{max} of synthesized compounds (a) **113g**, (b) **117f**, (c) **118c**, and (d) **122c**

Table 13: Solvent parameters of the studied solvents and fluorescence intensity of the synthesized compounds. E_T^N: normalized polarity parameter of Dimroth–Reichardt; solvent parameters of Kamlet–Taft: π^*, polarity–polarizability

Solvent	E_T^N	π^*	113g	117f	118c	122c
MeOH	0.76	0.60	7.0	25.9	9.4	8.2
EtOH	0.65	0.54	52. 8	100.4	41.3	44.6
			60.5	180.5	119.6	45.3
DMSO	0.44	1.00	179.8	239.3	240.2	215.1
DMF	0.39	0.88	113.5	29.9	40.4	60.0
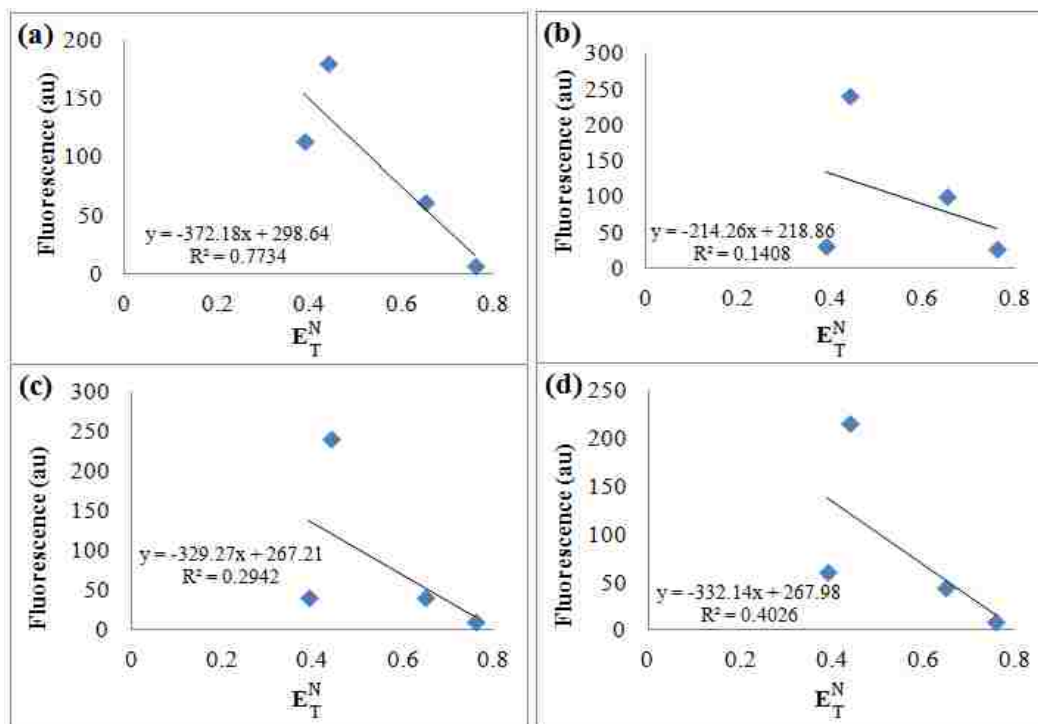
Figure 73: Solvents normalized polarity parameter (E_T^N) versus fluorescence intensity of the synthesized compounds (a) **113g**, (b) **117f**, (c) **118c**, and (d) **127c**
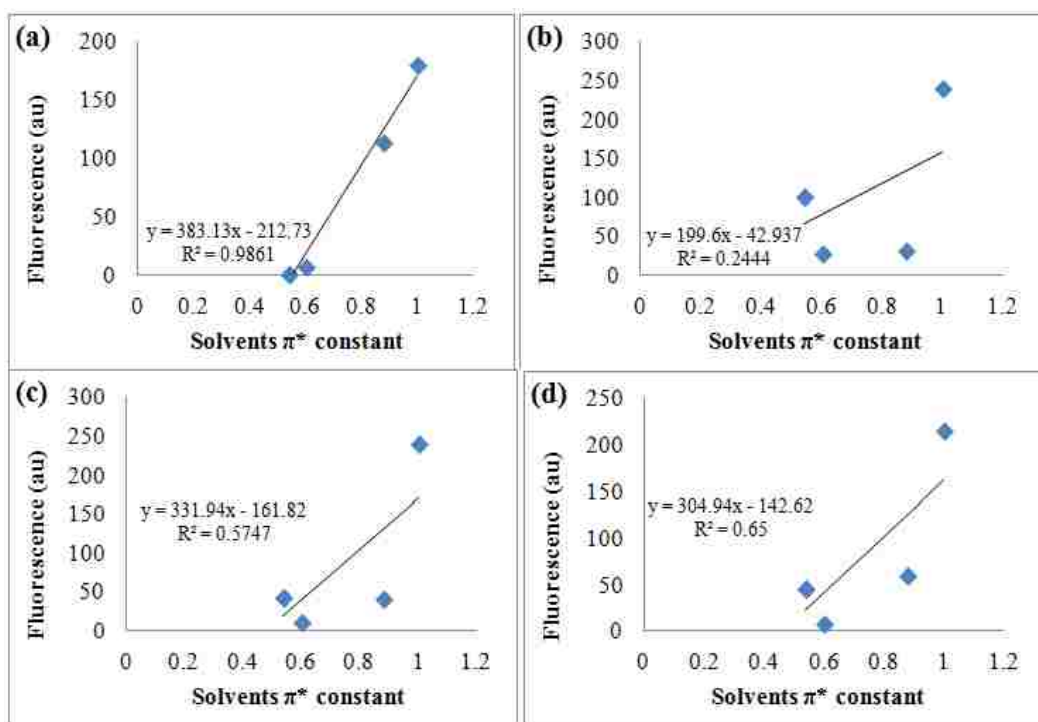
Figure 74: Solvents polarity–polarizability (π^*) versus fluorescence intensity of the synthesized compounds (a) **113g**, (b) **117f**, (c) **118c**, and (d) **127c**

4.5.2 Effect of pH

Effect of pH (3-11) on the obtained products was studied using UV-Vis spectrophotometer. The compounds were scanned after incubating in phosphate buffer for 30 minutes. Figure 74 shows compounds **113g** and **118c**. **113g** shows maximum absorption at 411 nm. There is no change in this band in pH 3, 4, 8, 9, 10 and11. While there is an increase in the absorption intensity in pH 5, 6 and 7. On other hand, **118c** shows two maximum absorption while increasing the pH. It has two absorption maxima at pH 3.5 (340 and 417 nm). By increasing the pH, the intensity of the band at 340 nm decrease while the other one increase. The is because of the Keto-Enol tutomarizm,

Figure 75 (b) shows also at two band absorbtion band appears at good intensity at pH 7.13 and 7.68. Therefore, natural pH is the optimum to use in the interaction experiments between this compound and the DNA.
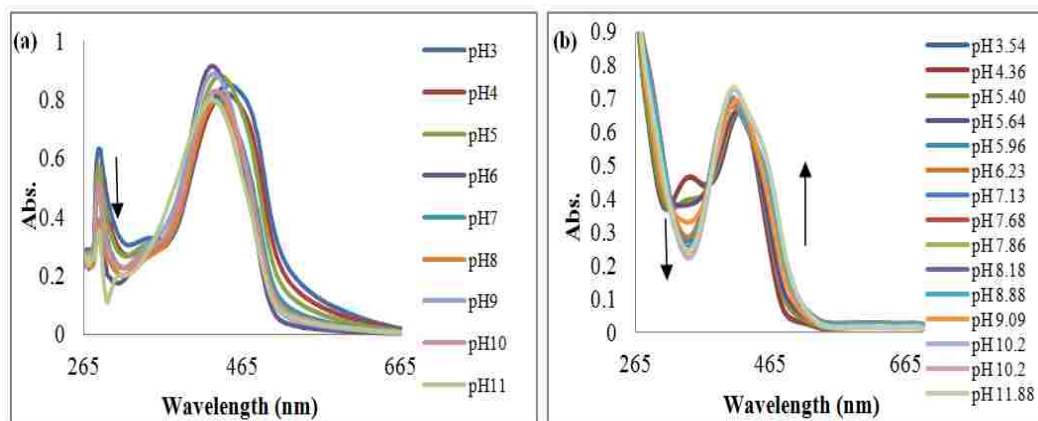
Figure 75: The absorption spectra for effect of pH (3-11) on (1 x 10^{-5} M) of synthesized drug (a) **113g**, (b) **118c** using phosphate buffer (0.01 M) and 5 % DMSO

4.5.3 Pyrazolones-DNA Interaction

The interaction of the synthesized compounds with DNA was studied to their binding affinity, nature of binding and effect of binding on DNA conformation of. The knowledge of these parameters can aid in drug designing, so as to design the drugs target specific sites on DNA and producing minimal side effects. The UV-Vis titration gave information regarding the nature of interaction of the drug with DNA, and was used for calculating the binding affinity of the drug with DNA [119]. The circular dichroism (CD) was used to observe conformational change occurred after the binding of pyrazolone molecules with DNA. It was also utilized for calculating the melting temperature of DNA molecules. CD has proved the best techniques for studying structural changes accompany with the interactions between biomolecules and ligands [120]. Fluorescence titration technique was employed to investigate the mode of interaction between the molecules and DNA [119].

4.5.3.1 Melting Temperature Curves

Melting temperature (T_m) is the temperature at which the duplex DNA is mid transition to the single stranded state [121]. Its value is used as an indication of drug's stabilizing capability upon binding with the DNA [121]. The temperature curve of ct-DNA complex with pyrazolones and pyrazolone ribosides were studied in this part. Studying the effect of the drugs on the thermal stability of the double stranded DNA structure help in developing knowledge about the mode of interaction between the drug molecules and *ct*-DNA.

The melting temperature curves for *ct*-DNA, and its complex with **114g**, **117f** and **118c**, were constructed using (CD) spectroscopy. The 1.00 mL *ct*-DNA (1.07 x 10^{-5} M, 107.0 ppm) solution in Tris-KCl-buffer pH 7.4 was heated up in 5.0 °C

increments within the range 25 to 98 °C. Then a 1.0 mL of *ct*-DNA - ligands complexes solution contain *ct*-DNA (1.07×10^{-5} M) and ligands (4.0×10^{-6} M) in Tris-KCl buffer pH 7.4 was heated from 25 to 98 °C. Incubation time intervals of 5 minutes at room temperature to ensure that the solution attained the required. The experiments were repeated with 1-2 °C increments in temperature in the CD jump range. The CD spectra were recorded in the range 200 – 400 nm against temperature.

Figure 76 shows the melting temperature curves of *ct*-DNA and its complexes with **113g**, **117f** and **118c**. Figure 76 shows that the pyrazoline azo day **113g** stabilized ct-DNA by $\Delta T_m = +4.5$ °C, (T_m,113g–*ct*-DNA − T_m, *ct*-DNA = 95.4 – 90.9 = +4.5 °C). The pyraoline acetylated riboside **117f** stabilized ct-DNA by $\Delta T_m = +2.9$ °C while the free pyrazoline riboside **118c** stabilized *ct*-DNA by $\Delta T_m = +4.8$ °C (Table 14). These results indicated that the pyrazolone azo dye **113g** and free pyrazoline nucleoside **118c** have nearly the same magnitudes and are more efficient in stabilizing the *ct*-DNA than the acetylated pyrazoline nucleoside **117f**. These differences in ΔT_m values between the three compounds **113g**, **117f** and **118c** may be attributed to the number of H-bond centers [122-125].

Table 14: Drug structures and ΔT_m of drug-DNA complexes comparing with the *ct*-DNA T_m (90.9 °C)

Drug	ΔT_m (°C)
113g	4.5
117f	2.9
118c	4.8
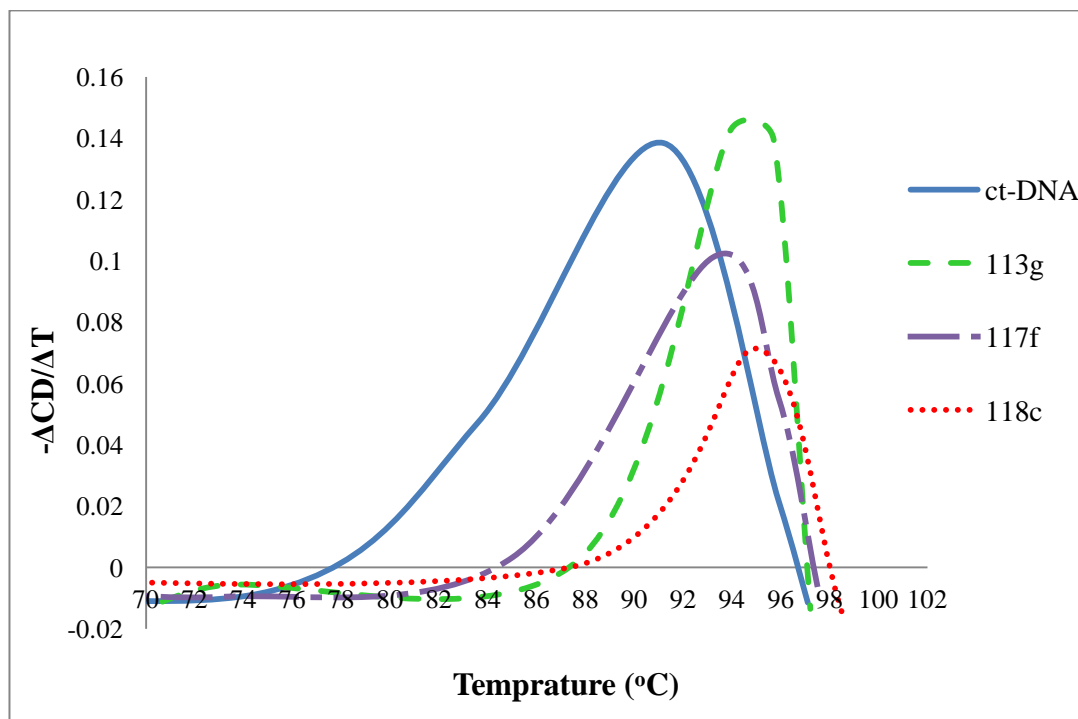
Figure 76: Melting temperatures' curves for *ct*-DNA and *ct*-DNA-ligands complexes. 1.0 mL of *ct*-DNA (1.07×10^{-5} M) solution in tris-KCl buffer, pH 7.4 was heated up in the range 25-98 $^{\circ}$C. A 1.0 mL of *ct*-DNA-ligands complexes solution contain *ct*-DNA (1×10^{-9} M) and ligands (1.10×10^{-5} M) in Tris-KCl buffer pH 7.4 was heated from 25-98 $^{\circ}$C

Pyrazolone derivaitives used in this section is illustrate in Figure 76. The pyrazolone azo dye **113g** has three hygdogen-bond donors and two hydrogen-bond– acceptor. While forming the glycosidc bond via the pyrazoline nitrogen atom reduced the number of hydrogen-bond-acceptor centers in the pyrazoline riboside **117f**. Then the de-accetylation of the pyrazoline riboside compound and forming the free derivative **118c**, which has thee free hydroxyl groups, increase the number of hydrogen-bond-centers. These groups can form hydrogen bonds with the hydrogen bonding sites available on ct-DNA structure providing much more stabilizing for ct-DNA [122-125].
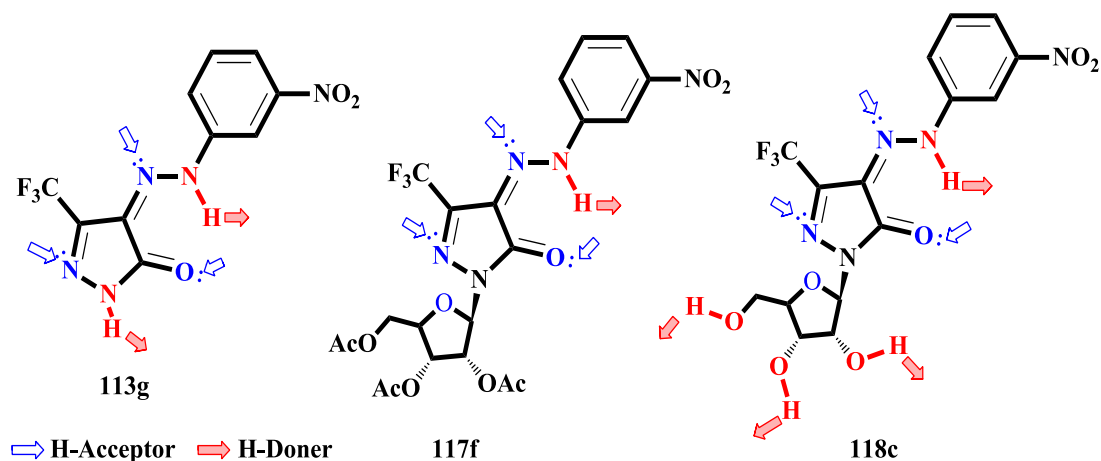
Figure 77: The H-bond-donors-acceptors in the ligands' structures

4.5.3.2 UV-Visible Titration

The UV-Vis absorption spectroscopy is a suitable technique for studying interactions between drugs and DNA. This interaction is indicated by the changes in the absorption properties of the drug or DNA. The DNA maximum absorption in the UV region is at 260 nm. This absorption is referred to the electronic transitions of the chromophoric groups in the DNA base pairs. This band could be used to estimate the binding mode. If the absorbing decrease, with red shift, then it is intercalation binding mode between the drug and the DNA. In this mode, the aromatic chromophore of the drug inter between the DNA base pairs. Therefore the drugs' π-electrons merged to the DNA bases-π electrons which leads the decreasing in the energy level of the π– π^* electron transition which appears in a longer wavelength (red shift) [126, 127]. Shifting to longer wavelength (red shift) is also could observed if there is an electrostatic interaction between the ligand and the phosphate group of the DNA backbone [128, 129].

On the other hand, Tabernero L. and co-workers illustrate that seventy-seven interactions between the drugs and the DNA base pairs can be classified as hydrogen bonds. Furthermore, there is a relationship between hydrogen bond geometry and the biding of the drug through the minor groove [130].

To study the interaction between the Drug and DNA, the UV absorption should be observed. Changes in intensity and/or shifting could be refer to the strength of the interaction between the DNA and its ligand. Some of the Drug-DNA interaction parameters such as binding mode, constant and number of the binding sites could be considered by titration process between DNA and the drug [131-134].

DNA-Drug interaction study was carried on the free riboside 3-(β-D-ribofuranosyl)-4-(3'-nitrophenylhydrazono)-5-trifluoromethyl-2,4-dihydropyrazol-3-one (**118c**) since it is the most efficient ligand in stabilizing the *ct*-DNA ($\Delta T_m = + 4.8$ °C).

The compound **118c** was titrated with different concentrations of calf thymus DNA and the absorption spectra was obtained Figure 77. The addition of DNA causes change in the UV-Vis spectrum of the free ribosed **118c**. Figure 78 shows increasing in absorbance at 260 nm, decrease in at 380 nm and blue shift in λ_{max} from 380 to 260 nm. The hyperchromism, an increase in absorbance, around 260 nm indicates the increasing of the DNA concentration as the maximum absorption of the DNA bases pairs appears around 260 nm. While the hypochromism, a decrease in absorbance, at 380 nm indicates the reduced n–π* electronic transition. This hypochromism could be coursed by forming H-bond between **118c** and the polar hydrogens of DNA [135]. This H-bonding formed supports the bonding of **118c** with the DNA, which also improve the chances of π-stacking. As a result of this stacking,

the interaction between π-orbitals of the drug (**118c**) and DNA increases, which also support the drug-DNA interaction [135].

On the other hand, this existence of hyperchomism and hypochromism formed an isosbestic point, which confirm the presence of two types of interactions (H-bonding and π-stacking) in equilibrium.
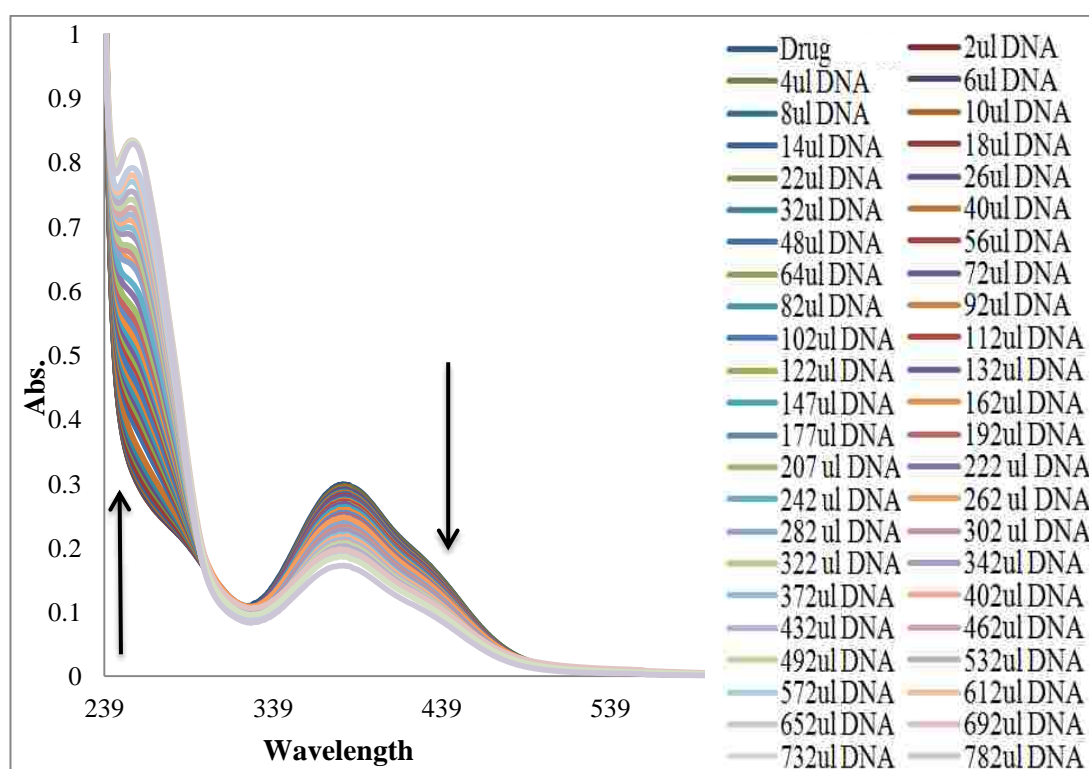
Figure 78: UV-visible spectrum of compound of **118c** (2.46 x 10^{-5}M) without *ct*-DNA and with *ct*-DNA (1.07 x 10^{-5} M) interaction (2.0 – 782.0 μL) in 5 % DMSO and Tris-KCl buffer, pH 7.4

Regarding to the change in the DNA concentration, at the constant drug **118c** concentration (2.46 x 10^{-5}M), the drug-DNA binding constant has been calculated. The following host–guest equation (2) was used to calculate the DNA binding constant (K).

$$\frac{A_\text{o}}{A-A_\text{o}} = \frac{\varepsilon_\text{G}}{\varepsilon_\text{H-G}-\varepsilon_\text{G}} + \frac{\varepsilon_\text{G}}{\varepsilon_\text{H-G}-\varepsilon_\text{G}} x \frac{1}{K[DNA]} \quad \text{-------------------- (2)}$$

Where A_o and A are the absorbance of drug, at λ_{max}, and ε_G and $\varepsilon_\text{H–G}$ are the drug molar absorptivities, at λ_{max}, in the absence and presence of DNA respectively. The value of binding constant (K) was calculated from the intercept to slope ratio of the linear plot between A_o /A− A_o and 1/[DNA]. From the linear equation (Figure 79) the binding constant (K) was calculated between the drug **118c** and the *ct*-DNA K = 5.4 x 10^6 M^{-1} which indicates that **118c** has a high affinity with DNA double helix [136].
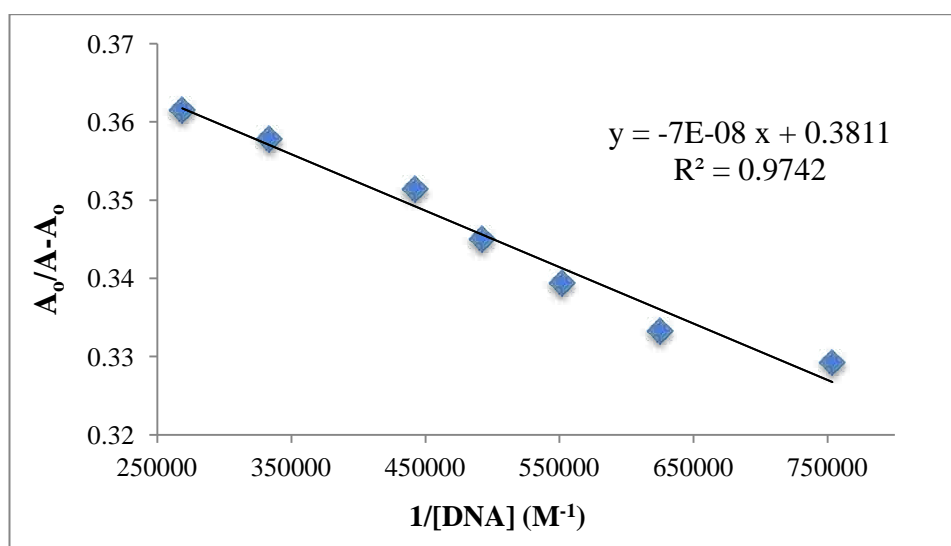
Figure 79: Graph between A_o/(A−A_o) and 1/[DNA] for the calculation of binding constant. where A_o and A are the absorbance of test sample, at λ_{max}, in the absence and presence of DNA respectively. And [DNA] is the *ct*-DNA concentration during the UV titration process with the drug **118c** (2.46 x 10^{-5}M)

The Drug-DNA stoichiometry was determined by mole-ratio method keeping the drug **118c** concentration constant (2.46 x 10^{-5}M) and varying the *ct*-DNA concentration. Change in absorbance was measured at 380 nm and plotted against

ratio of the drug to *ct*-DNA concentrations (Figure 80). Two straight lines were obtained intersection of which determines stoichiometry of the drug-DNA complex. Figure 80 suggests formation of a 30:1 drug: DNA complex at neutral pH.
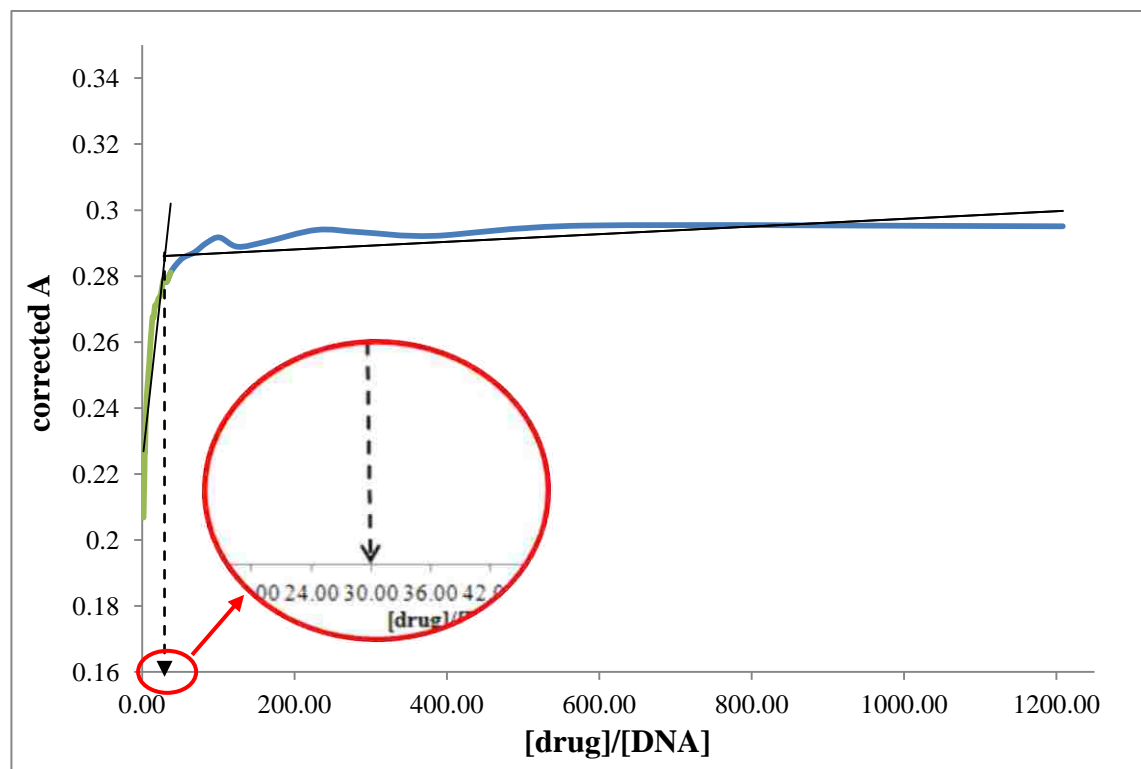
Figure 80: Mole-ratio plot showing the interaction of **118c** with *ct*-DNA at neutral pH. Inset is the graph with zoom in the intersection area

4.5.3.3 Fluorescence Titration

Fluorescence spectroscopy is an emission technique depends on the emission of photon from an exited molecule in order to relaxed into its ground state. The emitted energy is less than the absorption one; therefore the emitted light is usually in the visible range while the absorbed light is in the ultraviolet range [137].

Fluorescence titration experiment was done as an additional confirmation for DNA-drug interaction. As it is one of the most used techniques to study the interactions between small drug molecules and DNA [134]. The intensity of the

fluorescence emission band changes during the drug-DNA titration process which indicates the existence of the drug-DNA interaction [137, 138].

The fluorescence titration of the fixed concentration of the synthesized drug **118c** ($1.0x10^{-5}$ M) was carried against different concentrations of *ct*-DNA ($1.07x10^{-5}$M) in Tris-KCl buffer, pH 7.4 and 5% DMSO. The interactions of **118c** with ct-DNA were followed fluorimetrically at λ_{max} of emission 425 nm and excitation of 280 using slits width of 10.00 nm. After each DNA addition, solutions were shacked for 3 times, incubated for 3 min and scanned for its fluorescence spectra in the range 300-600 nm. The titrations process were stopped; when no change in fluorescence intensity observed.

Figure 81 shows the fluorescence spectrum of the compound **118c** obtained at excitation λ_{max} of 280 nm and emission band was obtained at 425 nm, with sequential additions of ct- DNA to the fixed drug concentration. The spectrum showed increase in fluorescence intensity, which could be attributed to the groove binding, electrostatic, or hydrogen bonding of the drug with DNA, resulting in the proximity of molecules to the sugar-phosphate backbone [119]. The fluorescence titration results confirm the UV-Vis titration results for the same complex.

4.5.3.4 Circular Dichroism Titration

Circular dichroism spectroscopy is also used to confirmed the interactions between drug **118c** and DNA. As it is an effective technique used to study interaction between DNA and drugs. CD is used mainly to study the changes in DNA conformations and melting temperature curves (as discusses previously). Circular dichroism spectroscopy technique depends on the measurements of the difference between the left and the right handed absorption of a chiral molecule which

circularly polarized light. CD spectrum illustrates the average molecular conformation in the whole sample. Consequently, it is useful to track the structural changes in a biomacromolecule due binding with a drug molecule or changing in temperature [139]. Though, CD results could limit the number of duplex DNA types; it can't certainly determine the type of quadruplex structure [140].
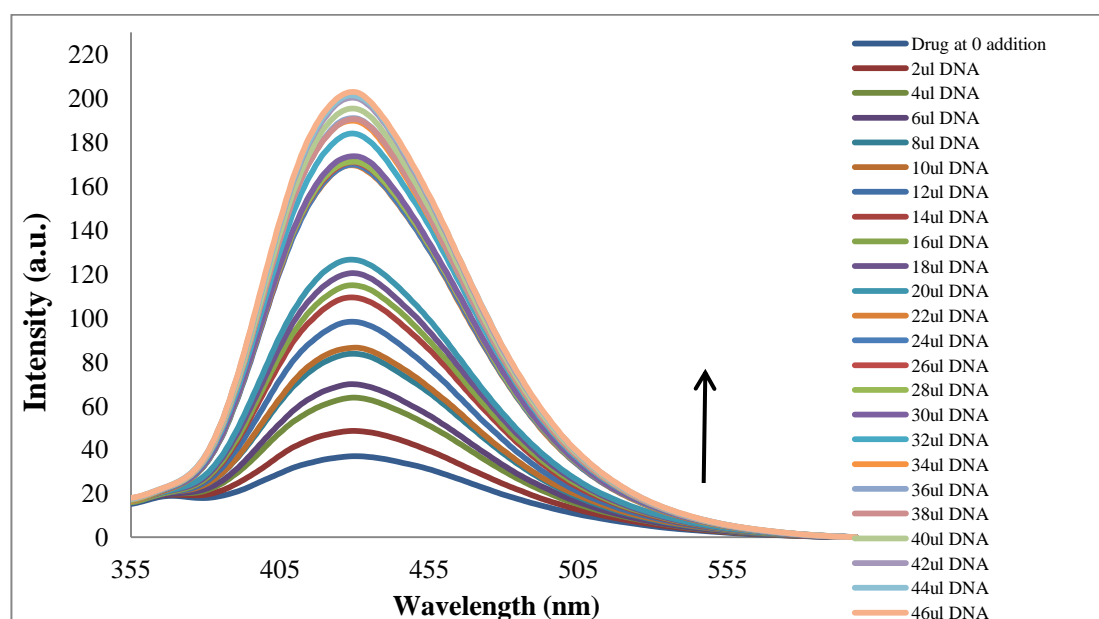
Figure 81: Fluorescence titration spectra of **118c** (5 x 10^{-6} M) in Tris-KCl buffer, pH 7.4 with *ct*-DNA (1.07 x 10^{-5} M) (2.0 - 46.0 µL) and 5 % DMSO

Figure 82 shows the CD spectrum of free calf thymus DNA (blue line), there are two major bands. at 243 nm (negative), 281 nm (positive). These bands are considered as the marker bands for B-form of DNA which is the most frequently observed conformation of DNA [136, 141].

The circular dichroism titration was carried out for the newly synthesized compound 3-(β-D-Ribofuranosyl)-4-(3'-nitrophenylhydrazono)-5-trifluoromethy-2,4-dihydropyrazol-3-one **118c** as it produced the maximum thermal stability effect (ΔTm = + 4.8 $^{\circ}$C). the interactions between **118c** and *ct*-DNA were studied. The *ct*-

DNA (1.07 x 10^{-6} M) was prepared using Tris-KCl buffer, pH 7.4 then titrated with successive amounts of the drug solution (1.0 x 10^{-3} M) in 5 % DMSO. Solution after each addition was shacked well, incubated for three minutes at room temperature and scanned in the range 200 - 400 nm with 50 nm/min, band width 1 nm and 3 accumulations.

The CD spectra (Figure 82) shows that the *ct*-DNA molecule gave a positive band at 280 nm, negative band at 240 nm and crossover occurred at 258 nm. Upon sequential addition of drug to *ct*-DNA changes in the CD spectra were observed, which indicated the change in conformation of the DNA molecules upon binding of the drugs. When the drug concentration was increased the intensity of the positive band at 280 nm decreased, and the crossover frequencies also changed beside the increase in absorbance on negative bands. These changes showed that compound **118c** interacted actively with DNA molecules, although preserving the B-form conformation of the DNA.
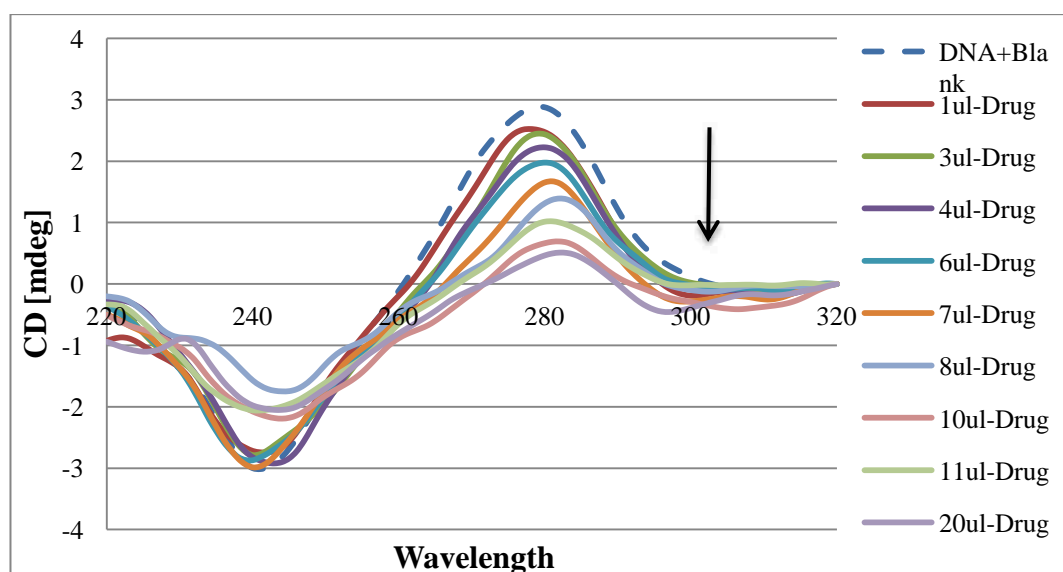
Figure 82: CD spectra of *ct*-DNA (1.07 x 10^{-5} M) in Tris-KCl buffer, pH 7.4 titrated with (1.0 x 10^{-3} M) of **118c** (1.0 - 20.0 μL)

4.5.3.5 Docking Study

Some of the synthesized pyrazolones (**117c**, **118c**, **124a,b**) underwent preliminary docking experiments into the DNA minor groove as well as into the intercalating site of the DNA-topoisomerase complex. As shown in Table 15, the synthesized compounds had favourable binding energies in either binding sites where **118c** always scoring the best amongst the newly synthesized compounds. However, and in line with the previous spectroscopic data, **118c** and the rest of the compounds in this series display better scores when they intercalate into the DNA-topoisomerase complex as compared to the minor groove binding site. Looking at the Ligands efficiency scores, it is clear that **118c** had a comparable scoring to the standard inhibitor Doxorubicin whereas it was not able to match the standard groove binder's (Daphnetin) scoring. As shown in the Figure 83 (A) and (B). **118c** seems to have more reasonable binding mode in the DNA-topoisomerase complex the minor groove as **118c** nitro aromatic moiety seems to be better inserted in between the DNA nucleotides, forming clear stacking interactions with their nitrogen bases. In the other hand, the **118c** sugar moiety forms several hydrogen bonds with the DNA backbone as well as with the topoisomerase basic residues. To sum up, the obtained docking results suggest that these compounds, especially **118c**, would rather act as intercalating agents than minor groove binders.

Table 15: Docking results of test compounds into the *ct*-DNA major and intercalation binding side

Compound code	Minor groove		Intercalation binding side		Structure
	Glide_XP Score kcal/mol	Ligand efficiency* kcal/mol	Glide_XP Score kcal/mol	Ligand efficiency* kcal/mol	
117e	-3.383	-0.103	-5.047	-0.169	
118c	-2.606	-0.085	-5.440	-0.186	
124a	-0.980	-0.033	-5.181	-0.140	
124b	-4.582	-0.153	-7.101	-0.237	
Doxorubicin	-	-	-10.07	-0.26	
Daphnetin	-4.437	-0.340	-	-	

Figure 83: Docking results of **118c** into the *ct*-DNA **(A)** docked pose of **118c** in the *ct*-DNA minor groove, **(B)** docked pose of **118c** in the *ct*-DNA intercalation binding side
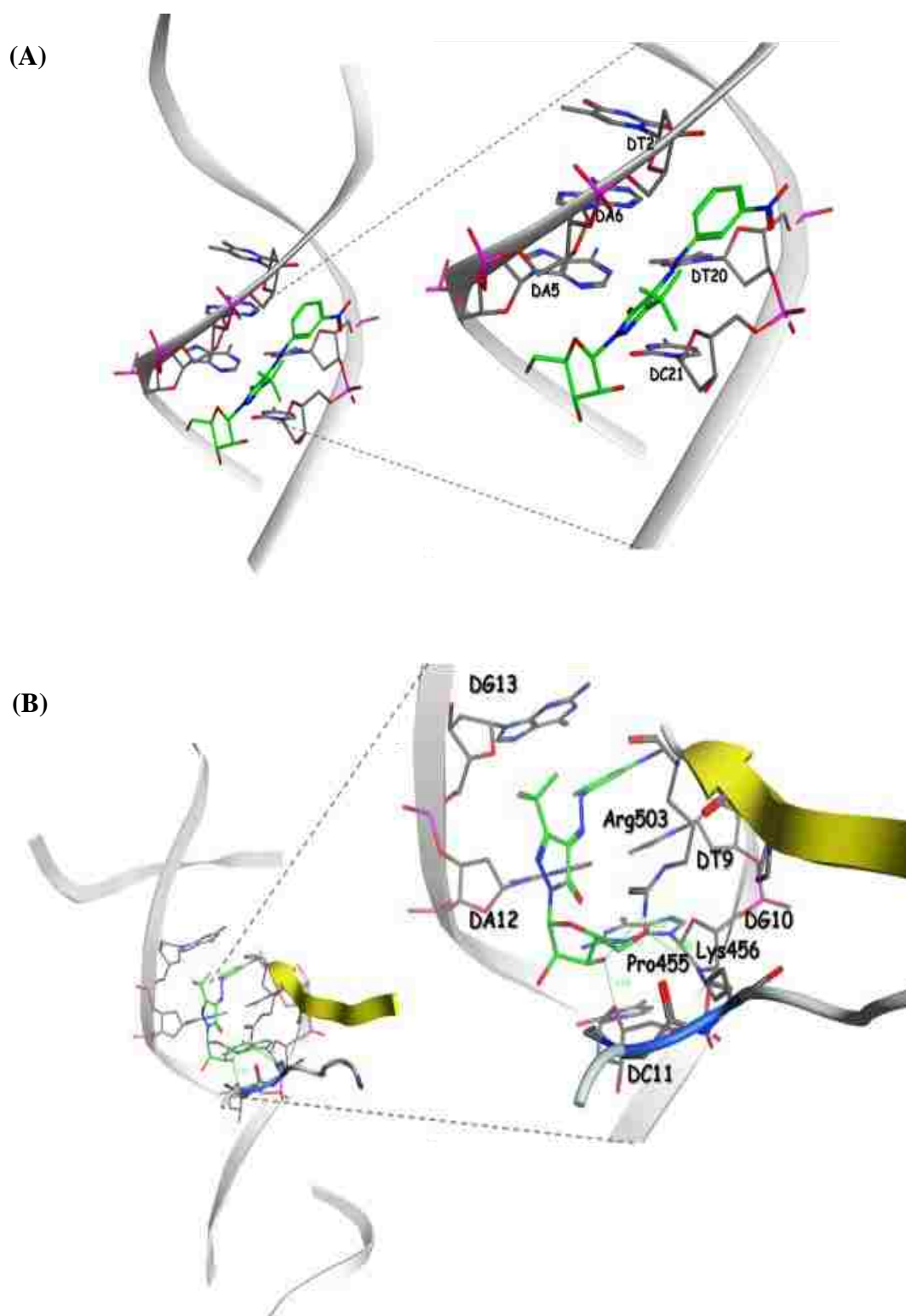
4.6 Summary

The study involved characterization of physical properties of the synthesized pyrazoline compounds, and testing for the nature of their interaction with the DNA (calf thymus), which is crucial for predicting their probable behavior with biological moieties. Among all the synthesized compounds, few compounds were subjected to the physical study and the most suitable compounds were selected pertaining to the results of their behavior in the different physical conditions. The effects of different physical conditions such as pH, solvent systems, upon the stability of ligands in the chemical compounds were studied.

The compounds 4-(3'-nitrophenylhydrazono)-5-trifluoromethyl-2,4-dihydropyrazol-3-one **113g**, 2-(2",3",5"-tri-*O*-acetyl-*β*-ribofuranosyloxy)-4-(3'-nitrophenylhydrazono)-5-trifluoromethyl-2,4-dihydropyrazol-3-one **117f**, 2-(*β*-ribofuranosyl)-4-(3'-nitrophenylhydrazono)-5-trifluoromethyl-2,4-dihydropyrazol-3-one **118c** and (*N*^{2}-Benzoyl)-4-(3'-nitrophenylhydrazono)-5-trifluoromethyl-pyrazolone **127c** were studied. The examined compounds were found to exhibit stability over different ranges of pH. The effect of four solvents (ethanol, methanol, dimethylformamide, dimethyl sulfoxide) with different dielectric constants upon the compounds **113g**, **117f**, **118c** and **127c** were studied, and DMSO was found to be the most stabilizing solvent for all the compounds.

Effects of solvents on electronic spectra of synthesized compounds were investigated. Good correlations with solvents parameters indicating the dependence of λ_{max} on solvent's dielectric constants, basicity, and polarity were obtained

Subsequent to stability studies of the compounds, the physical interaction of the compounds with *ct*-DNA was studied through different techniques which

involved melting temperature curve (measuring $\Delta T_{m)}$. The compound **118c** were found to have the highest ΔT_m amoung the examined compounds. Therefore, its interaction with *ct*-DNA was under more investigation. UV-Vis, fluorescence and circular dichroism spectroscophic techniques towards *ct*-DNA were studied as well. These helped in understanding the nature, mode and strength of interaction of the drugs with DNA. **118c** absorption spectra with DNA exhibited hypochromism and bathochromic shifts. The fluorescence spectra, further, gave details about the mode of binding of **118c** with *ct*-DNA. The results showed that compound **118c** was found to exhibit strong intercalation binding, and increased fluorescence intensity. The circular dichroism titration was thus carried out only with the compound 3-(*β*-ribofuranosyl)-4-(3'-nitrophenylhydrazono)-5-trifluoromethyl-2,4-dihydropyrazol-3-one **118c** to observe the changes in conformation brought about by binding of the compound. therefore, on the basis of physical studies, the free riboside compound, **118c** was found to be the most suitable and effective in interacting with *ct*-DNA, and subsequently poses as a potent compound for further investigative studies as a therapeutic agent in the near future.

Chapter 5: Conclusion and Recommendations

5.1 Summary

The purpose of our study was to synthesize new pyrazolones derivatives that can be used as antimicrobial or anticancer agents. The synthetic part includes four main categories: azopyrazolones, pyrazoline riboside, pyrazoline deoxyriboside and benzoyl pyrazoline derivatives. In the first part, a new series of nine azopyrazoline **113a-i** were synthesized in an environmentally and efficiently procedure in a good yield avarge 94 % and the products screened for their antifungal and antibacterial activities. Among the newly synthesized derivatives, compound **113c** exhibited the highest potent antibacterial activities MIC = 0.151 µg/mL against *yeast* and MIC = 0.075 µg/mL against *Bacillus.*

In the second part, a series of 10 new pyrazoline riboside **116a,b** and **117a-h** were synthesized using silyl-method to activate the pyrazolone ring, while the ribose was used as 1-acetyl analog that activated by Lewis acid catalyst to achieve the final products **116** and **117** in yield 63%. The synthesis of *O*- and *N*-isomer was controlled by the reaction time. The silyl intermediate reacts with an activated surge in either dry acetonitrile or methylene chloride for 4 hours at room temperature to affords a mixture of *O*- and *N*-ribosides . The study of the effect of the solvent and/or catalyst on regioselective showed the time is the most significant effect as it is noticed when solvents and catalyst are fixed, in which the yield of *O*-isomer decrease dramatically while the yield of *N*-isomer increase gradually with increasing the time, this is may be attributed to the stability of *N*-isomer. The structure of *O*- and *N*-ribose products were confirmed using FT-IR, ^{1}H-NMR, ^{13}C-NMR and LC-MS. The *O*-isomer **116a** was found to be potent antimicrobials when tested against Gram-positive bacteria;

bacillus with MIC value of 0.034 µg/mL. While **118c** showed high selectivity against the tested fungal with minimum inhibitory concentrations of 0.124 µg/ml, against *Yeast.* On the other hand, the *N*-isomer **117a, 117e** and **117f** showed superior anticancer activity against HL-60 and A-549 cell lines.

In the third part, a new series of pyrazoline deoxyribosides **112a-c** and **123a-c** were designed and synthesized. 1,3,5-tri-*O*-acetyl-2-deoxy-D-ribofuranos has introduced to the two different nucleophlic centers in the pyrazolone ring. As in the ribosides synthesis, the silyl-method is used to activate the pyrazolone ring, while the sugar moiety was used as 1-acetyl analog that activated by Lewis acid catalyst. The silyl intermediate reacts with the activated surge in dry methylene chloride for 8 hours at room temperature. The reaction afford *O*- and *N*-nucleosides in a good yield 53% and 47%; respectively. Among the new discovery; the structures of the obtained products were fully confirmed using elemental and spectroscopic techniques. The newly synthesized compounds were screened for their antibacterial activities against pathogenic bacteria. The results indicated that compounds **122b** and **123b** showed high selectivity against the tested microbs with inhibition zones of (23.0 and 27.8 mm) respectively, against control compound show better anti bacterial activity against *Proteusd* (19.3 and 19.2 mm) respectively in comparing with the positive control (Ceftriaxon 16.7 mm). Synthesized pyrazoline deoxyribosides have significant effect on cancer cell lines. **122b** showed the best decreasing in cell viability aganist HL-60 cell line among all tested compounds. While **122a** showed promising activity against A-549 cell line.

In the last part, The benzoyl Pyrozoline compounds **124a-h** and **127a-c** were prepared using two different synthetic methods, In the first method, a simple

nucleophlic substitution reaction was used to introduce the benzoyl group into the pyrazolone ring. The activating pyrazolone will enhanced the nucleophilicity of both O- and N^2 center of the pyrazolone ring to afforad O-isomer **124a-h**. While, In the second method, the benzoyl group introduced directly into the hydrazine nitrogen then cyclizaed followed by diazotization to afforded the N-benzoyl analogue **127a-c**. The structures of both O-benzoylation and N- benzoylation were confirmed and the antimicrobial, anti-cancer activity were evaluated. Antimicrobial activity results revealed that **124g** and **127c** were found to be the most potent antimicrobial agent with Inhibition zone value of (20.0 and 17.2 mm) respectively against *Proteus* which are higher than the positive control (Ceftriaxon 16.7 mm). Results of anticancer study indicated that the synthesized compound **124c, 124d, 124f** and **124g** have significant effect on of A-549 cell line. **124d** showed the best decreasing in cell viability (almost 15 %) against A-549 among the tested compounds. Which make it most potent anticancer agent against the cancerous A-549 cell lines.

5.2 Research Implications

Pyrazolones are one of the most studied compounds, and constitute a large area of research in organic chemistry, posing as a universal, chemically active moiety which can be utilized in broad spectrum of drugs. The present research yielded important information regarding the significance of the newly synthesized pyrazolones. Among the various compounds; **113c,116a, 117a, 117e, 117f, 118c, 122a, 122b, 123b,124c, 124d, 124f, 124g** and **127c** were found to exhibit important chemical and physical properties. Such a characterization and identification can be helpful in present studies being conducted on the scope of these compounds, and also the future researches. A large number of researches have been already conducted into

the wide range of biological properties such as antiviral, antimicrobial, anti-inflammatory, anticancer, exhibited by pyrazolones and their derivatives, and the present research contributed significantly towards the existing information. The information can also find important implications in the field of therapeutics and drug designing, as a large number of infectious diseases continue to spread around the world, characterized with new and resistant strains of microbes. The knowledge of pyrazolone compounds and their ability to be designed and formulated as per the requirement of the infection or diseased condition is also another area which this research aims to contribute to. Further, since the newly synthesized compounds showed significant biological and DNA-interacting properties, it has added to the existing repository of potential compounds capable of providing lifesaving opportunities.

5.3 Limitations and Future Scope of the Study

Although the study resulted in the synthesis of a large number of derivatives of pyrazolones, among which several compounds showed significant biological and physical activities, the study also showed several limitations, with respect to the research methodology. First and foremost, only three families of derivatives were synthesized in this study, ribonucleosides, deoxyribonucleosides and benzolyated compounds, thereby leaving out other important derivatives of this important compound. Furthermore, during the studies evaluating the biological properties, only five microorganisms were chosen, excluding variation in fungal pathogens. Although the compounds showed activity against these commonly found pathogens, other equally important pathogens were not tested for. Further, for the physical studies, while testing the DNA-compound interactions, only few compounds were selected,

therefore leaving out the rest of the compounds. Furthermore, more investigations need to be done to understand the nature of the interaction between the synthesized drug and DNA.

Through this study, several newly synthesized derivatives of pyrazolones were studies for their chemical structure, biological properties as well as physical interactions. Subsequently, few compounds were found to have significant potential as a future drug candidate. However, further research is needed with respect to its studies on anti-microbial activities against other groups of microbes, besides studying their effect against other cell lines. Also, other synthesized compounds need to be studied for their interaction with a broader range of solvents as well as testing the interactions of the remaining compounds with DNA.

References

1. Uramaru, N., Shigematsu, H., Toda, A., Eyanagi, R., Kitamura, S., & Ohta, S. (2010). Design, synthesis, and pharmacological activity of nonallergenic pyrazolone-type antipyretic analgesics. *Journal of Medicinal Chemistry*, *53*(24), 8727-8733.

2. Hassan, A. E., Moustafa, A. H., Tolbah, M. M., Zohdy, H. F., & Haikal, A. Z. (2012). Synthesis and antimicrobial evaluation of novel pyrazolones and pyrazolone nucleosides. *Nucleosides, Nucleotides and Nucleic Acids*, *31*(11), 783-800.

3. Rani, P., Srivastava, V. K., & Kumar, A. (2004). Synthesis and antiinflammatory activity of heterocyclic indole derivatives. *European Journal of Medicinal Chemistry*, *39*(5), 449-452.

4. Tseng, C. K. (2005). Overview of antiviral drug discovery and development. *Antiviral Drug Discovery for Emerging Diseases and Bioterrorism Threats*, 31-82.

5. Gamage, S. A., Spicer, J. A., Rewcastle, G. W., Milton, J., Sohal, S., Dangerfield, W., ... & Denny, W. A. (2002). Structure− activity relationships for pyrido-, imidazo-, pyrazolo-, pyrazino-, and pyrrolophenazinecarboxamides as topoisomerase-targeted anticancer agents. *Journal of Medicinal Chemistry*, *45*(3), 740-743.

6. Rajiv D, S., S., Sonwane, S.K. and Srivastava, S.K., Pharmacological Significance of synthetic heterocycles scaffold: *A Review.* . A*dvances in Biological Research*, 2011. **5** (3): p. 120-144.

7. Antre, R. V., Cendilkumar, A., Gurubasavrajswamy, P. M., Divakar, G., & Oswal, R. J. (2011) Pyrazolone part 3: Antibacterial activity of novel 4-substituted pyrazolone derivatives. *Der Pharma Chemica*, *3*(5),7-12.

8. Gouda, M. A., Eldien, H. F., Girges, M. M., & Berghot, M. A. (2016). Synthesis and antitumor evaluation of thiophene based azo dyes incorporating pyrazolone moiety. *Journal of Saudi Chemical Society*, *20*(2), 151-157.

9. Gürsoy, A., & Terzioğlu, N. (2005). Synthesis and isolation of new regioisomeric 4-thiazolidinones and their anticonvulsant activity. *Turkish Journal of Chemistry*, *29*(3), 247-254.

10. Rescifina, A., Zagni, C., Romeo, G., & Sortino, S. (2012). Synthesis and biological activity of novel bifunctional isoxazolidinyl polycyclic aromatic hydrocarbons. *Bioorganic & Medicinal Chemistry*, *20*(16), 4978-4984.

11. Manfredini, S., Bazzanini, R., Baraldi, P. G., Guarneri, M., Simoni, D., Marongiu, M. E., ... & Tramontano, E. (1992). Pyrazole-related nucleosides. Synthesis and antiviral/antitumor activity of some substituted pyrazole and

pyrazolo [4, 3-d]-1, 2, 3-triazin-4-one nucleosides. *Journal of Medicinal Chemistry*, *35*(5), 917-924.

12. Kumar, K. A., & Jayaroopa, P. (2013). Pyrazoles: synthetic strategies and their pharmaceutical applications-an overview. *International Journal of PharmTech Research*, *5*(4), 1473-1486.

13. Wiley, R. H., & Behr, L. C. (1967). *Pyrazoles, pyrazolines, pyrazolidines, indazoles and condensed rings-* (Chemistry of Heterocyclic Compounds; vol. 22). John Wiley & Sons, 3-20.

14. Peruncheralathan, S., Khan, T. A., Ila, H., & Junjappa, H. (2005). Regioselective Synthesis of 1-Aryl-3, 4-substituted/annulated-5-(methylthio) pyrazoles and 1-Aryl-3-(methylthio)-4, 5-substituted/annulated Pyrazoles §. *The Journal of Organic Chemistry*, *70*(24), 10030-10035.

15. Knorr, L. (1883). Einwirkung von acetessigester auf phenylhydrazin. *European Journal of Inorganic Chemistry*, *16*(2), 2597-2599.

16. Heller, S. T., & Natarajan, S. R. (2006). 1, 3-Diketones from acid chlorides and ketones: a rapid and general one-pot synthesis of pyrazoles. *Organic letters*, *8*(13), 2675-2678.

17. Aggarwal, V. K., de Vicente, J., & Bonnert, R. V. (2003). A novel one-pot method for the preparation of pyrazoles by 1, 3-dipolar cycloadditions of diazo compounds generated in situ. *The Journal of Organic Chemistry*, *68*(13), 5381-5383.

18. Deng, X., & Mani, N. S. (2006). Reaction of N-monosubstituted hydrazones with nitroolefins: a novel regioselective pyrazole synthesis. *Organic Letters*, *8*(16), 3505-3508.

19. Fustero, S., Simón-Fuentes, A., & Sanz-Cervera, J. F. (2009). Recent advances in the synthesis of pyrazoles. A review. *Organic Preparations and Procedures International*, *41*(4), 253-290.

20. Katritzky, A. R., Wang, M., Zhang, S., Voronkov, M. V., & Steel, P. J. (2001). Regioselective synthesis of polysubstituted pyrazoles and isoxazoles. *The Journal of Organic Chemistry*, *66*(20), 6787-6791.

21. Bishop, B. C., Brands, K. M., Gibb, A. D., & Kennedy, D. J. (2004). Regioselective synthesis of 1, 3, 5-substituted pyrazoles from acetylenic ketones and hydrazines. *Synthesis*, *2004*(01), 43-52.

22. Cacchi, S., Fabrizi, G., & Carangio, A. (1997). Functionalised pyrazoles through a facile one-pot procedure from N-tosyl-N-propargyl-hydrazine and aryl iodides or vinyl triflates. *Synlett*, *1997*(08), 959-961.

23. Jordheim, L. P., Durantel, D., Zoulim, F., & Dumontet, C. (2013). Advances in the development of nucleoside and nucleotide analogues for cancer and viral diseases. *Nature reviews. Drug Discovery*, *12*(6), 447-448

24. Romeo, G., Chiacchio, U., Corsaro, A., & Merino, P. (2010). Chemical Synthesis of Heterocyclic− Sugar Nucleoside Analogues. *Chemical reviews*, *110*(6), 3337-3370.

25. Fischer, E., & Helferich, B. (1922). Synthetische Glucoside der Purine. In *Untersuchungen Über Kohlenhydrate und Fermente II (1908–1919)* (pp. 137-162). Berlin: Springer.

26. Kazimierczuk, Z., Cottam, H. B., Revankar, G. R., & Robins, R. K. (1984). Synthesis of 2'-deoxytubercidin, 2'-deoxyadenosine, and related 2'-deoxynucleosides via a novel direct stereospecific sodium salt glycosylation procedure. *Journal of the American Chemical Society*, *106*(21), 6379-6382

27. Diekmann, E., Friedrich, K., & Fritz, H. G. (1993). Didesoxy-Ribonucleoside durch Schmelzkondensation. *Advanced Synthesis & Catalysis*, *335*(5), 415-424.

28. Niedballa, U., & Vorbrüggen, H. (1970). A general synthesis of pyrimidine nucleosides. *Angewandte Chemie International Edition*, *9*(6), 461-462.

29. Zhang, Q., Sun, J., Zhu, Y., Zhang, F., & Yu, B. (2011). An Efficient approach to the synthesis of nucleosides: Gold (I)-catalyzed *n*-glycosylation of pyrimidines and purines with glycosyl ortho-alkynyl benzoates. *Angewandte Chemie*, *50*(21), 4933-4936.

30. Framski, G., Gdaniec, Z., Gdaniec, M., & Boryski, J. (2006). A reinvestigated mechanism of ribosylation of adenine under silylating conditions. *Tetrahedron*, *62*(43), 10123-10129.

31. Dibble, D. J. (2010). *Electrostatic effects in exocyclic iminium, hydrazonium, and oxocarbenium ions-* PhD Dissertation, University of California, Irvine.

32. Larsen, C. H., Ridgway, B. H., Shaw, J. T., Smith, D. M., & Woerpel, K. A. (2005). Stereoselective C-glycosylation reactions of ribose derivatives: Electronic effects of five-membered ring oxocarbenium ions. *Journal of the American Chemical Society*, *127*(31), 10879-10884.

33. Smith, D. M., Tran, M. B., & Woerpel, K. A. (2003). Nucleophilic additions to fused bicyclic five-membered ring oxocarbenium ions: evidence for preferential attack on the inside face. *Journal of the American Chemical Society*, *125*(46), 14149-14152.

34. Tran, V. T., & Woerpel, K. A. (2013). Nucleophilic addition to silyl-protected five-membered ring oxocarbenium ions governed by stereoelectronic effects. *The Journal of Organic Chemistry*, *78*(13), 6609-6621.

35. Alonso, E., Ramón, D. J., & Yus, M. (1997). Direct generation of lithium homoenolates from 3-aryl α, β-unsaturated ketones or esters by an arene-catalysed lithiation: Synthesis of substituted tetrahydrofurans and γ-butyrolactones. *Tetrahedron*, *53*(7), 2641-2652.

36. Tvaroŝka, I., & Bleha, T. (1989). Anomeric and exo-anomeric effects in carbohydrate chemistry. *Advances in Carbohydrate Chemistry and Biochemistry*, *47*, 45-123

37. Demchenko, A. V. (2003). Stereoselective chemical 1, 2-cis-*O*-glycosylation: from 'sugar ray'to modern techniques of the 21st century. *Synlett*, *2003*(09), 1225-1240..

38. Demchenko, A. V. (2003). 1, 2-cis-O-glycosylation: Methods, strategies, principles. *Current Organic Chemistry*, *7*(1), 35-79.

39. Gelin, M., Ferrieres, V., & Plusquellec, D. (1997). Synthesis of new glycofuranosyl donors and their use in glycosylation reactions. *Carbohydrate Letters*, *2*, 381-388.

40. Lowary, T. L. (2002). D-Arabinofuranosides from mycobacteria: Synthesis and conformation. *Journal of Carbohydrate Chemistry*, *21*(7-9), 691-722.

41. Niedballa, U., & Vorbrüggen, H. (1974). Synthesis of nucleosides. 9. General synthesis of N-glycosides. I. Synthesis of pyrimidine nucleosides. *The Journal of Organic Chemistry*, *39*(25), 3654-3660.

42. Yin, H., D'Souz, F. W., & Lowary, T. L. (2002). Arabinofuranosides from mycobacteria: synthesis of a highly branched hexasaccharide and related fragments containing β-arabinofuranosyl residues. *The Journal of Organic Chemistry*, *67*(3), 892-903.

43. Bogusiak, J., & Szeja, W. (2001). Studies on the synthesis of 1, 2-cis pentofuranosides from S-glycofuranosyl dithiocarbamates, dithiocarbonates and phosphorodithioates. *Carbohydrate Research*, *330*(1), 141-144.

44. Gadikota, R. R., Callam, C. S., & Lowary, T. L. (2001). Stereocontrolled synthesis of 2, 3-anhydro-*β*-D-lyxofuranosyl glycosides. *Organic Letters*, *3*(4), 607-610.

45. Marotte, K., Sanchez, S., Bamhaoud, T., & Prandi, J. (2003). Synthesis of oligoarabinofuranosides from the mycobacterial cell wall. *European Journal of Organic Chemistry*, *2003*(18), 3587-3598.

46. Zhu, X., Kawatkar, S., Rao, Y., & Boons, G. J. (2006). Practical approach for the stereoselective introduction of *β*-arabinofuranosides. *Journal of the American Chemical Society*, *128*(36), 11948-11957.

47. Crich, D., Pedersen, C. M., Bowers, A. A., & Wink, D. J. (2007). On the use of 3, 5-O-benzylidene and 3, 5-*O*-(di-tert-butylsilylene)-2-*O*-

benzylarabinothiofuranosides and their sulfoxides as glycosyl donors for the synthesis of β-arabinofuranosides: importance of the activation method. *The Journal of organic chemistry*, *72*(5), 1553-1565.

48. Ishiwata, A., Akao, H., & Ito, Y. (2006). Stereoselective synthesis of a fragment of mycobacterial arabinan. *Organic letters*, *8*(24), 5525-5528.

49. Wu, X. (2014). *Stereoselectivity in Furanose Glycosylation*- MSc Thesis, University of Helsinki, Finland

50. Lalonde, M., & Chan, T. H. (1985). Use of organosilicon reagents as protective groups in organic synthesis. *Synthesis*, *1985*(09), 817-845.

51. Elgemeie, G. H., Zaghary, W. A., Amin, K. M., & Nasr, T. M. (2005). New trends in synthesis of pyrazole nucleosides as new antimetabolites. *Nucleosides, Nucleotides, and Nucleic Acids*, *24*(8), 1227-1247.

52. Matsumoto, S. S., Fujihaki, J. M., Nord, L. D., [...], & Jolley, W. B (1990). Inhibition of pyrimidine metabolism in myeloid leukemia cells by triazole and pyrazole nucleosides. *Biochemical pharmacology*, *39*(3), 455-462.

53. Basu, N., Oyama, K. I., & Tsukamoto, M. (2017). A solid-supported acidic oxazolium perchlorate as an easy-handling catalyst for the synthesis of modified pyrimidine nucleosides via Vorbrüggen-type N-glycosylation. *Tetrahedron Letters*, *58*(20), 1921-1924.

54. Michigami, K., Uchida, S., Adachi, M., & Hayashi, M. (2013). Synthesis of novel nucleosides and stereoselectivity of *N*-glycosidation. *Tetrahedron*, *69*(2), 595-599.

55. Chandra, T., Zou, S., & Brown, K. L. (2004). Low temperature dehydrogenation of α-indoline nucleosides. *Tetrahedron letters*, *45*(41), 7783-7786.

56. Chandra, T., & Brown, K. L. (2005). Direct glycosylation: Synthesis of α-indoline ribonucleosides. *Tetrahedron letters*, *46*(12), 2071-2074.

57. Abdou, I. M., & Strekowski, L. (2000). A facile synthesis of 6-aryl-5-cyano-1-(β-d-pyranosyl or β-d-furanosyl)-2-thiocytosines. *Tetrahedron*, *56*(44), 8631-8636.

58. Chanteloup, L., & t Thuong, N. (1994). Efficient synthesis of 2′-*O*-alkyl ribonucleosides using trichloroacetimidate d-ribofuranosides as ribosyl donors. *Tetrahedron letters*, *35*(6), 877-880.

59. Chanteloup, L., & t Thuong, N. (1994). Efficient synthesis of 2′-*O*-alkyl ribonucleosides using trichloroacetimidate d-ribofuranosides as ribosyl donors. *Tetrahedron letters*, *35*(6), 877-880.

60. Šnajdr, I., Janoušek, Z., Takagaki, M., Císařová, I., Hosmane, N. S., & Kotora, M. (2014). Alpha (α-) and beta (*β*-carboranyl-C-deoxyribosides: Syntheses, structures and biological evaluation. *European journal of medicinal chemistry*, *83*, 389-397.

61. Křen, V., Olšovský, P., Havlíček, V., Sedmera, P., Witvrouw, M., & De Clecq, E. (1997). N-Deoxyribosides of ergot alkaloids: Synthesis and biological activity. *Tetrahedron*, *53*(12), 4503-4510.

62. Marzabadi, C. H., & Franck, R. W. (2000). The synthesis of 2-deoxyglycosides: 1988–1999. *Tetrahedron*, *56*(43), 8385-8417.

63. Jung, M. E., & Castro, C. (1993). New approach to the synthesis of. beta.-2'-deoxyribonucleosides: intramolecular Vorbrueggen coupling. *The Journal of Organic Chemistry*, *58*(4), 807-808.

64. Lessor, R. A., & Leonard, N. J. (1981). Synthesis of 2'-deoxynucleosides by deoxygenation of ribonucleosides. *The Journal of Organic Chemistry*, *46*(21), 4300-4301.

65. Robins, M. J., & Wilson, J. S. (1981). Smooth and efficient deoxygenation of secondary alcohols. A general procedure for the conversion of ribonucleosides to 2'-deoxynucleosides. *Journal of the American Chemical Society*, *103*(4), 932-933.

66. Barai, V. N., Zinchenko, A. I., Eroshevskaya, L. A., Kalinichenko, E. N., Kulak, T. I., & Mikhailopulo, I. A. (2002). A universal biocatalyst for the preparation of base-and sugar-modified nucleosides via an enzymatic transglycosylation. *Helvetica chimica acta*, *85*(7), 1901-1908.

67. Robins, M. J., & Robins, R. K. (1965). Purine Nucleosides. XI. The synthesis of 2'-deoxy-9-α-and-β-d-ribofuranosylpurines and the correlation of their anomeric structure with proton magnetic resonance spectra1. *Journal of the American Chemical Society*, *87*(21), 4934-4940

68. Bryson, H. M., & Sorkin, E. M. (1993). Cladribine. *Drugs*, *46*(5), 872-894.

69. Mikhailopulo, I. A., Zinchenko, A. I., Kazimierczuk, Z., Barai, V. N., Bokut, S. B., & Kalinichenko, E. N. (1993). Synthesis of 2-chloro-2′-deoxyadenosine by microbiological transglycosylation. *Nucleosides & Nucleotides*, *12*(3-4), 417-422.

70. Sugimura, H., Osumi, K., Yamazaki, T., & Yamaya, T. (1991). Coupling reaction of 1-thiopentofuranosides with silylated pyrimidine bases by activation with *N*-bromosuccinimide: synthesis of 3′-azido-3′-deoxythymidine and its related nucleoside analogs. *Tetrahedron Letters*, *32*(15), 1813-1816.

71. Kolla, N. K., Neelam, U. K., Baddam, S. R., & Gangula, S. (2011). *U.S. Patent Application No. 13/282,921*.

72. Li, B., Zhang, B., Zhang, X., & Fan, X. (2016). Synthesis of 3-Cyano-1 H-indoles and Their 2′-Deoxyribonucleoside Derivatives through One-Pot Cascade Reactions. *The Journal of Organic Chemistry*, *81*(20), 9530-9538.

73. Rizk, H. F., Ibrahim, S. A., & El-Borai, M. A. (2017). Synthesis, dyeing performance on polyester fiber and antimicrobial studies of some novel pyrazolotriazine and pyrazolyl pyrazolone azo dyes. *Arabian Journal of Chemistry*, *10*, S3303-S3309.

74. Ghorab, M. M., Ragab, F. A., Heiba, H. I., Youssef, H. A., & El-Gazzar, M. G. (2010). Synthesis of novel pyrrole and pyrrolo [2, 3-d] pyrimidine derivatives bearing sulfonamide moiety for evaluation as anticancer and radiosensitizing agents. *Bioorganic & Medicinal Chemistry Letters*, *20*(21), 6316-6320.

75. Koca, I., Özgür, A., Coşkun, K. A., & Tutar, Y. (2013). Synthesis and anticancer activity of acyl thioureas bearing pyrazole moiety. *Bioorganic & Medicinal Chemistry*, *21*(13), 3859-3865.

76. Vijesh, A. M., Isloor, A. M., Shetty, P., Sundershan, S., & Fun, H. K. (2013). New pyrazole derivatives containing 1, 2, 4-triazoles and benzoxazoles as potent antimicrobial and analgesic agents. *European Journal of Medicinal Chemistry*, *62*, 410-415.

77. Said, S. A., Amr, A. E. G. E., Sabry, N. M., & Abdalla, M. M. (2009). Analgesic, anticonvulsant and anti-inflammatory activities of some synthesized benzodiazipine, triazolopyrimidine and bis-imide derivatives. *European journal of medicinal chemistry*, *44*(12), 4787-4792.

78. Khunt, R. C., Khedkar, V. M., Chawda, R. S., Chauhan, N. A., Parikh, A. R., & Coutinho, E. C. (2012). Synthesis, antitubercular evaluation and 3D-QSAR study of *N*-phenyl-3-(4-fluorophenyl)-4-substituted pyrazole derivatives. *Bioorganic & Medicinal Chemistry Letters*, *22*(1), 666-678.

79. Raffa, D., Maggio, B., Raimondi, M. V., Cascioferro, S., Plescia, F., Cancemi, G., & Daidone, G. (2015). Recent advanced in bioactive systems containing pyrazole fused with a five membered heterocycle. *European Journal of Medicinal Chemistry*, *97*, 732-746.

80. Rana, D. N., Chhabria, M. T., Shah, N. K., & Brahmkshatriya, P. S. (2014). Discovery of new antitubercular agents by combining pyrazoline and benzoxazole pharmacophores: design, synthesis and insights into the binding interactions. *Medicinal Chemistry Research*, *23*(5), 2218-2228.

81. Horrocks, P., Pickard, M. R., Parekh, H. H., Patel, S. P., & Pathak, R. B. (2013). Synthesis and biological evaluation of 3-(4-chlorophenyl)-4-substituted pyrazole derivatives. *Organic & Biomolecular Chemistry*, *11*(29), 4891-4898.

82. Yeong, L. T., Abdul Hamid, R., Saiful Yazan, L., Khaza'ai, H., & Awang Hamsin, D. E. Z. (2014). Synergistic action of compounds isolated from the hexane extract of Ardisia crispa root against tumour-promoting effect, in vitro. *Natural Product Research*, *28*(22), 2026-2030.

83. Lv, P. C., Li, H. Q., Sun, J., Zhou, Y., & Zhu, H. L. (2010). Synthesis and biological evaluation of pyrazole derivatives containing thiourea skeleton as anticancer agents. *Bioorganic & Medicinal Chemistry*, *18*(13), 4606-4614.

84. Manfredini, S., Bazzanini, R., Baraldi, P. G., Guarneri, M., Simoni, D., Marongiu, M. E., ..[...].. & Tramontano, E. (1992). Pyrazole-related nucleosides. Synthesis and antiviral/antitumor activity of some substituted pyrazole and pyrazolo [4, 3-d]-1, 2, 3-triazin-4-one nucleosides. *Journal of Medicinal Chemistry*, *35*(5), 917-924.

85. Franchetti, P., Marchetti, S., Cappellacci, L., Yalowitz, J. A., Jayaram, H. N., Goldstein, B. M., & Grifantini, M. (2001). A new C-nucleoside analogue of tiazofurin: synthesis and biological evaluation of 2-β-d-ribofuranosylimidazole-4-carboxamide (imidazofurin). *Bioorganic & Medicinal Chemistry Letters*, *11*(1), 67-69.

86. Buckingham, L. (2011). *Molecular diagnostics: fundamentals, methods and clinical applications*. FA Davis, 1-9

87. Smith, F. W., & Feigon, J. (1992). Quadruplex structure of Oxytricha telomeric DNA oligonucleotides. *Nature*, *356*(6365), 164.

88. Ho, P. S., & Carter, M. (2011). DNA structure: alphabet soup for the cellular soul. In *DNA Replication-Current Advances*. InTech.

89. Haq, I., & Ladbury, J. (2000). Drug–DNA recognition: energetics and implications for design. *Journal of Molecular Recognition*, *13*(4), 188-197.

90. Alzeer, J., & Luedtke, N. W. (2010). pH-mediated fluorescence and G-quadruplex binding of amido phthalocyanines. *Biochemistry*, *49*(20), 4339-4348.

91. Hurley, L. H. (2002). DNA and its associated processes as targets for cancer therapy. *Nature Reviews Cancer*, *2*(3), 188-200.

92. Kaufmann, S. H., & Earnshaw, W. C. (2000). Induction of apoptosis by cancer chemotherapy. *Experimental cell research*, *256*(1), 42-49.

93. Kaufmann, S. H. (1989). Induction of endonucleolytic DNA cleavage in human acute myelogenous leukemia cells by etoposide, camptothecin, and other cytotoxic anticancer drugs: a cautionary note. *Cancer Research*, *49*(21), 5870-5878.

94. Barry, M. A., Behnke, C. A., & Eastman, A. (1990). Activation of programmed cell death (apoptosis) by cisplatin, other anticancer drugs, toxins and hyperthermia. *Biochemical Pharmacology*, *40*(10), 2353-2362.

95. Mahmoud, S. A. M. (2006). *Effects of Novel Synthetic Nucleosides as Anti-Tumor Agents on Human Acute Promyelocytic Leukemia Cell Line* (HL-60)-MSc Thesis, the UAE University.

96. Song, Y. M., Wu, Q., Yang, P. J., Luan, N. N., Wang, L. F., & Liu, Y. M. (2006). DNA Binding and cleavage activity of Ni (II) complex with all-trans retinoic acid. *Journal of Inorganic Biochemistry*, *100*(10), 1685-1691.

97. Kuntz, I. D., Blaney, J. M., Oatley, S. J., Langridge, R., & Ferrin, T. E. (1982). A geometric approach to macromolecule-ligand interactions. *Journal of Molecular Biology*, *161*(2), 269-288.

98. Morris, G. M., Goodsell, D. S., Halliday, R. S., Huey, R., Hart, W. E., Belew, R. K., & Olson, A. J. (1998). Automated docking using a Lamarckian genetic algorithm and an empirical binding free energy function. *Journal of Computational Chemistry*, *19*(14), 1639-1662.

99. Wang, R., Lai, L., & Wang, S. (2002). Further development and validation of empirical scoring functions for structure-based binding affinity prediction. *Journal of Computer-Aided Molecular Design*, *16*(1), 11-26.

100. Prakhov, N. D., Chernorudskiy, A. L., & Gainullin, M. R. (2010). VSDocker: a tool for parallel high-throughput virtual screening using AutoDock on Windows-based computer clusters. *Bioinformatics*, *26*(10), 1374-1375.

101. Sharma, P. K., Kumar, S., Kumar, P., Kaushik, P., Sharma, C., Kaushik, D., & Aneja, K. R. (2012). Synthesis of 1-(4-aminosulfonylphenyl)-3, 5-diarylpyrazoline derivatives as potent antiinflammatory and antimicrobial agents. *Medicinal Chemistry Research*, *21*(10), 2945-2954.

102. Abdou, I. M., Saleh, A. M., & Zohdi, H. F. (2004). Synthesis and antitumor activity of 5-trifluoromethyl-2, 4-dihydropyrazol-3-one nucleosides. *Molecules*, *9*(3), 109-116.

103. Abdelhamid, A. O., Zohdi, H. F., & Ziada, M. M. (2001). A facile synthesis of pyrimido [2″, 3″: 5′, 1′] pyrazolo [3′, 4′: 4, 5] pyrimido [1, 6-a] benzimidazoles and [1, 2, 4] triazino [3″, 4″: 5′, l′] pyrazolo [3′, 4′: 4, 5]-pyrimido [6, 1-a] benzimidazoles. *Indian Journal of Chemistry, Section B: Organic Chemistry and Medicinal Chemistry, 40*(4), 284-289.

104. Gorin, P. A. J., & Jones, J. K. N. (1953). A New Synthesis of 2-Deoxy-D-ribose. *Nature*, *172*(4388), 1051-1052.

106. Yokozeki, K., & Tsuji, T. (2000). A novel enzymatic method for the production of purine-2′-deoxyribonucleosides. *Journal of Molecular Catalysis B: Enzymatic*, *10*(1), 207-213.

107. Jones, R. N., Gavan, T. L., & Barry, A. L. (1980). Evaluation of the sensititre microdilution antibiotic susceptibility system against recent clinical isolates: three-laboratory collaborative study. *Journal of Clinical Microbiology*, *11*(4), 426-429.

108. Mechkarska, M., Attoub, S., Sulaiman, S., Pantic, J., Lukic, M. L., & Conlon, J. M. (2014). Anti-cancer, immunoregulatory, and antimicrobial activities of the

frog skin host-defense peptides pseudhymenochirin-1Pb and pseudhymenochirin-2Pa. *Regulatory Peptides*, *194*, 69-76.

109. Keri, R. S., Chand, K., Ramakrishnappa, T., & Nagaraja, B. M. (2015). Recent Progress on Pyrazole Scaffold-Based Antimycobacterial Agents. *Archiv der Pharmazie*, *348*(5), 299-314.

110. Burkhardt, O., Ewig, S., Haagen, U., Giersdorf, S., Hartmann, O., Wegscheider, K., ..[...].. & Welte, T. (2010). Procalcitonin guidance and reduction of antibiotic use in acute respiratory tract infection. *European Respiratory Journal*, *36*(3), 601-607.

111. Chen, H., Li, Z., & Han, Y. (2000). Synthesis and Fungicidal Activity against Rhizoctoniasolani of 2-Alkyl (Alkylthio)-5-pyrazolyl-1, 3, 4-oxadiazoles (Thiadiazoles). *Journal of agricultural and food chemistry*, *48*(11), 5312-5315.

112. Zakerhamidi, M. S., Ghanadzadeh, A., & Moghadam, M. (2012). Solvent effects on the UV/visible absorption spectra of some aminoazobenzene dyes. *Chemical Science Transactions*, *1*(1), 1-8.

113. Homocianu, M. (2011). Solvent effects on the electronic absorption and fluorescence spectra. *Journal of Advanced Research in Physics*, *2*(1).

114. Božić, B. Đ., Alimmari, A. S., Mijin, D. Ž., Valentić, N. V., & Ušćumlić, G. S. (2014). Synthesis, structure and solvatochromic properties of novel dyes derived from 4-(4-nitrophenyl)-3-cyano-2-pyridone. *Journal of Molecular Liquids*, *196*, 61-68.

115. Masoud, M. S., Ali, A. E., Shaker, M. A., & Ghani, M. A. (2004). Solvatochromic behavior of the electronic absorption spectra of some azo derivatives of amino pyridines. *Spectrochimica Acta Part A: Molecular and Biomolecular Spectroscopy*, *60*(13), 3155-3159.

116. Hadjmohammadi, M. R., Chaichi, M. J., & Yousefpour, M. (2008). Solvatochromism effect of different solvents on UV-Vis spectra of flouresceine and its derivatives. *Iranian Journal of Chemistry and Chemical Engineering (IJCCE)*, *27*(4), 9-14.

117. Reichardt, C., & Welton, T. (2011). *Solvents and solvent effects in organic chemistry*. John Wiley & Sons, 408-447.

118. Blum, K. (2013). Phototransformation of pharmaceuticals in the environment: Multivariate modeling and experimental determination of photolysis half-lives, 8895-912.

119. Sirajuddin, M., Ali, S., & Badshah, A. (2013). Drug–DNA interactions and their study by UV–Visible, fluorescence spectroscopies and cyclic voltametry. *Journal of Photochemistry and Photobiology B: Biology*, *124*, 1-19.

120. Dodero, V. I., Quirolo, Z. B., & Sequeira, M. A. (2011). Biomolecular studies by circular dichroism. *Frontiers in Bioscience*, *16*, 61-73.

121. Watson, J. D., & Crick, F. H. (1953). Genetical implications of the structure of deoxyribonucleic acid. *Nature*, *171*(4361), 964-967.

122. Tabernero, L., Bella, J., & Alemán, C. (1996). Hydrogen bond geometry in DNA-minor groove binding drug complexes. *Nucleic Acids Research*, *24*(17), 3458-3466.

123. Moorhouse, A. D., Santos, A. M., Gunaratnam, M., Moore, M., Neidle, S., & Moses, J. E. (2006). Stabilization of G-quadruplex DNA by highly selective ligands via click chemistry. *Journal of the American Chemical Society*, *128*(50), 15972-15973.

124. Panigrahi, S. K., & Desiraju, G. R. (2007). Strong and weak hydrogen bonds in drug-DNA complexes: A statistical analysis. *Journal of Biosciences*, *32*(4), 677-692.

125. Ferreira, R., Artali, R., Benoit, A., Gargallo, R., Eritja, R., Ferguson, D. M., ..[..].. & Mazzini, S. (2013). Structure and stability of human telomeric G-quadruplex with preclinical 9-amino acridines. *PloS one*, *8*(3), e57701.

126. Sirajuddin, M., Ali, S., Shah, N. A., Khan, M. R., & Tahir, M. N. (2012). Synthesis, characterization, biological screenings and interaction with calf thymus DNA of a novel azomethine 3-((3, 5-dimethylphenylimino) methyl) benzene-1, 2-diol. *Spectrochimica Acta Part A: Molecular and Biomolecular Spectroscopy*, *94*, 134-142.

127. Sirajuddin, M., Ali, S., Haider, A., Shah, N. A., Shah, A., & Khan, M. R. (2012). Synthesis, characterization, biological screenings and interaction with calf thymus DNA as well as electrochemical studies of adducts formed by azomethine [2-((3, 5-dimethylphenylimino) methyl) phenol] and organotin (IV) chlorides. *Polyhedron*, *40*(1), 19-31.

128. Arjmand, F., & Jamsheera, A. (2011). DNA binding studies of new valine derived chiral complexes of tin (IV) and zirconium (IV). *Spectrochimica Acta Part A: Molecular and Biomolecular Spectroscopy*, *78*(1), 45-51.

129. Shahabadi, N., Kashanian, S., Khosravi, M., & Mahdavi, M. (2010). Multispectroscopic DNA interaction studies of a water-soluble nickel (II) complex containing different dinitrogen aromatic ligands. *Transition Metal Chemistry*, *35*(6), 699-705.

130. Tabernero, L., Bella, J., & Alemán, C. (1996). Hydrogen bond geometry in DNA-minor groove binding drug complexes. *Nucleic Acids Research*, *24*(17), 3458-3466.

131. Bhadra, K., & Kumar, G. S. (2011). Interaction of berberine, palmatine, coralyne, and sanguinarine to quadruplex DNA: a comparative spectroscopic and calorimetric study. *Biochimica et Biophysica Acta (BBA)-General Subjects*, *1810*(4), 485-496.

132. Wei, C., Wang, J., & Zhang, M. (2010). Spectroscopic study on the binding of porphyrins to (G 4 T 4 G 4) 4 parallel G-quadruplex. *Biophysical Chemistry*, *148*(1), 51-55.

133. Jaumot, J., & Gargallo, R. (2012). Experimental methods for studying the interactions between G-quadruplex structures and ligands. *Current Pharmaceutical Design*, *18*(14), 1900-1916.

134. Sun, H., Xiang, J., Liu, Y., Li, L., Li, Q., Xu, G., & Tang, Y. (2011). A stabilizing and denaturing dual-effect for natural polyamines interacting with G-quadruplexes depending on concentration. *Biochimie*, *93*(8), 1351-1356.

135. Altaf, A. A., Hashmat, U., Yousaf, M., Lal, B., Ullah, S., Holder, A. A., & Badshah, A. (2016). Synthesis and characterization of azo-guanidine based alcoholic media naked eye DNA sensor. *Open Science*, *3*(11), 160351.

136. Agarwal, S., Jangir, D. K., & Mehrotra, R. (2013). Spectroscopic studies of the effects of anticancer drug mitoxantrone interaction with calf-thymus DNA. *Journal of Photochemistry and Photobiology B: Biology*, *120*, 177-182.

137. Lakowicz, J. R., & Masters, B. R. (2008). Principles of fluorescence spectroscopy. *Journal of Biomedical Optics*, *13*(2), 029901.

138. Suh, D., & Chaires, J. B. (1995). Criteria for the mode of binding of DNA binding agents. *Bioorganic & Medicinal Chemistry*, *3*(6), 723-728.

139. Rodger, A. (2006). Circular dichroism and linear dichroism (p. 1-34). In *Encyclopedia of Analytical Chemistry*. New York: Wiley.

140. Paramasivan, S., Rujan, I., & Bolton, P. H. (2007). Circular dichroism of quadruplex DNAs: applications to structure, cation effects and ligand binding. *Methods*, *43*(4), 324-331.

141. Kypr, J., Kejnovská, I., Renčiuk, D., & Vorlíčková, M. (2009). Circular dichroism and conformational polymorphism of DNA. *Nucleic Acids Research*, *37*(6), 1713-1725.